

# **Role of WD domain of ATG16L1 and LC3 associated endocytosis in control of influenza virus infection**

---

**By Yingxue Wang**

**Norwich Medical School**

**University of East Anglia**

**March 2020**

**A thesis submitted for the degree of Doctor of Philosophy. This copy of the thesis has been supplied on the condition that anyone who consults it is understood to recognise that its copyright rests with the author and that use of any information derived there from must be in accordance with current UK Copyright Law. In addition, any quotation or extract must include full attribution.**



## Abstract

Autophagy is a conserved self-eating process that delivers intracellular material to lysosomes for degradation (Yu, Chen, & Tooze, 2018). Autophagy is activated by multiple cellular stresses, including starvation and pathogen infection and plays crucial roles in maintaining cellular homeostasis and in controlling pathogen infection and inflammation (Florey, Gammoh, Kim, Jiang, & Overholtzer, 2015) (Levine & Kroemer, 2008). Degradation during conventional (or canonical) autophagy is facilitated by autophagy protein ATG8/LC3 (LC3) which facilitates fusion of double-membraned autophagosomes with lysosomes. Recent work has revealed non-canonical autophagy pathways that use LC3 to target single-membraned endolysosome compartments to lysosomes during the uptake of extracellular material (Heckmann, Boada-Romero, Cunha, Magne, & Green, 2017). LC3-associated phagocytosis (LAP) has been used to describe recruitment of LC3 to phagosomes in phagocytic cells, while LC3-associated endocytosis describes a similar pathway targeting endosomes in non-phagocytic cells (Heckmann et al 2019).

Conventional autophagy is a well-established as a defence against infection, but the roles played by non-canonical autophagy during infection 'in vivo' are less clear. This study uses a mouse model ( $\delta$ WD) with systemic loss of non-canonical autophagy to study the roles played by LAP and LC3-associated endocytosis during influenza A virus (IAV) infection. The  $\delta$ WD mice were exquisitely sensitive to IAV with elevated lung virus titres leading to exacerbated pro-inflammatory cytokine responses, fulminant pneumonia, extensive pulmonary inflammation and high mortality. Bone marrow transfers from control mice were unable to protect  $\delta$ WD mice from IAV. Protection against IAV infection 'in vivo' was therefore independent of LAP in phagocytic cells. In a reciprocal experiment *LysMcre* was used to delete LAP specifically from myeloid cells. These  $LAP^{-/-}$  mice, which maintain LC3-associated endocytosis in other tissues were resistant to IAV suggesting that LC3 associated endocytosis, rather than LAP, provides a defence against IAV. Ex vivo studies suggest that this defence is most likely to take place in the epithelial cells that line the respiratory tract.

## **Keywords**

Autophagy, non-canonical autophagy, LC3-associated phagocytosis, LC3-associated endocytosis, influenza A virus, lung infection, epithelial barrier.

# Contents

<b>Chapter 1 introduction:</b> .....	15
<b>1.1 Autophagy and non-canonical autophagy</b> .....	15
<b>1.1.i Autophagy</b> .....	15
<b>1.1.ii Non-canonical autophagy</b> .....	15
<b>1.2 Molecular mechanism of autophagy.</b> .....	16
<b>1.2.i Initiation and nucleation</b> .....	16
<b>1.2.ii Autophagosome expansion</b> .....	17
<b>1.2.iii Cargo recognition and degradation during autophagy</b> .....	19
<b>1.3. Autophagy reduces pathogen load and inflammation during infection</b> .....	19
<b>1.3.i Pathogen capture</b> .....	19
<b>1.3.ii Autophagy and the control of inflammation.</b> .....	20
<b>1.4 Non-canonical autophagy and LC3 associated phagocytosis</b> .....	22
<b>1.4.i LC3 associated phagocytosis (LAP)</b> .....	22
<b>1.4.ii Molecular mechanism of LAP</b> .....	22
<b>1.5 Roles played by LAP during infection and inflammation</b> .....	24
<b>1.5.i Clearance of pathogens by LAP</b> .....	24
<b>1.5.ii LAP in efferocytosis and immunological silence</b> .....	27
<b>1.5.iii LAP participates in antigen presentation</b> .....	27
<b>1.6. Non-canonical autophagy and LANDO</b> .....	29
<b>1.7. Non-canonical autophagy and ATG16L1 WD40-repeats</b> .....	29
<b>1.7.i ATG16L1 WD40 domain interacting proteins</b> .....	30
<b>1.7.ii The T300A mutation in ATG16L1 impairs function of the WD40 domain</b> .....	30
<b>1.8. Generation of a mouse model to study the role played by non-canonical autophagy and LAP ‘in vivo’.</b> .....	31
<b>1.9. Influenza A virus (IAV) as a model to study the role played by non-canonical autophagy during viral infection.</b> .....	32
<b>1.9.i Virus types strains and structure</b> .....	32
<b>1.9.ii. Virus entry</b> .....	34
<b>1.9.iii. Replication and transcription</b> .....	35
<b>1.9.iv. Virion assembly</b> .....	36
<b>1.9.v Potential role for non-canonical autophagy and LAP during innate immune responses to Influenza A virus infection.</b> .....	37
<b>1.10 Inflammatory response and cytokine storm induced by influenza infection</b> .....	42
<b>1.10.i Inflammatory responses</b> .....	42

1.10.ii Innate immune cells involved in influenza infection .....	44
1.10.iii Cytokines, chemokines and interferons involved in influenza infection .....	45
1.10.iv. Cytokine storms and tissue damage during IAV infection .....	51
1.11 Mouse model and specific aims.....	53
Chapter 2 Methods: .....	56
2.1 Cell culture.....	56
2.1.i Cell lines.....	56
2.1.ii Tissue culture media and reagents .....	56
2.1.iii Primary cells isolation: .....	56
2.2 Immunofluorescence microscopy.....	57
2.2.i Autophagy and non-canonical autophagy stimulation.....	57
2.2.ii Fluorescent microscopy .....	58
2.3 Western blotting .....	58
2.3.i Cell lysis preparation .....	58
2.3.ii BCA assay .....	58
2.3.iii Western blotting .....	59
2.4 DNA amplification and genotyping .....	59
2.5 Virus infection .....	60
2.6 Plaque assay .....	60
2.6.i Tissue homogenise .....	60
2.6.ii Serial dilution .....	60
2.6.iii Overlay medium preparation .....	60
2.6.iv Fixation and staining .....	61
2.7 q-PCR for RNA expression level of cytokines and IAV .....	61
2.7.i Tissue homogenise .....	61
2.7.ii RNA extraction .....	62
2.7.iii RNA clean up .....	62
2.7.iv Reverse transcription .....	62
2.7.v Run q-PCR and data analysis.....	63
2.8 Flow cytometry.....	64
2.8.i Prepare single cell suspension .....	64
2.8.ii Antibody labelling .....	65
2.9 Elisa (enzyme-linked immunosorbent assay).....	66
2.9.i Antigen preparation and plates coating.....	66
2.9.ii Antibody detection by Elisa .....	66
2.10 Luminex Simplex Assay .....	67

2.10.i Sample preparation: .....	67
2.10.ii Luminex Assay .....	67
2.11 Generation and analysis of Radiation Chimeras .....	69
2.12 Histology, immunohistology .....	70
2.13 Statistical analysis .....	71
2.14 Mice model .....	71
Results Part I .....	73
Chapter 3: Analysis of IAV infection of mice lacking the WD domain of ATG16L1.....	74
3.1 Introduction and aims .....	74
3.2 Genotyping $\delta$ WD mice .....	76
3.3 Characterisation of autophagy and LAP in cells from $\delta$ WD mice lacking the WD domain of ATG16L1.....	78
3.4. Role played by WD domain of ATG16L1 during airway challenge with IAV .....	81
3.4.i Weight loss and mortality .....	81
3.4.ii Role played by WD domain of ATG16L1 on virus lung titre during IAV infection.....	81
3.4.iii Role played by WD domain of ATG16L1 on cytokine production during IAV infection. ....	84
3.4.iv Role played by WD domain of ATG16L1 on lung pathology following IAV infection .....	97
3.5. Discussion and summary.....	105
Results Part II.....	108
Chapter 4: Analysis of IAV infection of mice lacking the WD domain of ATG16L1 in phagocytic cells. ....	109
4.1 Introduction and aims:.....	109
4.2 Genetic background and genotyping results of <i>Atg16L1<sup>F1/F1</sup></i> and $\delta$ WD <i>LysMcre</i> mice model. ....	109
4.2.1 Genetic background and genotyping results of <i>Atg16L1<sup>f1/f1</sup></i> mice .....	109
4.2.2 Genetic background and genotyping results of $\delta$ WD <i>LysMcre</i> mice.....	110
4.3 Characterisation of autophagy and LAP in cells from $\delta$ WD- <i>LysMcre</i> mice. ....	115
4.4. Effect of specific loss of LAP in phagocytes on IAV infection .....	120
4.4.1 Weight loss and viral titre in lung.....	120
4.4.2 Effect of loss of LAP in phagocytes on cytokine production during IAV infection .....	120
4.4.3 Effect of loss of LAP in phagocytes on immune cell infiltration into lung during IAV infection.....	121
4.5 Discussion: .....	121
Results Part III.....	122
Chapter 5: Analysis of $\delta$ WD mice reconstituted with wildtype ( <i>LAP<sup>+/+</sup></i> ) bone marrow. ....	123
5.1 introduction.....	123

5.2 Generation and analysis of radiation chimeras .....	123
5.3 $\delta$ WD mice reconstituted with wild type bone marrow remain highly sensitive to IAV .....	123
5.4 $\delta$ WD mice reconstituted with wild type bone marrow does not protect against immune infiltration into the lungs during IAV infection .....	128
5.5 Discussion and summary .....	128
Result Part IV .....	131
Chapter 6: Role played by WD domain of ATG16L1 on acquired immune response following IAV infection .....	132
6.1 Introduction and Aims: .....	132
6.2 The effect of Atg16L1 WD domain in immune cells population on the lung during IAV infection .....	137
6.3 The effect of WD domain of Atg16L1 on immunoglobulin production during IAV infection .....	139
.....	140
6.4 Discussion .....	140
Discussion .....	142
Chapter 7 Discussion: .....	143
7.1 $\delta$ WD mice do not exhibit alterations in lymphocyte populations .....	143
7.2 correlative analysis across IAV mRNA level, cytokines expression level, viral titre and IAV histology quantification .....	145
7.3 Could LAP in phagocytic cells play a role in controlling IAV infection? .....	146
7.4 How loss of non-canonical autophagy/LAP causes high viral titre and cytokine expression after infection .....	147
7.5 How does the WD domain of ATG16L1 promote lipidation of endolysosome compartments? .....	149
7.6 Future work .....	150
References .....	152

## **Abbreviations:**

**ATG16L1:** Autophagy-related 16-like 1

**ATG5:** Autophagy-related 5

**ATG12:** Autophagy-related 12

**BMDM:** Bone marrow-derived macrophages

**BSA:** Bovine serum albumin

**CCD:** Coiled-coil domain

**DAPI:** 4', 6-Diamidion-2-Phenylindole

**DCs:** dendritic cells

**DMEM:** Dubelcco's modified Eagle's medium

**DMSO:** Dimethyl supfoxide

**EDTA:** Ethylenediaminetetraacetic acid

**FACs:** Fluorescence-activated cell sorting

**FIP200:** Focal adhesion kinase family interacting protein of 200 kDa

**HA:** haemagglutinin

**HBSS:** Hanks balanced salt solution

**HEPES:** 4-(2-hydroxyethyl)-1-piperazineethanesulfonic acid

**IAV:** Influenza A virus

**IFNs:** Interferons

**IL:** Interleukin

**IRF:** IFN-regulatory factor

**ISGs:** Interferon-stimulated genes

**LAP:** LC3-associated phagocytosis

**LANDO:** LC3-associated endocytosis

**LC3:** Microtubule-associated protein 1 light chain 3

**LIR:** LC3-interacting region

**LoxP:** locus of X-over P1 Bacteriophage

**M1:** matrix 1 protein

**M2:** matrix 2 protein

**M-CSF:** Macrophage colony-stimulating

**MDCK:** Madin-Darby Canine Kidney Epithelial Cells

**MEFs:** mouse embryonic fibroblast

**MHCII:** major-histocompatibility complex class II molecules

**MIIC:** MHC classII compartments

**MyD88:** Myeloid differentiation protein 88

**M $\phi$ :** Macrophage

**NA:** neuraminidase

**NETs:** neutrophil extracellular traps

**NF- $\kappa$ B:** nuclear factor- $\kappa$ B

**Nox:** NADPH oxidase

**NP:** nucleoprotein

**NS:** nonstructural protein

**OPN:** optineurin

**P62/SQSTM1:** sequestosome 1

**PA:** polymerase acidic protein

**PAMPs:** pathogen-associated molecular patterns

**PB:** polymerase basic protein

**PBS:** Phosphate Buffered Saline

**PCR:** Polymerase chain reaction

**PE:** phosphatidylethanolamine

**PFU:** plaque-forming unit

**PI:** phosphatidylinositides

**PI3P:** phosphatidylinositol 3-phosphate

**PRR:** pattern recognition receptors

**q-PCR:** quantitative polymerase chain reaction

**RIG-I:** retinoic acid-inducible gene-I

**ROS:** Reactive oxygen species

**RPMI:** Roswell Park Memorial institute medium

**SDS:** sodium dodecyl sulphate

**TBK1:** Tank binding kinase

**TLR:** toll-like receptor

**TNF:** Tumor necrosis factor

**ULK1:** unc-51-like kinase 1

**UVRAG:** UV Radiation Resistance Associated

**V-ATPase:** Vacuolar-type H<sup>+</sup>-ATPase

**VPS:** vacuolar protein sorting

**vRNPs:** viral ribonucleoproteins

**WD:** WD-40 domain

**WIPI:** WD repeat domain phosphoinositide-interacting protein 1

**WT:** Wild type

## List of figures:

**Figure 1.1.** Mechanism of mammalian autophagy.

**Figure 1.2.** Ubiquitin targets intracellular pathogens to autophagosomes via autophagy receptors.

**Figure 1.3.** Autophagy reciprocally regulates the inflammasome activity.

**Figure 1.4.** Canonical autophagy versus LC3-associated phagocytosis.

**Figure 1.5.** Molecular mechanism of LC3-associated phagocytosis.

**Figure 1.6.** Antigen presentation by MHC class II molecules in DCs.

**Figure 1.7.** The ATG16L1 structure difference between yeasts and mammals.

**Figure 1.8.** Generation of mouse model lacking the WD domain of ATG16L1.

**Figure 1.9.** Diagram of Influenza A virus.

**Figure 1.10.** Receptor-mediated cell entry of IAVs.

**Figure 1.11.** Viral replication, transcription and assembly.

**Figure 1.12.** Description of non-canonical autophagy deficiency increases viral load and exacerbate inflammatory responses.

**Figure 1.13.** Cell receptor mediated pathways involved in influenza virus infection

**Figure 1.14.** IFNs induced signalling pathway

**Figure 1.15.** Cytokine storm induced by influenza infection in the lung.

**Figure 3.1.** Strategy for removal of the linker and WD domains from ATG16L1. A. Protein domain and interaction map of ATG16L1.

**Figure 3.2.** Genotyping mice.

**Figure 3.3.** Analysis of autophagy in cells cultured from mouse strains.

**Figure 3.4.** Analysis of non-canonical autophagy and LAP in cells cultured from mouse strains.

**Figure 3.5.** Weight loss and mortality following challenge of mice with influenza virus.

**Figure 3.6.** Analysis of virus replication in lungs following challenge of mice with low dose of influenza virus.

**Figure 3.7.** Analysis of virus replication in lungs following challenge of mice with high dose of influenza virus.

**Figure 3.8.** Analysis of basal cytokine expression level in lungs from *Atg16L1<sup>fl/fl</sup>*-LysMcre and  $\delta$ WD mice model.

**Figure 3.9.** Analysis of interferon expression in lungs following challenge of mice with low dose of influenza virus.

**Figure 3.10.** Analysis of pro-inflammatory cytokine expression in lungs following challenge of mice with low dose of influenza virus.

**Figure 3.11.** Analysis of interferon expression in lungs following challenge of mice with high dose of influenza virus.

**Figure 3.12.** Analysis of pro-inflammatory cytokine expression in lungs following challenge of mice with high dose of influenza virus.

**Figure 3.13.** Analysis of interferon expression in lungs following challenge of mice with high dose of influenza virus

**Figure 3.14.** Analysis of pro-inflammatory cytokine expression in lungs following challenge of mice with high dose of influenza virus.

**Figure 3.15.** Cytokines level in lungs detected by luminex assay, following challenge of mice with high dose of influenza virus.

**Figure 3.16.** Immunohistochemical analysis of lung sections following challenge of mice with high dose of influenza virus.

**Figure 3.17.** Immunohistochemical analysis of virus antigen in lung sections following challenge of mice with high dose of influenza virus.

**Figure 3.18.** Immunohistochemical analysis of neutrophil migration in lung sections following challenge of mice with high dose of influenza virus.

**Figure 3.19.** Immunohistochemical analysis of neutrophil netosis in lung sections following challenge of mice with high dose of influenza virus.

**Figure 3.20.** Immunohistochemical analysis of macrophage migration in lung sections following challenge of mice with high dose of influenza virus.

**Figure 4.1.** Genome map and location of PCR primers for genotyping.

**Figure 4.2.** Representative agarose gel showing PCR products and genotype.

**Figure 4.3.** Breeding strategy of  $\delta$ WD-LysMcre mice model.

**Figure 4.4.** Genome map and PCR primers for analysis of  $\delta$ WD-LysMcre mice genotype.

**Figure 4.5.** Representative agarose gel showing PCR products and genotype.

**Figure 4.6.** Analysis of non-canonical autophagy and LAP in cells cultured from  $\delta$ WD<sup>phag</sup> mouse strains. A and B: non-canonical autophagy.

**Figure 4.7.** Weight loss and viral titer following challenge of  $\delta$ WD<sup>phag</sup> mice with influenza virus.

**Figure 4.8** Analysis of basal cytokine expression level in  $\delta$ WD<sup>phag</sup> mice model

**Figure 4.9.** Analysis of interferon and cytokines expression in lungs following challenge of  $\delta$ WD<sup>phag</sup> mice with influenza virus.

**Figure 4.10.** Comparison of Cytokine mRNA expression level in  $\delta$ WD and  $\delta$ WD<sup>phag</sup> mice lung

**Figure 4.11.** Immunohistochemical analysis of  $\delta$ WD<sup>phag</sup> mice in lung sections following challenge of mice with high dose of influenza virus.

**Figure 5.1.** Confirmation of bone marrow transplant radiation chimaeras

**Figure 5.2.** Weight loss, mortality and viral titer following challenge of reconstituted mice with influenza virus.

**Figure 5.3** Immunohistochemical analysis of lung following challenge with high dose influenza virus.

**Figure 5.4** Immunohistochemical analysis of lung following challenge with high dose influenza virus.

**Figure 6.1.** Gating strategy used to identify T cells and B cells in mice lung

**Figure 6.2.** Gating strategy used to identify alveolar macrophages in mice lung.

**Figure 6.3.** Gating strategy used to identify neutrophils in mice lung.

**Figure 6.4.** FACs results in mice lung following high dose infection

**Figure 6.5.** Quantification of immunoglobulins level in the serum by Elisa following challenge of mice with high dose of influenza virus.

**Figure 7.1.** Mice deficient in non-canonical autophagy have normal leukocyte populations.

**Figure 7.2:** The correlation plots between IAV mRNA level, cytokines expression level, viral titre and IAV histology quantification.

**Figure 7.3** Diagram of full-length (FL) 229–242 deletion ( $\Delta$ FBD) and 1–336 ( $\delta$ WD) ATG16L1 constructs used in this study.

## List of tables:

**Table 1:** List of studies for LC3-associated phagocytosis

**Table 2:** Primer information for genotyping

**Table 3:** 2×overlay Medium recipe for 100ml

**Table 4:** Annealing system

**Table 5:** q-PCR master mix for 1 reaction

**Table 6:** Resources of q-PCR primers for target genes

**Table 7:** List of antibody source and dilutions

**Table 8:** Expect bands size for each genotype

# **Chapter 1**

## **Introduction**

## Chapter 1 introduction:

### 1.1 Autophagy and non-canonical autophagy

#### 1.1.i Autophagy

The word “autophagy” is derived from the Greek meaning ‘self-eating’. It was invented by Christian de Duve in 1963, based on the discovery of lysosomes (Klionsky, 2008). The autophagy – related genes was identified in the 1990s, allows scientists further investigate the mechanisms of autophagy (Baba, Takeshige, Baba, & Ohsumi, 1994; Harding, Morano, Scott, & Klionsky, 1995; Klionsky, Cueva, & Yaver, 1992; Takeshige, Baba, Tsuboi, Noda, & Ohsumi, 1992; Tsukada & Ohsumi, 1993; Yorihuri & Ohsumi, 1994). Japanese scientist Yoshinori Ohsumi was awarded the Nobel Prize in Physiology or Medicine in 2016 "for his discoveries of mechanisms for autophagy".

Autophagy describes an intracellular degradation process activated by multiple cellular stresses, including starvation and pathogen infection. It plays crucial roles in maintaining cellular homeostasis and control of intracellular pathogens and pathogen-induced inflammation (Florey et al., 2015) (Levine & Kroemer, 2008). Three major types of autophagy have been described: macroautophagy, microautophagy, and chaperone-mediated autophagy (CMA), all of which promote the degradation of cytosolic components via lysosomes (Glick, Barth, & Macleod, 2010). Among them, macroautophagy, hereafter referred to as autophagy or canonical autophagy, is the most studied form. When autophagy is initiated, a double-membraned vesicle known as an autophagosome is generated within the cell that delivers damaged organelles, long-lived proteins or pathogens to lysosomes for degradation, and recycles the cellular components for other processes (Kundu & Thompson, 2008; Wileman, 2013). A key stage in autophagy is the recruitment of autophagy protein LC3/ATG8 to the membranes of the autophagosome to facilitate fusion with lysosomes.

#### 1.1.ii Non-canonical autophagy

The lipidation of LC3 onto double membrane autophagosomes has become a hall mark of conventional (canonical) autophagy. Recent studies show that LC3 can also be conjugated to single-membraned endo-lysosome compartments. This is referred to as non-canonical autophagy (NCA) (Florey & Overholtzer, 2012). In phagocytic cells the non-canonical autophagy pathway is called LC3-associated phagocytosis (LAP) which is thought to play a key

role in microbial killing (Akoumianaki et al., 2016; Lam, Cemma, Muise, Higgins, & Brumell, 2013). A similar LAP-like non-canonical autophagy pathway operates in non-phagocytic cells during uptake of particulate material or apoptotic cells (Chen et al., 2014). Recently studies have called this LC3-associated endocytosis to distinguish it from LAP (Heckmann et al 2019).

### 1.1.iii Autophagy definitions assumed in this thesis:

**Autophagy** (also called canonical and conventional autophagy) describes macroautophagy where LC3 is conjugated to double-membraned autophagosomes during the capture of **intracellular** material.

**Non-canonical autophagy** describes the conjugation of LC3 to single membraned endo-lysosome compartments during the uptake of **extracellular** material. There are two versions.

- **LC3 associated phagocytosis (LAP)** describes non-canonical autophagy where LC3 is conjugated to phagosomes in phagocytic cells.
- **LC3 associated endocytosis (LANDO)** describes non-canonical autophagy where LC3 is conjugated to endosomes and lysosomes in non-phagocytic cells.

## 1.2 Molecular mechanism of autophagy.

Autophagy can be divided into 3 main steps: initiation and nucleation, phagophore expansion, fusion with lysosome and degradation of sequestered cargo.

### 1.2.i Initiation and nucleation

Initiation of autophagy [Figure 1.1] is mediated by two membrane-associated protein complexes: ULK1 complex and class III PtdIns3K complex (Birgisdottir et al., 2019). In nutrient-rich conditions, autophagy is inhibited by the mammalian target of rapamycin complex 1 (mTORC1) which is the key regulator of autophagy induction (Jung, Ro, Cao, Otto, & Kim, 2010). Inactivation of mTORC1 during starvation or other stressors, leads to the activation of the ULK1 complex (composes of ULK1, ATG13, ATG101 and FIP200 in mammalian cells) and initiation of autophagy (Yang & Klionsky, 2010). In mammalian cells, the double membraned phagophore of autophagosome emerges from an omega-shaped structure (omegasome) on the ER, which provides a membrane platform for autophagy proteins, autophagosome membranes expansion, and autophagosome formation (Axe et al., 2008). The activated ULK1

complex which located on the ER translocates the class III PtdIns3K complex to the phagophore assembly site (Randall-Demllo, Chieppa, & Eri, 2013). The class III PtdIns3K complex, composing of ATG14L, Beclin-1, hVps34 (VPS34) and p150 (VPS15) in mammalian cells, is required for the induction of autophagy (Yang & Klionsky, 2010) (Yang & Klionsky, 2009). After translocation to the ER, ATG14L directs the class III PtdIns3K complex to the phagophore. This allows the activation of phosphoinositide 3-kinase (hVps34) in the complex, results in the phosphorylation of phosphatidylinositol (PI) to generate phosphatidylinositol (3)-phosphate (PI3P) on the phagophore membrane (Petiot, Ogier-Denis, Blommaert, Meijer, & Codogno, 2000). The PI3P then recruits and binds to WIPI (ATG18) and DFCP1 on the membrane, which is an essential step in the formation of the phagophore (Polson et al., 2010).

### **1.2.ii Autophagosome expansion**

The key step in autophagosome membrane expansion is attachment of LC3 to the limiting membrane of the autophagosome. Attachment involves the formation of a covalent bond between the C-terminus of LC3 and amine groups on phosphatidylethanolamine (PE) in membranes. There are two ubiquitin-like protein conjugation systems required in LC3 lipidation. One generates a covalent bond between ATG5 and ATG12 to generate the ATG5-ATG12 complex and the other attaches the C-terminus of LC3 to PE. The conjugation of ATG12 to ATG5 is activated by ATG7, which acting like an E1 ubiquitin-activating enzyme activates ATG12 in an ATP-dependent manner (Glick et al., 2010). The activated ATG12 is then transferred to ATG10, an E2 ubiquitin-conjugating enzyme, which catalyses the conjugation between ATG12 and ATG5 (Yang & Klionsky, 2009). Conjugated ATG5-ATG12 complexes then interact non-covalently with ATG16L, which allows the formation of an ATG16L1:ATG5-ATG12 tetrameric complex through the interaction between ATG16L1 coiled-coil domains (Mizushima et al., 2003).

The second ubiquitin-like system is responsible for conjugating of LC3 (ATG8) to the membrane lipid-PE. Upon induction of autophagy, the C-terminal arginine of pro-LC3 is cleaved by the ATG4, a cysteine protease, to release a soluble LC3-I into the cytosol (Glick et al., 2010). This cleavage allows the exposed C-terminal glycine residue of LC3-I to interact with the active site of ATG7. ATG7, again functions as a E1-like enzyme, transferring LC3-I to ATG3 (another E2-like enzyme) which catalyses the conjugation of LC3-I and PE to form LC3-II

(Randall-Demllo et al., 2013). In this step, ATG3 also interacts with ATG16L1:ATG5-ATG12 complex which localized to the phagophore by interaction between ATG16L1 and WIPI, allowing LC3 approach to the phagophore membrane (Hanada et al., 2007). The expansion of the autophagosome membranes also requires the activity of ATG9, a multispanning membrane protein, which delivers lipid vesicles from the Golgi to the forming phagophores, and facilitates LC3 lipidation (Yamamoto et al., 2012). LC3-II remains on the autophagosome membrane until fusion with lysosomes. This has resulted in LC3 becoming an established marker to detect autophagosomes and monitor the autophagy (Yang & Klionsky, 2009).

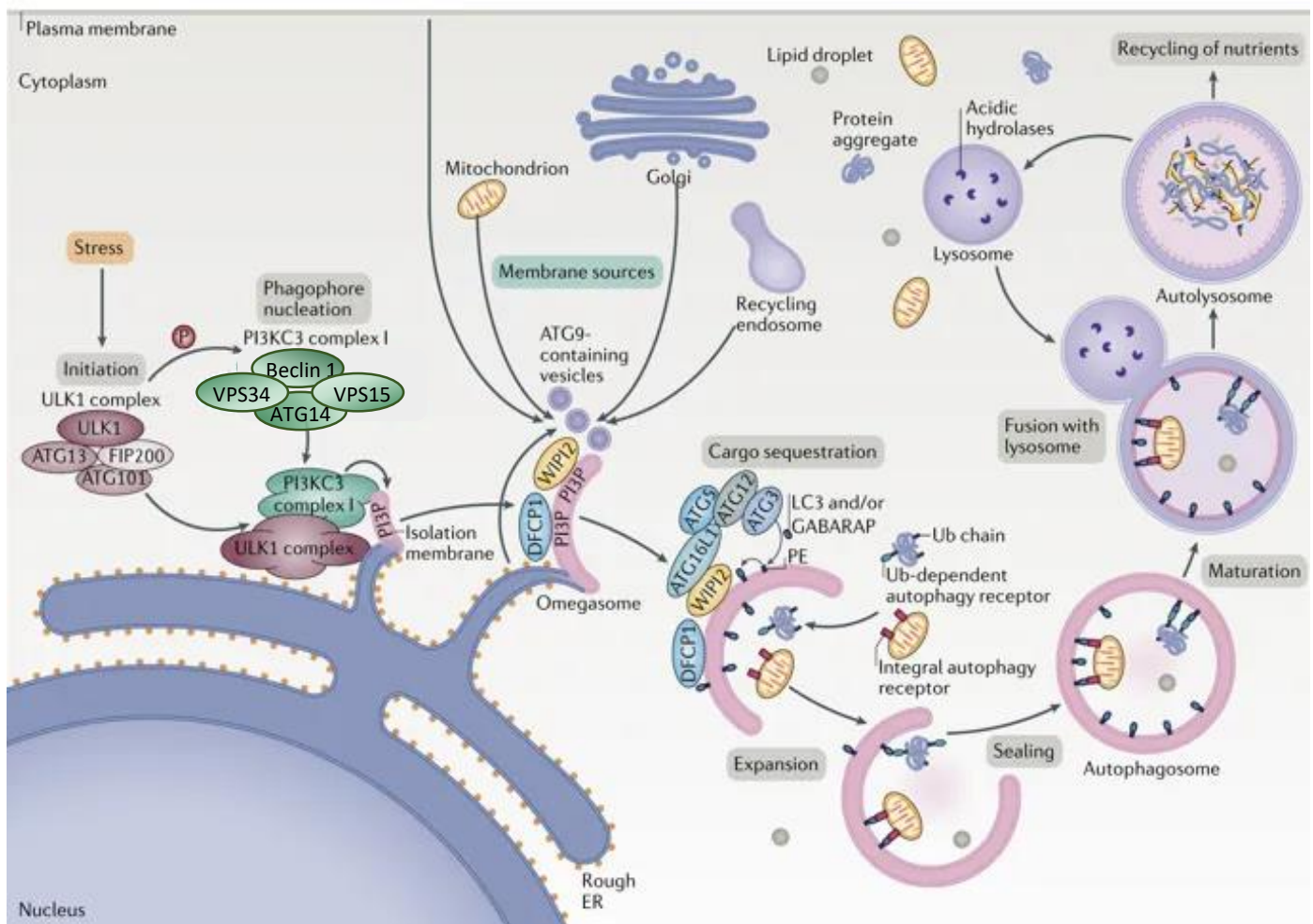


**Figure 1.1 Mechanism of mammalian autophagy.** The **initiation** of autophagy follows by ULK1 complex activation, which then phosphorylate and translocate the class III PtdIns3K complex (ATG14L, Beclin-1, VPS34 and VPS15) to the phagophore assembly site. This allows the activation of VPS34 (phosphoinositide 3-kinase) in the complex, results in the phosphorylation of phosphatidylinositol (PI) to generate phosphatidylinositol (3)-phosphate (PI3P) on the phagophore membrane. The PI3P recruiting DFCP1 and WIPI2 is essential for **expansion** of autophagosomes. WIPI2 is able to interact with ATG16L1 directly, to bring ATG16:ATG5-12 complex to autophagosomes. ATG16:ATG5-12 complex, conjugated with LC3I through Atg3, facilitates LC3 lipidation (LC3-I is converted into LC3-II) onto autophagosomes. LC3 could direct cargo into autophagosomes by interacts with autophagy receptors (shown as Un-dependent autophagy receptor). Sealing of the autophagosomal membrane give rise to a mature autophagosome which finally fuses with the lysosome for **degradation**. (Dikic & Elazar, 2018)

### **1.2.iii Cargo recognition and degradation during autophagy**

During autophagy a portion of the cytoplasm is engulfed by autophagosome membranes, this traps the cytoplasmic material in the lumen allowing degradation upon fusion with the lysosomes (Zaffagnini & Martens, 2016). Autophagy can be either non-selective or selective. Selective autophagy is responsible for specifically removing certain cargos such as damaged organelles, protein aggregates or invading microbes (Jin, Liu, & Klionsky, 2013). Selective autophagy mediated by ubiquitin and p62/SQSTM1 system is the most common pathway for autophagy-mediated protein degradation in the mammalian cells. Cargoes are ubiquitinated in the cytoplasm and then detected by autophagy receptors such as p62/SQSTM1 which bind both ubiquitin and the LC3 protein located on the autophagosome membrane. This mediates docking of ubiquitinated cargos to the autophagosome (Kirkin, McEwan, Novak, & Dikic, 2009), the autophagosome membrane is sealed and fusion with lysosome results in cargo degradation. Three sets of proteins are involved in the fusion step: Rab GTPases, membrane-tethering complexes and SNAREs (Ganley, 2013). Following fusion with lysosome, the cargo is degraded by lysosomal proteases such as cathepsins B, D, and L, and amino acids are recycled for other processes.

## **1.3. Autophagy reduces pathogen load and inflammation during infection**

### **1.3.i Pathogen capture**

Autophagy plays an important role in controlling infection by delivering intracellular pathogens to lysosomes for degradation, known as “xenophagy” (Johansen & Lamark, 2011). During xenophagy, autophagosomes recognise and engulf bacteria and viruses. Numerous molecules participate in this process, including sequestosome 1 (SQSTM1/p62), nuclear dot protein 52 kDa (NDP52), optineurin (OPTN), and neighbour of BRCA1 gene 1 (NBR1) (Jo, Yuk, Shin, & Sasakawa, 2013). In common with SQSTM1/p62, these molecules bind to LC3 and ubiquitin attached to pathogens, and drag pathogens into the autophagosome for degradation (Shaid, Brandts, Serve, & Dikic, 2013). [Figure 1.2]

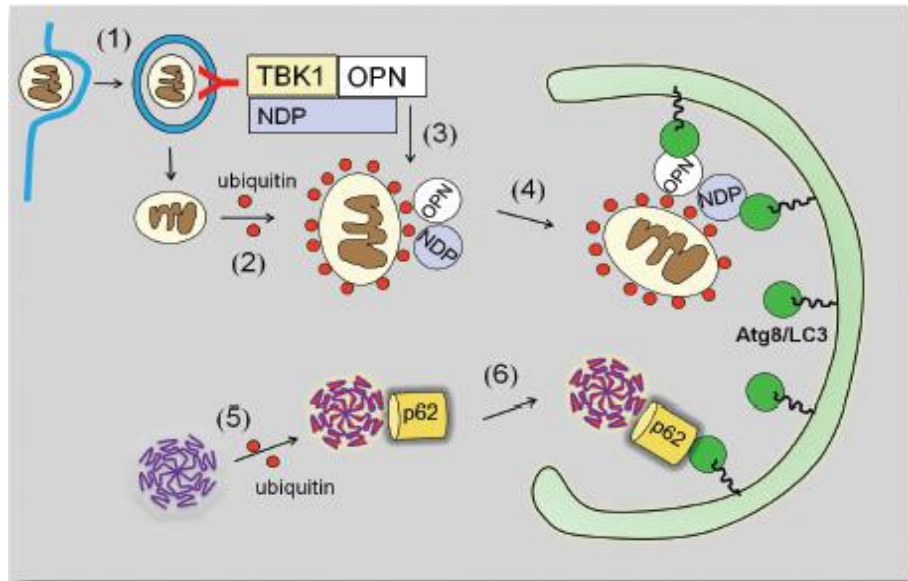


**Figure 1.2 Ubiquitin targets intracellular pathogens to autophagosomes via autophagy receptors.** Salmonella enter the cell by endocytosis (1). Some escape into the cytosol and are ubiquitinated (2). Recognition of bacterial lipopolysaccharide by TLR4 receptors in endosomes activates Tank binding kinase (TBK1) which forms a complex with two autophagy receptors called NDP52 (NDP) and optineurin (OPN). NDP52 and phosphorylated optineurin bind ubiquitin on cytosolic bacteria (3). NDP52 and optineurin also bind ATG8/LC3 allowing capture by autophagosomes (4). Sindbis virus capsids in the cytosol are ubiquitinated (5). The ubiquitin is recognised by autophagy receptor p62 which binds ATG8/LC3 allowing capture by autophagosomes (6).

### 1.3.ii Autophagy and the control of inflammation.

Apart from eliminating pathogens directly, autophagy is also involved in the innate immune response by controlling host inflammation. Inflammation is a conserved protective response, usually activated by pathogens, damaged cells, or irritants (H. Guo, Callaway, & Ting, 2015). Inflammation can be viewed as a double-edged sword in controlling host fitness. Deficient inflammation is unable to eliminate invading pathogens and leads to persistent infection, while excessive inflammation results in tissue damage and causes chronic or systemic inflammatory disease (H. Guo et al., 2015). Normally, inflammation is tightly regulated by the host, but inflammatory disorders can arise if inflammation in response to infection is excessive.

Recently, increasing studies revealed the role played by autophagy on suppression of excess inflammation (Deretic, 2012; Shi et al., 2012). During inflammation, molecular platforms known as inflammasomes are assembled to convert pro-caspase-1 to caspase-1. Then activated caspase-1 cleaves the precursor molecules of IL-18 and IL-1 $\beta$ , which belong to pro-

inflammatory IL-1 family, into mature bioactive cytokines IL-18 and IL-1 $\beta$ , and subsequently activates inflammation. Studies show that AIM2 and NLRP3 inflammasomes in macrophages activates RalB which binds with its effector Exo84 complex directly [Figure 1.3]. This binding activates the ULK1 and Beclin1-VPS34 complexes to induce autophagy (Bodemann et al., 2011; Shi et al., 2012). Moreover, the ubiquitination that inflammasomes underwent during assembly recruits p62 and by binding both ubiquitin and LC3, p62 is able to deliver inflammasomes into autophagosomes for degradation (Shi et al., 2012), thus reducing inflammasome level. Besides controlling inflammation by regulating inflammasomes, autophagy can also inhibit NF- $\kappa$ B pathway induced by pathogens. During viral infection, large amounts of viral envelope proteins accumulate in the lumen of the endoplasmic reticulum (ER), and results in ER stress (L. Zhang & Wang, 2012). The ER stress activates the transcription factor NF- $\kappa$ B, which induces the expression of pro-inflammatory cytokines, chemokines, and adhesion molecules, and leads to inflammation. Autophagy reduces inflammation by degrading the viral proteins held in the ER. In short, autophagy plays a crucial role in negative regulate of inflammation (Tam, Mercado, Hoffmann, & Niwa, 2012).

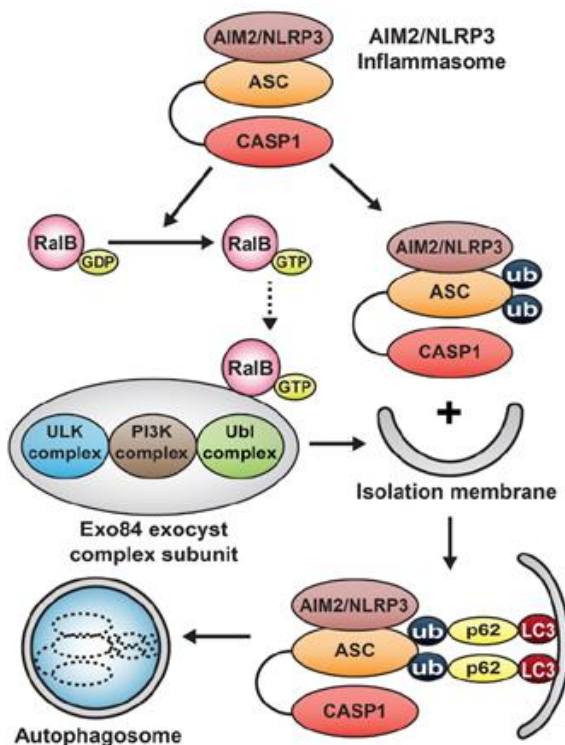


**Figure 1.3: Autophagy reciprocally regulates the inflammasome activity.** AIM2 or NLRP3 inflammasome triggers autophagy by activating RalB binding to Exo84 complex, which serves as platform for the formation of the isolation membrane. Ubiquitination that inflammasomes underwent recruits p62, by binding both ubiquitin and LC3, p62 is able to deliver inflammasomes into autophagosomes for degradation. (Oh & Lee, 2013)

## 1.4 Non-canonical autophagy and LC3 associated phagocytosis

Non-canonical autophagy involves the conjugation of LC3 to PE in single-membraned endolysosome compartments. There are two versions of non-canonical autophagy been known so far: LAP and LANDO.

### 1.4.i LC3 associated phagocytosis (LAP)

LC3 associated phagocytosis involves the conjugation of LC3 to phagosomes generating single-membraned LAPosomes [Figure 1.4]. These are generated during phagocytosis of extracellular pathogens which engage cell surface receptors such as TLRs, TIM4, or FcR (Lai & Devenish, 2012). Receptor engagement signals recruitment of LC3 to the cytosolic side of the phagosome membrane where it facilitates lysosome fusion and cargo destruction (Martinez et al., 2016). The LAP pathway requires components of the autophagy machinery such as ATG16L1:ATG5-ATG12 to conjugate LC3 to PE but is independent of upstream initiation components such as the ULK complex (Martinez et al., 2015). A defining feature of LAP is the activation of NADPH oxidase (Nox2) and production of reactive oxygen species (ROS) (J. Huang et al., 2009; Gluschko et al., 2018).

### 1.4.ii Molecular mechanism of LAP

*1.4.ii a Activation and nucleation of LAP.* In contrast to canonical autophagy, activation of LAP is not regulated by the mTOR-ULK1-ATG13 system and the absence of regulation by nutrients through the pre-initiation complex suggests that the function of LAP might be more important for pathogen clearance rather than during a starvation response (Martinez et al., 2015; Heckmann & Green, 2019). The activation of LAP is initiated by the ligation of cell surface receptors with pathogens or dead cells during phagocytosis, for example, pattern recognition receptors (PRR) ligate with pathogen-associated molecular patterns (PAMPs) from pathogens, immunoglobulin (Ig) receptors bound to antigens, or TIM4 receptor binds to phosphatidylserine (PtdSer)-displayed by dead cells (Heckmann et al., 2017; Martinez et al., 2011; Sanjuan et al., 2007).

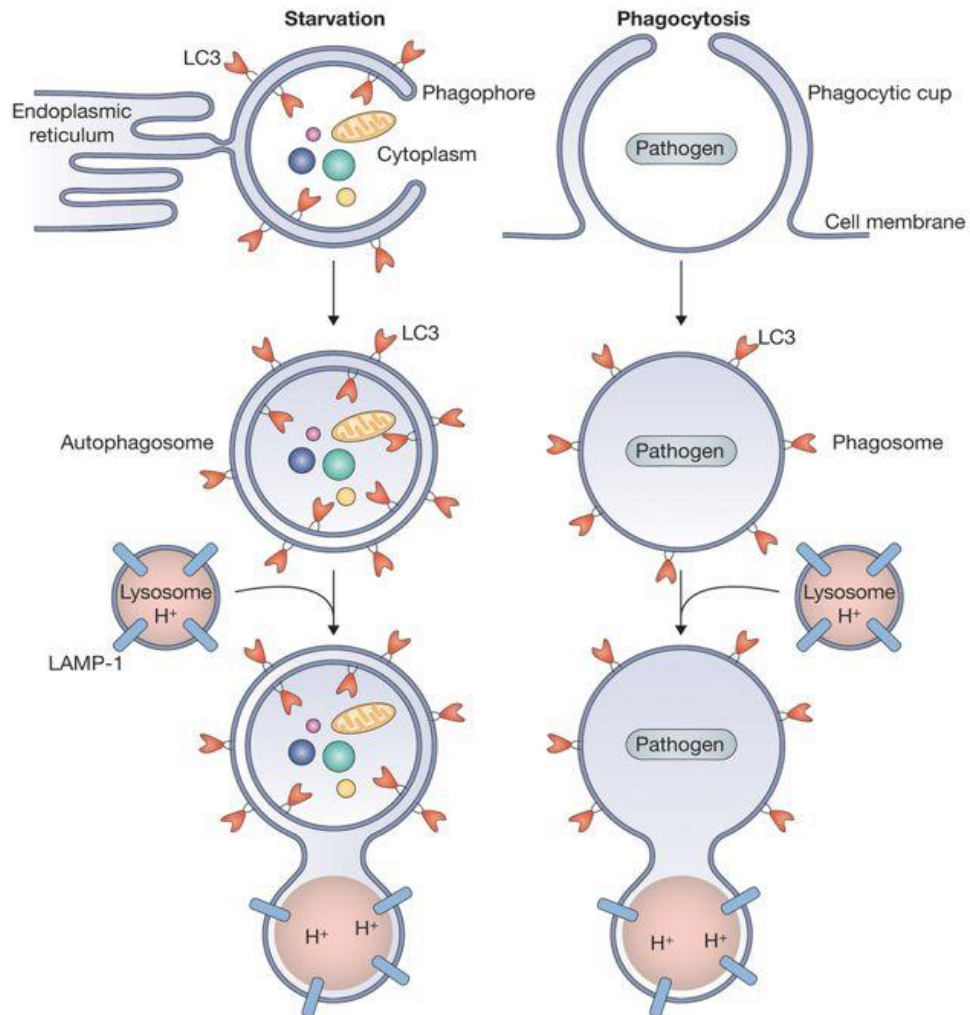


**Figure 1.4 Canonical autophagy versus LC3-associated phagocytosis.** During starvation induced canonical autophagy (left), a double-membrane autophagosome generates in the cell which engulf portions of their cytoplasm, and fuse with lysosome for degradation. Whereas LC3-associated phagocytosis is in terms of phagocytic cells internalizing extracellular microbes into single-membrane phagosomes (right). Followed by LC3 lipidates onto the single-membrane phagosomes, which aids trafficking of the vesicles and fusion to the degradative lysosome. (Boyle & Randow, 2015)

TLR signalling results in activation of the VPS34/Beclin Class III PI3kinase in the UVRAG complex (UVRAG, Beclin, VPS34 and VPS15) that phosphorylates lipids in the phagosome membrane. The phosphorylated lipids provide a platform for recruitment of the NOX2 (NADPH oxidase-2) complex with multiple subunits including RAC1, p22, p40, p47 and p67, responsible for reactive oxygen species (ROS) production in the lumen of the LAPosome. Rubicon is a RUN-domain-containing protein that binds the UVRAG complex required for PI3P generation induced by VPS34 on LAPosome membranes. Moreover, Rubicon facilitates ROS production induced by NOX2 complex. ROS is required for LC3 lipidation on LAPosomes (Martinez et al., 2015) by activating the ATG16L1:ATG5-ATG12 complex that conjugates LC3 to PE. ROS, which causes oxidative damage, is also a critical weapon for pathogen killing, allows LAP to be a vital pathway for clearance of extracellular microbes (Slauch, 2011). In addition, ROS can diffuse to the cytosol where they might activate ATG4 and ATG7 that promote further LC3-lipidation during LAP (Heckmann & Green, 2019). [Figure 1.5]

**1.4.ii.b LC3 conjugation on LAPosomes and lysosome fusion.** As described for autophagy, LC3 lipidation during LAP also requires two ubiquitin-like protein conjugation systems: ATG5-ATG12 and ATG8/LC3-PE conjugation system. Unlike autophagy, the LC3 conjugation does not promote membrane expansion and closure, as it occurs after phagosomes have formed and sealed (Heckmann & Green, 2019). While, LC3 does function in downstream events of LAP, which accelerates fusion between LAPosomes and lysosomes in mouse macrophages, therefore promoting microbial killing by LAP (Gluschko et al., 2018).

## **1.5 Roles played by LAP during infection and inflammation**

### **1.5.i Clearance of pathogens by LAP**

It is generally believed that LAP plays a key role in the clearance of pathogens, through direct engulfment, antimicrobial ROS production and rapid lysosomal degradation (Fang, 2011; Gluschko et al., 2018; Heckmann et al., 2017; Martinez et al., 2015). Much of the work has, however, been carried out in tissue culture. Previous studies show, LAP-deficient macrophages fail to efficiently clear *Saccharomyces cerevisiae* and *Aspergillus fumigatus* infection (Sanjuan et al., 2007; Sprenkeler, Gresnigt, & van de Veerdonk, 2016).

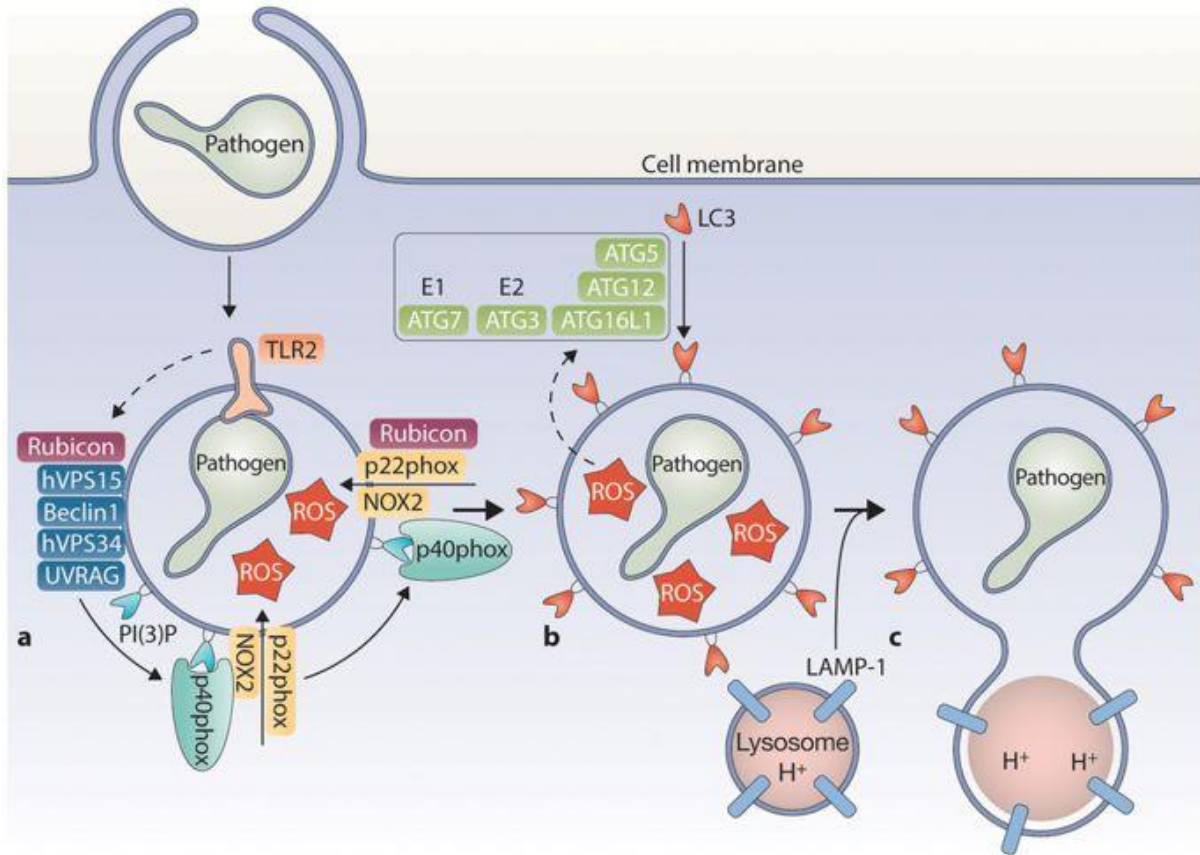


**Figure 1.5 Molecular mechanism of LC3-associated phagocytosis.** The activation of LAP is initiated by the ligation of cell surface receptors with pathogens during phagocytosis. A single membrane phagosome containing extracellular phagocytic cargos, is generated inside the cell, follows by recruitment of Rubicon on the membrane. Rubicon is required for assembling UVRAG-containing class III PtdIns3K to generate PI(3)P and recruiting the NADPH oxidase complex onto LAPosomal membrane. NADPH oxidase complex including p40phox, p22phox and NOX2 produces ROS in the LAPosome, which is necessary for recruitment of the LC3 lipidation machinery to enable attachment of LC3 and expedite fusion with lysosomes (Boyle & Randow, 2015).

Interestingly, *A. fumigatus* infection activates LAP-induced fungal killing, while the melanin on *A. fumigatus* cell wall inhibits LAP by excluding p22phox NADPH oxidase, promotes *Aspergillus* virulence (Akoumianaki et al., 2016). Moreover, an intracellular pathogen *Legionella dumoffii*, has been reported to use diverse strategies and virulence factors to escape autophagy meaning that the survival of the pathogen may be limited predominantly by LAP (Hubber et al., 2017). Furthermore, study in *Listeria monocytogenes* demonstrates

that infection of L.m. could activate NOX2 NADPH oxidase, results in ROS production and LAP activation. By accelerating fusion of L.m.-containing LAPosomes with lysosomes, LAP promotes L.m. killing and enhances anti-listerial immunity (Gluschko et al., 2018). Taken together, several in vitro studies suggest that LAP plays a key role in infection by promoting fusing of phagosomes with lysosomes leading to bacterial clearance and activation of immune response. Studies were listed on Table 1.

**Table 1. List of studies for LC3-associated phagocytosis**

Category	Pathogens	In vivo	In vitro	MΦ tropism	Reference
Virus	Influenza A		A549 cells, HCT116 cells, MDCK cells	+/-	(Beale et al., 2014)
			HCT116 cells	+/-	(Fletcher et al., 2018)
Bacteria	Listeria		RAW 264.7 macrophages	+	(Lam et al., 2013)
		Atg7 <sup>MYEL-KO</sup> , or FIP200 <sup>MYEL-KO</sup> Mice model	Peritoneal macrophages	+	(Gluschko et al., 2018)
	Salmonella	Zebrafish		+/-	(Masud et al., 2019)
	Legionella		MEFs, BMDM THP-1 cells, RAW264.7 cells	+	(Hubber et al., 2017)
Fungi	Aspergillus	Atg5 conditional KO (Atg5 <sup>flox/flox</sup> +vavCre)	Primary human monocytes, PMA-differentiated THP-1 cells, BMDMs	+/-	(Akoumianaki et al., 2016)
	Histoplasma capsulatum		Macrophages	+/-	(J. H. Huang et al., 2018)
Parasite	Leishmania		Bone marrow macrophage	+	(Matte et al., 2016)
Particulate material or aggregates	zymosan	ULK1 <sup>-/-</sup> , Rubicon <sup>-/-</sup> , and (FIP200 <sup>flox/flox</sup> , Atg7 <sup>flox/flox</sup> , Beclin1 <sup>flox/flox</sup> ) LysM-Cre <sup>+</sup> mice model	ULK1 <sup>-/-</sup> , NOX2 <sup>-/-</sup> , Rubicon <sup>-/-</sup> , and (FIP200 <sup>flox/flox</sup> , Beclin1 <sup>flox/flox</sup> , VPS34 <sup>flox/flox</sup> ) LysM-Cre <sup>+</sup> macrophages	+/-	(Martinez et al., 2015)
			E230 <sup>-/-</sup> BMDCs		(Fletcher et al., 2018)
	neurotoxic β-amyloid	FIP200 <sup>fl/fl</sup> and ATG5 <sup>fl/fl</sup> LysM-cre <sup>+</sup> mice model	FIP200 <sup>fl/fl</sup> and ATG5 <sup>fl/fl</sup> LysM-cre <sup>+</sup> primary microglia	+/-	(Heckmann et al., 2019)

### **1.5.ii LAP in efferocytosis and immunological silence**

Apart from clearance of pathogens, LAP also prevents the autoimmune or inflammatory response by cleaning up apoptotic dead cells, a process known as efferocytosis. During efferocytosis, the dead cells which release inflammatory signals in the tissue, are engulfed by professional phagocytes such as macrophages, thus limiting tissue damage (Elliott, Koster, & Murphy, 2017). This allows efferocytosis to be an important pathway to keep immunologically silent and tissue homeostasis. Evidences suggest, efferocytosis plays an effective regulatory role by inhibiting the pro-inflammatory cytokines and chemokines production such as IL-6, IL-8, IL-12, IL-1 $\beta$ , TNF- $\alpha$ , and inducing the anti-inflammatory cytokines IL-10 and TGF- $\beta$  production (Fadok et al., 1998; Heckmann et al., 2017; Martin, Peters, & Behar, 2014). Interestingly, studies demonstrate that in macrophages, LC3 translocation to dead cell-containing phagosomes requires ATG5, ATG7, Rubicon and NOX2-induced ROS production, but not ULK1 complex, indicating the role played by LAP rather than canonical autophagy (J. Huang et al., 2009; Martinez et al., 2011). In particular, LAP is triggered by the PtdSer-displaying dead cells which engage cell surface receptor TIM4, followed by engulfment and recruitment of LC3 to the LAPosomes (Martinez et al., 2011). In addition, LAP also responds to DNA containing immune complexes (DNA-IC) and dying tumor cells, results in promotion of IFN- $\alpha$  secretion and anti-inflammatory response (Cunha et al., 2018; Henault et al., 2012). Briefly, LAP plays the key role in efferocytosis and maintaining immunological silence.

### **1.5.iii LAP participates in antigen presentation**

In macrophages, as described previously, LAP is thought to promote bacterial clearance by enhancing fusion of phagosomes with lysosomes. While in dendritic cells (DCs), instead of leading to the direct degradation by lysosomes, a study reveals a LAP-related pathway, which enhances MHCII-mediated antigen presentation and plays a role in regulating immune responses. Romano and colleagues show that the presentation of antigen peptides requires ATG5 and is dependent on NOX2 (Romao et al., 2013). Moreover, electron micrographs show the LC3-labeled phagosomes harbouring pathogens have a single membrane (Romao et al., 2013) suggesting LAP. In this pathway, LAP facilitates antigen presentation by delaying phagosome maturation by blocking fusion with lysosomes. This allows peptides to be loaded onto major-histocompatibility complex class II molecules (MHCII) to activate CD4<sup>+</sup> cells to initiate immune response (Neerinx et al., 2013) [Figure 1.6]. In this process, the delayed

fusion with lysosomes gives antigens a better access to MHC classII compartments, and improves the antigenic peptides presenting on cell surface (Romao et al., 2013).

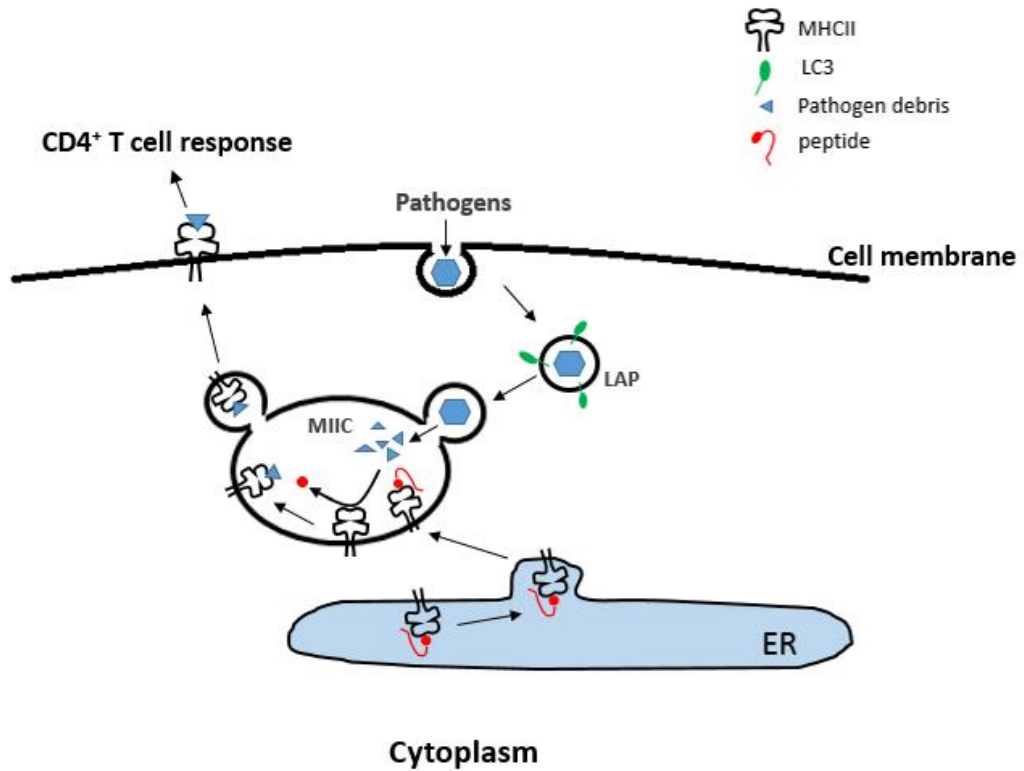


**Figure 1.6: Antigen presentation by MHC class II molecules in DCs.** MHC class II molecules synthesized from the endoplasmic reticulum are delivered to the phagolysosomes to form a MHC classII compartments (MIIC). LC3-labeled phagosomes harbouring pathogens fuse with (MIIC), which contain proteolytic enzymes that cleave the phagocytosed proteins into small peptides and loaded with peptide. Peptide-loaded MHC class II complexes are transported to the cell surface, allowing antigen presentation to CD4+ T cells. Modified from (Neerinx, Castro, Guarda, & Kufer, 2013)

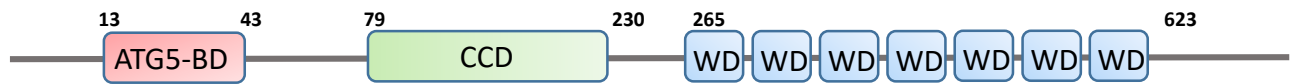
## 1.6. Non-canonical autophagy and LANDO

LANDO terms of non-canonical autophagy where LC3 is conjugated to endosomes and lysosomes in non-phagocytic cells. It has first been described in Oliver Flory's work (Florey et al., 2015), suggests that endolysosomal LC3 lipidation can be activated by chloroquine and monensin in a V-ATPase-dependent manner, demonstrates that LC3 lipidation onto endolysosomal compartments occurs during osmotic imbalances. In addition, a recent work from Douglas Green's lab (Heckmann et al., 2019) demonstrate LC3 LANDO in microglia is a critical regulator of immune-mediated aggregate removal and microglial activation in a murine model of Alzheimer's Disease. However, the studies about LC3 associated endocytosis is limited so far and the molecular mechanisms and the role played by LC3 associated endocytosis during pathogen infection is still unclear.

## 1.7. Non-canonical autophagy and ATG16L1 WD40-repeats

ATG16L1 is essential for both conventional autophagy and non-canonical autophagy/LAP. ATG16L1 interacts with ATG5-12 to mediate the conjugation of phosphatidylethanolamine (PE) to LC3. Mammalian ATG16L1 [Figure 1.7] is composed of N-terminal ATG5 binding motif (residues 13–43 of ATG16L1), a coiled-coil domain (residues 79-230), a linker region (residues 231-265) and C-terminal WD-40 repeats (residues 266-623). ATG5 interacts with ATG16L1 by ATG5 binding motif, the coiled-coil domain is responsible for WIPI and FIP200 binding during autophagy (Dooley et al., 2014). The yeast ATG16L1 only has ATG5 binding domain and coiled coil domain while the C-terminal WD-40 repeats are seen in *Atg16L1* genes expressed by higher eukaryotes. This suggests that the WD domain has been added during evolution, but the function is still not fully understand. Over recent years several studies show that WD-40 repeats may play a role in pathways linked to pathogen detection (Boada-Romero et al., 2013; Boada-Romero et al., 2016; Fletcher et al., 2018; Serramito-Gómez, Boada-Romero, & Pimentel-Muiños, 2016).

## Mammalian ATG16L1



## Yeast ATG16

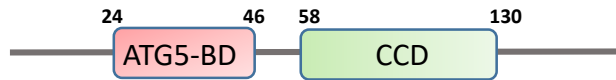


**Figure 1.7 The ATG16 structure difference between yeasts and mammals.** Schematic representation of mammal ATG16L1 and yeast ATG16. Both of the proteins share an ATG5-binding domain (ATG5-BD) at the N-terminus and followed by a coiled-coil domain (CCD). While, the WD-40 repeats are only present in mammal ATG16L1 at the C-terminus and absent in yeast Atg16.

### 1.7.i ATG16L1 WD40 domain interacting proteins

Interestingly, recent studies reveal novel interactions between the WD-repeat domain of ATG16L1 and a series of proteins which are involved in pathogen recognition including human transmembrane protein TMEM59, TME166, NOD1, NOD2 and Ubiquitin (Boada-Romero et al., 2013; Boada-Romero et al., 2016; Fujita et al., 2013; Travassos et al., 2010; Ver Heul, Fowler, Ramaswamy, & Piper, 2013; Xiong et al., 2018). Study in TMEM59 demonstrates that, during *Staphylococcus aureus* infection, TMEM59 binds ATG16L1 by WD-40 domain (residues 263–281) to induce a non-canonical autophagy that promotes LC3 recruitment on the single-membrane bacterial phagosomes, thus promoting lysosomal degradation (Boada-Romero et al., 2013). Also, loss of TMEM59 leads to reduced bacterial recovery from infected cells. Notably, a study on this non-canonical autophagy shows the LC3 recruitment to the phagosome requires PIK3C3, ATG5 and ATG7, but independent on BECN1, indicating the mechanism is different from canonical autophagy but quite similar with LAP (Boada-Romero et al., 2013; Pimentel-Muinos & Boada-Romero, 2014). Whether this pathway is LAP or not still needs to be demonstrated.

### 1.7.ii The T300A mutation in ATG16L1 impairs function of the WD40 domain

A single amino acid mutation (change from T to A at position 300) of ATG16L1 increase the risk of Crohn disease, which is a chronic inflammatory condition of the digestive tract.

Previous study suggests the mutation enhances ATG16L1 sensitization to caspase-3-mediated cleavage in stressful situation, results in compromise xenophagy and inflammation (Murthy et al., 2014). A recent study suggests the T300A mutation might cause a mild structural alteration of the WD domain that reduces its binding ability with proteins containing WD-binding motifs, without detectable caspase-3 activity, results in an unsuccessful bacterial clearance (Boada-Romero et al., 2016; Serramito-Gómez et al., 2016). This alteration impairs the non-canonical autophagy which requires WD40, whereas canonical autophagy remains unaffected, indicating the important role played by WD40 domain and non-canonical autophagy during bacterial infection.

### **1.8. Generation of a mouse model to study the role played by non-canonical autophagy and LAP 'in vivo'.**

It has been difficult to dissect the role played by non-canonical autophagy 'in vivo' because non-canonical autophagy, LAP and LC3-associated endocytosis share downstream pathways with conventional autophagy, and deletion of these genes such as ATG16L1, ATG7, ATG5 result in neonatal lethality (Yoshii et al., 2016). Non-canonical autophagy uses the E3-ligase like activity of the ATG16L1:ATG5-ATG12 complex within the core autophagy machinery to conjugate LC3 to phosphatidylethanolamine in endo-lysosome membranes. Work from our laboratory has shown that conjugation of LC3 to endo-lysosome membranes during non-canonical autophagy requires the WD domain of ATG16L1 (Fletcher et al 2018). This prompted us to generate a mouse lacking the WD domain of ATG16L1 to study the role played by non-canonical autophagy 'in vivo'. The mouse model ' $\delta$ WD' (*Atg16L1* <sup>$\delta$ WD/ $\delta$ WD</sup>) carries a stop codon after the CCD of ATG16L1 to prevent translation of the WD repeat and linker domains, and the mice have systemic loss of LAP and LC3 associated endocytosis (Rai et al 2019). The mice retain the N-terminal CCD and ATG5-binding domains of ATG16L1 required for conventional autophagy, allowing the mice to activate autophagy and grow normally and maintain tissue homeostasis (Rai et al 2019). [Figure 1.8]

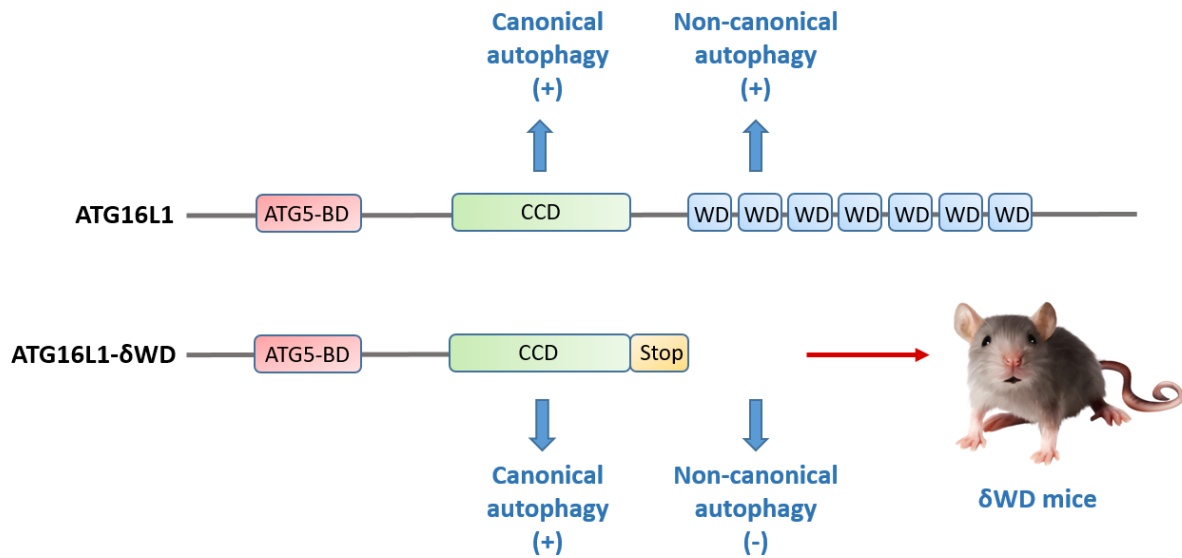


**Figure 1.8 Generation of mouse model lacking the WD domain of ATG16L1.** The WD repeats of Atg16L1 is only required for non-canonical autophagy, but not required for canonical autophagy. This allows us to generate a mice model with systemic loss of non-canonical autophagy by removing the WD repeats without effect of canonical autophagy.

## 1.9. Influenza A virus (IAV) as a model to study the role played by non-canonical autophagy during viral infection.

**Rationale:** IAV was chosen for study because the virus enters cells by endocytosis and activates non-canonical autophagy resulting in recruitment of LC3 to cellular membranes. Importantly, the recruitment of LC3 to membranes following IAV infection is dependent on the WD domain of ATG16L1 (Fletcher et al). ‘In vivo’ responses to mouse-adapted strains of IAV are well documented. This allowed us to use  $\delta$ WD mice to study the roles played by non-canonical autophagy during IAV infection ‘in vivo’ including analysis of virus replication in respiratory tissue and consequent effects on morbidity, pathology and immune responses. Finally, IAV is still an important pathogen of humans where severe infections cause a cytokine storm with high incidence of fatality. This means it is important for us to understand the molecular aspects of IAV–host cell interactions in detail.

### 1.9.i Virus types strains and structure

It’s over 100 years now since the worst pandemic influenza outbreak on the record, known as Spanish Flu (H1N1) in 1918. One third of the world's population (or  $\approx$ 500 million persons) were infected, and leads to approximately 50 million deaths worldwide (Taubenberger &

Morens, 2006). Since then there have been several pandemics. They are H2N2 pandemic strain on 1957, pandemic Hong Kong influenza H3N2 on 1968, re-emergence of a descendant of the 1918 H1N1 on 1977, novel pandemic H1N1 on 2009 (Taubenberger & Kash, 2010; Taubenberger & Morens, 2009). Apart from that, severe outbreaks of highly pathogenic avian influenza H5N1 spread throughout Asia and into Europe and Africa on 2003 (Neumann, Chen, Gao, Shu, & Kawaoka, 2010), followed by avian H7N9 on 2013.

Influenza viruses belong to the Orthomyxoviridae family, there are 4 four genera in this family: types A, B, C and Thogotovirus, only genera A and B are clinically relevant for humans ("Influenza Virus," 2009). The influenza A and B viruses are characterized by eight segmented, negative-strand RNA genomes loosely encapsidated by the nucleoprotein ("Influenza Virus," 2009). These eight RNA genomes (vRNAs), which encode at least 11 open reading frames, contain all the genetic information they need for passage.

The envelope of influenza A virus (IAV) contains the surface glycoproteins haemagglutinin (HA), neuraminidase (NA) and M2 matrix proteins (Taubenberger & Kash, 2010). The HA protein binds influenza virus to the host cells and it also mediates fusion between the viral and endosomal membranes, allowing the release of viral ribonucleoproteins (RNPs) into the cytoplasm during infection (Taubenberger & Kash, 2010). The sialidase activity of the neuraminidase (NA) protein is required for cleavage of host cell sialic acids to release the newly produced virions from the host cells (Taubenberger & Kash, 2010). As an ion channel, the M2 matrix protein transfers protons from endosomes into the core of viruses allowing the virion acidification for efficient release of vRNP to the cytoplasm (Gannage et al., 2009).

The nucleoprotein (NP), polymerase acidic protein (PA), polymerase basic protein (PB) and matrix 1 (M1), are involved in nucleic acid replication, alter antiviral responses in the host cell, and influence virulence (Sandbulte, Spickler, Zaabel, & Roth, 2015). In virions, a single viral RNA is wrapped around NP. The 5' and 3' of vRNA forms a helical hairpin, which is bound by the polymerase complexes -- three polymerase proteins (polymerase basic protein 2 [PB2], PB1 polymerase basic protein 1 [PB1] and polymerase acidic protein [PA]) (Dou, Revol, Ostbye, Wang, & Daniels, 2018). The matrix 1 (M1) protein, which locates underneath the plasma membrane, interacts with vRNP to support envelopment (Dou et al., 2018). [Figure 1.9]

The nonstructural protein NS1, present in the cytoplasm is a multifunctional protein, which is involved in the inhibition of interferon-mediated host defences and regulation of host gene expression. While, NS2 plays an important role in the nuclear export of the viral ribonucleoprotein complexes (Enami, 1997).

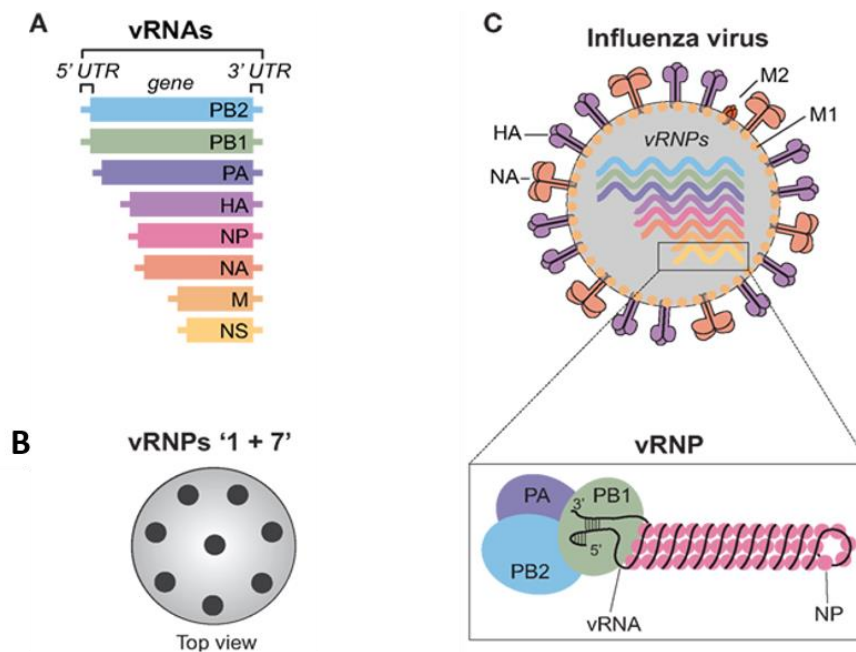


**Figure 1.9. Diagram of Influenza A virus.** (A) Eight viral RNA gene segments that comprise the influenza A genomes, including PB1, PB2, PA, HA, NP, NA, M and NS. (B) Top view of vRNAs organized in influenza virus capsid. (C) Structure of influenza A virus. HA, NA and M2 are inserted into viral lipid membrane, with M1 underneath to support the viral envelope. Eight vRNA gene segments are wrapped in the viral capsid. Each vRNA segment, consists of RNA joined with several proteins shown in the diagram: B1, PB2, PA and NP. (Dou et al., 2018)

### 1.9.ii. Virus entry

The HA protein of IAVs binds to glycoconjugates with terminal sialic acid residues triggering by HA-mediated internalisation (Dou et al., 2018). Once internalized, the virus is trapped in the endosomal compartment, which moves along the actin, and microtubules from the plasma membrane to the perinuclear region (Edinger, Pohl, & Stertz, 2014). The acidic pH in the endosome allows fusion between viral and endosomal membranes to release vRNPs into the cytoplasm (Edinger et al., 2014). During this process the pH in endosomes drops from 6.8-5.9 (early endosomes) to 6.0-4.8 (late endosomes), leading to a conformational change in HA

which exposes the fusion peptide. The fusion peptide moves 100 Å away from the original position and inserts into the endosomal membrane, that brings the viral and endosomal membranes into close proximity promote the formation of the fusion pore (Edinger et al., 2014; Superti, Agamennone, Pietrantonio, & Ammendolia, 2019). The M2 ion channel transfers protons from endosomes to inside of the viral particle which enables the release of the vRNPs into the host (Fodor, 2013) (Dou et al., 2018). Then, with the help of the importin- $\alpha$ -importin- $\beta$  nuclear import pathway, newly released cytoplasmic vRNPs are transported directly into the nucleoplasm (Dou et al., 2018). [Figure 1.10]

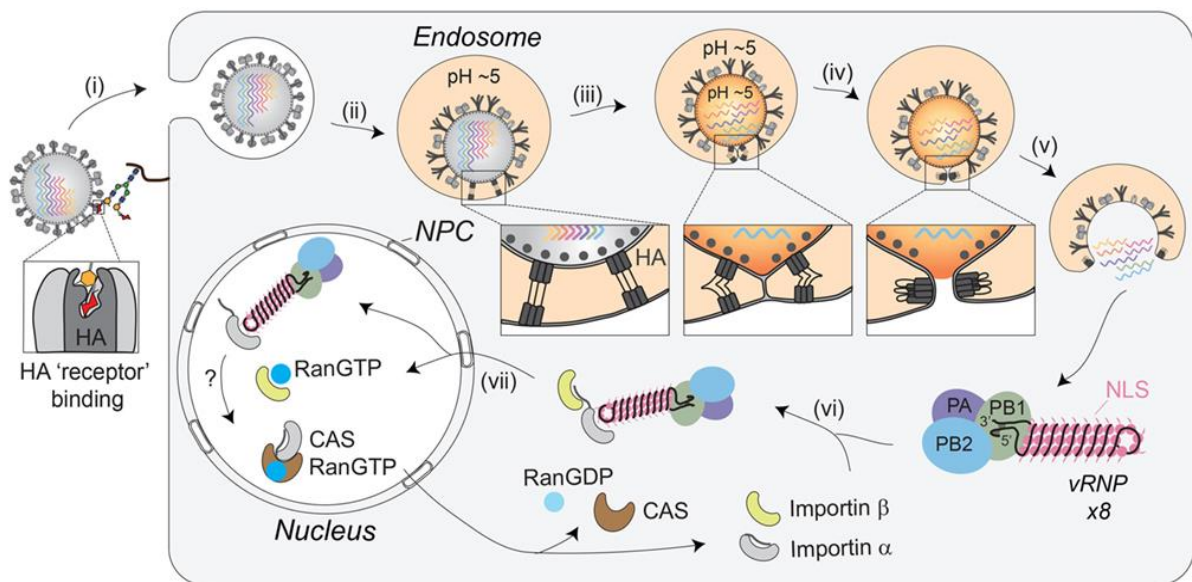


**Figure 1.10 Receptor-mediated cell entry of IAVs.** (i) IAVs entry is initiated by binding between HA and sialylated glycoconjugates (receptor) on the host cell surface. This binding triggers endocytosis. (ii) The viruses enter the endosome where the lower pH facilitates a conformational change in HA, allows HA inserted into the endosomal membrane. (iii) The M2 ion channel transfers protons from endosomes to inside of the viral particle facilitating the release of the packaged vRNPs from M1. (iv-v) HA further promote the formation of the fusion pore, which releases the vRNPs into the cytosol. (vi-vii) The new released vRNP are recognized by the adaptor protein importin- $\alpha$  and importin- $\beta$  which facilitates the transport of vRNP directly into the nucleoplasm. (Dou et al., 2018)

### 1.9.iii. Replication and transcription

Viral replication starts once the vRNP enters the host cell nuclei. Transcription of the cRNA is initiated by RNA-dependent RNA polymerase (PB2, PB1, and PA). The newly synthesized cRNA



**Figure 1.11 Viral replication, transcription and assembly.** Upon entry into the cell nucleus, the vRNP start transcription into (i) viral mRNAs and (iv) cRNAs. (ii) The mRNAs then exported to cytosolic ribosomes for translation. (iii) Newly synthesized viral polymerase subunits (PA, PB1, and PB2) and nucleoprotein (NP) are imported back into the nucleus, (v) for assembling cRNAs into cRNPs. (vi) The cRNPs can transcribes into viral RNA (vRNA), which then (vii) assembles into vRNPs by PA, PB1, PB2 and NP. After assembled, (viii) the new vRNPs are able to transcribe more viral mRNAs, (ix) new cRNA copies, or (x) associate with the newly synthesized M1 and NS2 to recruit CRM1, which (xi) mediates the vRNP exporting into cytoplasm. (xii) Once exported, the vRNPs are trafficked toward the plasma membrane for budding by the help of Rab11 which located in the modified endoplasmic reticulum (ER) membranes or microtubules. (Dou et al., 2018)

### **1.9.v Potential role for non-canonical autophagy and LAP during innate immune responses to Influenza A virus infection.**

Influenza viruses can infect diverse host species, including pigs, birds and humans. For infection of mammals, influenza virus enters the host through oral or nasal cavities. After passing through the mucous layer IAV invades respiratory epithelial cells to initiate infection in the respiratory tract (Iwasaki & Pillai, 2014). Innate immunity to IAV begins with recognition of single-stranded viral RNA by retinoic acid-inducible gene-I (RIG-I) and toll-like receptor (TLR) 7. This leads to production of type I IFNs and the pro-inflammatory cytokines mediated by NF- $\kappa$ B activation (Fukuyama & Kawaoka, 2011). Both of these pathways can be influenced by non-canonical autophagy. Beale and colleagues (Beale et al., 2014) describe induction of LC3 lipidation during IAV infection 'in vitro' and translocation of LC3 to the plasma membrane and perinuclear vesicles. This may involve direct binding of LC3 to M2, but recent work (Fletcher et al) shows that the relocation of LC3 requires the WD domain of ATG16L1 indicative of LAP. Recognition of IAV by TLRs in endosomes could activate LANDO in epithelial cells or LAP in phagocytic cells. Recruitment of LC3 would increase delivery of IAV to lysosomes. This would decrease viral load and could attenuate TLR signalling and reduce delivery of viral RNA to the cytoplasm for recognition by RNA sensors triggering interferon production. A failure in non-canonical autophagy could increase viral load in vivo and exacerbate inflammatory responses. A description of these pathways is provided below. [Figure 1.12]

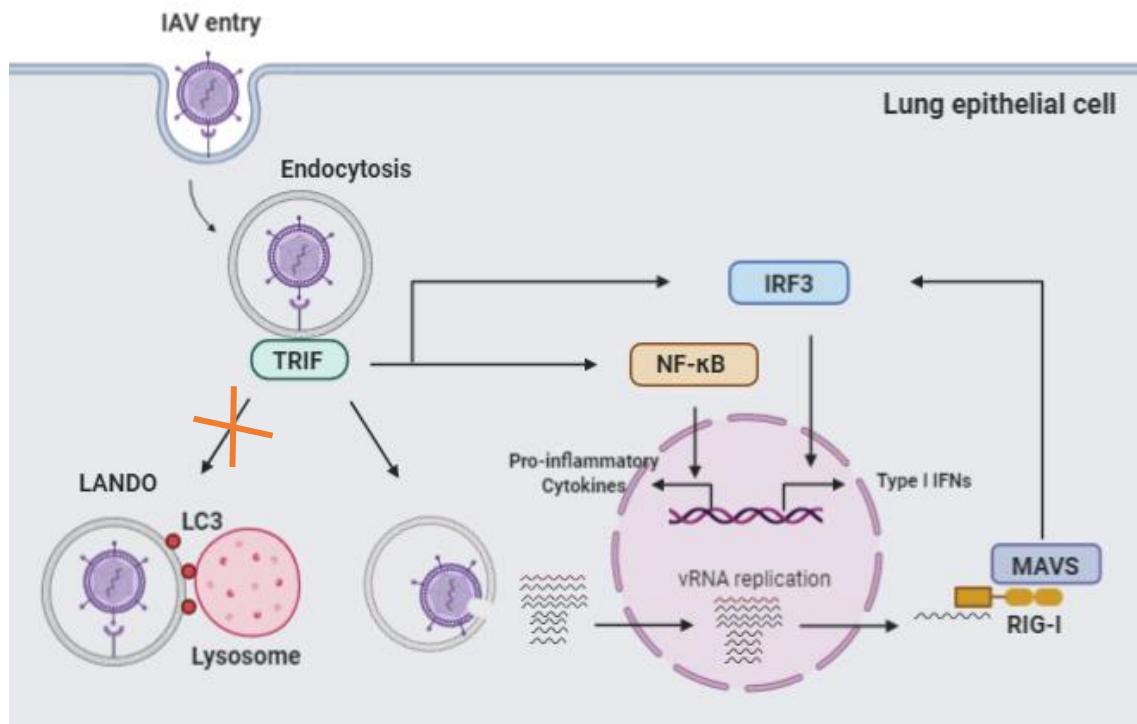


**Figure 1.12 Description of non-canonical autophagy deficiency increases viral load and exacerbate inflammatory responses.** During IAV enter to the non-canonical autophagy deficient cells, the phagosome that contain virus is failed to recruit LC3 on the membrane, thus block the access to the lysosomes. Thus, more vRNPs released in the cytoplasm that recognized by RNA sensors could trigger interferon production. In addition, more vRNPs access to the nucleus could result in increased viral load by promoting replication.

### 1.9.v. a Innate immunity to IAV in respiratory tissue.

As the primary target of influenza virus, the respiratory epithelial layer triggers the production of type I and type III IFNs (IFN- $\alpha$ , IFN- $\beta$ , IFN- $\lambda$ ) which upregulate hundreds of genes expression collectively, to inhibit viral replication, degrade viral nucleic acids, and induce viral resistance to neighbouring cells (Galani et al., 2017). In addition to the IFN-mediated antiviral response, respiratory epithelial cells produce various cytokines and chemokines such as IL-1 $\beta$ , TNF- $\alpha$ , IL-6, MCP-1, and CXCL-1. This is followed by the recruitment of an array of innate immune cells including neutrophils, macrophages, dendritic cells and NK cells which carry out viral clearance by taking up and eliminating the virus, killing infected cells, and guiding subsequent innate and adaptive immune response.

#### *1.9.v. b Detection of influenza virus infection by RIG-I mediated signalling pathways.*

RIG-I signalling pathway is mediated by RIG-I-like receptors (RLRs) which detect viral RNA in cytoplasm. RLRs (including RIG-I, MDA5, and LGP2) are expressed in both immune and non-immune cell types such as epithelial cells, conventional DCs and alveolar macrophages (Iwasaki & Pillai, 2014) [Figure 13 b]. During influenza infection, RIG-I recognizes the intact genomic ssRNA containing 5'-triphosphate, shorter genomic segments and 5'-triphosphate viral ssRNA that is generated after viral replication, and results in phosphorylation of IRF7/3 and NF- $\kappa$ B, which in turn induce type I IFNs, and pro-inflammatory cytokine and chemokine production, respectively (Iwasaki & Pillai, 2014; Pulendran & Maddur, 2015). RNA recognition leads to a conformational change in RIG-I that leads to association with MAVS (mitochondrial antiviral signalling protein) in the mitochondrial membrane. Subsequent MAVS signalling results in activation of NF- $\kappa$ B and the IRF7/3 pathways that triggers pro-inflammatory cytokine and type I IFNs production. The influenza nonstructural protein NS1 has evolved to block RIG-I signalling by binding to RIG-I/IPS-1 complexes that results in attenuation of type I IFN and inflammatory cytokine expression, indicates the key role played by RIG-I-mediated recognition in naturally infected hosts (Z. Guo et al., 2007).

#### *1.9.v. c Detection of influenza virus by TLR receptors.*

Toll-like receptors (TLRs) are a class of pattern recognition receptors (PRR) that act as key sensors of innate immunity against bacteria and viruses. TLR7/8, TLR3 and TLR4 are the key sensors during influenza infection.

TLR7 is highly expressed in plasmacytoid dendritic cells (pDCs), and it recognizes viral particles by binding to viral genomic single-stranded RNA (ssRNA). TLR7 signalling activates nuclear factor- $\kappa$ B (NF- $\kappa$ B) and IFN-regulatory factor 7 (IRF7) to induce production of inflammatory cytokines and type I IFNs, respectively (Iwasaki & Pillai, 2014) [Figure 13 a]. TLR7/MyD88-deficient mice shows enhance susceptibility to influenza virus with uncontrolled viral load and high mortality (Seo et al., 2010). Similarly, TLR8, which expressed by human monocytes and macrophages, is also stimulated by viral ssRNA that results in the production of IL-12. However, the relevance of TLR8 in influenza virus infection is remain unclear (Pulendran & Maddur, 2015).

TLR3 expression is detectable in macrophages, myeloid DCs (mDC), and primary respiratory epithelial cells, but not in plasmacytoid DCs (pDCs), monocytes, and neutrophils in mice and humans (Kadowaki et al., 2001; Le Goffic et al., 2006). TLR3 recognizes viral double-stranded RNA (dsRNA) in the endosomes. During influenza infection, dsRNA present in dying cells taken up by macrophages activates TLR3 (Iwasaki & Pillai, 2014) [Figure 13 a]. Subsequent activation of NF- $\kappa$ B and IFN-regulatory factor 3 (IRF3) pathways, results in the expression of pro-inflammatory cytokines and of type I interferon (IFN) and IFN-stimulated genes (ISGs) (Guillot et al., 2005). While the overexpression of pro-inflammatory leads to pathology, TLR3<sup>-/-</sup> mice survive longer than wild-type mice, despite higher viral loads in the lungs, during lethal influenza virus infection, suggesting that TLR3-triggered innate response inhibits viral replication but contributes to the negative effects of a detrimental host inflammatory response (Le Goffic et al., 2006).

TLR4 is mainly expressed on myeloid cells including neutrophils, monocytes, macrophages, mDCs and moDCs, is able to detect the damage associated molecular patterns (DAMPs) released from virus infected cells (Pulendran & Maddur, 2015). A DAMP molecule S100A9 was found to trigger TLR4-MyD88-signaling pathway in macrophages to enhance inflammation during IAV infection (Tsai et al., 2014). Similar with TLR3, the TLR4<sup>-/-</sup> mice were protected from influenza A virus-induced lethal infection when compared to wild type mice (Nhu et al., 2010), suggesting the activation of TLR4 signalling pathway during lethal influenza infection seems to induce an excessive inflammatory response that results in severe outcomes (Pulendran & Maddur, 2015).

In summary, endosomal TLRs play different roles in influenza virus infection. TLR7 in pDCs, recognizing virus by ssRNA, induces IFN responses to block viral replication and to promote antibody responses. TLR3 and TLR4 induce an antiviral response by recognizing viral dsRNA and DAMP in infected cells, while they also cause the detrimental effect following lethal infection (Iwasaki & Pillai, 2014) . The link between TLR recognition and non-canonical autophagy/LAP makes it likely that mice lacking the WD domain of ATG16L1 will show defects in the control of IAV infection

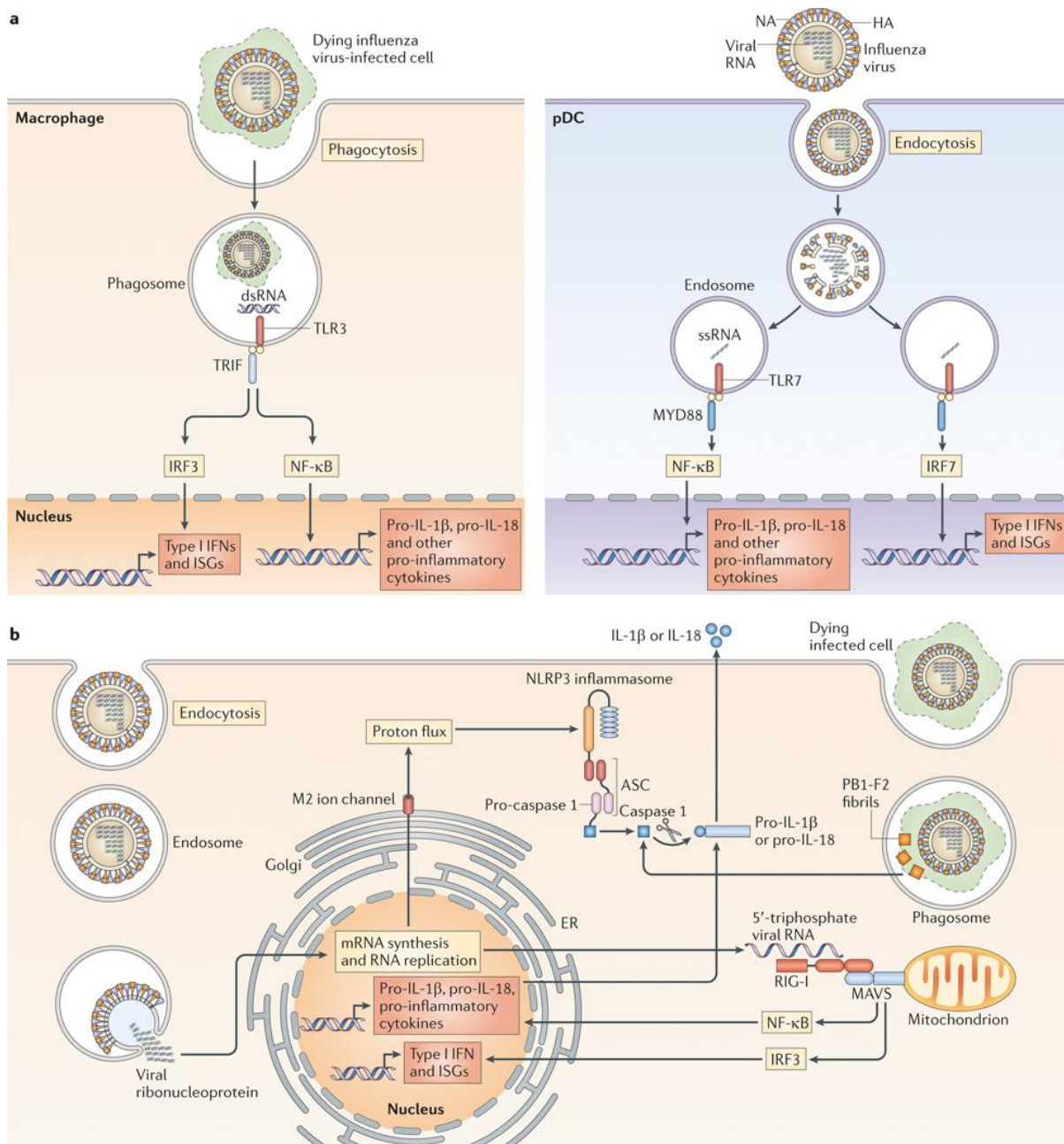


**Figure 1.13 Cell receptor mediated pathways involved in influenza virus infection**

Influenza virus infection can be detected by multiple host sensors during entry. **a.** When infected cells are phagocytosed by macrophages, double-stranded RNA from infected cells can be recognized by Toll-like receptor 3 (TLR3) in endosomes, which leads to the activation of IRF3 and NF- $\kappa$ B pathways, and release of IFNs, ISGs and pro-inflammatory cytokines. Similarly, the release of single-stranded RNA (ssRNA) within plasmacytoid dendritic cells (pDCs), can lead to TLR7 signalling inducing IRF7 and NF- $\kappa$ B activation, results in secretion of IFNs, ISGs and NF- $\kappa$ B-dependent cytokines. **b.** Single-stranded viral RNA in the cytosol of infected epithelial cells is recognized by retinoic acid-inducible gene-I (RIG-I), leading to activation of IRF3 and NF- $\kappa$ B pathways, which stimulate the expression of IFNs, ISGs and pro-inflammatory cytokines. (Iwasaki & Pillai, 2014)

## 1.10 Inflammatory response and cytokine storm induced by influenza infection

### 1.10.i Inflammatory responses

Inflammation is a protective response triggered by injurious factors such as microbial infection, tissue injury, and toxic compounds, and acts by removing harmful stimuli and repairing damaged tissue (Takeuchi & Akira, 2010). Typically, inflammatory responses requires four components: inflammatory inducers, the sensors on the immune cells, the inflammatory mediators and target tissue (Medzhitov, 2010). Influenza virus (inflammatory inducer) is recognized by TLR (sensors) on the immune cells leading to release of inflammatory mediators, including cytokines, chemokines and interferons. The inflammatory mediators then slow virus replication, kill infected cells and repair damaged tissue. Although the important role played by inflammatory response against influenza A infection, an uncontrolled and excessive response can result the severe lung injury and death (Tavares, Teixeira, & Garcia, 2017). Hence, the IAV induced inflammatory response can be described as a double edge sword, as it is essential for protecting host against viral infection but can also leads to severe outcomes (Tavares et al., 2017). Therefore, it is important to understand how inflammation is regulated 'in vivo' during IAV infection to identify factors that may predispose to cytokine storms which increase severity and mortality.

#### 1.10.i.a *NF- $\kappa$ B pathway*

The nuclear factor (NF)- $\kappa$ B transcription factor regulates the expression of numerous genes involved in different processes of the immune and inflammatory responses (Tavares et al., 2017). The activation of NF- $\kappa$ B pathway is triggered by pro-inflammatory cytokines, pattern-recognition receptors (PRR) and pathogen-derived substances (T. Liu, Zhang, Joo, & Sun, 2017). In resting cells, NF- $\kappa$ B proteins mainly present in the cytoplasm, and are inhibited by I $\kappa$ B proteins. Upon activation, I $\kappa$ B is phosphorylated and degraded by the proteasome, follows by releasing and activation of NF- $\kappa$ B (Moynagh, 2005). Subsequently, NF- $\kappa$ B enters the nucleus and turn on the expression of pro-inflammatory cytokines, chemokines and adhesion molecules, results in the initiation of inflammatory and immune responses.

### *1.10.i.b. IRF-mediated pathway*

Interferon regulatory factors (IRF) are involved in inflammatory and immune response by regulating transcription of interferons and several pro-inflammatory cytokines. To date, nine human cellular IRF genes have been identified including IRF-1, IRF-2, IRF-3, IRF-4, IRF-5, IRF-6, IRF-7, IRF-8 and IRF-9 (Paun & Pitha, 2007). IRF3 and IRF7 play a key role in antiviral response by regulating the type I IFNs gene expression (Paun & Pitha, 2007). Upon IAV infection, TLR3 and RIG-I signalling pathways are activated, leading to phosphorylation of IRF3. Subsequent nuclear translocation of IRF3 increases expression of type I IFNs and ISGs (Hiscott, Nguyen, Arguello, Nakhaei, & Paz, 2006; Iwasaki & Pillai, 2014). Similarly, activation of TLR7 or TLR9 leads to IRF7 mediated expression of type I IFNs and ISGs. Moreover, IRF5 is able to regulate the typical pro-inflammatory genes such as IL-6, TNF  $\alpha$  and IL12, although IRF5 may also contribute to IFN-I regulation in some status (Paun & Pitha, 2007; Platanitis & Decker, 2018). The IRF4 plays a role in T, B cell maturation, B cell differentiation and Th2 response, while IRF8 is important for pDC differentiation. IRF9 is able to induce an increased expression of ISGs via JAK–STAT pathway by interacting with STAT1 and STAT2 (Rengachari et al., 2018). In sum, IRF-mediated pathway plays an important role in regulating inflammatory and immune response during IAV infection.

### *1.10.i.c JAK-STAT pathway*

The Janus kinase and signal transducer and activator of transcription (JAK-STAT) pathway functions as a downstream mediator response for various cytokines, hormones and growth factors (Dodington, Desai, & Woo, 2018). To date, 4 members in JAK family: JAK1, JAK2, JAK3, and TYK2, and 7 members in STAT family: STAT1–4, STAT5A/B, and STAT6 have been identified. Different combinations of JAKs and STATs are activated depending on the cytokine or growth factor signal. For example, in macrophages, IL-6 binds to gp130 on the membrane, and activates STAT3 via JAK1 and JAK2. STAT proteins then translocated into the nucleus bind target gene promoter regions to regulate transcription of inflammatory genes (L. Chen et al., 2018; Cong, Iwasaki, Jiang, & Kisseleva, 2012). Thus, JAK-STAT pathway is a critical pathway in regulating inflammation, immune responses and cellular development (Kaplan, 2013).

## **1.10.ii Innate immune cells involved in influenza infection**

### *Macrophages*

In addition to lung epithelial cells and neutrophils, macrophages are one of the first cells in the respiratory tract to respond to IAV. Upon influenza infection, macrophages are activated to engulf virus and clean up virus-infected and apoptotic cells thus limiting viral spread (Pulendran & Maddur, 2015). The activation of macrophages is also associated with expression of multiple cytokines and chemokines to stimulate inflammatory response. Although lung epithelial cells and neutrophils release pro-inflammatory molecules in early infection stage, macrophages are believed to be the main producers of type I IFN, pro-inflammatory cytokines and chemokines (Pulendran & Maddur, 2015). Depletion of airway macrophages leads to enhanced influenza virus replication and greater disease severity and mortality in mice (Michelle D. Tate, Pickett, van Rooijen, Brooks, & Reading, 2010). Thus, macrophages appear to play critical role in the early innate response to influenza virus infection.

### *Neutrophils*

Neutrophils are the first responders to infection that act at the epithelial barrier to inactivate infectious virions, clear infected dying epithelial cells, and limit viral spread to neighbouring cells (Pulendran & Maddur, 2015). Neutrophil recruitment is triggered by the chemokine CXCL1 (IL-8 in human) released by lung epithelial cells. As phagocytic cells, neutrophils are able to uptake the influenza virus and virus-infected apoptotic cells in the lungs to control infection. Neutrophils are also the main source of pro-inflammatory cytokines in early infection to attract more immune cells and augment clearance of virus (Galani et al., 2017). Although neutrophils are an important contributor in the antiviral response, dysregulated or excessive neutrophil responses in the airways may cause severe outcomes during influenza infections (Sakai et al., 2000; M. D. Tate et al., 2011). The specific role of neutrophils during mild and severe influenza virus infections and their mechanisms in antiviral immunity, remain poorly understood.

### *Dendritic cells*

Known as professional antigen presenting cells (APC), dendritic cells (DCs) play a key role in antiviral innate and adaptive immunity by detecting foreign antigens and presenting them to the innate and adaptive immune responses (Michelle D. Tate et al., 2010). Toll-like receptor

3 (TLR3) and TLR7 recognise double-stranded viral RNA and single stranded RNA respectively leading to production of IFNs and pro-inflammatory cytokines (Michelle D. Tate et al., 2010). In addition, DCs play an important role during antigen presentation leading to presentation of viral peptides to CD4+ and CD8+ T cells.

### *NK cells*

Recent studies show that Natural Killer cells (NK) participate in the immune response against the orthomyxovirus influenza A virus through the production of cytokines and the direct killing of infected target cells (Hwang et al., 2012). Uniquely, NK have the ability to recognize and kill stressed cells directly in the absence of antibodies and MHC, allowing faster immune reaction, unlike other immune cells detecting major histocompatibility complex (MHC) presented on infected cell surfaces, triggering cytokine release, causing lysis or apoptosis (Vivier et al., 2011). NK cells have been recognized as major producers of cytokines such as interferon- $\gamma$  (IFN- $\gamma$ ), which boost macrophage and T cell responses. NK also produce an array of other cytokines, such as TNF- $\alpha$ , interleukin (IL)-10, and many chemokines, including CCL2 (MCP-1), CCL3 (MIP1- $\alpha$ ), CCL4 (MIP1- $\beta$ ), CCL5 (RANTES), XCL1 (lymphotactin), and CXCL8 (IL-8) (Walzer, Dalod, Robbins, Zitvogel, & Vivier, 2005). Those chemokines are key to their colocalization with other hematopoietic cells such as dendritic cells (DC) in areas of inflammation (Vivier et al., 2011). Accordingly, the NK cell depletion resulted in delayed virus clearance from the lungs in mouse with sublethal influenza virus infection (Ge et al., 2012). However, other study suggested in some conditions NK cells might contribute to the pathogenesis of influenza in the lungs, while mechanisms controlling NK cell activation during influenza infection remain unclear (Hwang et al., 2012).

## **1.10.iii Cytokines, chemokines and interferons involved in influenza infection**

### *1.10.iii.a Cytokines*

Cytokines are a large group of small and short-lived proteins that have a specific effect on the interactions and communications between cells (J. M. Zhang & An, 2007). They mainly released by immune cells, including monocytes, macrophages and lymphocytes, as well as endothelial cells, fibroblasts, and various stromal cells. Function as the inflammatory mediators, cytokines effect on the target cells and tissues by autocrine, paracrine or endocrine activities, to modulate the inflammatory and immune response (Tisoncik et al., 2012).

### Pro-inflammatory cytokines:

Pro-inflammatory cytokines are mainly produced by activated monocytes and macrophages to recruit immune cells to the infection site and enhance immune responses (J. M. Zhang & An, 2007). The main pro-inflammatory cytokines such as TNF $\alpha$ , IL-1 and IL-6, could trigger pathological pain, fever, inflammation and tissue destruction. Dysregulation of pro-inflammatory cytokines have been shown to correlate with the mortality during severe infection (Mokart et al., 2002). A balance between pro-inflammatory and anti-inflammatory cytokines is crucial to maintain the host fitness (Jaffer, Wade, & Gourlay, 2010).

### Interleukin (IL-1 $\beta$ )

Interleukins function as inflammatory modulators to stimulate, regulate, or modulate lymphocytes.

IL-1 $\beta$  is predominantly released by the activated monocytes and macrophages, also some fibroblasts and endothelial cells, which causes fever, pain, inflammation and autoimmune conditions (J. M. Zhang & An, 2007). Once TLRs is activated by pathogen or factors released by damaged cells, expression of IL-1 $\beta$  precursor is rapidly induced by signalling pathways such as NF-k $\beta$  (Borthwick, 2016). An active form is then made by caspase-1 by cleaving IL-1 $\beta$  precursor into IL-1 $\beta$  and IL-18. Once released, IL-1 $\beta$  binds to the IL-1R1 to initiate downstream signalling in a range of cell types, inducing the expression of hundreds of genes such as IL-6, IL-8, MCP-1, COX-2, I $\kappa$ B $\alpha$ , IL-1 $\alpha$ , IL-1 $\beta$ , MKP-1, that promote the pro-inflammatory response (Weber, Wasiliew, & Kracht, 2010).

### IL-6

IL-6 is expressed by a range of immune cells and non-immune cells such as epithelial cells, endothelial cells, fibroblasts and keratinocytes, in response to specific stimuli (Dienz et al., 2012). IL-6 is transiently produced at the site of inflammation in response to infections and tissue injury (Tanaka, Narazaki, & Kishimoto, 2014) and can stimulate T cell activation, B cell differentiation, and the regulation of the acute phase response (Hunter & Jones, 2015).

### Tumour Necrosis Factor $\alpha$ (TNF $\alpha$ )

In 1970s, Tumour necrosis factor (TNF $\alpha$ ) was initially identified as an endotoxin-induced serum factor that mediates endotoxin-induced tumor necrosis (Carswell et al., 1975). Now it is known to be a pleiotropic cytokine that plays a central role in mediating inflammatory and

immune responses, by inducing cytokine production, activating adhesion molecules expression and inhibiting tumorigenesis and viral replication (Smith, Farrah, & Goodwin, 1994; Turner, Nedjai, Hurst, & Pennington, 2014). TNF- $\alpha$  is primarily produced in activated macrophages in response to immunological challenges, although it can also be secreted by other cell types such as T cells, mast cells, NK cells, keratinocytes, fibroblasts and neurons (Turner et al., 2014). The expression of TNF- $\alpha$  can be triggered by bacterial products, LPS, and IL-1 $\beta$ . Once releasing, TNF- $\alpha$  binds to its receptor TNFR1 and TNFR2 with high affinity to initiate apoptotic signalling to induce cell death (Parameswaran & Patial, 2010).

#### *1.10.iii.b Chemokines*

Pro-inflammatory chemokines are released by stimulated cells to attract leukocytes from blood to the sites of infection or tissue injury (Turner et al., 2014).

##### *CXCL-1*

CXCL-1 belongs to CXC subfamily, primarily released by tissue residence macrophages and TNF-stimulated endothelial cells in response of pathogens and pro-inflammatory cytokines. It plays a crucial role in host immune response by recruiting neutrophils to the site of infection and also promoting the release of reactive oxygen species (ROS) and proteases for microbial killing in the tissue (Sawant et al., 2016). CXCL1 mediates neutrophil recruitment through binding to its receptor CXCR2 on the neutrophils, and induces integrin expression to facilitate the arrestment of neutrophils by endothelium (Turner et al., 2014). Neutrophils are the first immune cells to migrate into infected tissue sites, response to infections, tissue injury and induce inflammatory response. Therefore, releasing of CXCL-1 is an important step in initiating innate immune response (De Filippo, Henderson, Laschinger, & Hogg, 2008).

##### *MCP-1 (CCL2)*

MCP-1 (monocyte chemoattractant protein-1) also known as CCL2, belongs to CC chemokine subfamily (Deshmane, Kremlev, Amini, & Sawaya, 2009). As a potent chemotactic factor for monocytes, MCP-1 is able to recruit monocytes, memory T cells, and dendritic cells to the sites of inflammation induced by infection or tissue damage. MCP-1 is produced by a variety of cell types including monocytes, macrophages, dendritic cells, fibroblasts, endothelial and epithelial cells, among which monocyte and macrophages are the main source. And the expression of MCP-1 is triggered by oxidative stress, cytokines, or growth factors from

infection site (Deshmane et al., 2009). MCP-1 mediates the effect by binding to its receptor CCR2 which expressed in certain types of cells. This binding directly activates the target cells such as monocytes, memory T cells and natural killer cells, to promote inflammatory response.

#### *1.10.iii.c Interferons.*

Interferons (IFNs) are a group of signalling proteins that are expressed and released by infected cells following the detection of viral components (Killip, Fodor, & Randall, 2015). IFNs are named by their capability of "interfere" with viral replication. The IFNs are classified into three types: Type I IFNs (IFN- $\alpha$ , IFN- $\beta$ ), Type II IFNs (IFN- $\gamma$ ), and Type III IFNs (IFN- $\lambda$ ). All the three classes are important for restricting the early stages of virus infections and for the regulation of the immune system (Killip et al., 2015).

#### *IFN- $\alpha,\beta$*

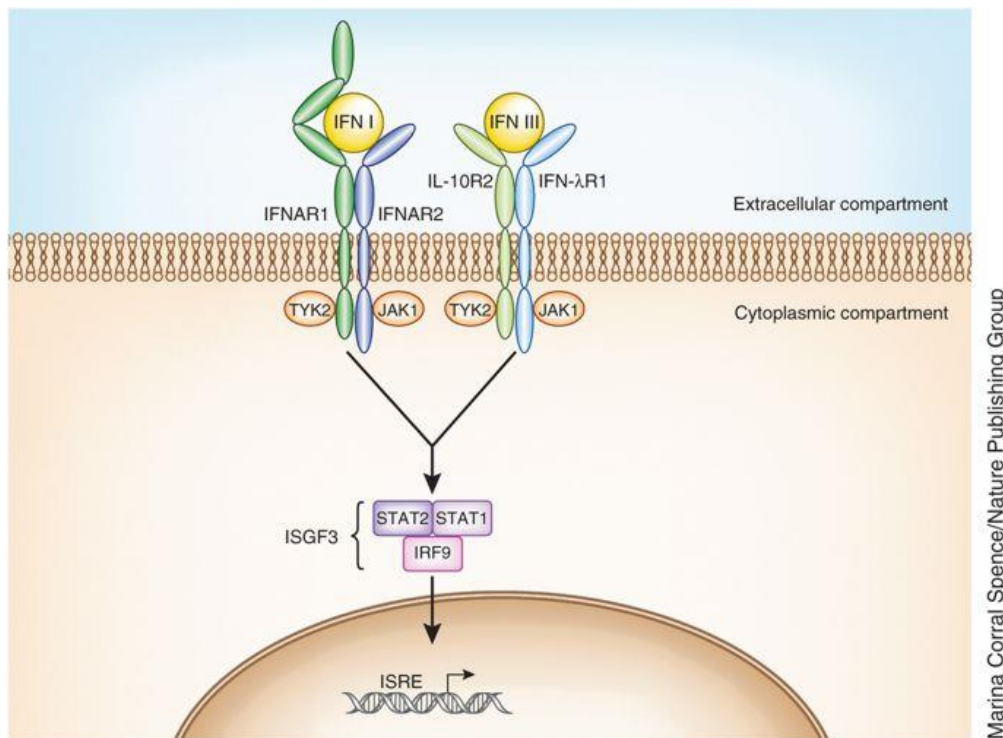
The type I IFNs is a group of cytokines with similar structures, including IFN $\alpha$ , IFN $\beta$ , IFN $\epsilon$ , IFN $\tau$ , IFN $\kappa$ , IFN $\omega$ , IFN $\delta$  and IFN $\zeta$  (McNab, Mayer-Barber, Sher, Wack, & O'Garra, 2015). IFN $\alpha$  and IFN $\beta$  are the most well-defined type I IFNs. Although type I IFNs are secreted by most cell types at low levels, whereas, haematopoietic cells, particularly plasmacytoid dendritic cells, are the predominant source of IFN $\alpha$ , and fibroblasts are a major source of IFN- $\beta$  (Ivashkiv & Donlin, 2014; Schroder, Hertzog, Ravasi, & Hume, 2004). Viral infection is the classic stimulus for IFN- $\alpha$  and IFN- $\beta$  expression (Schroder et al., 2004). There are 3 major roles played by type I IFNs during viral infection. First, IFN $\alpha/\beta$  promote an antiviral state and restrict the viral replication cycle in infected and neighbouring cells in vivo and in vitro by promoting the expression of IFN-stimulated genes (ISGs) (McNab et al., 2015). Second, they promote the innate immune responses by enhancing the function of dendritic cells and monocytes, also by effecting the cytolytic effector functions and the production of IFN $\gamma$  by NK cells (McNab et al., 2015). Third, they activate the adaptive immune system by promoting CD4+ and CD8+ T cell responses and enhancing B cell activities and immunological memory (Ivashkiv & Donlin, 2014).

#### *IFN- $\lambda$*

The type III IFN family comprises IFN $\lambda$ 1 (also known as IL-29), IFN $\lambda$ 2 (IL-28A) IFN $\lambda$ 3 (IL-28B) and the most recently described IFN $\lambda$ 4 (Prokunina-Olsson et al., 2013). Type III IFN can be expressed in a variety of primary cell types, pDCs and epithelial cells are primarily responsible

for type III IFN production (Coccia et al., 2004) (Wack, Terczyńska-Dyla, & Hartmann, 2015). Like type I IFNs, IFN $\lambda$ s could also restrict viral replication by regulating ISGs expression during infection, and activate the innate and adaptive immune responses. While, study shows IFN- $\lambda$  is produced earlier than type I IFN following viral infection, suggesting that IFN- $\lambda$  plays a non-redundant role in limiting initial viral spread in the respiratory tract (Galani et al., 2017). In addition, IFN- $\lambda$  is sufficient to protect host from low dose infection. If viral load is high in the first place that out of control by IFN- $\lambda$ , type I IFNs will be triggered to induce a systemic response and strong immune activation (Andreakos, Salagianni, Galani, & Koltsida, 2017). Studies also demonstrated that type I IFNs could upregulate pro-inflammatory cytokines such as TNF, IL-1b, and IL-6, with the associated risk of immune-mediated damage (Galani et al., 2017). While, IFN $\lambda$ s could only induce the expression of ISGs to restrict viral replication without upregulating the pro-inflammatory cytokines (Galani et al., 2017). Therefore, IFN $\lambda$ s play an important role in early antiviral response, with minimum host damage.

Upon signalling, type I IFNs bind to a heterodimeric transmembrane receptor composed of the subunits IFNAR1 and IFNAR2, which is expressed on most nucleated cells. While, the type III IFNs bind to the IFN- $\lambda$  receptor complex composed of the specific IFN- $\lambda$ R1 and the shared IL-10R2, which is highly expressed on epithelial cells (Klinkhammer et al., 2018). Despite using different receptors, both type I and III IFNs activate the expression of ISGs. Ligation of IFNAR or IFN- $\lambda$  receptor complex by IFNs leads to activation of the receptor-associated protein tyrosine kinases JAK1 and TYK2. The activated JAK1 and TYK2 then phosphorylate STAT1 and STAT2 molecules, leading to their dimerization and recruitment of IRF9 (IFN regulatory factor 9) to form the ISGF3 (ISG factor 3) complex [Figure 1.14] (Wack et al., 2015). The ISGF3 complex then enters the nucleus and induces the expression of several hundred ISGs, which function to induce an antiviral state within the cell (McNab et al., 2015).



Marina Corral Spence/Nature Publishing Group

**Figure 1.14 IFNs induced signalling pathway.** Upon signalling, type I IFNs bind to a heterodimeric transmembrane receptor composed of the subunits IFNAR1 and IFNAR2. While, the type III IFNs bind to the IFN-λ receptor complex composed of the specific IFN-λR1 and the shared IL-10R2. Ligation of IFNAR or IFN-λ receptor complex leads to activation of tyrosine kinases JAK1 and TYK2, follows by phosphorylation of STAT1 and STAT2 molecules and recruitment of IRF9 to form the ISGF3 (ISG factor 3) complex, which regulates the expression of genes containing an interferon response element (ISRE) (Wack et al., 2015).

### Interferon-stimulated genes (ISGs)

Interferon-stimulated genes (ISGs) are a group of gene products induced by IFNs that critical for controlling virus infections. Transcription of ISGs is rapidly stimulated by IFNs which secreted from the infected cell, follows by activating JAK/STAT pathway and transcriptional activation of ISGs (Wang, Xu, Su, Peppelenbosch, & Pan, 2017). Hundreds of ISGs released that target almost any step in a virus life cycle and carry out their antiviral effects. The most important steps in viral life cycle including virus entry, translation and replication, and viral budding, all become the potential target for ISG (Schneider, Chevillotte, & Rice, 2014). For instance, ISGs affect virus entry into cells including Myxovirus resistance (Mx), Cholesterol-25-hydroxylase (CH25H), IFITM proteins, TRIM proteins; a number of ISGs that inhibit translation and replication, including zinc-finger antiviral protein (ZAP), IFIT family, the OAS-RNaseL pathway, PKR and ISG15; virus inhibitory protein, endoplasmic reticulum-associated

IFN-inducible (Viperin) and Tetherin are involved in inhibiting virus budding at the host cell membrane (Schneider et al., 2014). Apart from the antiviral effects, ISGs could also positively and negatively regulate IFN signalling and other host responses (Schneider et al., 2014).

#### **1.10.iv. Cytokine storms and tissue damage during IAV infection**

The inflammatory response refers to the signalling pathways and their production such as cytokines and chemokines are crucial to active immune response and protect host from a variety of pathogens infection. While the inflammatory response can also be potential harmful that causes the host tissue damage and results in severe outcomes when it becomes uncontrolled. Act as inflammatory mediators, cytokines are the main contributor of uncontrolled inflammatory response. An excessive cytokine production, known as “cytokine storm” will lead to the vascular barrier damage and capillary leakage resulting in tissue edema, multiple organ failure and death (Sivro et al., 2011).

Generally, the cytokine storm is induced by the acute inflammatory response which triggered by harmful stimuli that results in activation of pro-inflammatory cytokines or chemokines [Figure 1.15]. A significantly higher level of pro-inflammatory cytokines including IFNs, TNFs and ILs, has been detected in patients suffering from severe influenza infections (Q. Liu, Zhou, & Yang, 2016). TNF- $\alpha$  and IL-1 $\beta$ , expressed in the early stages of infection, are the key cytokines driving of the cytokine storm, followed by an increasing expression of IL-6 and IL-8, and results in abundant immune cell infiltration and tissue damage (Aikawa, 1996). Redness, heat, pain, tissue swelling or edema, and organ dysfunction are the hallmarks of cytokine storm. The acute inflammatory response initiates at a local site and spreads throughout the whole body by the systemic circulation (Tisoncik et al., 2012).

Cytokine storm could induce by the exposure of new pathogens, for instance, specific mutations in influenza viral proteins have been linked to the propensity for cytokine storms induction. Moreover, the deficiencies in host immunity is another contributor of cytokine storms (Sivro et al., 2011). Therefore, to understand the immunopathology induced by host immunity deficiency is one of the key approach to investigate the mechanisms of cytokine storms and the potential therapies.

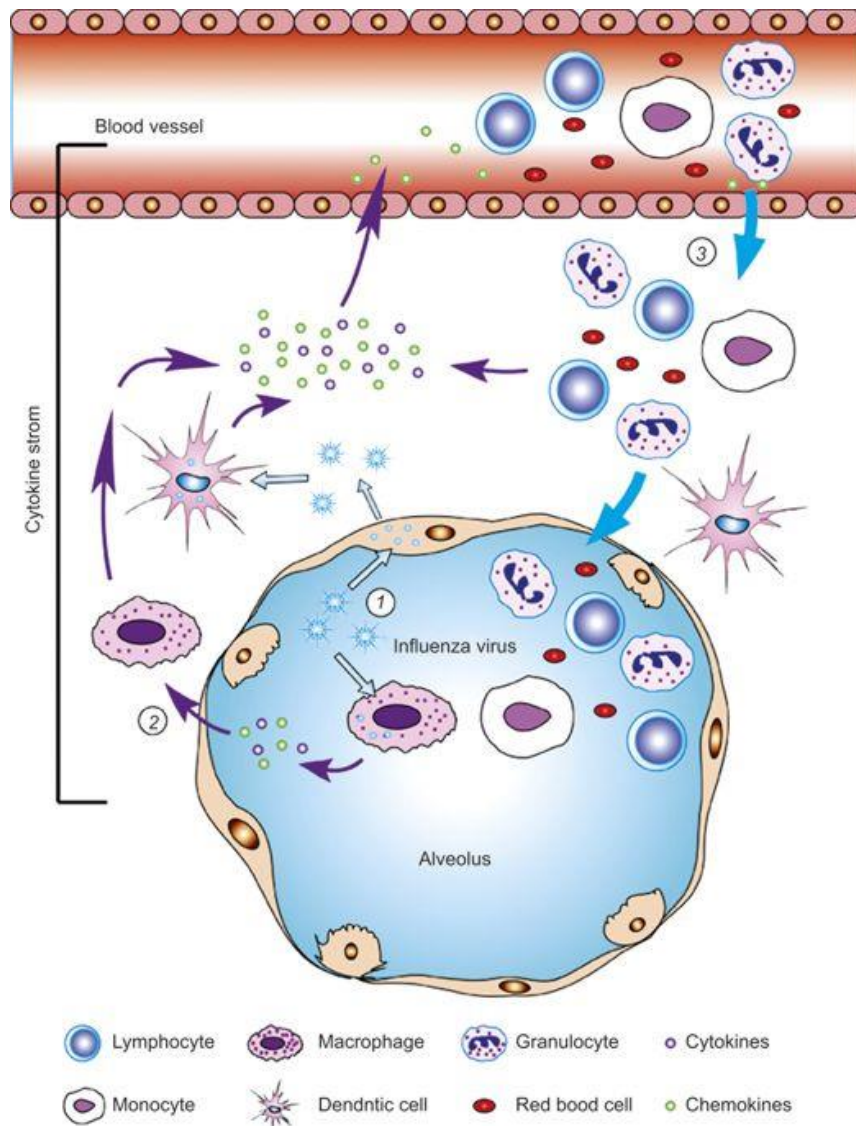


**Figure 1.15 Cytokine storm induced by influenza infection in the lung.** Upon enter to the lung epithelial cells or alveolar macrophages, influenza virus can be recognized by the sensors (as described above) that trigger innate immune responses (1). Cytokines released from infected cells including IFNs and pro-inflammatory cytokines, mainly to restrict viral replication and spreading, but can also activate macrophages and DCs to induce a more extensive immune response and initiate cytokine storm (2). Chemokines released by stimulated cells attract leukocytes from blood to the sites of infection, which release additional cytokines to amplify cytokine storm (3). (Q. Liu et al., 2016)

## 1.11 Mouse model and specific aims.

This project uses two mouse models to study the role played by LANDO and LAP in controlling IAV infection 'in vivo'.

1. **Atg16L1  $\delta$ WD mice ( $\delta$ WD).** These mice have systemic loss of the WD domain of ATG16L1, which requires for non-canonical autophagy. The remaining of CCD of ATG16L1 can still activate canonical autophagy to maintain tissue homeostasis.

**Specific aim:** The main aims of this project is to investigate the role played by non-canonical autophagy during influenza infection. Previous studies demonstrate the anti-infection role of non-canonical autophagy during bacterial or fungal induced infection, but less were known about viral infection 'in vivo'. The influenza A virus was chosen for this study as the virus enters cells by endocytosis, that activates non-canonical autophagy resulting in recruitment of LC3 to cellular membranes. In addition, the recruitment of LC3 to membranes following IAV infection is dependent on the WD domain of ATG16L1 (Fletcher et al), suggest the potential role of non-canonical autophagy during influenza infection. The  $\delta$ WD mice model generated in our lab allows us to do 'In vivo' studies, to further investigate the effect of non-canonical autophagy in host response against influenza infection.

There are several approaches used to examine the outcomes of influenza challenge: the viral replication level was measured by plaque assay and q-PCR, inflammatory level was indicated by cytokines expression and FACs, and pathology outcomes was explored by immunohistochemically analysis.

We assuming that loss of non-canonical autophagy would affect the innate immune response at early time point during IAV infection. As the existence of LANDO in the lung epithelial cells could tag the virus-containing endosomes to lysosomes for degradation, to control the viral infection at the early entry step. Moreover, the restricted viral entry could reduce the vRNP level in the cytoplasm, results in less activation of RIG-I and subsequent stimulation of IFNs and pro-inflammatory cytokines. Therefore, the loss of LANDO is possible to cause severe inflammatory response and leads to cytokine storm. In addition, the loss of LAP in phagocytic cells

result in the delayed clearance of infected cells, which would lead to enlarged viral spread and enhanced inflammatory signalling.

In short, these  $\delta$ WD mice model will be used to study the effects of combined loss of LANDO and LAP on IAV infection 'in vivo'.

2. ***Atg16L1*  $\delta$ WD<sup>fl/fl</sup>-LysMcre mice ( $\delta$ WD<sup>phag</sup>).** These mice carry cre recombinase controlled by a *LysM*<sup>cre</sup> promoter, a single *Atg16L1* <sup>$\delta$ WD</sup> allele and a single *Atg16L1*<sup>fl</sup> allele. The cre recombinase removes full length *Atg16L1* from myeloid cells leaving a *Atg16L1* <sup>$\delta$ WD</sup> allele. The myeloid cells of these mice are LAP negative while other tissues are positive for LANDO.

**Specific aims:** these mice will be used to study the specific role played by LAP in phagocytic cells during IAV infection 'in vivo. As the  $\delta$ WD mice loss both of LANDO and LAP, is not possible to identify which plays the key role in control of IAV infection. While, this  $\delta$ WD<sup>phag</sup> mice model with specifically loss of LAP in myeloid cells, but positive for LANDO in other tissues would clarify which pathway play the key role to control IAV infection.

## **Chapter 2**

### **Material and methods**

## Chapter 2 Methods:

### 2.1 Cell culture

#### 2.1.i Cell lines

Primary cells including Mouse embryonic fibroblast (MEFs), skin fibroblasts, Bone marrow derived macrophages (BMDMs) were isolated from  $\delta$ WD and  $\delta$ WD<sup>phag</sup> mice and their littermate controls.

#### 2.1.ii Tissue culture media and reagents

MEFs and skin fibroblasts were grown in Dulbecco's Modified Eagle's Medium (DMEM) (1X) + GlutaMAX™-I [+] 1g/L D-Glucose [+] Pyruvate (Gibco by Life Technologies 21885-025) with 10% fetal bovine serum (Heat Inactivated) (Gibco by Life Technologies 10500-064) and 100U/ml Penicillin Streptomycin (Gibco by Life Technologies 15140-122), in 5% CO<sub>2</sub> at 37°C. MEFs and skin fibroblasts were detached from flasks by 0.25% Trypsin-EDTA (Gibco by Life Technologies 25200-072) before plating. BMDMs were grown in RPMI Medium 1640 (1X) + GlutaMAX™-I (Gibco by Life Technologies 61870-010) containing 30ng/ml M-CSF (Peprotech 315-02) with 10% fetal bovine serum (Heat Inactivated) (Gibco by Life Technologies 10500-064) and 100U/ml Penicillin Streptomycin (Gibco by Life Technologies 15140-122), in 5% CO<sub>2</sub> at 37°C. BMDMs were detached by ice cold phosphate-buffered saline (PBS) before plating.

#### 2.1.iii Primary cells isolation:

##### *MEFs*

MEFs were isolated from embryos of WT and  $\delta$ WD mice. The embryos were harvested from pregnant mice at 12 d.p.c. (day post-coitum) after cervical dislocation. Individual embryos were separated from placenta and embryonic sac, head and organs were removed. Rest of the tissue was minced with scissors and incubated with 0.05% trypsin at 37°C for 30 min. After trypsin digestion, cell suspension was passed through 40 $\mu$ m filter and centrifuged at 1000xg for 10 mins in room temperature. Cell pellets were collected and placed in a 10 cm tissue culture dish containing DMEM (Dulbecco's modified Eagle's medium) supplemented with 10% FBS and 1% pen strep. Cells were incubated 37 °C and 5 % CO<sub>2</sub> for 2 days before move into the T-75 flasks.

### *Skin fibroblasts*

$\delta$ WD<sup>phag</sup> mice and littermate controls were sacrificed by cervical dislocation, the mice body were sterilized with 70% ethanol. Fur around incision site was shaved with a sharp sterile scalpel. A piece of skin sample (approximately 1 cm<sup>2</sup>) was cut with scissors and collected in a petri dish. The dermal side of the skin was scraped with a sterile scalpel to remove adipose tissue and fat tissue. Skin sample was flattened inside an empty sterile 6-well plates, with the dermis facing down. The plates were dried in the tissue culture hood for 15 minutes. 2 ml of DMEM media (with 10% FBS 1% pen strep) was added to each well, and the plates were placed in incubator at 37 °C, 5 % CO<sub>2</sub>. The skin fibroblast started to exit tissue fragments within 2-5 days.

### *Bone marrow derived macrophages*

Mice were sacrificed by cervical dislocation and sterilized with 70% ethanol. The abdomen and hind legs were removed from mice body and collected in a petri dish. Muscle was removed from the bone by a sterile blade, the femur and tibia were separated at the joint. The bones were cut at both ends, and bone marrow was flushed out by RPMI 1640 media carried by 10ml syringes with 25G needles. To obtain a single cell suspension, the bone marrow cells were passed through 40 $\mu$ m filter and centrifuged at 1000rpm 4 °C for 10 mins. Cell pellets were collected and cultured in RPMI 1640 media supplemented with 10% FBS and 1% pen strep. To differentiate bone marrow cells into mature macrophages, 30 ng/ml M-CSF was added to the culture media, and incubated them in standard 37 °C and 5 % CO<sub>2</sub> for 6 days.

## **2.2 Immunofluorescence microscopy**

### **2.2.i Autophagy and non-canonical autophagy stimulation.**

Autophagy was activated by incubating cells in Hanks balanced salt solution (HBSS) (ThermoFisher, 11550456) which lacks amino acids for 2 h at 37°C. Non-canonical autophagy (LAP) was stimulated in BMDMs by incubation with Zymosan. Non-canonical autophagy (LANDO) was stimulated in MEFs or skin fibroblasts in monensin (Sigma, M5273) 100  $\mu$ M for 2 h at 37°C.

## **2.2.ii Fluorescent microscopy**

For fixed cell imaging, cells were cultured on coverslips in 24-well plates (15000 cell/well) before drug treatment. Cells were fixed and permeabilized by 100% ice cold methanol for 7 min in -20°C, and blocked by goat serum (5% goat serum, 0.3% Triton-x in 1×PBS) for 30 min. Fixed cells were incubated with primary antibodies at 1:500 dilution in BSA buffer (1%BSA, 0.3% Trion-x in 1×PBS) slow rocking overnight. The day after, coverslips were washed three times with PBS, and incubated with secondary antibodies (1:1000 dilution) for 2 hrs at room temperature. Coverslips were mounted using ProLong Gold antifade reagent after 5 minutes DAPI (Thermo Scientific) staining (1:5000 dilution). The fixed cell images were obtained at x63 magnification on a Zeiss Axioplan confocal microscope (Zeiss, Oberkochen, Germany) (Cottam et al., 2011). The rabbit anti-LC3A/B (CST-4108s), was used as primary antibody and Goat anti-Rabbit IgG Alexa Fluor® 488, was used as secondary antibody to detect LC3.

## **2.3 Western blotting**

### **2.3.i Cell lysis preparation**

Cells were cultured on 6-well plates 150,000 per well over night before treat with HBSS to induce starvation. Cells were washed twice with PBS before protein extraction. 50µl Mper (mammalian protein extraction reagent) buffer with protease inhibitor was applied in each well, and the wells were scraped to dislodge cells. Cells were lysed in Mper buffer by incubation on ice for 30mins. Cell debris was separate by centrifuge the sample 7mins at 13000xg in 4°C, supernatant was transferred to a clean tube for western blotting.

### **2.3.ii BCA assay**

The BCA (Bicinchoninic Acid) assay was used for quantitation of total protein in a sample by Pierce BCA Protein Assay Kit (life technologies). 10µl of standards or samples (1:10 dilution in water) were loaded in 96-well plate along with BCA reagent (made up according to manufacturer's instructions). After 30 mins 37°C incubation, plate was read by Wallac EnVision 2013 Multilabel Reader (PerkinElmer). Protein concentration was calculated according to the absorption spectra, sample volume was adjusted according to the concentration before loading.

### 2.3.iii Western blotting

Protein samples were denatured in SDS lysis buffer (1% SDS, 10 mM Tris pH 6.8) and boiled for 5mins at 95°C before loading. Running buffer was made by 40ml of MOPS SDS Running Buffer (20x) (NuPAGE, Novex by Life technologies) with 760 ml water. Proteins were separated on 4–12% Bis-Tris gels (Novex, NP0322BOX) at 150v for 1h. Separated proteins were transferred from gels to PVDF membranes and probed by rabbit anti-LC3A/B (CST-4108s), mouse anti-Atg16L (MBL M150-3). Mouse anti-actin was used for loading controls. Rabbit 800 and Mouse 680 (LI-COR 926-3241) secondary antibodies were visualized with a LI-COR Odyssey Infrared imager.

### 2.4 DNA amplification and genotyping

Genomic DNA was extracted from mice ear punch lysed in 50µl of proteinase K lysis buffer at 4°C overnight. PCR amplification was performed using the forward and reverse primer pairs on the list Table 2. Each 20 µL PCR reaction mixture consisted of 1 µL of primer mix (20 pmol/µL), 5 µL 10 × buffer (includes MgCl<sub>2</sub>), 2 µL homemade Taq (TOD#3 1:10 diluted), 0.5 µL LidNTP (25 µM), 38.5 µL dH<sub>2</sub>O, 3 µL DNA (1:10 dilution direct from lysis). The PCR condition comprised initial denaturation at 95°C for 10 min; 10 cycles of denaturation at 95°C for 45 s, annealing at 65°C for 1 min, extension at 72°C for 1 min, 30 cycles of denaturation at 95°C for 45 s, annealing at 55°C for 1 min, extension at 72°C for 1 min and a final extension at 72°C for 10 min, 4°C on hold. The fragments were separated by electrophoresis on 5% agarose gels stained with ethidium bromide, photographed in ultraviolet light by ChemiDoc-It®2 810 Imager.

**Table 2: primer information for genotyping**

Primer name	Primer sequence
290 (forward)	5'-CAAATATGCCTTCAGAACTG
291 (reverse)	5'-GCTGTAGTTCCAATCCCTAA
223 (forward)	5'-CTGAACAGTTAAGTTCCTAG
226 (reverse)	5'-CCAAGAGACACTGACATAGG
19B (forward)	5'-GACATGTTTCAGGGATCGCCAGGCG
15B (reverse)	5'-GACGGAAATCCATCGCTCGACCAG

## 2.5 Virus infection

Animals were randomly assigned into multiple cohorts, anaesthetized lightly with KETASET i.m. and separate cohorts inoculated intra-nasally with influenza A virus in 50 µl sterile PBS. They were sacrificed at variable time-points after infection by cervical dislocation. Tissues were removed immediately for downstream processing. Sample sizes of n = 5-6 were used as determined using power calculations and previous experience of experimental infection with these viruses. Separate cohorts of mice were used for virological analysis, qRT-PCR and histopathology

## 2.6 Plaque assay

### 2.6.i Tissue homogenise

Frozen tissue were homogenized by TissueLyser LT with 0.5cm stainless steel bead and 2ml safe lock micro centrifuge tubes as previously described. 1 ml serum free DMEM was added in each tube immediately. TissueLyser LT was operated for 4 mins at 50Hz. Tubes were centrifuged at 2000xg, 5mins at 4°C, supernatant from samples was transferred into a new tube, followed by BCA and plague assay.

### 2.6.ii Serial dilution

Tissue homogenise samples were adjusted to same concentration based on BCA assay. 10-fold serial dilution were made from  $10^{-1}$  to  $10^{-7}$  by serum free DMEM supplemented with 1µg/ml of TPCK trypsin. MDCK (Madin-Darby canine kidney cells) were seeded on 6-well plates,  $1 \times 10^6$  cells/well one day before plague assay. Cells were wash by PBS once before 1ml virus dilution per well been added. Cells were incubated with virus dilution in 37°C for 1h, plates were gently rocked every 15 mins.

### 2.6.iii Overlay medium preparation

Overlay medium was prepared by mixing 2.4% Avicel RC-581 and 2xoverlay Medium (1:1). 2xoverlay Medium was made up according to Table 3. The overlay medium was placed to water bath 30 mins before use, 1µg/ml of TPCK trypsin was added immediately before use. After 1h incubation, virus dilution was taken, cells were covered by 4ml overlay medium per well and incubated at 37°C, 5% CO<sub>2</sub> for 72h before fix.

**Table 3: 2×overlay Medium recipe for 100ml**

10xMEM	(Sigma)	20ml
NaHCO <sub>3</sub>	(Gibco)	2ml
HEPES buffer	(Gibco)	4ml
L-glutamine	(Gibco)	2ml
Pen strap	(Gibco)	2ml
ddH <sub>2</sub> O		70ml

#### **2.6.iv Fixation and staining**

After 72h incubation, overlay medium was removed, cells were washed by PBS two or three times, to get rid of Avicel from monolayers. Cells were immediately fixed by ice-cold acetone: methanol (60:40) for 10 mins at room temperature. Fixation reagents were removed, plates were left to air dry completely. 1ml Crystal Violet Solution was added to each well for visible staining, incubated room temperature for 10 mins. Crystal Violet was washed away by water, plates were left to dry overnight. Negative staining plaques (transparent dots) can be counted and virus titer can be calculated using the formula:

$$\text{Number of plaques} \times \text{the dilution factor} \times \text{dilution number (10}^x\text{)} = \text{PFU/ml}$$

### **2.7 q-PCR for RNA expression level of cytokines and IAV**

#### **2.7.i Tissue homogenise**

Frozen tissue were taken from -80°C, 25mg tissue from each sample were cut and transferred to a 2ml safe lock micro centrifuge tubes containing one 0.5cm stainless steel bead (tubes contain beads were placed on dry ice for 15 mins before use). Tissue were incubated on dry ice for another 15 mins. Tubes containing beads and tissue were placed into the TissueLyser LT Adapter, and incubated at room temperature for 2 minutes to avoid freezing of reagents. 1 ml Trizol was added in each tube immediately. TissueLyser LT was operated for 4 mins at 50Hz. Tubes were centrifuged at 12000rpm, 5mins at 4°C, supernatant from samples was transferred into a new tube, followed by RNA extraction.

### **2.7.ii RNA extraction**

Trizol-Chloroform method was used for RNA extraction. 200µl chloroform was added to each sample homogenized in 1ml Trizol. Tubes were shaken vigorously for 15 secs (do not vortex), incubated at room temperature for 10 mins for phase separation, and spun at 12000xg, 4°C for 15 mins. The aqueous phase of the samples was transferred into a new tube, 500µl isopropanol was added to the samples which were vortexed vigorously and incubated in RT for 10 mins for precipitated RNA. Samples were spun at 12000xg, 4°C for 10 mins, supernatants were discarded and RNA pellets were washed with 1 ml 75% ethanol, then centrifuged at 12000g, 4°C for 5 mins. Supernatants were removed, and pellets were air dried for 10 mins, then 50µl nuclease free water was added to re-suspend RNA pellets.

### **2.7.iii RNA clean up**

After extraction, RNA samples were clean by RNeasy MinElute cleanup kit from Qiagen. Sample volume was adjusted by nuclease free water to 100µl, 350µl buffer RLT and 250µl 100% ethanol were added to each sample, well mixed by pipetting. 700µl sample was transferred to an RNeasy MinElute spin column which placed in a 2ml collection tube. Samples were centrifuged at 10000rpm for 15s, flow-through was discarded and 500µl buffer RPE was added to wash the spin column. Samples were spun at 10000rpm for 15s, flow-through was discarded, and wash step was repeated 1 time with 80% ethanol. Then spin columns were spun at full speed 5 mins the dry the membrane. RNeasy MinElute spin column were placed in new tubes, 14µl nuclease free water was added to elute RNA. Nano-drop spectrometer was used to measure RNA concentration.

### **2.7.iv Reverse transcription**

Random primer annealing was done according to the annealing system Table 4, the mixture was heated at 65°C for 5 mins, and chilled on ice. 4µl 5×FW buffer, 2µl 0.1M DTT and 1µl of superscript II were added to each sample mix, followed by 2hr incubation at 42°C for reverse transcription and 15 mins 70°C for enzyme heat inactivation. cDNA samples were store in -20°C before use.

**Table 4: Annealing system**

Random primer (Invitrogen)	1 $\mu$ l
10 mM dNTP mix (Invitrogen)	1 $\mu$ l
RNaseout (Invitrogen)	1 $\mu$ l
cDNA sample	2 $\mu$ g
ddH <sub>2</sub> O	make up to 13 $\mu$ l in total

### 2.7.v Run q-PCR and data analysis

q-PCR was performed using 2 $\times$ Bioline immomix, additional SYBR green and MgCl<sub>2</sub> were added according to Table 5 to optimize the reaction condition. 2  $\mu$ l of 10 $\times$ primers (Qiagen) for each target gene were added to each reaction, followed by 5  $\mu$ l of 1ng/ $\mu$ l cDNA samples. PCR was carried out by 7500 standard Real-Time PCR system (Applied Biosystems, Grand Island, NY). Amplification program including 3 stages: holding stage: 50 $^{\circ}$ C 2mins, 95 $^{\circ}$ C 10mins; cycling stage ( $\times$ 40): 95 $^{\circ}$ C 15s, 60 $^{\circ}$ C 30s; melt curve stage: 95 $^{\circ}$ C 15s, 60 $^{\circ}$ C 1min, 95 $^{\circ}$ C 30s and 60 $^{\circ}$ C 15s.

**Table 5: q-PCR master mix for 1 reaction**

2 $\times$ Bioline immomix	10 $\mu$ l
10mg/ml BSA (BioLabs)	2 $\mu$ l
50mM MgCl <sub>2</sub> (Bioline)	0.2 $\mu$ l
100x SYBR Green I nucleic acid gel stain (Invitrogen)	0.12 $\mu$ l
ROX reference (Invitrogen)	0.4 $\mu$ l
ddH <sub>2</sub> O	0.28 $\mu$ l

Transcript level were normalized by 18s RNA within each sample. After run, amplification curve and melt curve were checked to make sure there is no product formed for NTC (no contamination), and every reaction just has a single peak. Standard curves of each target gene were made by 6 serial 2-fold dilutions of cDNA template, intercept and slope generated by standard curve were used to calculate the initial concentration of each sample. Final concentration of each product was normalized by 18s before processed by graphpad. Resources of q-PCR primers for target genes are indicated in Table 6.

**Table 6: Resources of q-PCR primers for target genes**

Target	Catalogue number
IAV (Sigma)	-Fw 5'-GACCRATCCTGTCCACCTCTGAC -Rev 5'-AGGGCATTYTGGACAAKCGTCTA
ISG15 (Qiagen)	QT00322749
IFIT1 (Qiagen)	QT00322749
IFN- $\alpha$ (Qiagen)	QT00253092
IFN- $\beta$ (Qiagen)	QT00249662
IFN- $\lambda$ 2,3 (Sigma)	-Fw 5'-AGTGGAAGCAAAGGATTG -Rev 5'-GAGATGAGGTGGGAACTG
IL-1 $\beta$ (Qiagen)	QT01048355
TNF- $\alpha$ (Qiagen)	QT00104006
CXCL1 (Qiagen)	QT00115647
CCL2/MCP-1 (Qiagen)	QT00167832
IL-6 (Qiagen)	QT00098875
18S ribosomal RNA (Qiagen)	QT02448075

## 2.8 Flow cytometry

### 2.8.i Prepare single cell suspension

Fresh lungs were obtained from infected mouse, the heart and associated connective tissue were removed before transfer into a 10ml tube containing 2ml RPMI. Lungs were transferred to a sterile petri dish and cut into tiny pieces with small scissors. Lung pieces were transferred back to the Bijou tube with 2ml RPMI, petri dish was washed with 0.5ml RPMI to ensure lung pieces are in a final volume of 2.5ml. 50 $\mu$ l of collagenase D (final concentration of 1mg/ml) and 50 $\mu$ l of DNase I (final concentration of 200 $\mu$ g/ml) were added to the samples, followed by incubation for 1h at 37°C with moderate shaking (200rpm for SHBL LAB shaking incubator). After incubation, the contents were filtered through 10 $\mu$ m cell strainers into fresh 50ml centrifuge tubes. Lung pieces staying on the strainers were mashed with the plunger of a 10ml syringe. Remaining cells on the strainers were washed through the mesh by 2ml RPMI, and repeat rinse by additional 2ml RPMI. Samples were centrifuged at 900 $\times$ g for 5mins at RT.

Supernatant was discarded, cell pellet was re-suspended in 2ml ACK lysis buffer to lyse red blood cells. Samples were incubated with ACK buffer 2.5 mins at RT, vortex briefly, further incubated 2.5 mins at RT. 5ml RPMI was added into sample immediately after incubation to restore the osmotic balance. Cells were centrifuged at 900×g for 5mins at RT, re-suspended in 2ml RPMI prior counting.

### 2.8.ii Antibody labelling

After counting,  $1 \times 10^6$  cells were transferred to each well in a 96-well U bottom plate. Plates were centrifuged, supernatant was discarded, to get the cell pellets. Cell pellets were re-suspended and blocked by 100µl Fc block solution (anti-mouse CD16/CD32 diluted 1:500 in FACS buffer), incubated 15 mins at 4°C. 100µl of stain mix, single stain or unstained FACS buffer were added to each well as appropriate. Plates were incubated 30 min at 4°C, centrifuged at 600g for 5 mins at 4°C. Supernatant was removed, cells were re-suspended in 200µl 4% PFA to fix. After 15 mins fixation, plates were centrifuged, supernatant was discarded and cells were re-suspended in 200µl PBS prior analysing. Flow cytometric analysis was performed on MAC Miltenyi Biotec, and data analysed by Flowjo.

**Table 7: List of antibody source and dilutions**

Marker	Label	Clone	Dilution	Source
CD45	eFluor450	30-F11	1:200	eBioscience 48-0451-80
CD4	PE-Cy7	GK1.5	1:200	eBioscience 25-0041-81
CD8	APC	53-6.7	1:200	eBioscience 17-0081-81
B220	PE	RA3-6B2	1:200	eBioscience 12-0452-81
CD11b	APC	M1/70	1:200	eBioscience 17-0112-81
CD11b	FITC	M1/70	1:200	eBioscience 11-0112-41
CD11c	PE-Cy7	N-418	1:200	eBioscience 25-0114-82
Siglec F	PE	E50-2440	1:200	BD Pharmingen™ 552125
Ly6G	APC	RB6-8C5	1:200	eBioscience 17-5931-82

## 2.9 Elisa (enzyme-linked immunosorbent assay)

In order to investigate the antibody level changes after virus infection, serum from infected mice was analysed by Elisa to detect the antibody level.

### 2.9.i Antigen preparation and plates coating

Inactivated influenza A virus was used to coat the plates, which could bind directly with the antibody from serum. To obtain inactivated virus, a T175 flask of MDCK cells was infected by influenza A virus X31, with the ratio 1PFU/cell, and incubated 24-36 h ensure good CPE. Cells were scraped into 1 ml PBS containing 10 $\mu$ l protease inhibitor cocktail, and transferred to an Eppendorf tube. Tube was freeze-thaw 3 times on dry ice with mild vortex to disperse cell debris. Then 1ml of cell/virus solution was spread onto a sterile tissue culture dish, Hoefer UVC 500 box was set at 300mJ/cm<sup>2</sup> irradiate to inactivate the virus. 1ml virus was diluted in 50ml PBS before use. Flat bottom 96-well Elisa plates were coated by 100 $\mu$ l UV inactivated virus in PBS, left in sealed and left overnight at 4°C.

### 2.9.ii Antibody detection by Elisa

Antigen was discarded, plates were 3 times washed by PBS before blocked by PBS containing 1% BSA at 37°C for 1 h, 200 $\mu$ l/well. Then plates were washed 5 times by PBS containing 0.05% Tween 20 before incubation with the serum samples. Serum samples were diluted 1/20 in PBS, and 2-fold serial diluted in PBS containing 1% BSA and 0.05% Tween 20 until 1/640 (dilution range could be change depends on the samples), followed by 1 h incubation at 37°C in sealed Tupperware box. After incubation, plates were washed 5 times by PBS containing 0.05% Tween 20, 100 $\mu$ l anti-mouse Ig subtype HPX (Anti-Mouse IgG Sigma A3673 dilute 1:3000; Anti-Mouse IgA Sigma A4789 dilute 1:4000) was added in each well, followed by 1h 37°C incubation in sealed Tupperware box. Plates were washed 5 times by PBS containing 0.05% Tween 20, then 2 times by tap water. 100 $\mu$ l TMB solution (Sigma D50292) was added and plated were incubated in dark at room temperature for 30 mins. 100 $\mu$ l 0.5M HCL was added to each well to stop the reaction. Plates were read at 450nm by Spectra MAX M2 plate reader.

## 2.10 Luminex Simplex Assay

Luminex is a multiplex immunoassay based on Luminex xMAP technology that enables simultaneous detection and quantitation of multiple secreted proteins. It has been used to detect the cytokines released in mice lung after IAV infection in this project.

### 2.10.i Sample preparation:

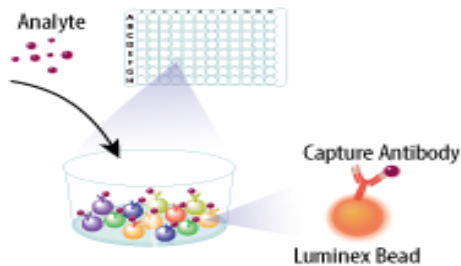
The lung lavage was collected from sacrificed mice by flushing 1 ml PBS into the lung through trachea, and kept in -20°C before Luminex assay. Separate lung samples were homogenised in media by TissueLyser LT and the supernatant was taken for Luminex assay. The BCA assay was applied to all of the samples to adjust the protein level before running Luminex.

### 2.10.ii Luminex Assay

The Luminex assay was operated following the ProcartaPlex™ Multiplex Immunoassay USER GUIDE (Simplex Kits and Combinable Panels). Reagents and antigen standard were prepared according to manufacturer's protocol. 50x Simplex beads for each cytokine (IL-1 $\beta$  eBioscience EPX01A-26002-901, IL-6 eBioscience EPX01A-20603-901, TNF- $\alpha$  eBioscience EPX01A-20607-901) were diluted in water at final concentration 1x, vortexed for 30 sec before use. Simplex beads for each cytokine were mixed and 150 $\mu$ l of the mixed beads were added to the appropriate wells of 96-well flat bottom plate (ProcartaPlex™ Mouse Basic Kit eBioscience EPX010-20440-901). Wells with magnetic beads were washed with 120 $\mu$ l wash buffer, and the wash buffer was removed by quickly inverting the Hand-Held Magnetic plate washer and 96-well flat bottom assembly over a sink. 50 $\mu$ l of standards or samples were added to appropriate wells of the 96-well plate containing the beads. The plate was sealed and incubated with shaking for 2h at RT, followed by 3 times washing with wash buffer. 25 $\mu$ l detection antigen mixture was added, and plate was covered with black lid and incubated with shaking for 30 min at RT. After 3 times washing with wash buffer, 50 $\mu$ l of SAPE solution was added to each well. Plate was covered with black lid and incubated with shaking for 30 min at RT, followed by 3 times washing with wash buffer. 120 $\mu$ l Reading buffer was added to each well, and plate was incubated with shaking for 5 min at RT before read on Luminex®100/200. The principle of luminex assay is indicated below.

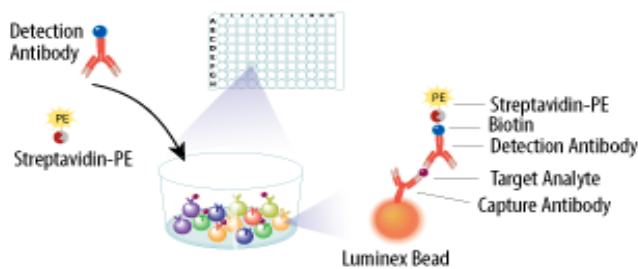
## Luminex Assay Principle

### Step 1



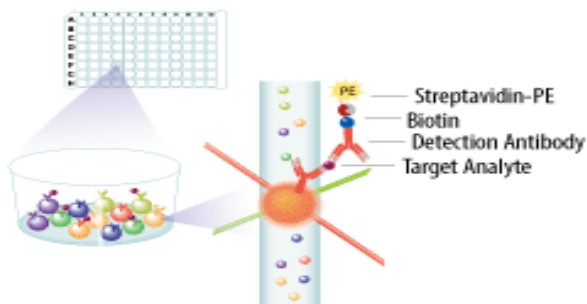
The standard or sample is added to a mixture of simplex beads, pre-coated with analyte-specific capture antibodies. The antibodies could bind to the analytes of interest.

### Step 2



Biotinylated detection antibodies specific to the analytes of interest are added and form an antibody-antigen sandwich. Phycoerythrin (PE)-conjugated streptavidin is added. It binds to the biotinylated detection antibodies.

### Step 3



Beads are read on a dual-laser flow-based detection instrument, such as the Luminex 100/200. One laser classifies the bead and determines the analyte that is being detected. The second laser determines the magnitude of the PE-derived signal, which is in direct proportion to the amount of analyte bound. Modified from R&D system, "Luminex Assay Principle".

## 2.11 Generation and analysis of Radiation Chimeras

The chimeras were generated at Liverpool University by Professor James Stewart. The procedure was approved by the University of Liverpool Animal Welfare and Ethical Review Body and performed under UK Home Office Project License 70/8599. Mice were subjected to whole body irradiation with 11 Gy in two doses separated by 4 hours using a  $^{137}\text{Cs}$  source in a rotating closed chamber. Bone marrow was collected from male C57BL/6-Ly5.1 (B6.SJL-*Ptprc<sup>a</sup>Pepc<sup>b</sup>*/BoyCrI) mice that are congenic for the CD45.1 allele or from  $\delta\text{WD}$  mice. The femur and tibia of the donor mouse was collected and sterilised for 2 minutes in 70% ethanol. The ends of the bones were removed and a needle with PBS was used to flush out the bone marrow through a 40 $\mu\text{m}$  cell sieve. Red blood cell lysis was performed using 0.83% ammonium chloride, the cells were washed twice in PBS and re-suspended at a concentration of  $10^7$  cells/ml. T-cell depletion was performed prior to transfusion by using commercial mouse hematopoietic progenitor cell isolation kit (catalogue no. 19856 EasySep, STEMCELL™ TECHNOLOGIES). Normal Rat serum (100  $\mu\text{l}$  /ml) was added into cell samples followed by isolation cocktail (50 $\mu\text{l}$ / ml) and transferred samples to 5 ml polystyrene round bottom tube. Samples tube were incubated at 2-8 $^{\circ}\text{C}$  for 15 minutes with a brief vortex, following by addition of streptavidin RapidSpheres (75 $\mu\text{l}$ /ml) and gently pipetted by addition of 2.5 ml of recommendation media (PBS without  $\text{Ca}^{2+}$  and  $\text{Mg}^{2+}$  with 2% FBS and 1mM EDTA. The tube was placed in EasySep magnet without lid at RT for 3 minutes. The tube was removed from magnet and inverted in a new 15 ml tube in one continuous motion. This process was repeated to get more number of cells.

After depletion,  $1 \times 10^6$  donor bone marrow cells were injected into each irradiated mouse by tail vein injection 3 hours following irradiation. Mice were then allowed to recover for 12 weeks with daily monitoring of mouse weights and general condition for at least the first two weeks to monitor for any severe radiation sickness or illness due to being immunocompromised.

For chimaerism analysis, approximately  $1 \times 10^6$  spleen cells were incubated in 100 $\mu\text{l}$  of Fc block (clone 2.4G2, BD Bioscience) diluted in PBS, 2% FCS (PBS-FCS) for 15 min at 4  $^{\circ}\text{C}$  prior to the addition of fluorochrome-conjugated monoclonal antibodies specific for CD45.1 (clone A20 eBioscience) CD45.2, (clone 104 eBioscience) CD8a, (clone 53-6.7 eBioscience) CD4 (clone GK

1.5 eBioscience), CD3 (clone 17A2 eBioscience) and B220 (clone RA3-6B2 eBioscience in PBS-FCS and incubation for 30 min at 4 °C in the dark. Cells were then washed in PBS-FCS, fixed in PBS, 4% paraformaldehyde for 15 min at 20°C prior to analysis on a MACSQuant Analyzer 10 (Miltenyi Biotech UK). Data were analysed using FlowJo.

## 2.12 Histology, immunohistology

The histology work undertaken by Anja Kipar at Institute of Veterinary Pathology, University of Zurich, Switzerland. Tissues were fixed in 4% buffered paraformaldehyde (PFA) for 24h and routinely paraffin wax embedded. Consecutive sections (3-5 µm) were either stained with haematoxylin and eosin (HE), used for immunohistology (IH).

IH was performed to detect viral antigen and to identify neutrophils and neutrophil extracellular traps (NETs), macrophages, T cells and B cells, using the horseradish peroxidase (HRP) and the avidin biotin complex (ABC) method. The following primary antibodies were applied: goat anti-IAV (Meridian Life Sciences Inc., B65141G), rat anti-mouse Ly6G (clone 1A8, Biolegend; neutrophil marker), rabbit anti-Iba-1 (antigen: AIF1; Wako Chemicals; macrophage marker), mouse anti-human CD3 (clone F7.2.38, Agilent Technologies; T cell marker), rat anti-mouse CD45R (clone B220, BD Biosciences; B cell marker), and rabbit anti-histone H3 (citrulline R2 + R8 + R17; abcam; NET marker). Briefly, after deparaffination, sections underwent antigen retrieval in citrate buffer (pH 6.0, 20 min at 98°C; for Ly6G, Iba-1 and CD45R) and EDTA buffer (pH 9.0, 20 min at 98°C; for CD3), followed by blocking of endogenous peroxidase (peroxidase block, S2023, Dako) for 10 min at room temperature (RT). Slides were then incubated with the primary antibodies (diluted in dilution buffer, Dako) for a) CD3 and Iba-1 (60 min at RT), followed by a 30 mins incubation at RT with the secondary antibody (Envision mouse and rabbit, respectively, Dako) in an autostainer (Dako), and b) Ly6G (60 min at RT) and CD45R (overnight at 4°C), followed by rabbit anti-rat IgG and the ABC kit (both 30 min at RT; Ventana). Staining for histone H3 was undertaken with an autostainer (Discovery XT, Ventana), using citrate buffer, dilution buffer and detection kits provided by the manufacturer. The antibody reaction was visualized with 3,3'-diaminobenzidin and sections counterstained with hemalum.

## 2.13 Statistical analysis

Data were analysed using the Graphpad Prism package. *P* values were set at 95% confidence interval. A repeated-measures two-way ANOVA (Bonferroni post-test) was used for time-courses of weight loss; two-way ANOVA (Bonferroni post-test) was used for other time-courses; log-rank (Mantel-Cox) test was used for survival curves; one-way ANOVA (Tukey's post-hoc) was used to compare three or more groups side-by-side; Mann-Whitney U test was used to compare two groups. All differences not specifically stated to be significant were not significant ( $p > 0.05$ ). For all figures, \* $p < 0.05$ , \*\* $p < 0.01$ , \*\*\* $p < 0.001$ , \*\*\*\* $p < 0.0001$ .

## 2.14 Mice model

All experiments were performed in accordance with UK Home Office guidelines and under the UK Animals (Scientific procedures) Act1986.

The generation of  $\delta$ WD mice (*Atg16L1* <sup>$\delta$ WD/ $\delta$ WD</sup>) has been described previously (Rai et al., 2019). Generation of  $\delta$ WD<sup>phag</sup> and *Atg16L1*<sup>fl/fl</sup>-LysMCre mice is described in detail in Figure 4.3. Comparisons were made using littermate control mice for each individual genotype. Studies were approved by the University of East Anglia Animal Welfare and Ethical Review Body and performed under UK Home Office Project License 70/8232.

Infection studies were performed at the University of Liverpool, approved by the University of Liverpool Animal Welfare and Ethical Review Body and performed under UK Home Office Project License 70/8599. Studies used 2-3 m old male and female mice that had been backcrossed to C57BL/6J. Mice were maintained under specific pathogen-free barrier conditions in individually ventilated cages (Greenline GM500, Techniplast) at a temperature of 22°C ( $\pm$  2°C), humidity 55% ( $\pm$  10%), light/dark cycle 12/12 hours (7 am to 7 pm), food CRM(P) and RO or filtered water *ad lib*. Colonies were screened using the Charles River surveillance plus PRIA health screening profile every 3 months to ensure SPF status.

For virus infection, animals were randomly assigned into multiple cohorts, anaesthetised lightly by the i.m. route with 150 mg/kg ketamine (Ketavet, Zoetis UK Ltd) and separate cohorts inoculated intra-nasally with 10<sup>3</sup> PFU IAV strain X31 in 50  $\mu$ l sterile PBS. Mice were infected between 9 and 11 AM. Animals were sacrificed at variable time-points after infection

by cervical dislocation. Tissues were removed immediately for downstream processing. Sample sizes of  $n = 6$  were used as determined using power calculations and previous experience of experimental infection with these viruses. For survival analysis, a humane endpoint was determined using a scoring matrix that included excessive ( $>20\%$ ) weight loss.

# **Chapter 3**

## **Results Part I**

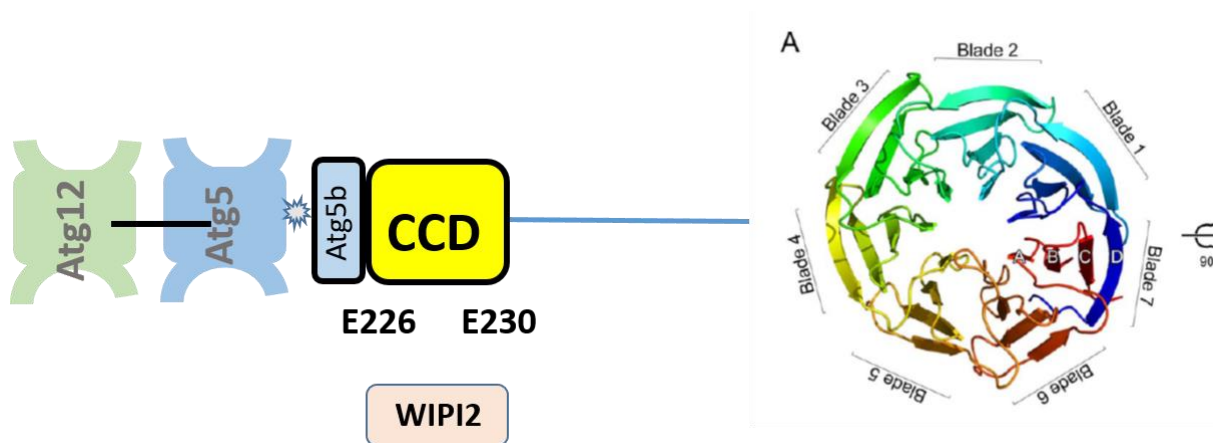
## Chapter 3: Analysis of IAV infection of mice lacking the WD domain of ATG16L1.

### 3.1 Introduction and aims

As described above, Atg16L1 is an essential protein for both canonical and non-canonical autophagy. Previous studies have identified the main protein interaction regions of ATG16L1. The ATG5 binding region occupies the N-terminal 1-78aa, followed by coiled-coil domain (CCD) located on residues 79-230 followed by a linker domain (231 to 265aa) that links the coiled-coil domain to a large C-terminal WD-domain which ranges from 266 to 623aa [Figure 3.1]. Notably, the WIPI2b-binding site needed for canonical autophagy is located on the CCD of ATG16L1 between amino acids 207 and 230 (Dooley et al., 2014). As a PtdIns(3)P effector, WIPI2b interacts with ATG16L1 directly and makes the link between (ER)-localized production of PtdIns3P on ER lipids, and the LC3-conjugation complex containing ATG16L1:ATG5-12. This complex is crucial for autophagosome formation during starvation-induced autophagy (Wilson, Dooley, & Tooze, 2014). Fine mapping studies suggest that mutation of glutamic acid residue E226 or E230 in the CCD of ATG16L1 to arginine (E226R and E230R) abolished binding of ATG16L1 to WIPI2b and mutant proteins cannot rescue starvation-induced autophagy (Dooley et al., 2014). Recent studies by Fletcher et al (2018) have focussed on recruitment of LC3II to endosomes and lysosomes and show that the WD-40 repeats of ATG16L1 are required for non-canonical recruitment of LC3 to endo-lysosome membranes. Work from our laboratory has generated mice lacking the WD and linker domains of ATG16L1 (Rai et al., 2019). These mice cannot activate non-canonical autophagy or LAP but are able to activate starvation-induced autophagy. They maintain tissue homeostasis, grow normally and are fertile.

In this study the mice lacking the WD domain of ATG16L1 were used to see if non-canonical recruitment of LC3 to endosome or phagosome membranes plays a role in innate immunity to viral infection.

The recruitment of LC3 to endosomes and phagosomes has the potential to defend cells against infection by increasing the delivery of endocytosed microbes to lysosomes for degradation. Lung epithelial cells are the primary target for influenza A virus, due to highly



**B**

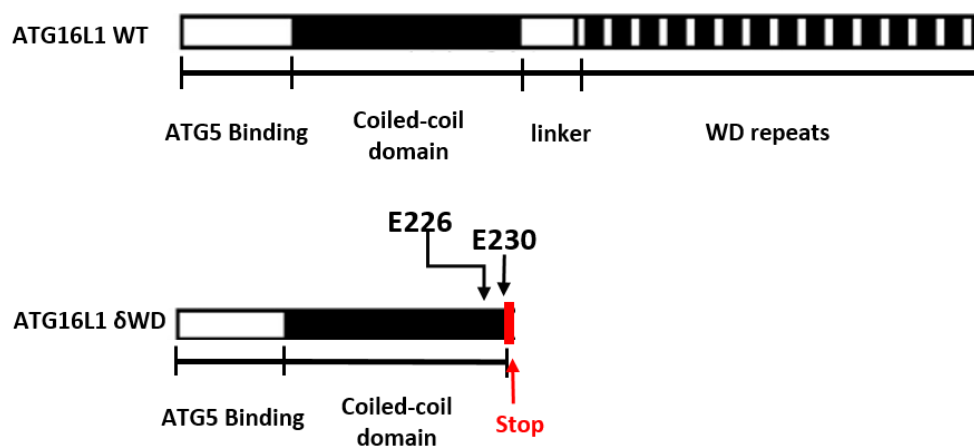


**Figure 3.1. Strategy for removal of the linker and WD domains from ATG16L1. A. Protein domain and interaction map of ATG16L1.** The ATG5 binding domain (Atg5bd) binds the ATG5-ATG12 complex. The coiled coil domain (CDD) contain two glutamate residues (**E226 and E230**) required for binding to WIPI2 during autophagy. The WD domain at the C-terminus contains a seven blade  $\beta$ -propeller attached to the CCD by the linker domain. **B. Location of stop codon used to remove WD domain.** The wild type mouse contains the N-terminal ATG5 binding domain (white box), CCD (black box), linker region and WD repeats (Striped box). The stop codon in the  $\delta$ WD mouse is placed after the E230 glutamate residue required for WIPI2 binding. The mutation removed the WD domain and the linker region. [Modified from Dooley, HC., Razi, M., Polson, HE., et al. 2014. Mol Cell. 55(2):238-52.]

expressed sialic acid residues on the plasma membrane. Viral replication takes place in the epithelial cells throughout the respiratory tract, thus an airway challenge model involving lung tissue is a relevant model for IAV infection studies. As described previously (Beale et al., 2014; Fletcher et al., 2018) IAV infection results in the lipidation of LC3 and its re-localisation to perinuclear vesicles and the plasma membrane. This depends on the proton channel activity of M2 and the WD40 domain of Atg16L1. The results above and those of Florey and colleagues (Fletcher et al., 2018) show that the WD40 domain, is only required for non-canonical autophagy including LAP and LANDO, but not for canonical autophagy. How non-canonical autophagy affects influenza infection is still unclear. One possibility is that, when IAV enters to the host cells by endocytosis, LC3 lipidation at the plasma membrane and/or endosomes enhances the fusion between virus containing endosomes and lysosomes, thus reducing the chance of vRNP import to the nuclei and this restricts viral replication. Therefore, in absence of non-canonical autophagy viral replication could be increased. Another possibility could be through an effect of efferocytosis of dead cells killed by IAV infection which requires the intact LAP pathway in phagocytic cells, such as macrophages. During IAV infection, the dead cells containing large numbers of virions, are engulfed by professional phagocytes, thus limiting viral spreading. The absence of LAP in phagocytic cells may therefore result in increased viral replication and spread.

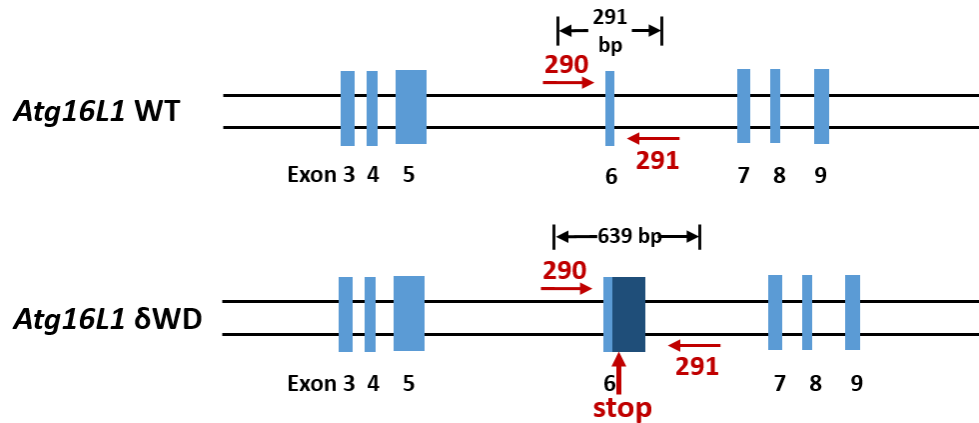
The aim of this chapter is to use the  $\delta$ WD mice to understand the role played non-canonical autophagy pathways during infection without off pathway reactions resulting from loss of canonical autophagy.

### 3.2 Genotyping $\delta$ WD mice

Mice lacking the WD domain of Atg16L1 were generated in the lab by Julia Maryam Arasteh during her Ph.D. In the  $\delta$ WD mice, two stop codons are introduced straight after the CCD (E230), to prevent translation of the WD domain. The coiled-coil domain is intact and can bind WIPI2b, so  $\delta$ WD mice should be autophagy positive and LAP negative [Figure 3.1]. PCR primers used to genotype the mice, designed and optimized by Julia Maryam Arasteh, are shown in Figure 3.2A. The 290-291 primers produce a 291pb band in wild type mice but the

band increases in size to 639bp following introduction of the stop codon into exon 6 (Arasteh 2012).

A



B

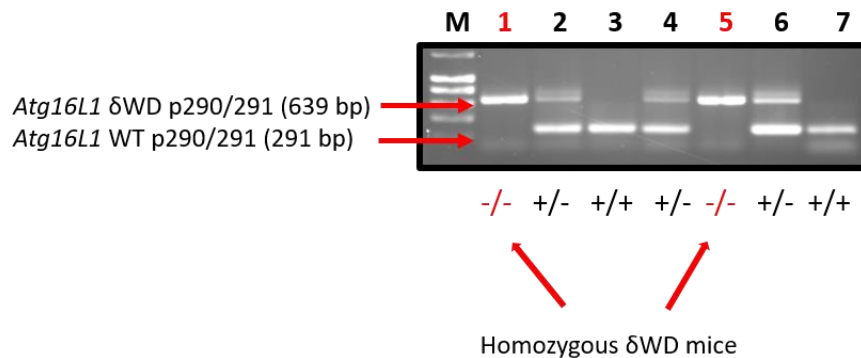


**Figure 3.2. Genotyping mice. A. Location of PCR primers.** The PCR primers are designed to anneal to exon 6. In wild type mice primers 290 and 291 generate a 291bp fragment. The stop codon in the  $\delta$ WD mouse increases the size of the fragment to 639bp. **B. Representative agarose gel showing PCR products and genotype.** DNA extracted from 7 mice were analysed by PCR using primers 290 and 291 and resolved on an agarose gel. Molecular size markers are in lane M. A single band at 291 (3,7) indicates wild type mice (+/+), a single band at 639 (1,5) indicates homozygous  $\delta$ WD mouse (-/-), heterozygous mice (2,4,6) have both bands (+/-).

Representative PCR reactions separated on agarose gel are shown in Figure 3.2B. Wild type mice (+/+) generate a single band at 291bp, while homozygous mutant mice (-/-) generate a single band at 639bp. Heterozygotes (+/-) produce both bands. The genotyping allowed homozygous  $\delta$ WD mice to be selected for experiments, with wild type mice from the same litter being used as littermate controls.

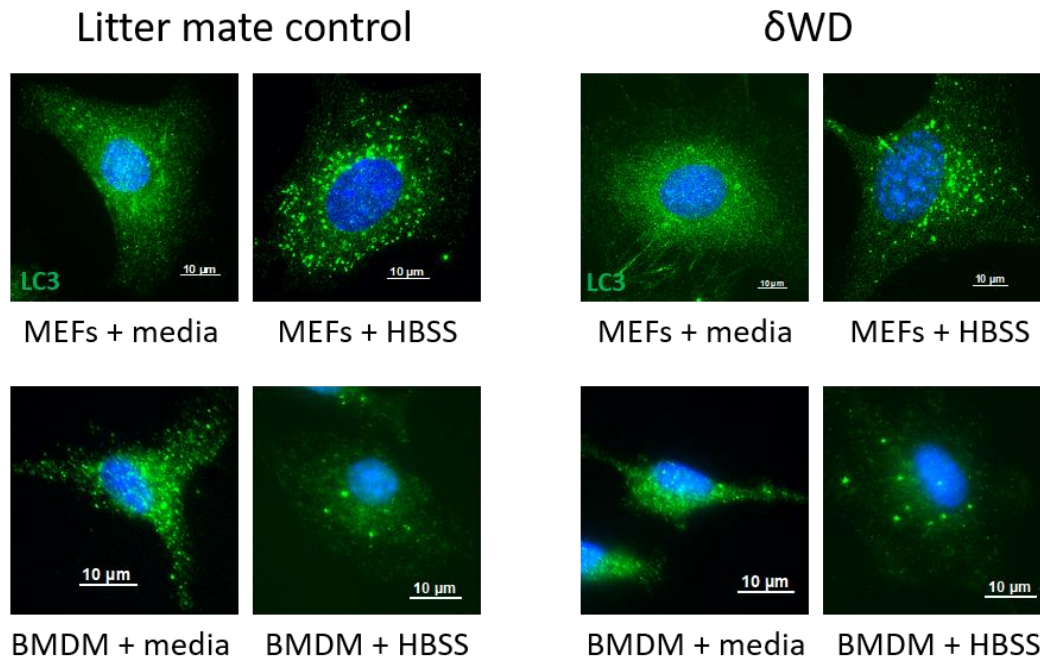
### 3.3 Characterisation of autophagy and LAP in cells from $\delta$ WD mice lacking the WD domain of ATG16L1.

Mouse embryonic fibroblasts (MEFs) and bone marrow-derived macrophage (BMDM) were isolated from  $\delta$ WD and WT (litter mate control) mice to study the effect of loss of the WD domain and linker region of Atg16L1 on starvation induced autophagy. The distribution of LC3 was analysed by immunofluorescence microscopy in cells incubated in control nutrient media or HBSS to induce autophagy [Figure 3.3]. MEFs and BMDM from WT and  $\delta$ WD mice generated LC3-positive puncta during starvation. This indicates that the Atg5-binding domain and CCD of ATG16L1 were sufficient for autophagy induced by starvation and that autophagy did not require the WD domain.

The ability of cells from control and  $\delta$ WD mice to active non-canonical autophagy was tested using monensin which activates non-canonical autophagy by changing the osmotic balance and pH in endosomes resulting in recruitment of LC3 onto endo-lysosomal membranes. After 2hrs, cells were fixed, and the location of LC3 was analysed by immunostaining. In control MEFs LC3 was tightly associated with swollen endo-lysosomal membranes induced by monensin, indicated by a ring structure of LC3 labelling [Figure 3.4A]. While, in  $\delta$ WD MEFs, LC3 accumulated as small puncta but failed to form a ring of LC3 surrounding the endo-lysosomal membranes [Figure 3.4B]. A similar experiment incubated BMDM with Zymosan to induce LAP. Zymosan is a preparation of killed *S. cerevisiae* conjugated Alexa Fluor™ 594. Zymosan particles engulfed by control macrophages were trapped in phagosomes which recruited LC3 thus indicating LAP [Figure 3.4C], while in  $\delta$ WD macrophages, LC3 failed to label phagosomes containing Zymosan and remained distributed throughout the cytoplasm [Figure 3.4D]. These results show that cells from littermate control mice were able to active non-

canonical autophagy and LAP, while cells from  $\delta$ WD mice were deficient in non-canonical autophagy and LAP.

**A**



**B**

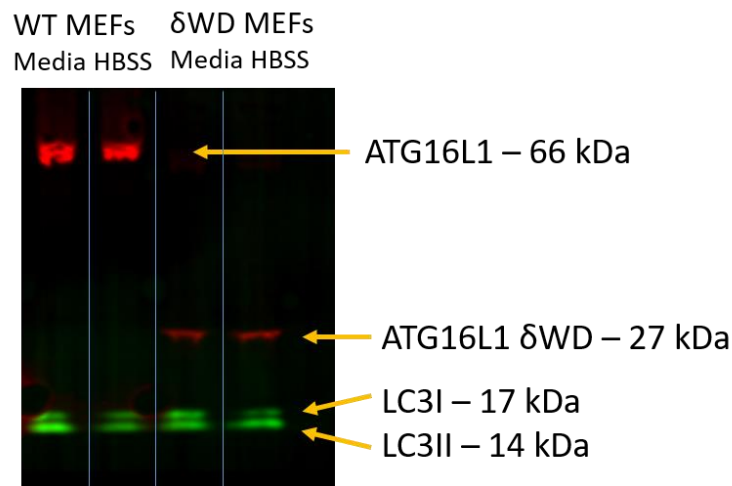


**Figure 3.3. Analysis of autophagy in cells cultured from mouse strains.** Mouse embryonic fibroblasts (MEFs) or bone marrow derived macrophages (BMDM) were incubated in control nutrient media or in HBSS for 2 hours to induce autophagy. Litter mate controls indicate cells from wild type mice,  $\delta$ WD indicates mice lacking WD domain of ATG16L1. **A.** Autophagosomes were identified as fluorescent puncta following immunofluorescence staining for LC3 (Alexafluor 488 green). Nuclei were counterstained using DAPI (blue). Bars: 10 $\mu$ m. **B.** Activation of autophagy was analysed by LC3 western blot. Production of LC3II indicates lipidation of LC3.

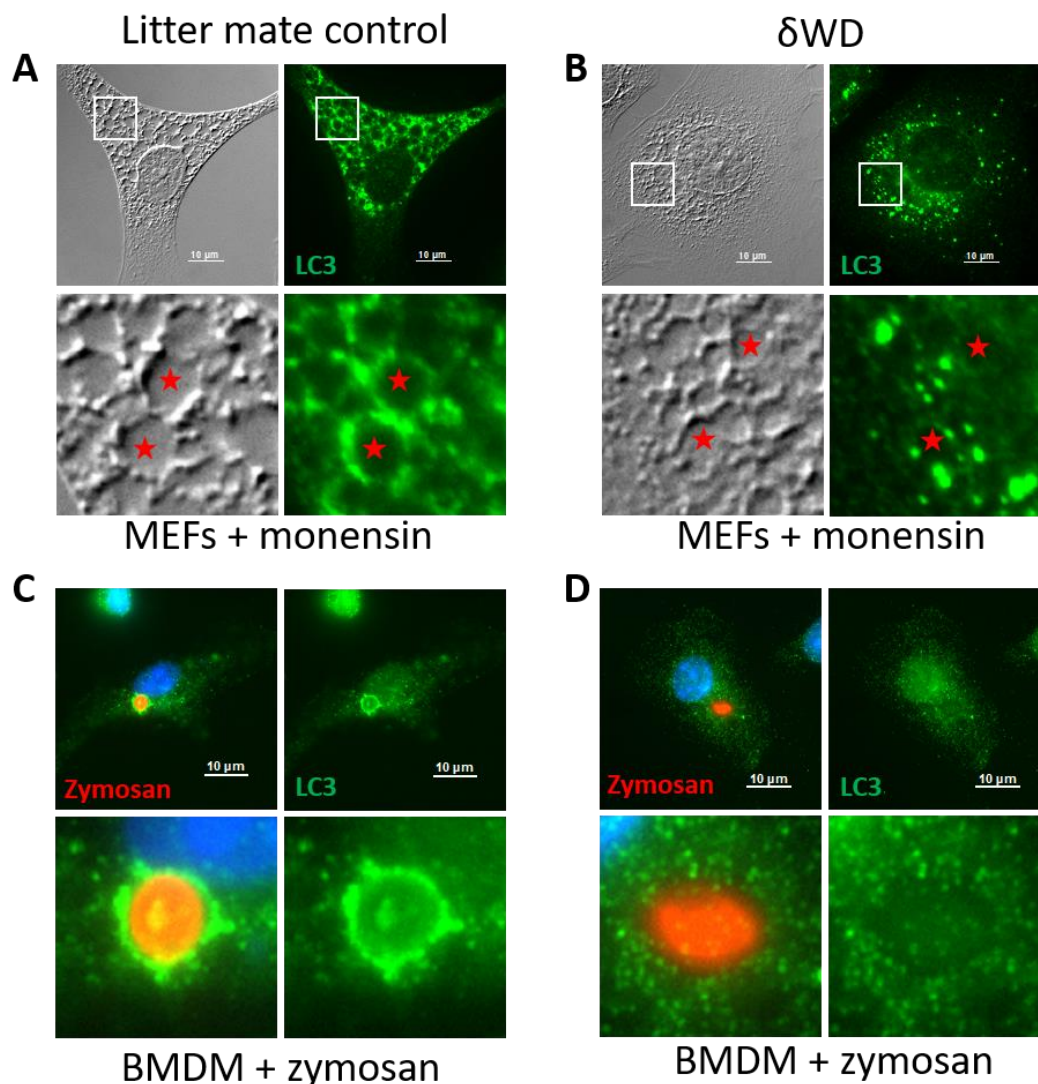


**Figure 3.4. Analysis of non-canonical autophagy and LAP in cells cultured from mouse strains. A and B: non-canonical autophagy.** Mouse embryonic fibroblasts (MEFs) were incubated in control nutrient media or in media containing monensin for 2 hours to induce non-canonical autophagy. Non-canonical autophagy was indicated by the recruitment of LC3 to swollen vesicles following immunofluorescence staining for LC3 (Alexafluor 488 green). Litter mate controls indicate cells from wild type mice,  $\delta$ WD indicates mice lacking WD domain of ATG16L1. **C and D: LAP.** Bone marrow derived macrophages (BMDM) were incubated in nutrient media containing Zymosan for 2 hours. LAP was indicated by the recruitment of LC3 to phagosomes containing Zymosan (red) following immunofluorescence staining for LC3 (Alexafluor 488 green).

In conclusion, the  $\delta$ WD mice are able to power starvation induced autophagy but have a defect in non-canonical autophagy including LAP. Therefore,  $\delta$ WD mice provide an excellent system to understand the role played non-canonical autophagy pathways during infection without confounding off pathway reactions resulting from loss of canonical autophagy.

### **3.4. Role played by WD domain of ATG16L1 during airway challenge with IAV**

#### **3.4.i Weight loss and mortality**

There are two mouse adapted strains of influenza A virus, H1N1 PR8 and H3N2 X31, and they were verified in mice models (Groves et al., 2018). The X31 strain have been choose to do the in vivo infection as it is less lethal than PR8 (Bouvier & Lowen, 2010). Mice were challenged with H3N2 X31 (a low dose of 100pfu and a high dose of 1000pfu separately) by inhalation, weight loss and mortality were monitored. According to figure 3.5A, both  $\delta$ WD mice and littermate controls lost weight from day1-7 post infection, and recovered from day7.  $\delta$ WD mice showed more rapid weight loss compared to littermate controls, significant different start from day 5. At day 7, the littermate controls lost nearly 20% body weight, while  $\delta$ WD mice showed greater weight loss reaching 27% loss, after day 7,  $\delta$ WD mice recovered more slowly from infection, and many were culled reaching 30% weight loss according to the home office [Figure 3.5B].

#### **3.4.ii Role played by WD domain of ATG16L1 on virus lung titre during IAV infection**

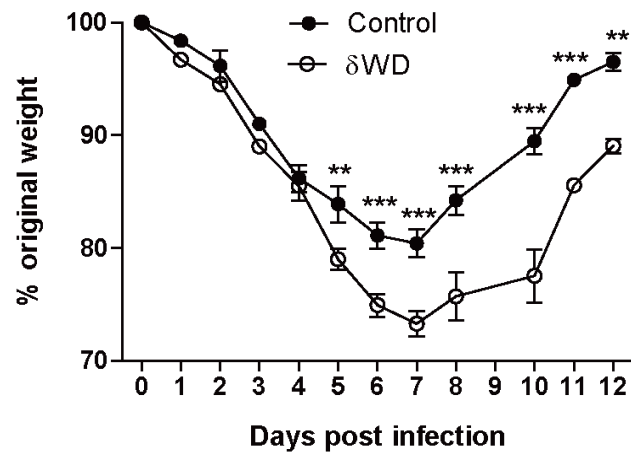
Two viral doses were tested in the mouse model: a low dose of 100pfu and a high dose of 1000pfu.

##### *3.4.ii.a Low dose IAV infection (100pfu).*

Mice were challenged with H3N2 X31 (100 pfu/mice) and sacrificed at day 1, 5 and 6, and lungs were taken to assess viral replication level by q-PCR and plaque assay separately. According to Figure 3.6A, q-PCR result showed the viral mRNA level in lungs of  $\delta$ WD mice was more than 5 times higher than littermate controls on day 5 pi, no significant difference was observed on day 6 pi. Consistently, the plaque assay results show the viral titre was approximately 5 times higher in  $\delta$ WD mice compared to control at day 5 and again, viral load was reduced in both mice on day 6 pi, with no significant difference observed between mice at day 6 Figure 3.6B. Both the q-PCR and plaque assay results demonstrated that IAV X31

shows a higher viral replication level and viral load in  $\delta$ WD mice than littermate controls, suggesting the  $\delta$ WD mouse has increased sensitivity to IAV infection.

A



B

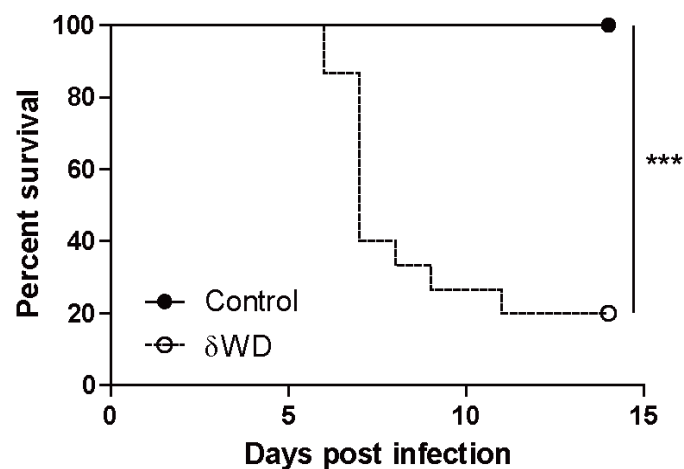


**Figure 3.5. Weight loss and mortality following challenge of mice with influenza virus.** Mice were given intranasal challenge of influenza virus strain X31 (1000pfu). Mice (n=6) were monitored for weight loss (**panel A**) or mortality (**panel B**) at the indicated time points. Significance was determined by 2-way ANOVA. A repeated-measures two-way ANOVA (Bonferroni post-test) was used for time-courses of weight loss; log-rank (Mantel-Cox) test was used for survival curves; P values were set at 95% confidence interval.

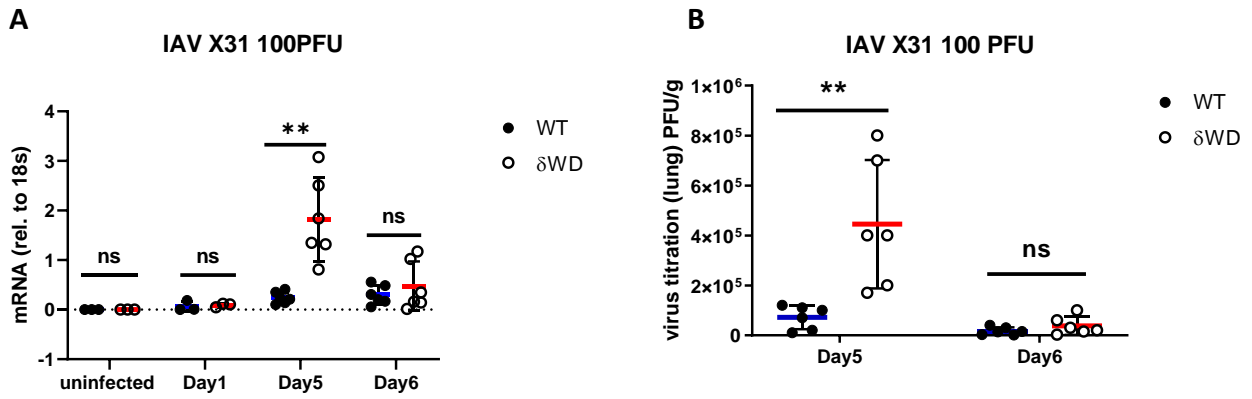


**Figure 3.6. Analysis of virus replication in lungs following challenge of mice with low dose of influenza virus.** Mice were given intranasal challenge of influenza virus strain X31 (100pfu). Lungs were removed from mice (n=6) at the indicated times and analysed for virus genome by q-PCR (**panel A**), or virus by plaque assay (**panel B**). Significance was determined by 2-way ANOVA with Bonferroni post-tests (\* $p < 0.05$ ), data represent the mean value  $\pm$  SD.

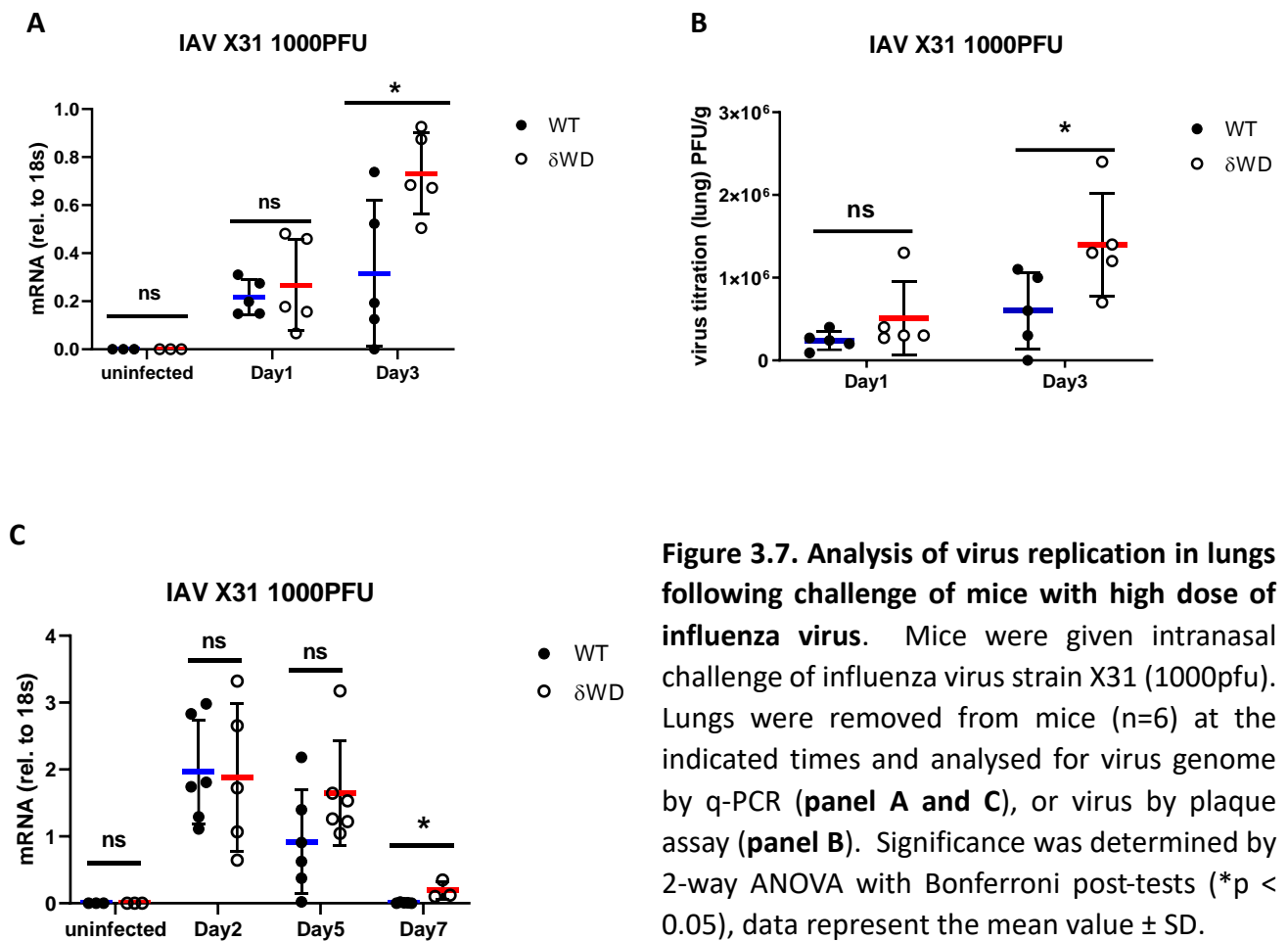


**Figure 3.7. Analysis of virus replication in lungs following challenge of mice with high dose of influenza virus.** Mice were given intranasal challenge of influenza virus strain X31 (1000pfu). Lungs were removed from mice (n=6) at the indicated times and analysed for virus genome by q-PCR (**panel A and C**), or virus by plaque assay (**panel B**). Significance was determined by 2-way ANOVA with Bonferroni post-tests (\* $p < 0.05$ ), data represent the mean value  $\pm$  SD.

#### *3.4.ii.b. High dose IAV infection (1000pfu).*

In the next experiment mice were challenged with 1000 pfu and the q-PCR and plaque assay results are shown [Figure 3.7]. Both the viral mRNA level and viral load in  $\delta$ WD mice were approximately 2 times higher than littermate controls at day 3 pi, suggesting  $\delta$ WD mice are more susceptible than WT mice to high dose IAV infection, indicating an important role played by non-canonical autophagy in suppressing IAV replication early during infection. The experiment was repeated to cover more time points. Lung samples from different time points (day2, 5, 7 pi) following high viral dose challenge were collected and viral mRNA expression was measured by q-PCR. Results in Figure 3.7C show that the viral mRNA level increased rapidly on day 2 pi in both of the mouse models, and it was not possible to see a difference in the mean levels between control and  $\delta$ WD mice. On day 5 pi, the viral mRNA level was reduced by half in control mice compared to day 2 pi, while in  $\delta$ WD mice the mean viral mRNA level fell more slowly. There was high variability and the difference between control and  $\delta$ WD mice was not significant. On day 7 pi, viral mRNA level decreased dramatically in both of the mouse models to close to basal levels.

In general, the mean level of viral replication either assayed by plaque assay or measured by qPCR shows significant increase in  $\delta$ WD mice than littermate controls. This is seen on day 5 pi with the low dose around 5-fold increases in  $\delta$ WD mice, and on day 3 and 7 pi with high dose around 2-fold increases in  $\delta$ WD mice. In summary, the study of viral replication in the lung suggest that the  $\delta$ WD mice is more susceptible than control mice to IAV infection indicating the important role played by non-canonical autophagy in suppressing IAV replication.

### **3. 4.iii Role played by WD domain of ATG16L1 on cytokine production during IAV infection.**

#### *3.4.iii.a Introduction*

The outcome of IAV infection is dependent on the balance between protective innate immune responses that limit infection and the damage caused by excessive inflammation arising from cytokine secretion into the lungs (X. Chen et al., 2018). The host mucosal layer covering the respiratory epithelial cells is the first barrier to influenza infection. After breaking the mucosal barrier, influenza virus binds to sialic acid receptors on the respiratory epithelial cells and

enters cells via endocytosis to start replication (Ramos & Fernandez-Sesma, 2015). Innate immune signalling pathways activated during infection of lung epithelial cells and resident alveolar macrophages, result in the release of interferons (IFN  $\alpha/\beta/\lambda$ , ISGs) which generate a central antiviral effect in neighbouring cells (Camp & Jonsson, 2017; Cole & Ho, 2017). IFNs also stimulate production of pro-inflammatory cytokines such as IL-1 $\beta$ , IL-6 and TNF $\alpha$ . Pro-inflammatory cytokines released by lung epithelial cells and resident alveolar macrophages then signal endothelial cells to secrete chemokines to help spread inflammatory signals. Chemokines, such as CCL2 (MCP-1) and CXCL, spread throughout the circulation, recruiting neutrophils, monocytes and NK cells (Camp & Jonsson, 2017). Neutrophils, recruited by CXCL-1 (IL-8 in humans), secrete cytokines, reactive oxygen species (ROS) and neutrophil extracellular traps (NET) to control pathogen spread (Camp & Jonsson, 2017).

The acquired immune response begins when monocytes recruited primarily by CCL2, differentiate into macrophages or DCs to contribute to inflammation and antigen presentation, bridging the innate and adaptive immune responses during the IAV infection (Camp & Jonsson, 2017; Cole & Ho, 2017); NK cells, also recruited by CCL2, can induce an antiviral state by secretion of type II IFNs (IFN $\gamma$ ), and induce apoptosis of infected cells by secretion of granzyme B, thus limiting viral replication, propagation and spreading (Cole & Ho, 2017).

As the major inflammatory mediator during IAV infection, cytokines and IFNs are released rapidly by lung epithelial and innate immune cells through 3 main pathways. Single-stranded viral RNA in the cytosol of infected epithelial cells is recognized by retinoic acid-inducible gene-I (RIG-I), leading to activation of IRF3 and NF- $\kappa$ B pathways, which stimulate the expression of IFNs, ISGs and pro-inflammatory cytokines. When infected cells are phagocytosed by macrophages, double-stranded RNA from infected cells is recognized by Toll-like receptor 3 (TLR3) in endosomes, which also leads to the activation of IRF3 and NF- $\kappa$ B pathways, and release of IFNs, ISGs and pro-inflammatory cytokines. The release of single-stranded RNA (ssRNA) within plasmacytoid dendritic cells (pDCs), can lead to TLR7 signalling inducing IRF7 and NF- $\kappa$ B activation, leads to secretion of IFNs, ISGs and NF- $\kappa$ B-dependent cytokines (Iwasaki & Pillai, 2014). As a result, large amount of IFNs and cytokines are produced and released in the lung to defence against IAV infection.

IFNs and cytokines are crucial to restrict virus replication, active inflammatory and immune response that protect host from pathogens infection. While the excessive cytokine production can also be a potential weapon that causes the host tissue damage when it becomes uncontrolled and results in tissue edema, multiple organ failure and death (Sivro et al., 2011). Studies suggest that the pro-inflammatory cytokines such as IL-6, IL-1 $\beta$  and TNF- $\alpha$  are overexpressed at higher serum levels in patients with severe infection compared with the moderate disease (Chiaretti et al., 2013; Garcia-Ramirez et al., 2015; Zuniga et al., 2011). Therefore, the regulation of cytokines production seems to be the key factor to determine the outcomes of influenza infection.

Previous studies suggest autophagy plays an important role in regulating inflammatory response and controlling the cytokine production (Crisan et al., 2011; Harris et al., 2011; Shi et al., 2012), while the role played by non-canonical autophagy is still unclear. The aim of this experiment is to identify roles played by non-canonical autophagy in regulating of cytokine production and innate immune response during influenza infection in vivo. To do this the  $\delta$ WD mouse model is used utilized to determine if non-canonical autophagy deficiency affects cytokine expression after IAV infection.

#### *3.4. iii.b The role of non-canonical autophagy in maintaining inflammatory threshold*

Non-canonical autophagy shares core autophagy proteins required to conjugate LC3 to PE in cellular membranes. Many studies describe the important role played by autophagy in controlling the inflammatory response (Kuballa, Nolte, Castoreno, & Xavier, 2012; Qian, Fang, & Wang, 2017). In vitro studies in macrophages taken from mice lacking ATG16L1 for example, show increases in IL-1 $\beta$  secretion in response to TLR ligands. A study based on autophagy deficient mouse models suggests that LysMcre-mediated loss of autophagy from myeloid cells raises the inflammatory threshold 'in vivo'. In the lung, this raised cytokine-based inflammation results in a resistance to lethal influenza virus infection (Lu et al., 2016). It was therefore important to consider if the  $\delta$ WD mutation increased the levels of inflammatory cytokines in the lung before challenge with IAV.

The basal mRNA expression levels of interferons and cytokines in the mouse models were tested before challenge with IAV. The results in Figure 3.8, shows that in mice with LysMcre mediated loss of *ATG16L1* from myeloid cells (*Atg16<sup>fl/fl</sup>-LysMcre*) there was an increased

expression of CXCL-1, IL-1 $\beta$  and IL-6 compared to the littermate control. Importantly, there was no difference observed between  $\delta$ WD and littermate controls. These results indicate that, as described previously, autophagy deficiency in phagocytic cells resulting from complete loss of ATG16L1 generates a pro-inflammatory environment in mouse lung prior to infection. The results in Figure 3.8, however, show that loss of the WD domain in the whole animal model does not induce a pro-inflammatory response. Taken together, these results allow us to investigate the direct role played by WD dependent non-canonical autophagy during influenza infection rather than indirect effects on inflammation.

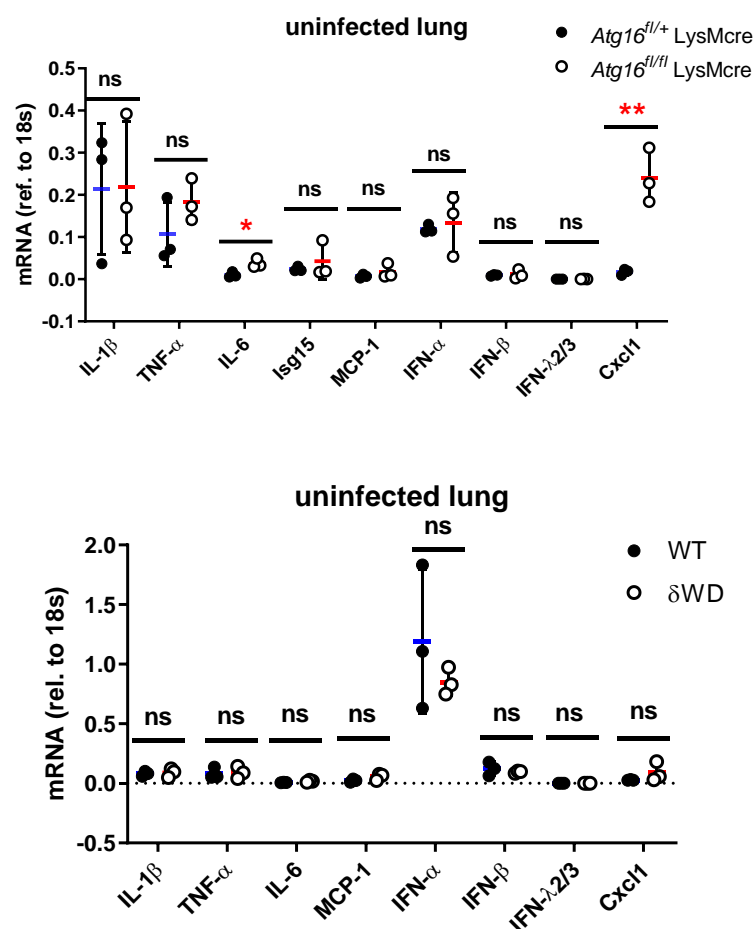


**Figure 3.8 Analysis of basal cytokine expression level in lungs from *Atg16L1<sup>fl/fl</sup>*-LysMcre and  $\delta$ WD mice model.** Mice from *Atg16L1<sup>fl/fl</sup>*-LysMcre,  $\delta$ WD and their littermate controls were sacrificed. Lungs were removed from mice (n=3) and analysed for indicated cytokine genes by q-PCR. Significance was determined by T-tests (\*p < 0.05), data represent the mean value  $\pm$  SD.

### *3.4.iii.c Analysis of cytokine mRNA expression after IAV infection*

Mice were challenged with H3N2 X31 by inhalation, mRNA expression levels of IFNs, cytokines and chemokines were determined by q-PCR at certain days post infection (dpi). Two viral dose were given to the mice model: 100PFU (low dose) and 1000PFU (high dose).

**Expression of interferons.** The interferon family play a major role in antiviral responses which is critical in restricting the early stages of virus infections before the activation of the adaptive immune system (Killip et al., 2015). IFN- $\lambda$  is released by lung epithelial cells at the initial stage of infection, acts locally at epithelial barrier to restrict virus replication and limit viral spread without activating inflammatory responses. Once infection escapes IFN- $\lambda$  control, IFN- $\alpha/\beta$  are induced to enhance antiviral responses and induce pro-inflammatory responses (Galani et al., 2017). Neutrophils participate in antiviral defence by expression numerous of ISGs in response of both type I and type III IFNs, while they express pro-inflammatory mediators only in response to type I IFNs at early stage of infection responses (Galani et al., 2017).

**Expression of pro-inflammatory cytokines.** Pro-inflammatory cytokines including IL-1 $\beta$ , IL-6 and TNF $\alpha$  play crucial roles in inflammation, infection, and responses to stress induced by infections. Interleukin-1 $\beta$  (IL-1 $\beta$ ) is considered as a central cytokine that mediates inflammatory response by recruiting immune cells against virus infection, it also induces the expression of pro-inflammatory genes such as IL-6, Cxcl1 (IL-8), CCL2 (MCP-1), that promoting the pro-inflammatory response (Kim, Jung, Shin, Choi, & Kim, 2015; Weber et al., 2010). IL-6, which play a key role in regulating the immune and acute phase responses during infection, can be induced by other pro-inflammatory cytokines, such as TNF- $\alpha$  and IL-1 $\beta$  (Hunter & Jones, 2015; Scheller, Chalaris, Schmidt-Arras, & Rose-John, 2011). TNF- $\alpha$  mediates a wide spectrum of multiple pro-inflammatory and immunological functions, which triggers the local immune response and controls infection (Sladkova & Kostolansky, 2006).

Mice were challenged with H3N2 X31 (100 PFU/mice) and sacrificed at day 1, 5 and 6 pi. Lungs were taken to measure the cytokine mRNA expression levels by q-PCR. Figure 3.9 shows the expression levels of IFNs including, IFN- $\alpha$ , IFN- $\beta$ , IFN- $\lambda$ 2,3 and ISG15. Expression of ISG15 and all the IFNs in  $\delta$ WD mice were significantly higher than littermate controls on day 5 pi, but no significant difference was observed on day 6 pi.

The expression level of pro-inflammatory cytokines including IL-1 $\beta$ , TNF- $\alpha$  and IL-6; chemokines including MCP-1 and Cxcl-1 in lung were measured. The q-PCR result [Figure 3.10] shows that with low dose (100 PFU/mice) infection, the mRNA levels for all the cytokines and chemokines were significantly higher ( $\approx$  5-fold) in  $\delta$ WD mice compared to littermate controls on day 5 pi. Same with interferons no significant difference was observed on day 6 pi. These results demonstrate that all the IFNs, pro-inflammatory cytokines and chemokines were expressed at higher levels in  $\delta$ WD mice compared to the littermate controls after IAV infection, suggesting that non-canonical autophagy may suppress cytokine production in control mice.

The experiment was repeated using a high dose of IAV (1000 PFU/mice). Two independent trials were carried out, first trial including day 1 and 3 pi, second trial with day 2, 5 and 7 dpi. q-PCR results show that IAV induced a transient rise in interferon (ISG15, IFIT1, IFN- $\alpha$ ,  $\beta$ ,  $\lambda$ 2,3) [Figure 3.13] and pro-inflammatory cytokines [Figure 3.14] expression in the lungs of control and  $\delta$ WD mice lung at day 2 pi. RNA expression levels of all the interferons [Figure 3.11] and cytokines [Figure 3.12] tested show significant increases in  $\delta$ WD mice compared to litter mate control at 3 dpi. Increased cytokine expression was resolved in control mice, while in  $\delta$ WD mice IL-1 $\beta$  and Isg15 and TNF- $\alpha$  levels remain high on day7 pi [Figure 3.13 and 3.14], coincident with accelerated virus titre and weight loss [Figure 3.7, 3.5A]. The lungs of these mice showed high expression of CXCL1 and MCP-1 mRNA, they are chemotaxis factors for neutrophil and monocyte recruitment to the infection sites. These results demonstrate mice lacking non-canonical autophagy failed to control excessive cytokine production and lung inflammation during high dose IAV X31 infection.

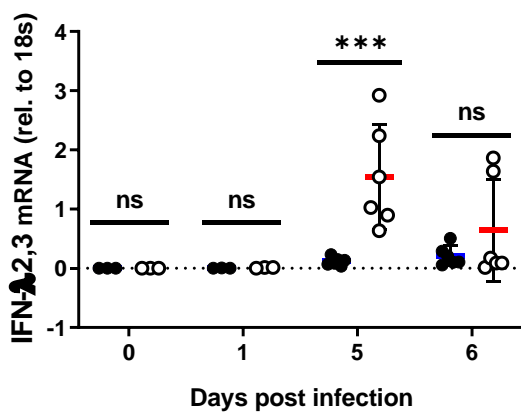
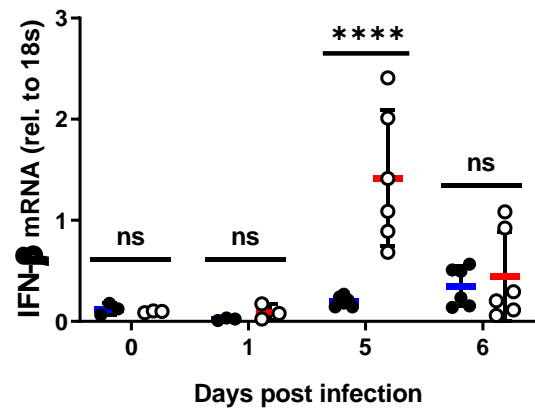
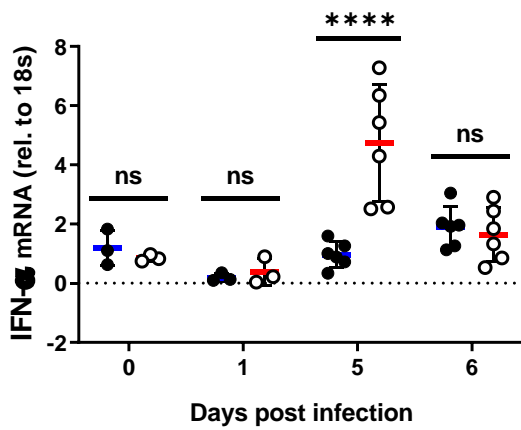
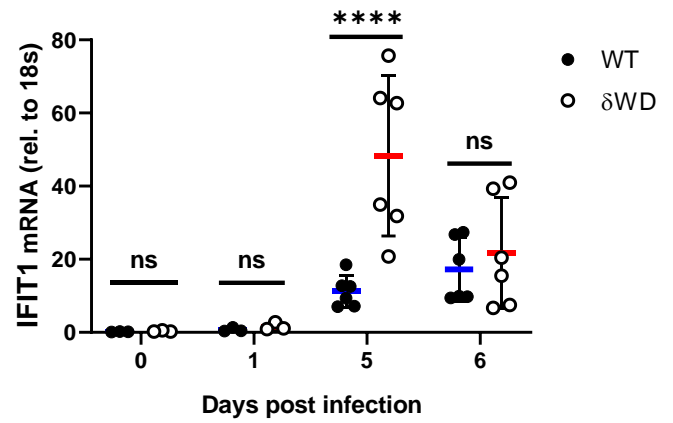
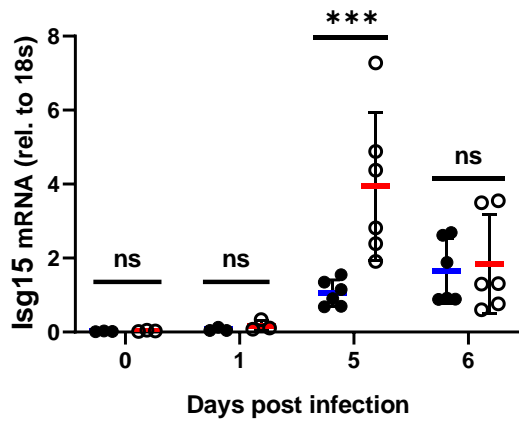


**Figure 3.9. Analysis of interferon expression in lungs following challenge of mice with low dose of influenza virus.** Mice were given intranasal challenge of influenza virus strain X31 (100pfu). Lungs were removed from mice (n=6) at the indicated times and analysed for indicated interferon genes by q-PCR. Significance was determined by 2-way ANOVA with Bonferroni post-tests (\* $p < 0.05$ ), data represent the mean value  $\pm$  SD.

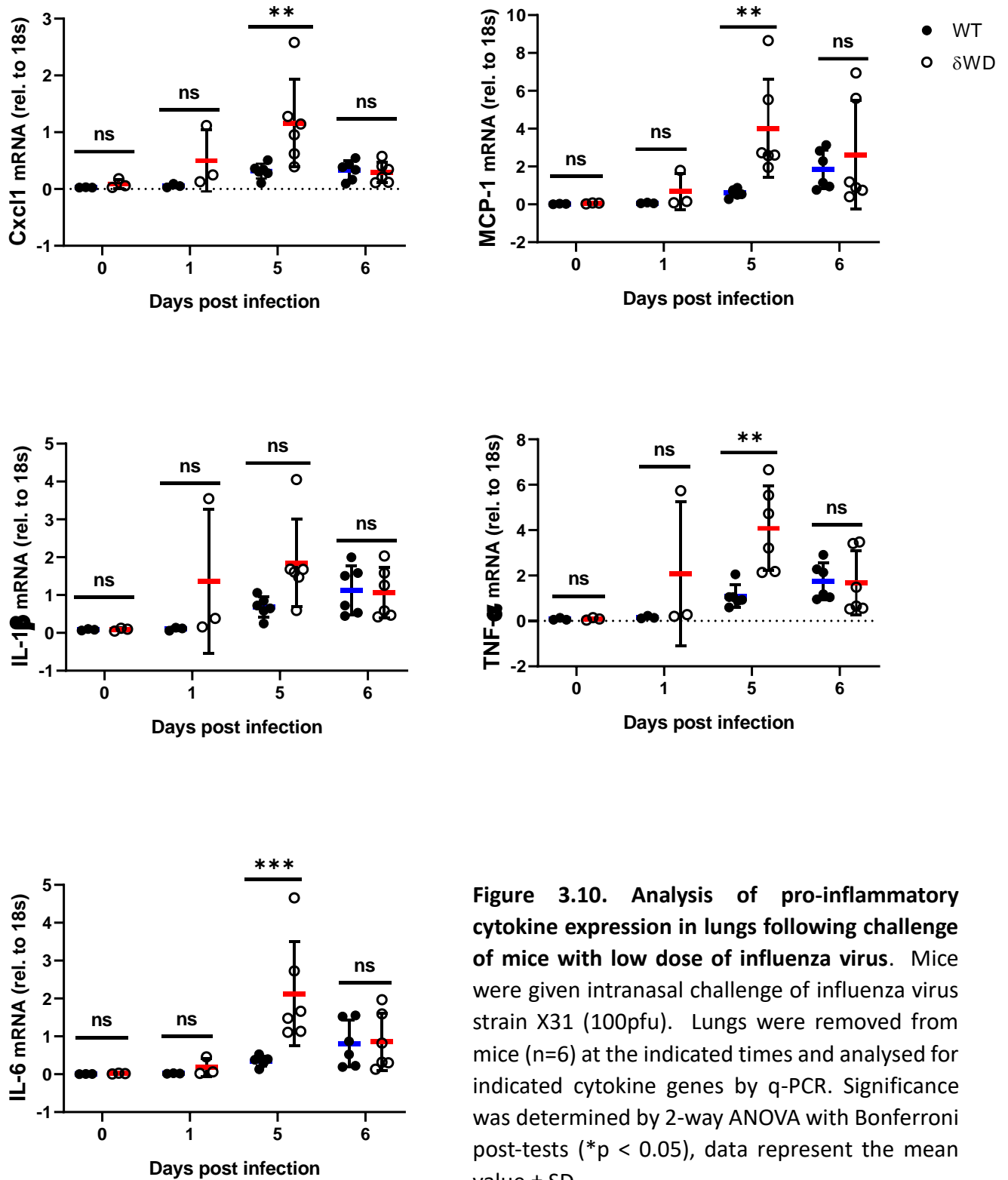


**Figure 3.10. Analysis of pro-inflammatory cytokine expression in lungs following challenge of mice with low dose of influenza virus.** Mice were given intranasal challenge of influenza virus strain X31 (100pfu). Lungs were removed from mice (n=6) at the indicated times and analysed for indicated cytokine genes by q-PCR. Significance was determined by 2-way ANOVA with Bonferroni post-tests (\*p < 0.05), data represent the mean value  $\pm$  SD.

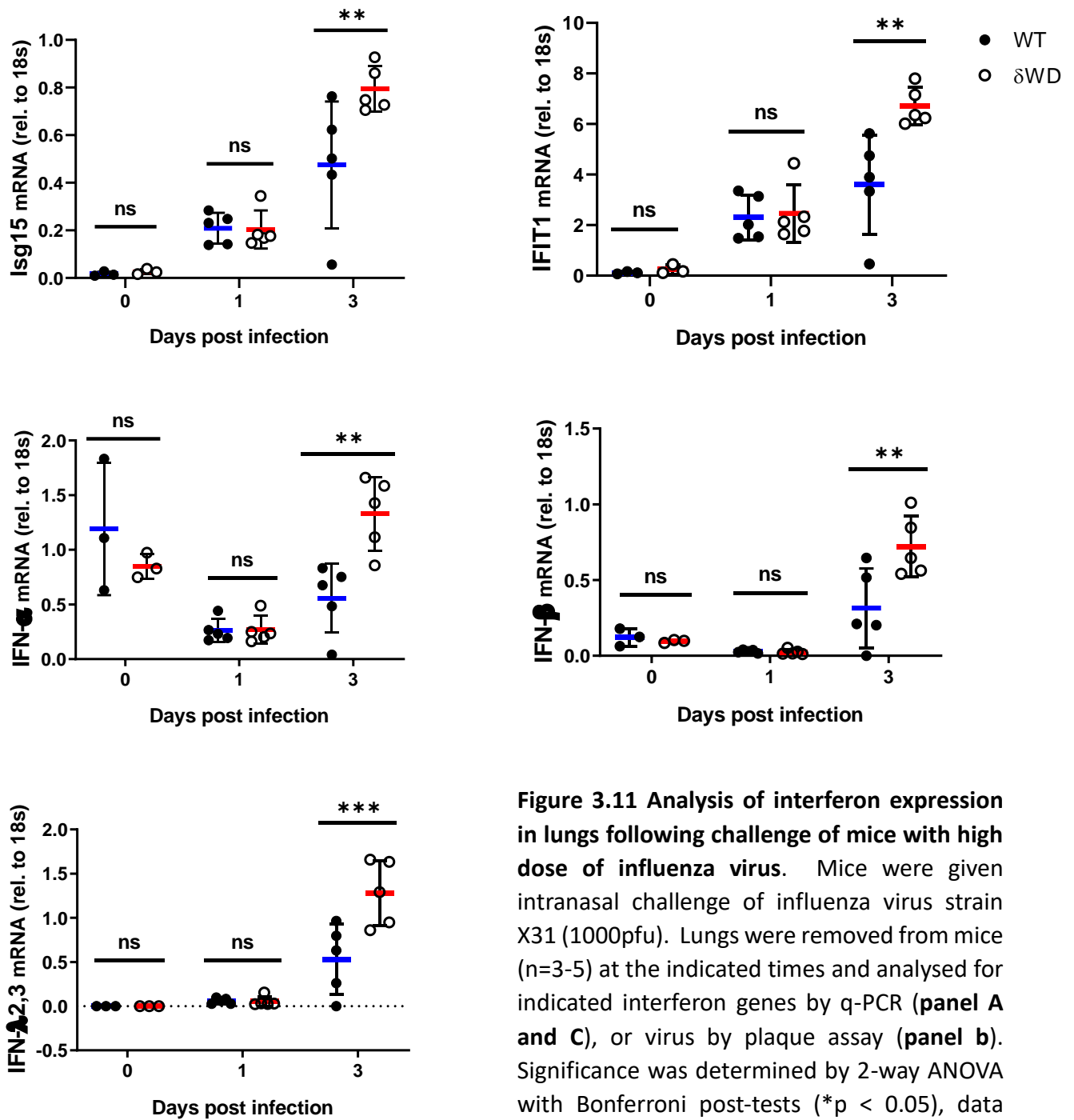


**Figure 3.11 Analysis of interferon expression in lungs following challenge of mice with high dose of influenza virus.** Mice were given intranasal challenge of influenza virus strain X31 (1000pfu). Lungs were removed from mice (n=3-5) at the indicated times and analysed for indicated interferon genes by q-PCR (**panel A and C**), or virus by plaque assay (**panel b**). Significance was determined by 2-way ANOVA with Bonferroni post-tests (\*p < 0.05), data represent the mean value  $\pm$  SD.

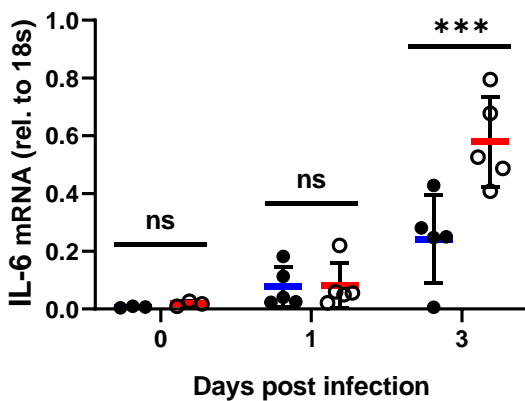
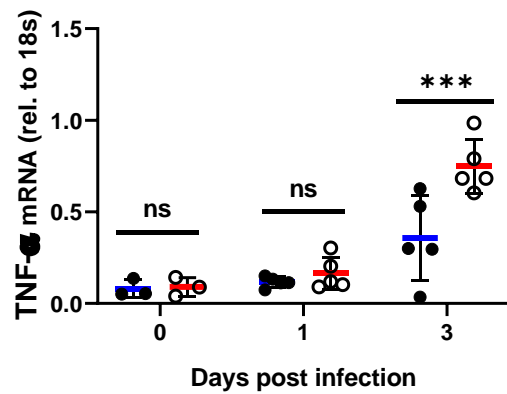
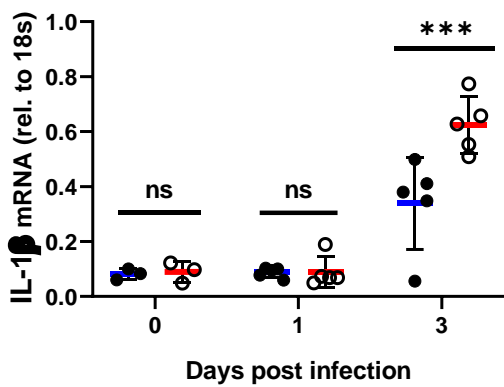
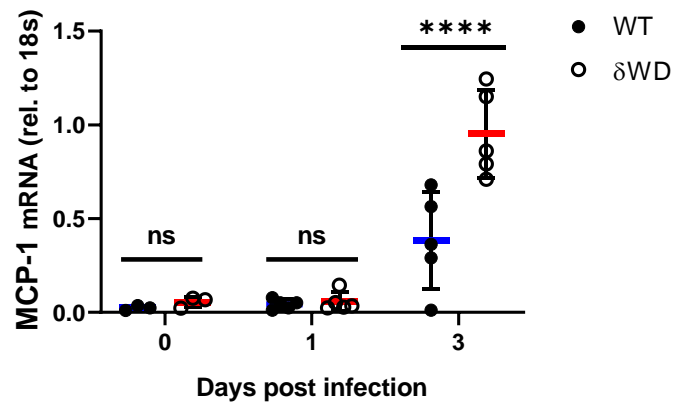
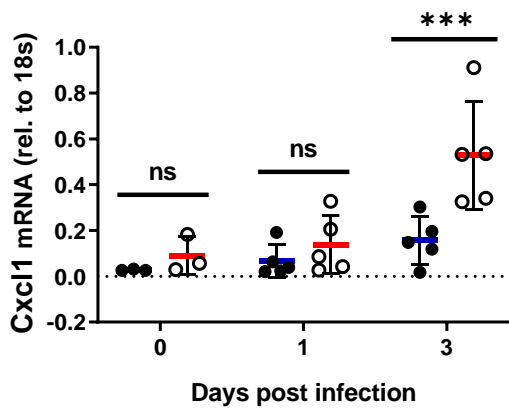


**Figure 3.12. Analysis of pro-inflammatory cytokine expression in lungs following challenge of mice with high dose of influenza virus.** Mice were given intranasal challenge of influenza virus strain X31 (1000pfu). Lungs were removed from mice (n=3-5) at the indicated times and analysed for indicated cytokines. Significance was determined by 2-way ANOVA with Bonferroni post-tests (\*p < 0.05), data represent the mean value  $\pm$  SD.

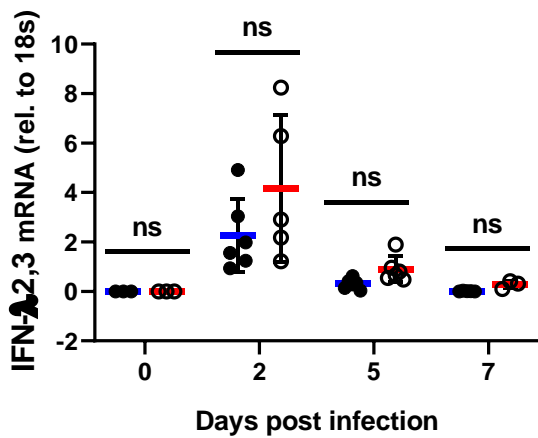
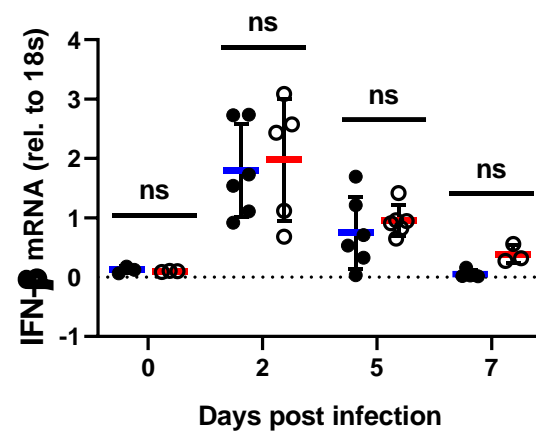
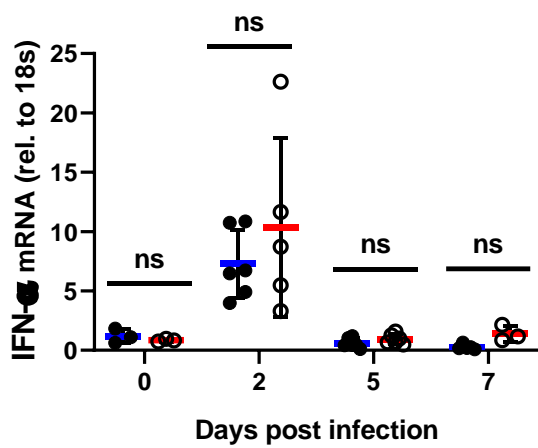
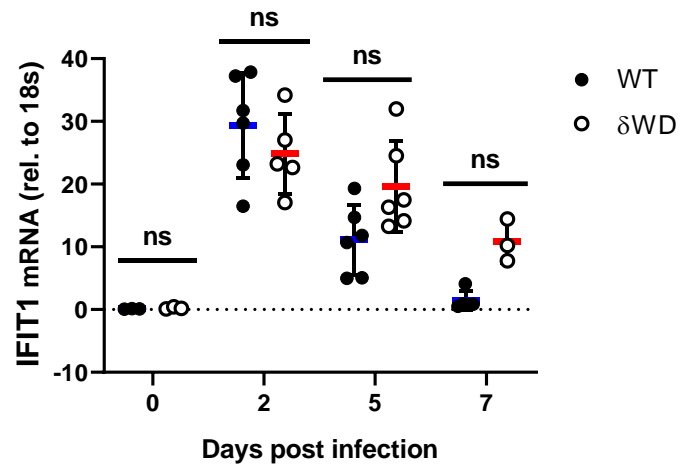
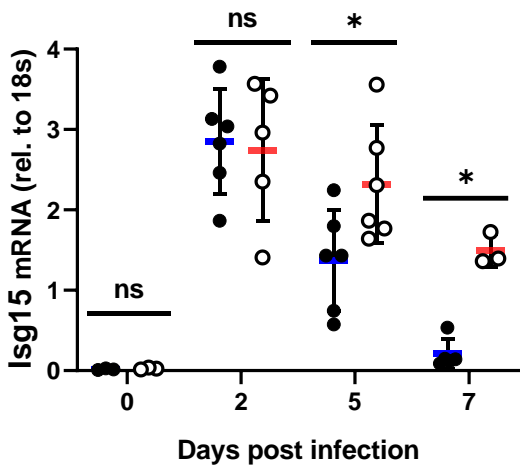


**Figure 3.13 Analysis of interferon expression in lungs following challenge of mice with high dose of influenza virus.** Mice were given intranasal challenge of influenza virus strain X31 (1000pfu). Lungs were removed from mice (n=3-6) at the indicated times and analysed for indicated interferon genes by q-PCR (**panel A and C**), or virus by plaque assay (**panel b**). Significance was determined by 2-way ANOVA with Bonferroni post-tests (\* $p < 0.05$ ), data represent the mean value  $\pm$  SD.

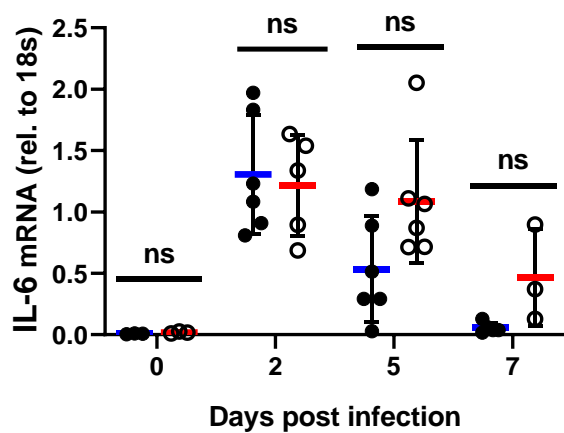
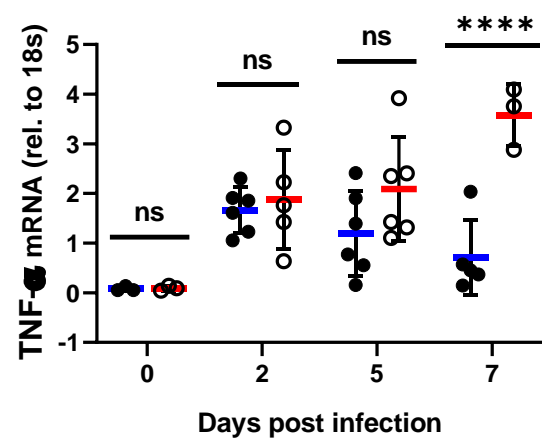
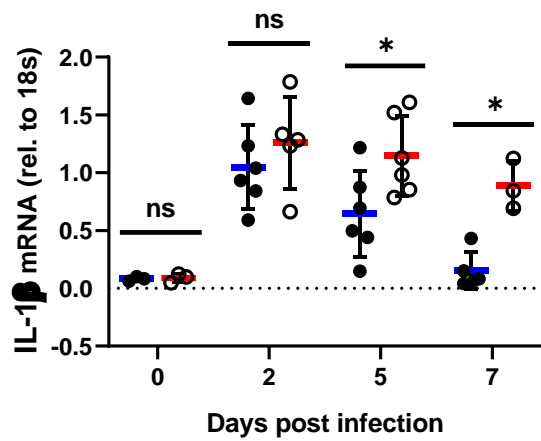
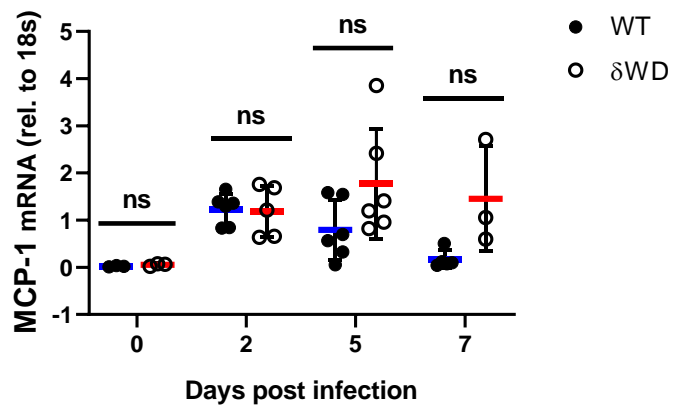
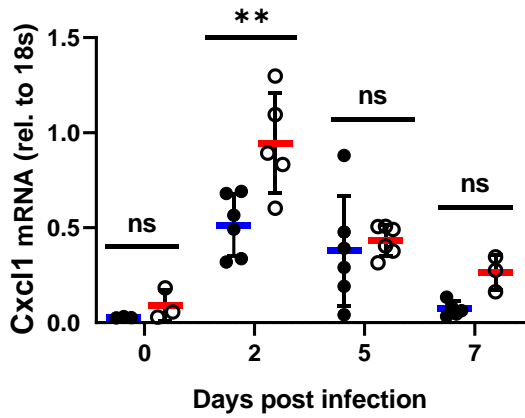


**Figure 3.14. Analysis of pro-inflammatory cytokine expression in lungs following challenge of mice with high dose of influenza virus.** Mice were given intranasal challenge of influenza virus strain X31 (1000pfu). Lungs were removed from mice (n=3-6) at the indicated times and analysed for indicated cytokines. Significance was determined by 2-way ANOVA with Bonferroni post-tests (\*p < 0.05), data represent the mean value  $\pm$  SD.

### 3.4.iii.d Analysis of cytokine protein expression after IAV infection

The results above showed that mRNA for pro-inflammatory cytokines increased in  $\delta$ WD mice compared to littermate control following IAV infection. The experiments below describe the use of a Luminex assay to determine if it was possible to detect increases in cytokine protein levels in lung.

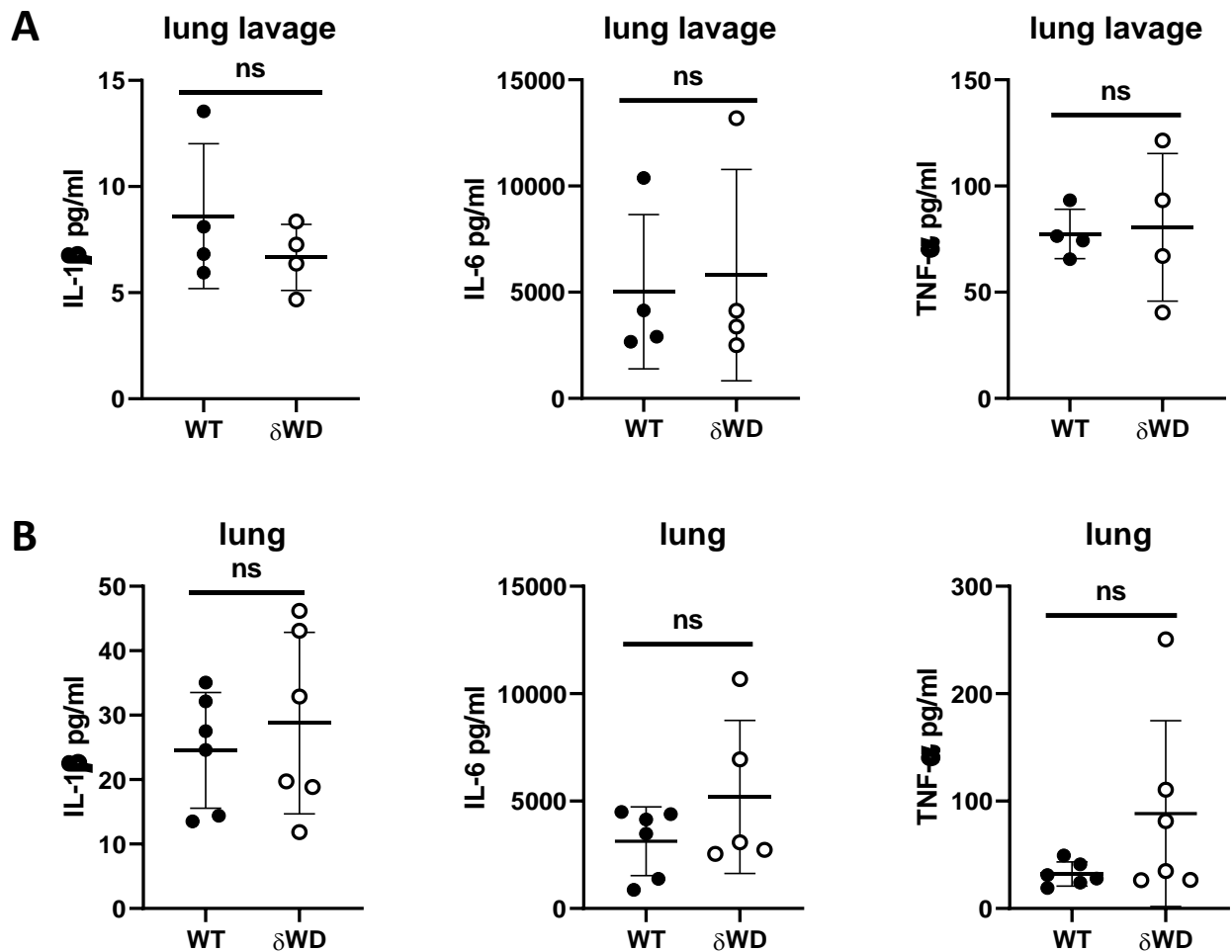


**Figure 3.15: Cytokines level in lungs detected by luminex assay, following challenge of mice with high dose of influenza virus.** Mice were given intranasal challenge of influenza virus strain X31 (1000pfu). Lung lavage were taken from mice (n=4) at 7 days post infection (A); lung samples were removed from mice (n=6) at 5 days post infection (B). The cytokines level in the lung or lung lavage were analysed by luminex assay. Significance was determined by Mann-Whitney U test (\* $p < 0.05$ ), data represent the mean value  $\pm$  SD.

Figure 3.15 shows the levels of cytokines released present in lung lavage or homogenised lung after IAV infection as detected by Luminex assay. The lung lavage was taken at 7 days post infection, and lung samples were taken at 5 days post infection from WT and  $\delta$ WD mice. This pilot experiment studied levels of pro-inflammatory cytokines including IL-1 $\beta$ , IL-6 and TNF- $\alpha$  that showed significant differences at the mRNA level between  $\delta$ WD mice and littermate controls during IAV infection.

The results show that it was not possible to detect significant differences in cytokine levels in lung lavage or homogenised lung tissue by Luminex. There was a slight increase in level of TNF- $\alpha$  in  $\delta$ WD mice lung samples at 5 days post infection, but no significance statistically. As the process of sample preparation and Luminex assay is time-consuming, and cytokines are not stable, it is possible that cytokines might degraded during sample processing. This may explain the large variation in the data sets. A similar problem with high variation in cytokine expression levels detected in lung is reported by Lu et al (2016) in a study of IAV infection of mice lacking Vici Syndrome gene Epg5. They required comparison of as many as 15 animals to achieve significant differences between mutant and control. Challenging this number of mice was not feasible in our study and the analysis concentrated on measurement of mRNA.

#### **3.4.iv Role played by WD domain of ATG16L1 on lung pathology following IAV infection**

##### *3.4.iv.a. Introduction:*

The results above suggest that the  $\delta$ WD mice are unable to control cytokine expression during IAV infection of the lung. It therefore seemed likely that excessive cytokine secretion would lead to a lung pathology indicating excessive inflammation. The pathology of animals infected with the IAV has been described previously (Fislova et al., 2009; Guarner & Falcon-Escobedo, 2009; van den Brand, Haagmans, van Riel, Osterhaus, & Kuiken, 2014). Accordingly, diffuse alveolar damage (DAD) is the usual pathologic manifestation of acute respiratory distress syndrome (ARDS) which could occur during extensive lung injury induced by IAV infection. The stages of DAD can be divided into an early exudative (acute) phase, a subacute proliferative (organizing) phase and a late fibrotic phase, depends on the pathologic changes (van den Brand et al., 2014). The exudative phase is most prominent in the first week of injury. The pathologic changes in the exudative phase include the interstitial and intra-alveolar hemorrhage and edema induced by the increased capillary permeability; lymphocytes

infiltrating the interstitium; development of hyaline membranes on alveolar wall where epithelium is denudated and disrupted (Guarner & Falcon-Escobedo, 2009). The proliferative phase begins after 1 week which is characterized by fibroblastic proliferation in alveolar spaces and interstitium, and epithelial cell regeneration characterized by type II pneumocyte hyperplasia (van den Brand et al., 2014). In the late fibrotic phase after 14 days, fibrosis appears in alveolar spaces and interstitium, with cellular fibroblastic proliferation and collagen deposition.

Leukocyte infiltration of the hyperemic alveolar septa is a sign of inflammation during influenza infection. The leukocytes are predominantly neutrophils and occasionally eosinophils in the early stages of influenza virus pneumonia. In the later stages, interstitial infiltrates of mononuclear leukocytes occur, predominantly lymphocytes and plasma cells. Necrotic areas are associated with leukocytic infiltrates, exudation of fibrin, and disappearance of alveolar lining cells. Hemorrhage into the alveolar air spaces is often observed near necrotic areas, associated with the exudation of plasma and strands of fibrin (Taubenberger & Morens, 2008). This chapter is going to use pathology to investigate the severity of lung infection in the mouse genotypes mice after influenza infection.

#### *3.4.iv.b General pathology*

The mice described above were challenged with H3N2 X31 by inhalation and sacrificed at indicated days post infection. Half of each lung was taken for analysis of cytokine expression and virus replication. The other half was fixed for histology. Each mouse received a high dose of X31 IAV (1000pfu). Lung tissues were harvested at 7 days pi. The lungs sections were stained with H&E or anti-IAV and processed for immunohistochemistry to detect IAV antigen. According to Figure 3.16, control mice exhibit clear signs of infection with necrosis, and lymphocytes migrating through the bronchiolar epithelium. Surrounding vessels contain inflammatory infiltrates dominated by lymphocytes. This inflammation often extended into the surrounding alveoli, with lymphocytes and oedema. According to Figure 3.17, IAV antigen is present rarely in a few bronchioles, in the debris which is present in the lumen. Lung sections from the  $\delta$ WD mice exhibited similar lesions, but they were more extensive, extending more distally in the lung, to smaller bronchioles and to the majority of the alveolar lumen. Severe inflammatory infiltration and oedema distributed throughout the lung lobes. There was also more IAV antigen in the bronchiolar epithelium and alveoli area in  $\delta$ WD mice

compared to littermate controls. The percentage area of anti-IH labelling (for IAV detection) were quantified by ImageJ. The quantification results suggest the percentage of IAV infected area is significant high in  $\delta$ WD mice than littermate controls at 7 days pi.

#### *3.4.iv.c. Lymphocyte infiltration*

The data following cytokine expression showed high expression of neutrophil chemotaxis factor at day 2 and 3 pi. To detect neutrophils infiltration and netosis, the  $\delta$ WD and littermate control mice were infected with 1000 pfu IAV X31 and lung tissues were harvested at 3d p.i. Neutrophils and H3 (marker of netosis) were labelled by anti-Ly6G and anti-H3, immunohistochemistry of sections counter-stained with hematoxylin. Micrographs of representative areas from lungs of 2-3 mice are shown, and the percentage area of antibody labelling were quantified by ImageJ. According to Figure 3.18, there was an accumulation of neutrophils in bronchi and bronchioles of both mice and obvious bronchiolitis. Far less neutrophils were, however, detected in alveolar space in littermate controls. There was a dramatic increase in numbers of neutrophils infiltrating the airways (bronchi and bronchioles) and lung parenchyma in  $\delta$ WD mice, accompanied by significantly-increased netosis [Figure 3.19]. In addition, there were large consolidated, cell rich areas in  $\delta$ WD mice, often with necrosis of cells, which was absent in littermate controls. The quantification results suggest, the main level of neutrophil infiltration and netosis are high in  $\delta$ WD mice at 3 days pi. No significant difference was shown, due to the limited sample size.

## Day7 p.i. H&E staining

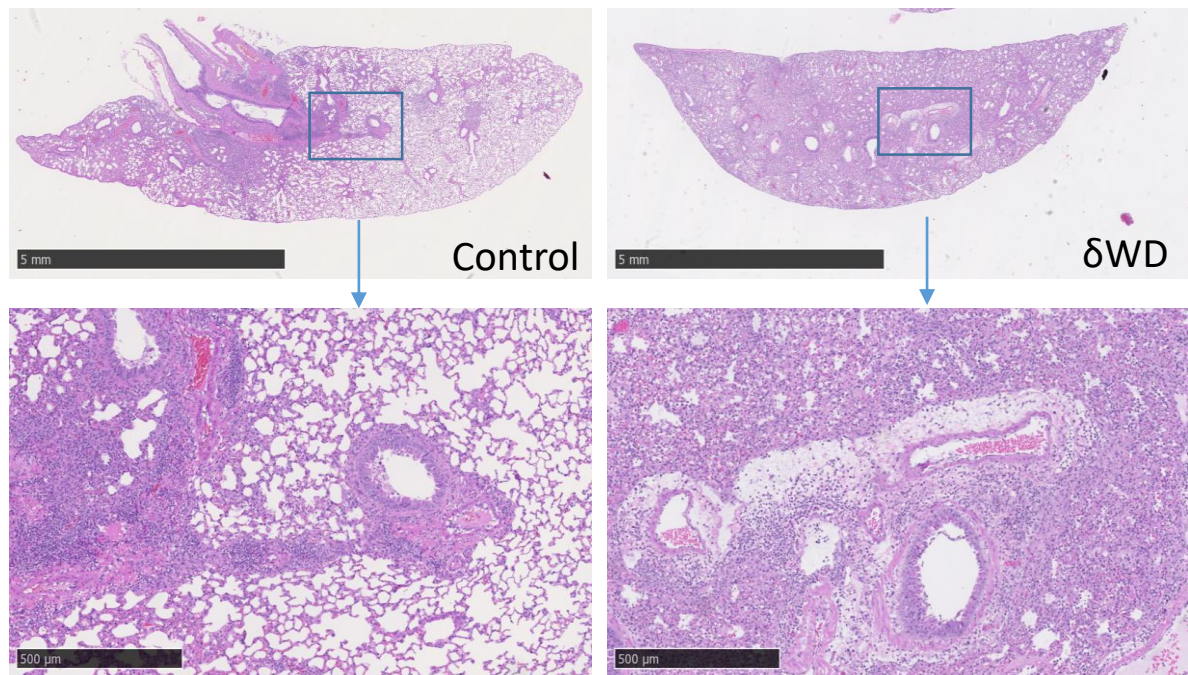


**Figure 3.16. Histochemical analysis of lung sections following challenge of mice with high dose of influenza virus.** Mice were given intranasal challenge of influenza virus strain X31 (1000pfu). Lungs were removed from mice at day 7 pi and subject to H&E stain. The images show increased inflammatory infiltration in the lung parenchyma of  $\delta$ WD mice.

### Day7 p.i. IH (IAV) staining

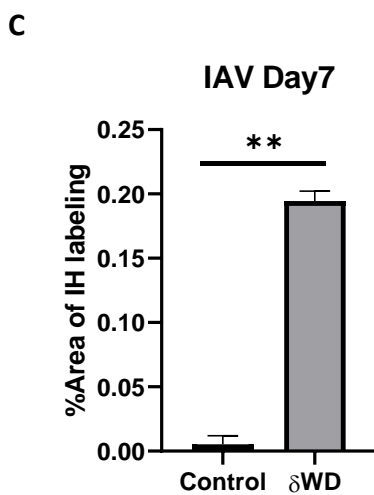
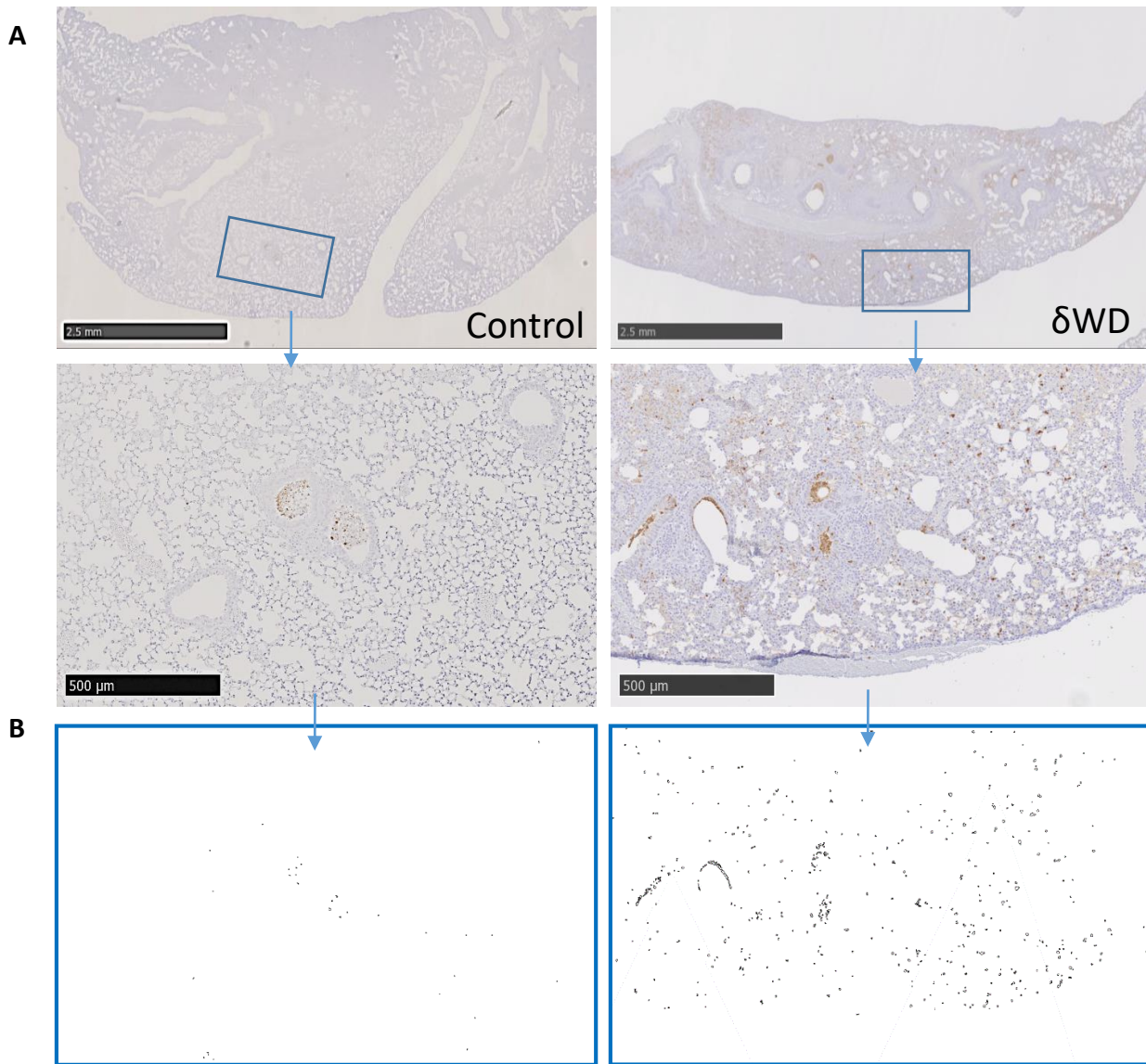


**Figure 3.17. Immunohistochemical analysis of virus antigen in lung sections following challenge of mice with high dose of influenza virus.** Mice were given intranasal challenge of influenza virus strain X31 (1000pfu). Lungs were removed from mice at day 7 pi. Influenza antigen was detected using antibodies against IH, visualised by DAB stain (**panel A**). Regions of interest are boxed and shown at higher magnification as indicated. Scale bars represent 5mm (upper panels) or 500μm (lower images). Micrographs of representative areas from lungs of 2 mice are shown. The percentage area of antibody labelling were converted to digital data (**panel B**) and quantified by ImageJ (**panel C**). Significance was determined by T-tests (\* $p < 0.05$ ), data represent the mean value  $\pm$  SD.

## Day3 p.i. Ly6G (neutrophils) staining

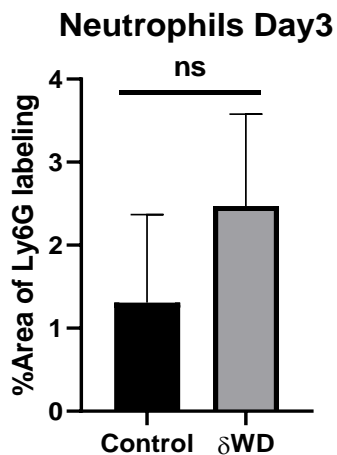
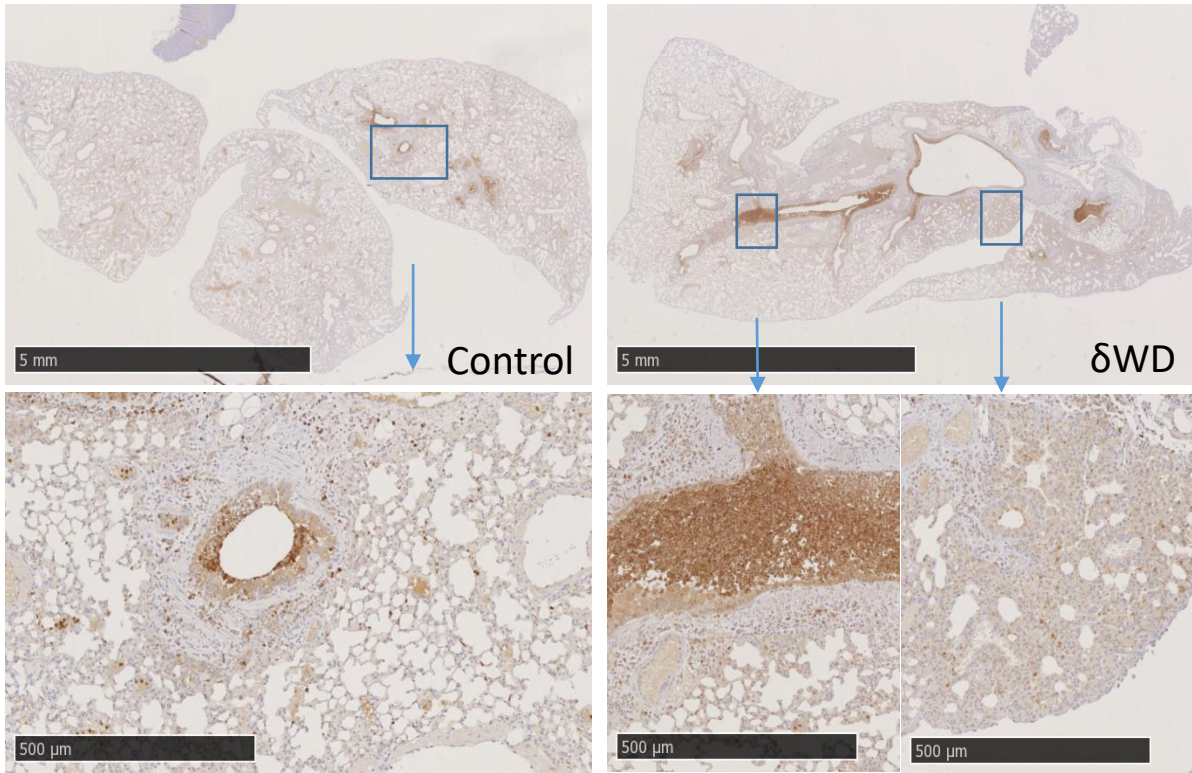


**Figure 3.18. Immunohistochemical analysis of neutrophil migration in lung sections following challenge of mice with high dose of influenza virus.** Mice were given intranasal challenge of influenza virus strain X31 (1000pfu). Lungs were removed from mice at day 3 pi. Neutrophil antigen was detected using antibodies against Ly6G visualised by DAB stain. Regions of interest are boxed and shown at higher magnification as indicated. Scale bars represent 5mm (upper panels) or 500 $\mu$ m (lower images). Micrographs of representative areas from lungs of 4 mice are shown. The percentage area of antibody labelling were quantified by ImageJ. Significance was determined by T-tests (\* $p < 0.05$ ), data represent the mean value  $\pm$  SD.

## Day3 p.i. H3 (netosis) staining

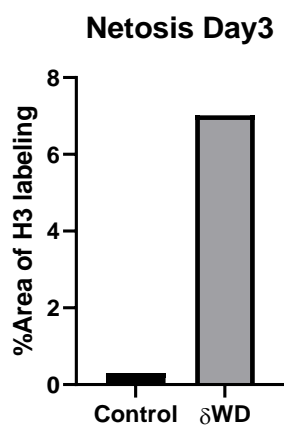
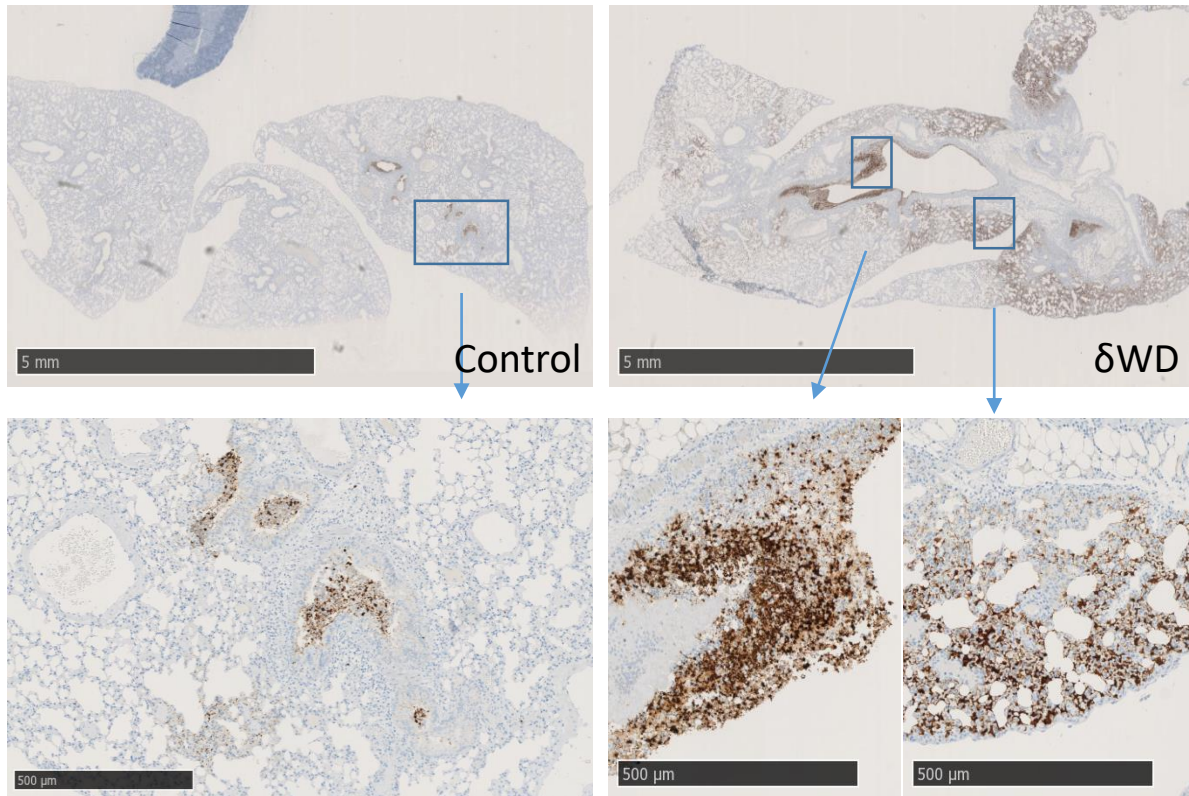


**Figure 3.19. Immunohistochemical analysis of neutrophil netosis in lung sections following challenge of mice with high dose of influenza virus.** Mice were given intranasal challenge of influenza virus strain X31 (1000pfu). Lungs were removed from mice at day 3 pi. Neutrophil chromosomal histone antigen H3, a marker for netosis was detected using antibodies against H3 visualised by DAB stain. Regions of interest are boxed and shown at higher magnification as indicated. Scale bars represent 5mm (upper panels) or 500mm (lower images). The micrographs show increased netosis in the bronchi and bronchioles and lung parenchyma of  $\delta$ WD mice. The percentage area of antibody labelling were quantified by ImageJ.

## Day7 p.i. Iba-1 (macrophages) staining

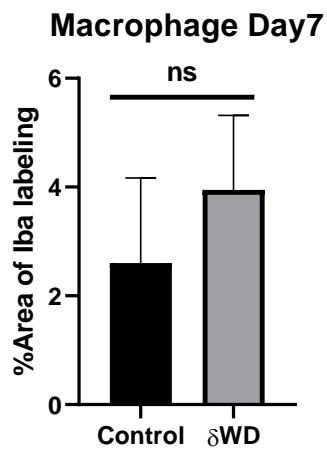
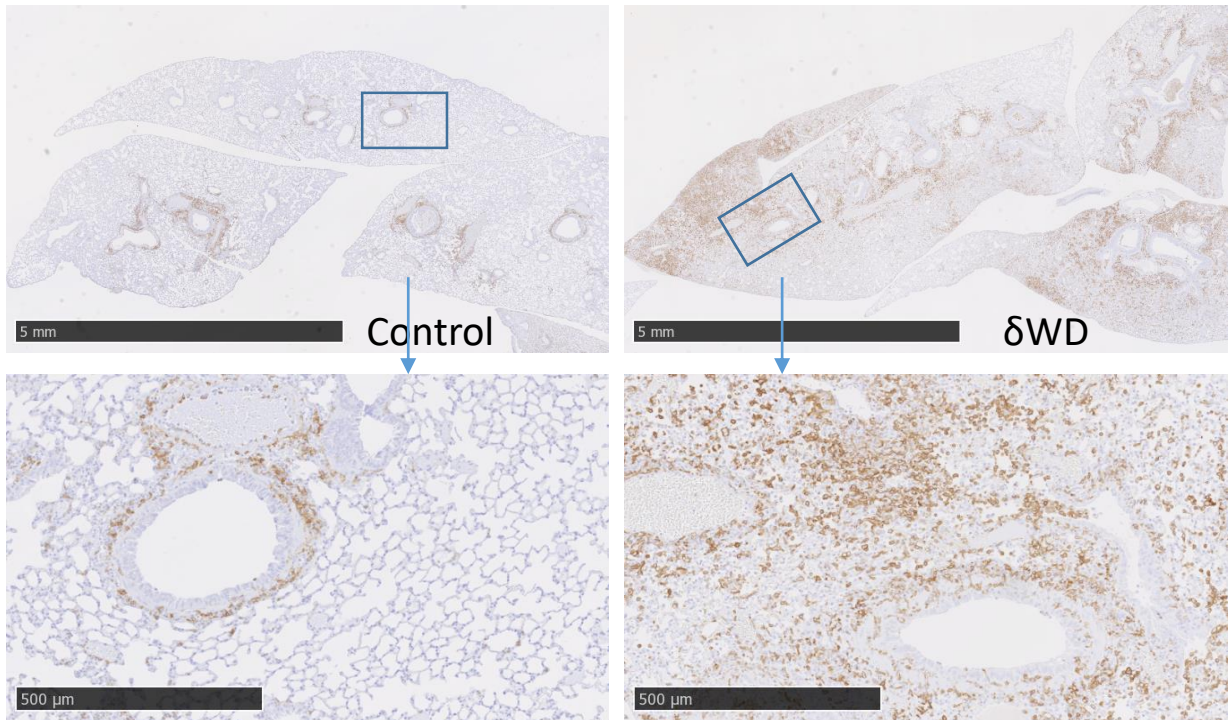


**Figure 3.20. Immunohistochemical analysis of macrophage migration in lung sections following challenge of mice with high dose of influenza virus.** Mice were given intranasal challenge of influenza virus strain X31 (1000pfu). Lungs were removed from mice at day 7 pi. Macrophage antigen was detected using antibodies against iba-1 visualised by DAB stain. Regions of interest are boxed and shown at higher magnification as indicated. Scale bars represent 5mm (upper panels) or 500mm (lower images). Micrographs of representative areas from lungs of 3 mice are shown. The percentage area of antibody labelling were quantified by ImageJ. Significance was determined by T-tests (\* $p < 0.05$ ), data represent the mean value  $\pm$  SD.

Cytokine profiles showed increased expression of MCP-1 (monocyte chemoattractant protein-1) later (day 6 pi) in infection. Lung tissue harvested at day 7 pi was therefore analysed for presence of macrophages by anti-Iba. Micrographs of representative areas from lungs of 2 mice are shown, and the percentage area of antibody labelling were quantified by ImageJ. According to Figure 3.20, macrophages accumulated around the bronchioles in both  $\delta$ WD mice and littermate controls but there clearly more macrophages in the lung parenchyma of  $\delta$ WD mice compared to littermate controls. This is consistent with the quantification results which suggest the percentage of area labelled by anti-Iba is high in  $\delta$ WD mice than littermate controls. Due to the limited sample size, it failed to show significant difference statistically.

### 3.5. Discussion and summary

The generation of mice defective in non-canonical autophagy and LAP is complex because the pathways share many downstream components with conventional autophagy. Both pathways require ATG16L1 and complete knock out of ATG16L1 results in loss of autophagy and the mice die shortly after birth (Saitoh et al., 2008). Mice with tissue-specific loss of ATG16L1 survive, but the tissues lacking ATG16L1 accumulate damaged proteins and organelles and are prone to ER stress and inflammation (Tschurtschenthaler et al., 2017). Attempts to remove LAP from phagocytic cells by deletion of ATG16L1 are problematic because parallel loss of autophagy in myeloid cells leads to a pro-inflammatory state because of over secretion of IL-1 $\beta$ . A study by (Lu et al., 2016) has demonstrated that myeloid-specific deletion of essential autophagy genes in mice actually protects mice from lethal influenza infection, because the lungs are in a pro-inflammatory state caused by deficient of canonical autophagy. To understand the role of LAP during influenza infection, it is therefore important to find a way to inhibit LAP without effecting canonical autophagy.

During the course of this thesis project several publications suggested that the WD-40 repeats of ATG16L1 are not essential for conventional canonical autophagy, but play a role in non-canonical autophagy (Boada-Romero et al., 2013; Boada-Romero et al., 2016; Fletcher et al., 2018; Serramito-Gómez et al., 2016). This prompted our lab to generate  $\delta$ WD mice (*Atg16L1* <sup>$\delta$ WD/ $\delta$ WD</sup>) to study non-canonical autophagy during infection. Work by Martinez et al (Martinez et al., 2015) has generated a mouse defective in LAP by exploiting differences in upstream

signalling pathways, rather than the central ATG16L1:ATG5-ATG12 autophagy machinery. During LAP, activation of the UVRAG complex containing RUBICON conjugates LC3 to PE in single membraned endo-lysosome compartments. Deletion of RUBICON therefore results in a loss of LAP, but does not affect autophagy. A LAP deficient mouse model based on Rubicon KO has been established to investigate the function of LAP (Martinez et al., 2015). However, Rubicon is however also involved in a plethora of signalling pathways and act as a sentinel in the inflammatory response, thus *Rubicon* KO mice with exaggerated inflammatory responses not be an ideal mouse model to study LAP during infection (Wong, Sil, & Martinez, 2018). In contrast the  $\delta$ WD mice (*Atg16L1* <sup>$\delta$ WD/ $\delta$ WD</sup>) lack the WD repeat domain of ATG16L1, but remain the ATG5-binding and CC-domain required for canonical autophagy are growing normally and maintain tissue homeostasis and do not have raised serum cytokine levels including IL-1B, IL-12 (p70), IL-13, TNF, IL-6 and CCL2/MCP-1 (Rai et al., 2019).

The challenge experiments showed that the  $\delta$ WD mouse was highly susceptible to IAV.  $\delta$ WD mice showed accelerated weight loss and increased morbidity. The lungs of  $\delta$ WD mice contained 5-fold higher titres of IAV compared to littermate controls and this led to severe inflammation. There was a positive correlation between severity of lung pathology and cytokine expression suggesting the  $\delta$ WD mice fail to control lung inflammation during IAV infection.  $\delta$ WD mice had extensive infiltration of neutrophils and macrophages into airways and parenchyma. This result is highly consistent with the higher expression of neutrophil chemotaxis factor CXCL1 mRNA in  $\delta$ WD mice at day 2 p.i. and increased expression of macrophage chemotaxis factor MCP-1 mRNA in  $\delta$ WD mice at day 7 p.i. It suggests the high expression levels of chemotaxis factors could be one of the reasons that leads to extensive neutrophil infiltration and macrophage-rich inflammation in  $\delta$ WD mice.

The high virus titre could be one of the reasons for increased cytokine production in  $\delta$ WD mice. The increased cytokine expression level in both control and  $\delta$ WD mice during IAV infection was co-incident with increased virus titre and accelerated weight loss. Increased cytokine expression was resolved in control mice and they started to recover at day 7. This raises the possibility that the uncontrolled cytokine production in  $\delta$ WD mice is triggered by increased viral load. Interestingly, even though high levels of cytokines are produced in  $\delta$ WD mice they do not efficiently restrict viral replication.

The q-PCR results of CXCL-1 mRNA expression level on day 2 pi suggest that CXCL-1 is highly expressed in  $\delta$ WD mice compared to litter mate controls, whereas IAV replication levels shows little difference on day 2 pi. High cytokine production is not therefore linked directly to virus replication in  $\delta$ WD mice at early time points. This raises the possibility that excessive cytokine production in  $\delta$ WD mice is not only triggered by the high viral replication levels, but non-canonical autophagy might also play a role in controlling of cytokine production induced by IAV infection.

There are 3 main pathways involved in IAV-induced cytokine production, each takes place in lung epithelial cells, macrophages and DCs respectively. Within infected epithelial cells, the single-stranded viral RNA in the cytosol is recognized by retinoic acid-inducible gene-I (RIG-I), results in stimulating the expression of IFNs, and pro-inflammatory cytokines. Therefore, it is possible that the non-canonical autophagy in lung epithelial cells could reduce the amount of viral RNA in the cytosol by promoting the fusion of virus-contain endosomes and lysosomes. An increased delivery of viral RNA to interferon sensors in  $\delta$ WD mice may contribute to excessive cytokine expression during IAV infection. Whether non-canonical autophagy regulates cytokine production directly or not, still needs to be further investigated.

# **Chapter 4**

## **Results Part II**

## Chapter 4: Analysis of IAV infection of mice lacking the WD domain of ATG16L1 in phagocytic cells.

### 4.1 Introduction and aims:

The role of systemic loss of the WD domain in ATG16L1 during IAV infection has been demonstrated in Chapter 3. In the  $\delta$ WD mouse model, the WD domain of ATG16L1 is deficient in all tissues. As described in Chapter 1, there are many cell types involved during IAV infection, including lung epithelial cells, macrophages, dendritic cells and neutrophils. The pathology results in Chapter 3 suggest there is more IAV antigen in the bronchiolar epithelium and alveoli area accompanied with severe infiltration of macrophage and neutrophils in the lung parenchyma in  $\delta$ WD mice. Therefore, it was interesting to determine which cell type was important for controlling IAV infection by non-canonical autophagy/LAP.

In order to understand the role of non-canonical autophagy more specifically, a  $\delta$ WD-LysMcre mice model was established with specific knock out of the WD domain in myeloid cells, including macrophage, dendritic cells and neutrophils. The full length ATG16L1 was expressed in other cell types. With this mouse model, we were able to investigate the role of WD domain in these phagocytic cells during IAV infection.

### 4.2 Genetic background and genotyping results of *Atg16L1*<sup>F1/F1</sup> and $\delta$ WD lysMcre mice model.

#### 4.2.1 Genetic background and genotyping results of *Atg16L1*<sup>fl/fl</sup> mice

The cre-Lox system is a widely-used tool to introduce gene deletions, insertions, translocations and inversions on specific target sites. Cre recombinase is a recombinase enzyme discovered in P1 Bacteriophage, which could recognize and crop the specific DNA sequences, called LoxP sites. LoxP (locus of X-over P1 Bacteriophage) sites consist of 34 base pairs: two symmetric 13-bp sequences and an asymmetric 8-bp region, allow the cre recombinase-catalysed deletion, insertion and translocation of DNA sequence between the sites, depending on orientation of these LoxP sites.

The tissue specific *Atg16L1* KO mice were generated based on cre-Lox system in our lab by Julia Maryam Arasteh during her Ph.D (Arasteh, 2012). The exon 2 of *Atg16L1* was chosen to be flanked by LoxP sites, the removal of exon 2 leads to a frame shift results in a premature stop codon (Arasteh, 2012). As shown in the diagram, two loxP sites have been inserted on either side of exon 2. Two PCR primers (primers 223 and 226) were designed by Julia Maryam Arasteh for the two loxP sites, with this pair of primers, an 801 bp band is produced in *Atg16L1*<sup>flox/flox</sup> mice [Figure 4.1] (Arasteh, 2012). As an example, in our genotyping results, No.7 got a single band in 801 bp which means it is a homozygous mouse [Figure 4.2]. Homozygous mice were selected for generating  $\delta$ WD-LysMcre mice.

#### 4.2.2 Genetic background and genotyping results of $\delta$ WDLysMcre mice

*Atg16L1*<sup>flox/flox</sup> mice have been selected and crossed with the “Cre positive mouse” to generate tissue specific loss of the full length *Atg16L1* KO. The crossing work done by Ph.D students Matthew Jefferson and Weijiao Zhang in our lab (data not published). “Cre positive mouse” is genetically modified in which the recombinase Cre is expressed in the specific cell lineages or tissues. A mouse line that specifically expresses Cre under control of the murine M lysozyme gene in macrophages and neutrophils (named LysMcre mice), have been described previously (Clausen, Burkhardt, Reith, Renkawitz, & Förster, 1999). In order to investigate the role of LAP in myeloid cells, LysMcre mice have been utilized to generate tissue specific loss of the *Atg16L1* allele in myeloid cells (macrophages, DCs, eosinophils and neutrophils).

This diagram [Figure 4.3] describes how  $\delta$ WD-LysMcre ( $\delta$ WD<sup>phag</sup>) mice have been generated. First, LysMcre mice were crossed with homozygous  $\delta$ WD mice. Offspring were selected that expressed Cre recombinase in myeloid cells and  $\delta$ WD in all tissues (*Atg16L1* <sup>$\delta$ WD/ $\delta$ WD</sup>/LysMcre<sup>+/-</sup>). These mice were then crossed with mice carrying *Atg16L1*<sup>fl/fl</sup> in all tissues. Cre positive offspring were selected that are heterozygous for floxed *ATG16L1* and  $\delta$ WD (*Atg16L1*<sup>fl/ $\delta$ WD</sup>/LysMcre<sup>+/-</sup>). Mice lacking cre recombinase were used as littermate controls (*Atg16L1*<sup>fl/ $\delta$ WD</sup>/LysMcre<sup>-/-</sup>). In cre positive mice cre recombinase is expressed in myeloid cells where it inactivates the full length *Atg16L1* gene. Myeloid cells therefore loss of *Atg16L1* but express one  $\delta$ WD allele that is sufficient for autophagy but not LAP, resulting in a specific LAP deficiency in myeloid cell. This mouse was named as  $\delta$ WD<sup>phag</sup> mice.

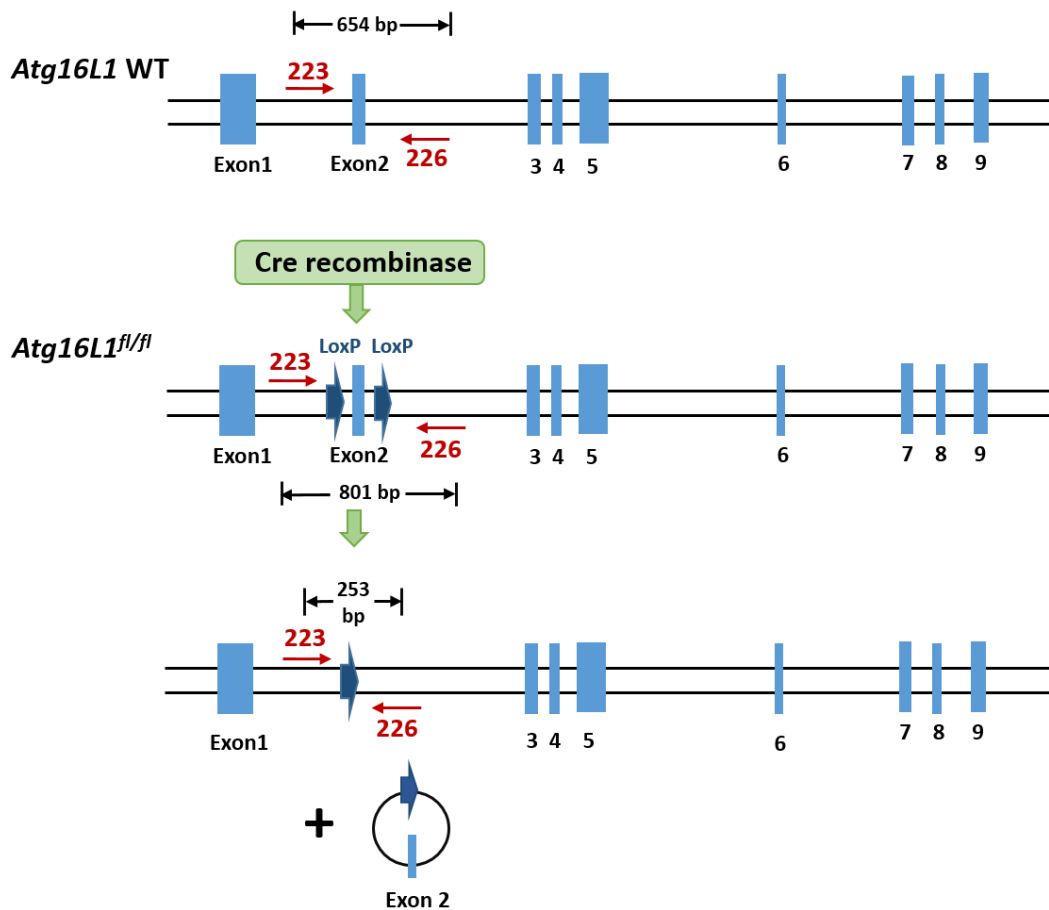


**Figure 4.1: Genome map and location of PCR primers for genotyping** - The PCR primers are designed to anneal to exon 2. In wild type mice primers 223 and 226 generate a 654bp fragment. The cre recombinase in *Atg16L1*<sup>fl/fl</sup> increases the size of the fragment to 801bp. (modified from Arasteh, 2012)

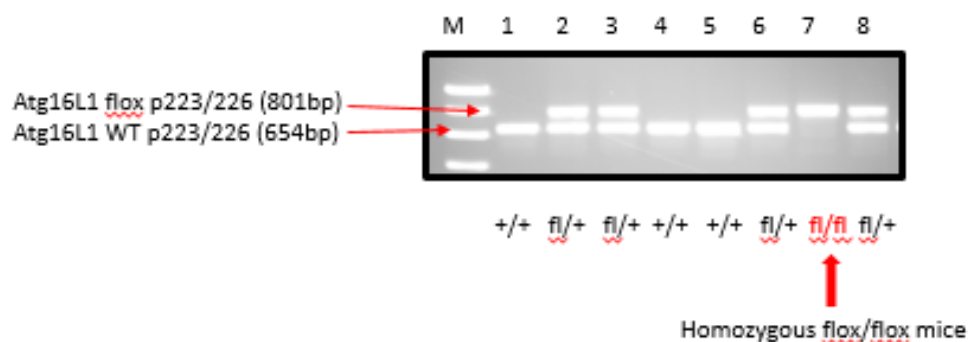


**Figure 4.2: Representative agarose gel showing PCR products and genotype.** DNA extracted from 8 mice were analysed by PCR using primers 223 and 226 and resolved on an agarose gel. Molecular size markers are in lane M. The 801 bp band corresponds to a PCR product from floxed sequence amplified by primers (223 and 226). The 654 bp band corresponds to a PCR product from WT mice. Sample 7 has a single 801 bp band, indicating it is a homozygous *fl/fl* mice.

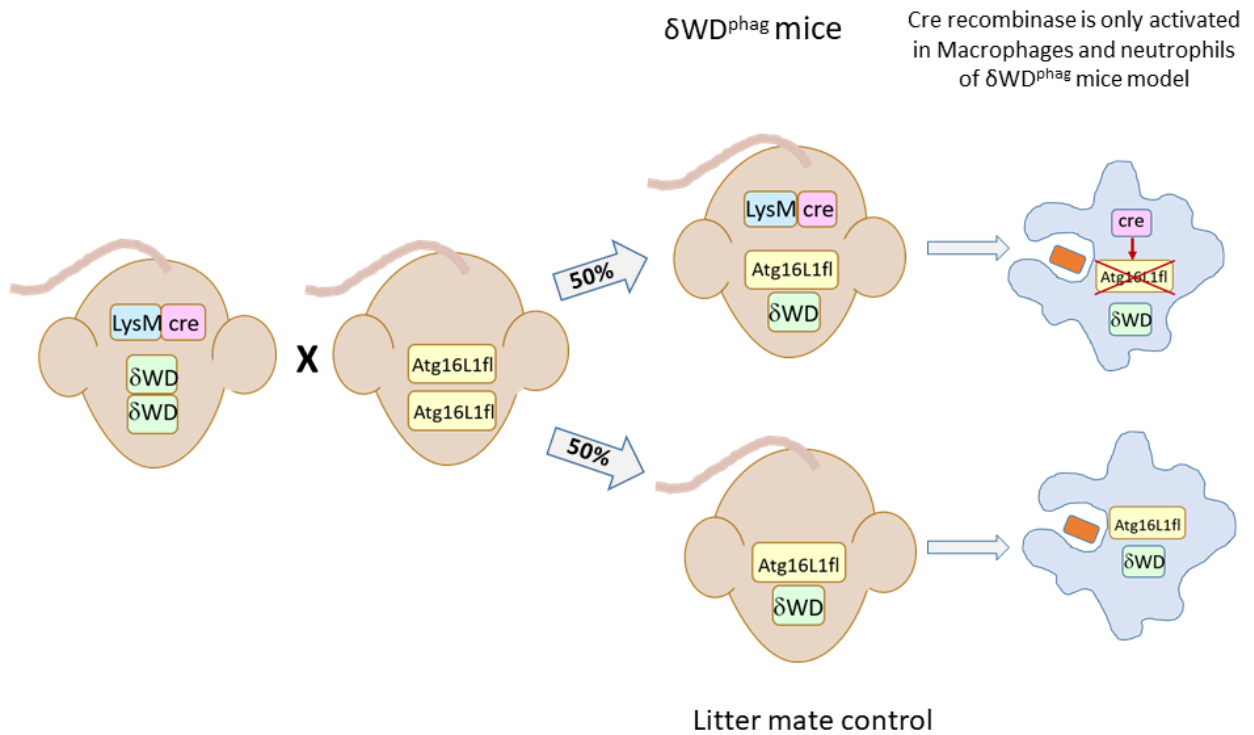


**Figure 4.3 Breeding strategy of  $\delta\text{WDLysMcre}$  mice model.** Homozygous  $\delta\text{WD}$  mice carrying  $\text{LysMcre}$  were crossed with  $\text{Atg16L1}^{\text{fl/fl}}$  mice. 50% of progeny are  $\text{Atg16L1}\delta\text{WD}^{\text{phag}}$  ( $\delta\text{WD}^{\text{phag}}$ ) and carry  $\text{LysMcre}$  and one allele each of  $\delta\text{WD}$  and floxed  $\text{Atg16L1}$ . Cre recombinase expressed in myeloid cells of these mice inactivates  $\text{Atg16L1}$  by removing exon 2 from  $\text{Atg16L1}$ . The myeloid cells only express  $\delta\text{WD}$ . Cre recombinase is not expressed in non-myeloid tissues and  $\text{Atg16L1}$  is preserved to power autophagy. 50% of progeny provide littermate controls because they lack  $\text{LysMcre}$  and preserve  $\text{Atg16L1}$  in all tissues.

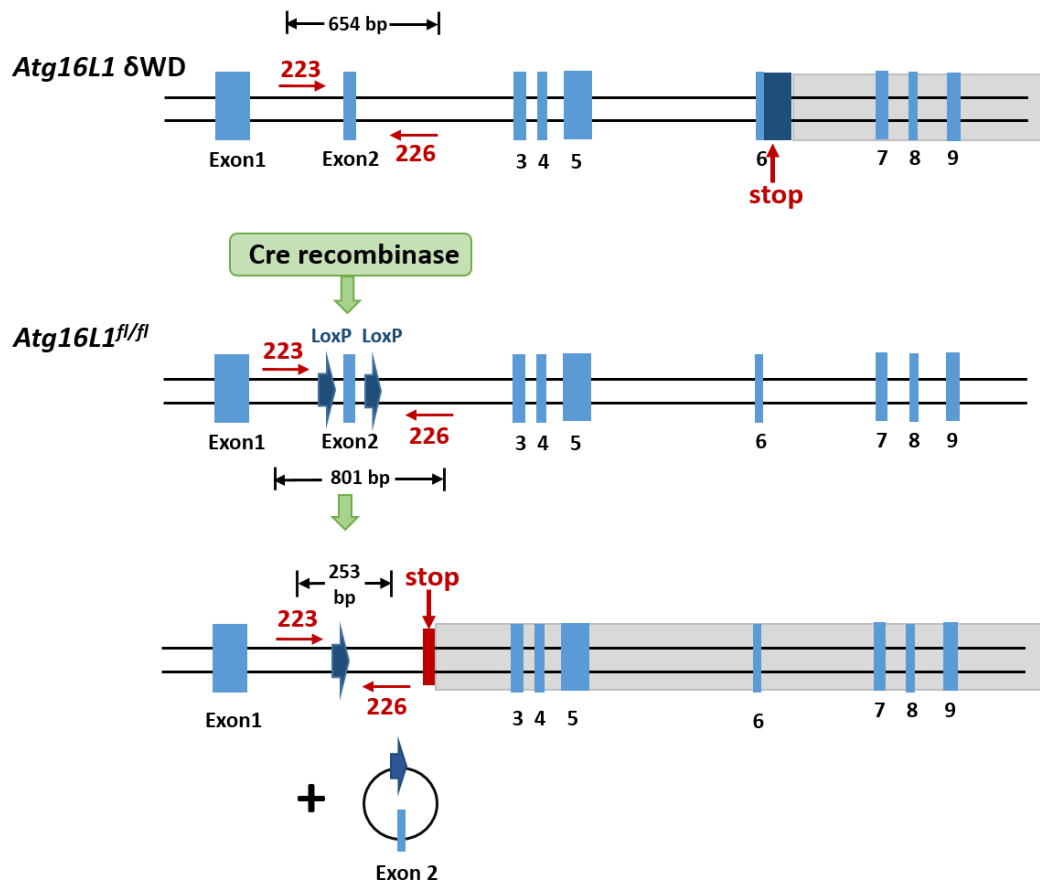


**Figure 4.4 Genome map and PCR primers for analysis of  $\delta$ WD-LysMcre mice genotype.** *Atg16L1*<sup>fl/fl</sup> and  $\delta$ WD allele were identified using primers flanking exon 2 (223, 226). In  $\delta$ WD allele, primers 223 and 226 generate a 654bp fragment. In *Atg16L1*<sup>fl/fl</sup> allele, Loxp sites flanking exon 2 increase the PCR product of exon 2 from 654 bp to 801 bp. In *Atg16L1*<sup>fl/fl</sup>-LysMcre removal of exon 2 by Cre recombinase reduces the PCR product of exon 2 from 801 bp to 253 bp.

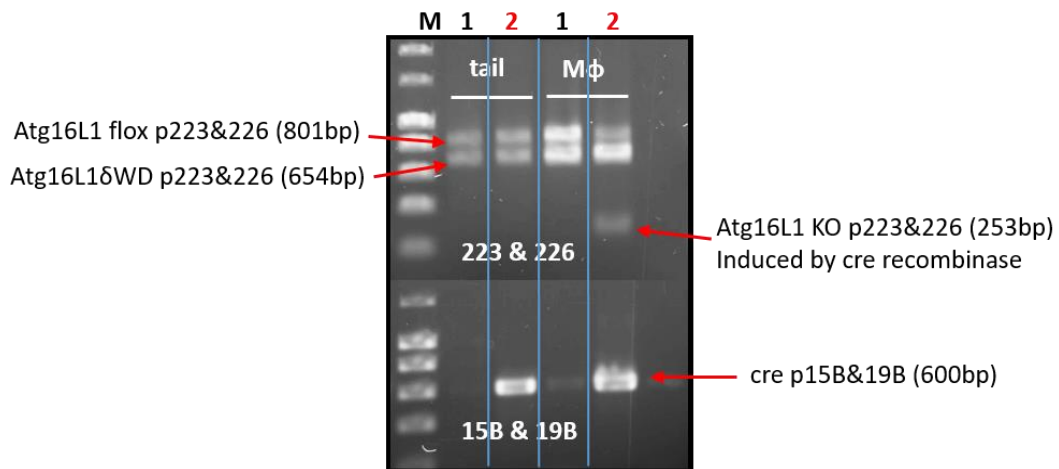


**Figure 4.5 Representative agarose gel showing PCR products and genotype.** DNA samples are acquired from tails and bone marrow-derived macrophages from M1 and M2, the 801 bp and 654 bp bands are corresponds to the PCR product from *Atg16L1<sup>fl</sup>* allele and *Atg16L1<sup>δWD</sup>* allele amplified by primers (223 and 226) respectively. The 253bp band is a shorter product released from *Atg16L1<sup>fl</sup>* allele which cleaved by activated cre recombinase. The cre gene is identified by primer 15B&19B, M2 has a 600 bp band, indicating it is a cre positive mice and M1 is cre negative.

**Table 8: Expect bands size for each genotype**

Genotype	<i>Atg16L1<sup>fl/δWD</sup></i> <i>/LysMcre<sup>-/-</sup></i>	<i>Atg16L1<sup>fl/δWD</sup></i> <i>/LysMcre<sup>+/-</sup></i>
P 223&226 in tail	801bp 654bp	801bp 654bp
P 223&226 in Mφ	801bp 654bp	253bp 654bp
P 15B&19B	Nothing	600bp

The genome diagram [Figure 4.4] and Table 8 indicate the primer binding positions and the expected sizes of DNA products for different genotypes. According to these, offspring with 2 genotypes can be identified. Figure 4.5 is an example of genotyping results for identifying *Atg16L1<sup>fl/δWD</sup>/LysMcre<sup>+/-</sup>* and *Atg16L1<sup>fl/δWD</sup>/LysMcre<sup>-/-</sup>* mice. DNA samples are acquired from tails and bone marrow-derived macrophages from M1 and M2, primer 223&226 have been used to test *Atg16L1*; primer 15B&19B have been used for identify cre gene. According to Figure 4.5 and Table 8, M1 is cre negative, the *Atg16L1<sup>fl</sup>* allele is intact (801bp) in both tail and Mφ DNA samples. While M2 is cre positive, in which cre recombinase is activated in Mφ, results in a shorter product (253bp) released from *Atg16L1<sup>fl</sup>* allele, and *Atg16L1<sup>fl</sup>* allele still intact (801bp) in tail DNA samples.

### 4.3 Characterisation of autophagy and LAP in cells from $\delta\text{WD}^{\text{phag}}$ mice.

The activity of canonical and non-canonical autophagy/LAP pathways in  $\delta\text{WD}^{\text{phag}}$  mice was studied using skin fibroblasts and BMDM from  $\delta\text{WD}^{\text{phag}}$  mice and litter mate control.

The ability of skin fibroblast cells from control and  $\delta\text{WD}^{\text{phag}}$  mice to active non-canonical autophagy was tested using monensin as described in chapter 3. After 2hrs, cells were fixed, and the location of LC3 was analysed by immunostaining. In control fibroblasts and fibroblasts from  $\delta\text{WD}^{\text{phag}}$  mice LC3 was associated with swollen endo-lysosomal membranes [Figure 4.6A,B] showing that non-canonical autophagy was active ion fibrobalsts. A similar experiment incubated BMDM with Zymosan to induce LAP. Zymosan particles engulfed by control macrophages were trapped in phagosomes which recruited LC3 thus indicating LAP [Figure 4.6C], while in  $\delta\text{WD}^{\text{phag}}$  macrophages, LC3 failed to label phagosomes containing Zymosan and remained distributed throughout the cytoplasm [Figure 4.6D]. These results show that  $\delta\text{WD}^{\text{phag}}$  mice have a specific loss of LAP from myeloid cells.

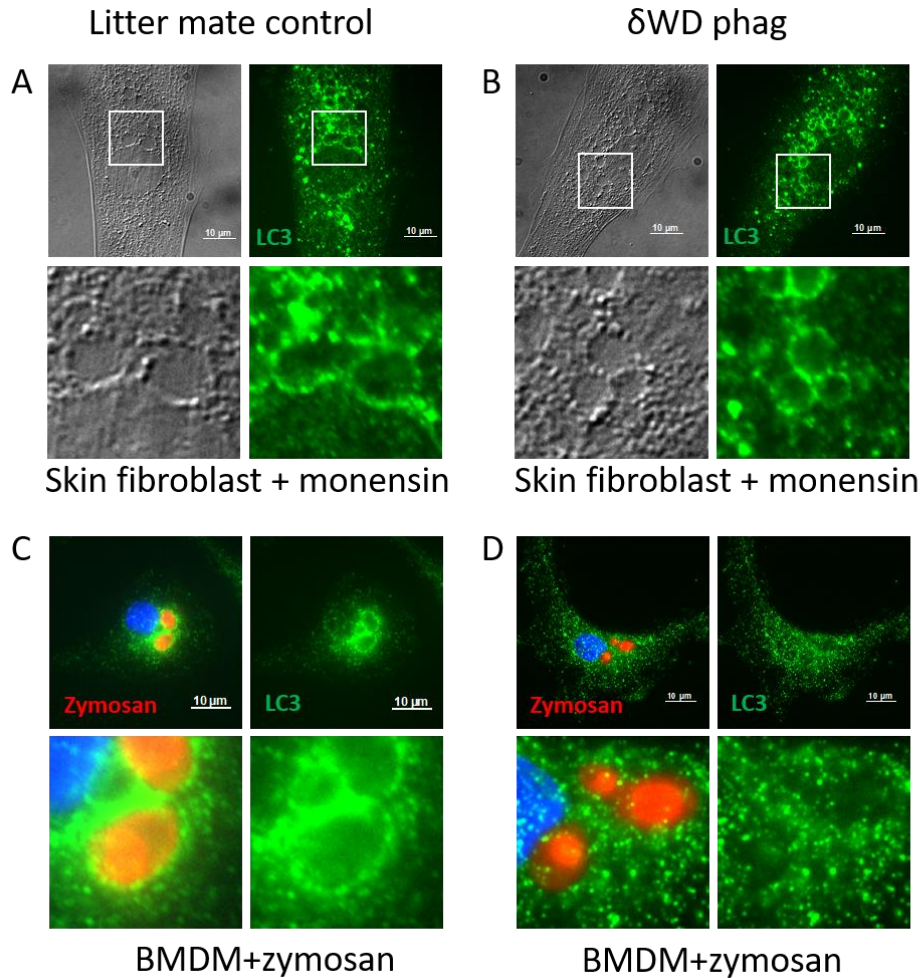


**Figure 4.6. Analysis of non-canonical autophagy and LAP in cells cultured from  $\delta\text{WD}^{\text{phag}}$  mouse strains. A and B: non-canonical autophagy.** Skin fibroblast from  $\delta\text{WD}^{\text{phag}}$  mice and litter mate control were incubated in nutrient media containing monensin for 2 hours to induce non-canonical autophagy. Non-canonical autophagy was indicated by the recruitment of LC3 to swollen vesicles following immunofluorescence staining for LC3 (Alexafluor 488 green). Litter mate controls indicate cells from wild type mice,  $\delta\text{WD}^{\text{phag}}$  indicates mice lacking WD domain of ATG16L1 in phagocytic cell. **C and D: LAP.** Bone marrow derived macrophages (BMDM) from  $\delta\text{WD}^{\text{phag}}$  mice and litter mate control were incubated in nutrient media containing Zymosan for 2 hours. LAP was indicated by the recruitment of LC3 to phagosomes containing Zymosan (red) following immunofluorescence staining for LC3 (Alexafluor 488 green).

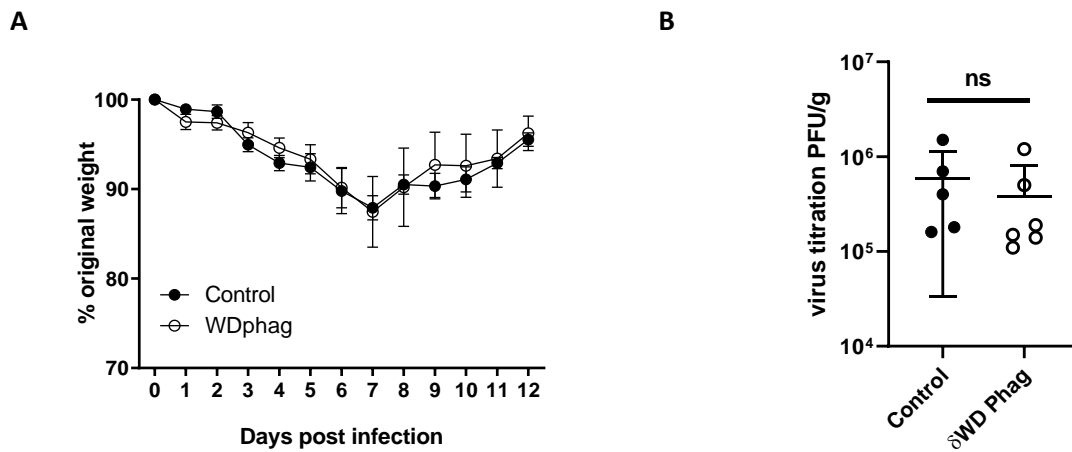


**Figure 4.7 Weight loss and viral titer following challenge of  $\delta$ WD<sup>phag</sup> mice with influenza virus.** Mice were given intranasal challenge of influenza virus strain X31 (1000pfu). Mice were monitored for weight loss (**A**) at the indicated time points. Lung tissues (n=5 or 6) were taken at 5 d.p.i. and virus titer determined by plaque assay (**B**). Data represent the mean value  $\pm$  SD. Analysis using the Mann-Whitney U test showed a significant difference (\* $p < 0.05$ ).

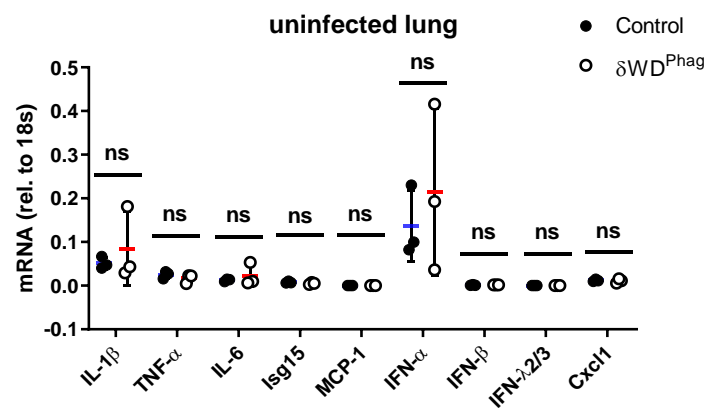


**Figure 4.8 Analysis of basal cytokine expression level in  $\delta$ WD<sup>phag</sup> mice model.**  $\delta$ WD<sup>phag</sup> mice and litter mate controls were sacrificed. Lungs were removed from mice (n=3) and analysed for indicated cytokine genes by q-PCR. Significance was determined by T-tests (\* $p < 0.05$ ), data represent the mean value  $\pm$  SD.

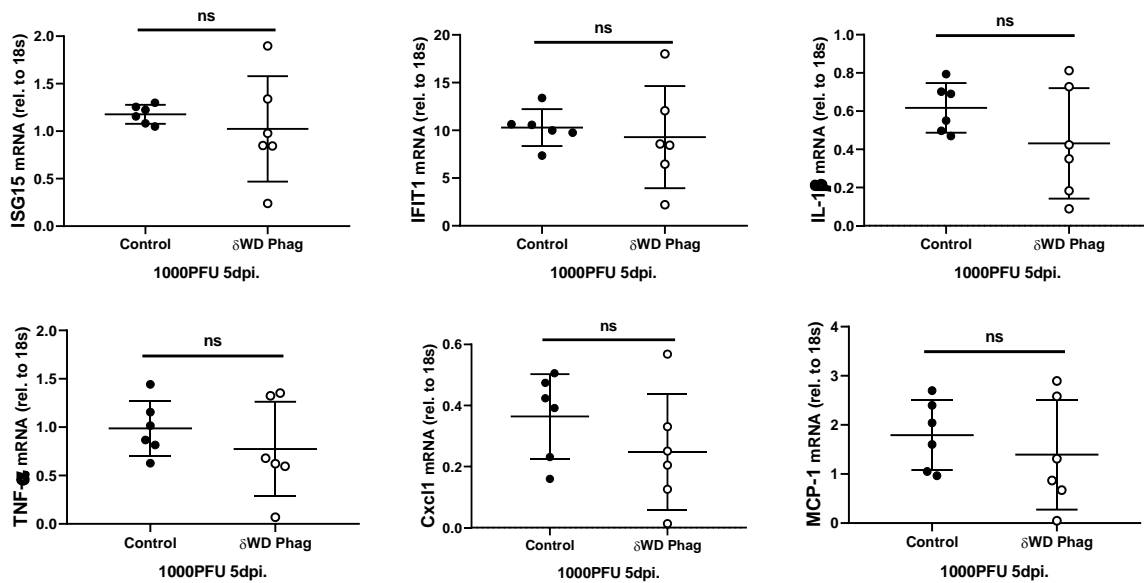


**Figure 4.9 Analysis of interferon and cytokines expression in lungs following challenge of  $\Delta$ WD<sup>phag</sup> mice with influenza virus.** Mice were given intranasal challenge of influenza virus strain X31 (1000pfu). Lungs were removed from mice (n=6) at 5 d.p.i and analysed for indicated interferon genes by q-PCR. Plots data represent individual animals with bars representing mean  $\pm$  SD. Analysis using the Mann-Whitney U test showed a significant difference (\* $p < 0.05$ ).

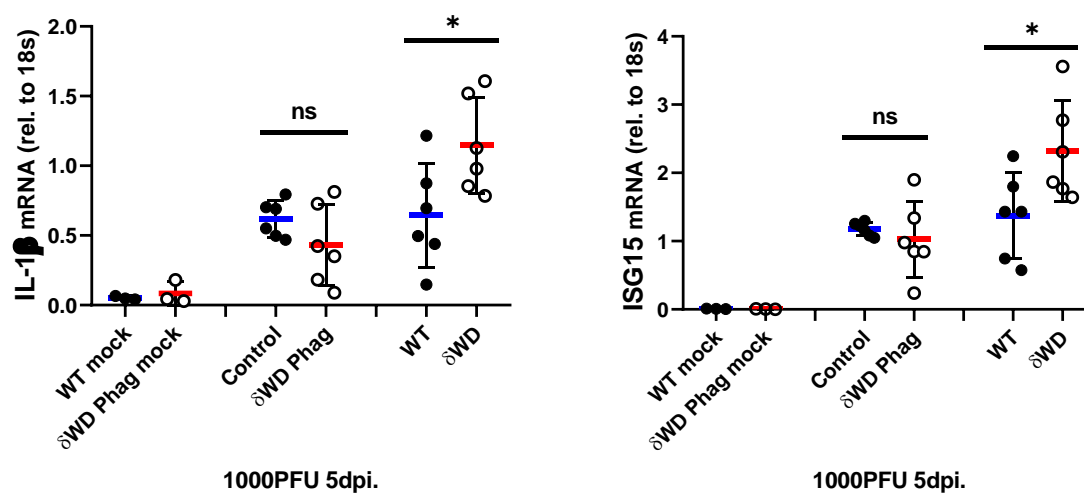
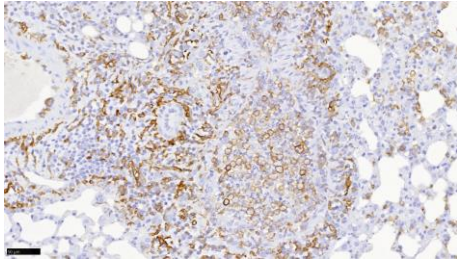


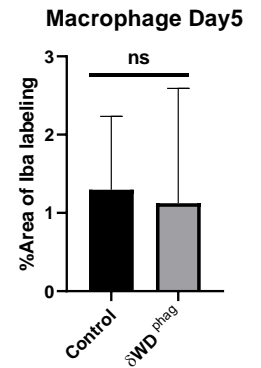
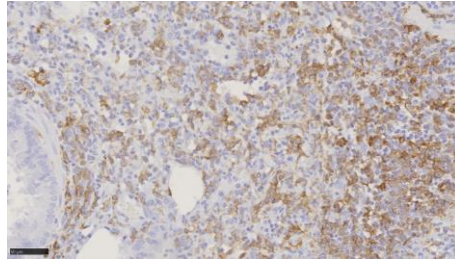
**Figure 4.10 Comparison of Cytokine mRNA expression level in  $\Delta$ WD and  $\Delta$ WD<sup>phag</sup> mice lung** - Mice were given intranasal challenge of influenza virus strain X31 (1000pfu). Lungs were removed from mice (n=6) at 5 d.p.i and analysed for indicated interferon genes by q-PCR. Plots data represent individual animals with bars representing mean  $\pm$  SD. Significance was determined by multi-T-test.

## Day 5 p.i.

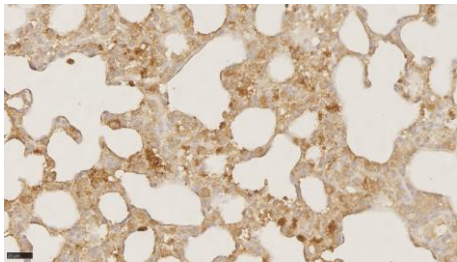
Control Iba-1 (macrophages)



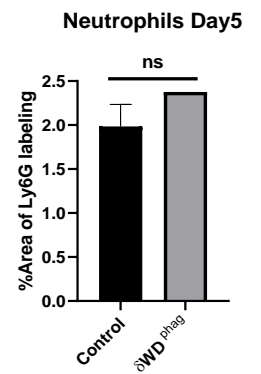
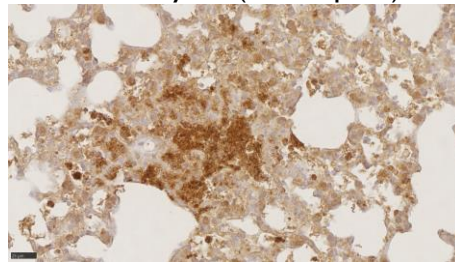
$\delta$ WD<sup>phag</sup> Iba-1 (macrophages)



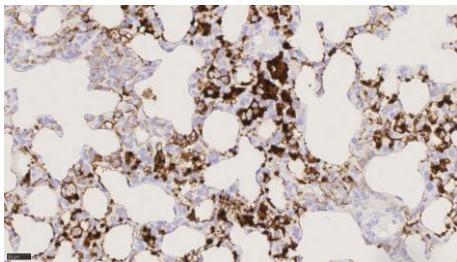
Control Ly6G (neutrophils)



$\delta$ WD<sup>phag</sup> Ly6G (neutrophils)



Control H3 (netosis)



$\delta$ WD<sup>phag</sup> H3 (netosis)

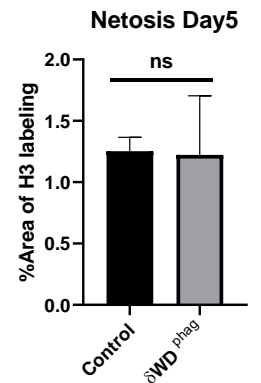
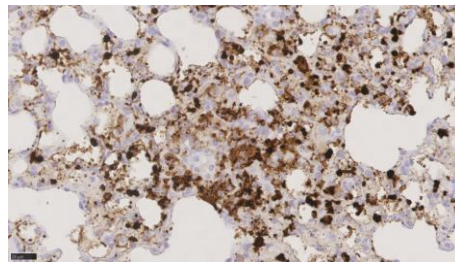


**Figure 4.11 Immunohistochemical analysis of  $\delta$ WD<sup>phag</sup> mice in lung sections following challenge of mice with high dose of influenza virus.** Mice were given intranasal challenge of influenza virus strain X31 (1000pfu). Lungs from  $\delta$ WD<sup>phag</sup> mice and litter mate controls were removed at day 5 d.p.i. Macrophages were detected by using anti-Iba-1, neutrophils with anti-Ly6G and netosis with anti-H3, visualized with DAB and counter-stained with hematoxylin. Micrographs of representative areas from lungs of 6 mice are shown. Regions of interest are boxed and shown at higher magnification as indicated. Scale bars represent 5mm (upper panels) or 500 $\mu$ m (lower images). There are similar numbers of macrophages, neutrophils and levels of netosis in the lung parenchyma of  $\delta$ WD<sup>phag</sup> and control mice. The percentage area of antibody labelling were quantified by ImageJ. Significance was determined by T-tests (\* $p < 0.05$ ), data represent the mean value  $\pm$  SD.

## 4.4. Effect of specific loss of LAP in phagocytes on IAV infection

### 4.4.1 Weight loss and viral titre in lung

$\delta$ WD<sup>phag</sup> mice and litter mate controls were challenged with 1000 PFU H3N2 X31 by inhalation, weight loss was monitored and viral titre was determined by plaque assay. According to the results, the  $\delta$ WD<sup>phag</sup> mice retained 90% of original weight at day 4 following challenge [Figure 4.7A] and failed to show the raised virus titre in lung [Figure 4.7B] seen in  $\delta$ WD mice. The resistance of these mice, which lack LAP in phagocytic cell to IAV was similar to control mice. The results, which show that a loss of LAP in phagocytic cells does not make mice more sensitive to IAV, suggested that resistance to IAV was provided by cells other than phagocytic cells.

### 4.4.2 Effect of loss of LAP in phagocytes on cytokine production during IAV infection

Phagocytic cells such as macrophages, neutrophils and pDCs are the predominant source of cytokine production. Besides, the efferocytosis during infection executed by phagocytes possibly mediated through LAP plays could play an effective regulatory role by inhibiting pro-inflammatory cytokine and chemokines production (Fadok et al., 1998; Heckmann et al., 2017; Martin et al., 2014). Therefore, the effect of LAP in phagocytes on cytokine production was worth investigating. The basal mRNA expression levels of interferons and cytokines in  $\delta$ WD<sup>phag</sup> mouse models have been tested by q-PCR before challenge with IAV. Result [Figure 4.8] suggests there was no different observed between  $\delta$ WD<sup>phag</sup> and littermate controls. This allows us to detect the cytokines expression level during IAV infection without considering the pro-inflammatory response. Cytokine mRNA levels from  $\delta$ WD<sup>phag</sup> mice challenged with 1000PFU X31 5dpi were analysed by q-PCR. Figure 3.14 shows an increased cytokine expression level in  $\delta$ WD mice after 5 days infection [Figure 4.9], while there was no difference observed between  $\delta$ WD<sup>phag</sup> mice and litter mate controls. The results suggested that unlike  $\delta$ WD mice, the absence of LAP only in phagocytes does not lead to the uncontrolled cytokine production. Indicating that LAP in phagocytes cells does not play predominant role in the regulation of cytokines IAV infection.

#### 4.4.3 Effect of loss of LAP in phagocytes on immune cell infiltration into lung during IAV infection

$\delta$ WD<sup>phag</sup> and littermate control mice were infected with 1000 pfu IAV X-31. Lung tissues were harvested at 5 d p.i. Macrophages were detected by using anti-Iba-1, neutrophils with anti-Ly6G and netosis with anti-H3. According to results Figure 4.11, there are similar numbers of macrophages, neutrophils and levels of netosis in the lung parenchyma of  $\delta$ WD<sup>phag</sup> and control mice, suggesting that LAP in phagocytes cells does not play predominant role in the regulation of immune cell infiltration into lungs during IAV infection. The percentage area of antibody labelling was quantified by ImageJ, suggesting there is almost no difference between  $\delta$ WD<sup>phag</sup> and control mice, in the levels of macrophage accumulation, neutrophil infiltration and netosis.

#### 4.5 Discussion:

The  $\delta$ WD<sup>phag</sup> mouse model was established for understanding the role of LAP in phagocytic cells during IAV infection. Genotyping and western blot analysis of phagocytic cell (bone derived macrophages) and non-phagocytic cells (skin fibroblast and tail) suggested that cre recombinase was only activated in myeloid cells. This results the inactivation of the *Atg16L1*<sup>fl/fl</sup> allele and the expression of  $\delta$ WD allele to power autophagy. The LAP assays on skin fibroblast and macrophages taken from  $\delta$ WD<sup>phag</sup> mice confirmed that they are LAP deficiency in phagocytic cells but can activate LC3 conjugation to endo-lysosome compartments by non-canonical autophagy in non-phagocytic cells. Thus,  $\delta$ WD<sup>phag</sup> mice can be used as a model to investigate the role of LAP in myeloid cells.

q-PCR results and viral titre showed that loss of LAP from phagocytic cells did not increase the sensitivity of mice to IAV infection. The 2-fold increase in virus titre see following systemic loss of non-canonical autophagy in  $\delta$ WD mice was absent, as was evidence for uncontrolled cytokine production and inflammatory infiltration into the lungs. The results suggest that the predominant role played by non-canonical autophagy in protecting against severe IAV infection may lie in lung epithelial cells rather than the LAP in phagocytes.

**Chapter 5**  
**Results Part III**

## Chapter 5: Analysis of $\delta$ WD mice reconstituted with wildtype (LAP<sup>+/+</sup>) bone marrow.

### 5.1 introduction

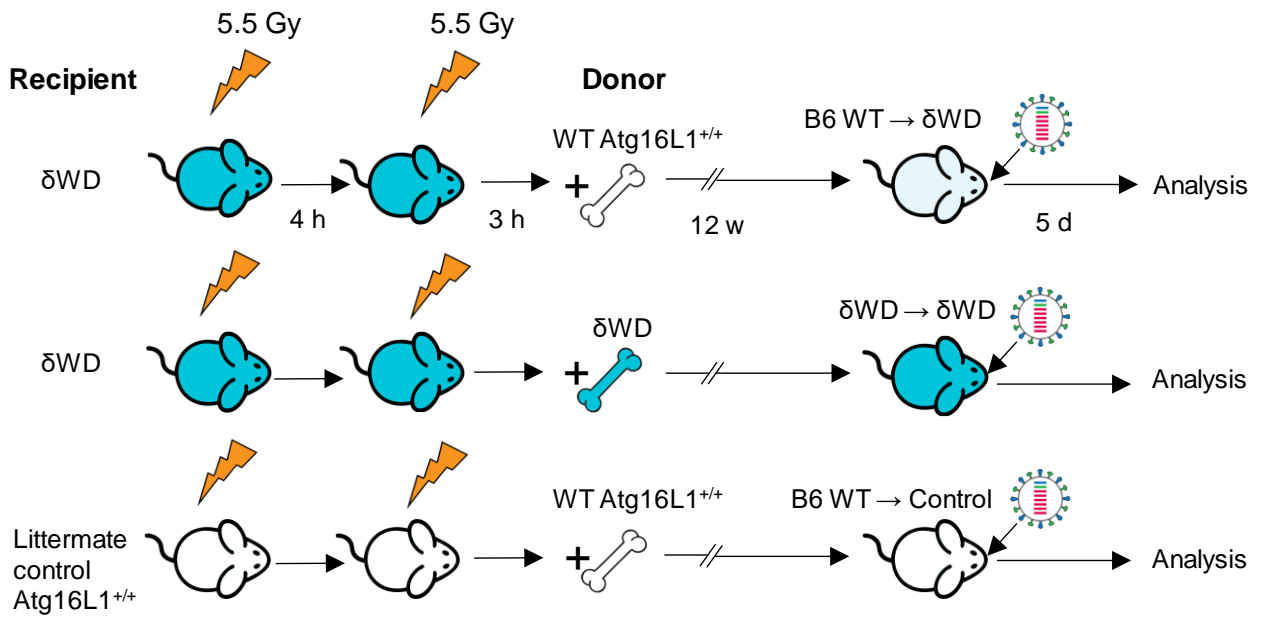
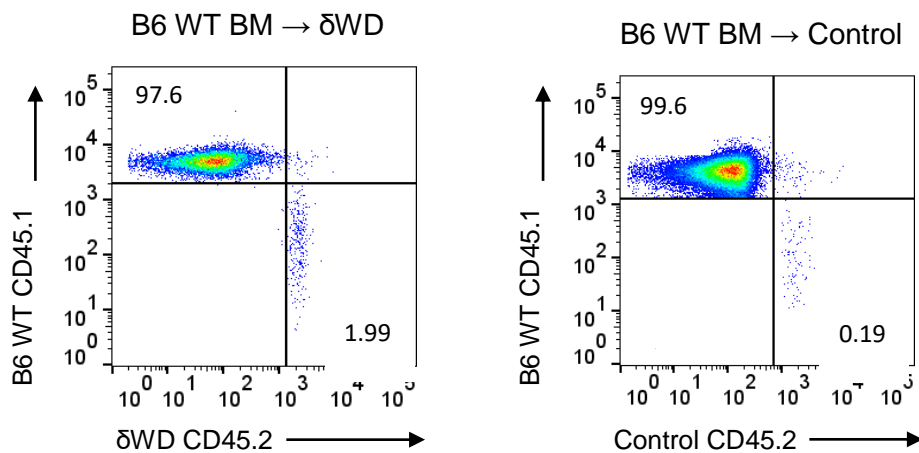
In order to investigate the role of non-canonical autophagy in lung epithelial cells during IAV infection, a reciprocal experiment was carried out by reconstituting wild type bone marrow into  $\delta$ WD mice. As a result, these chimera mice are carrying wild type *Atg16L1* in all the bone-marrow-derived cells, such as phagocytic cells and lymphocytes, while the rest of the tissues, including lung epithelial cells, lack the WD domain and are defective in non-canonical autophagy. These mice can be used to determine if phagocytic cells from wild type *Atg16L1*<sup>+/+</sup> bone marrow can protect susceptible  $\delta$ WD mice from lethal IAV infection, or if the non-canonical autophagy in lung epithelial cells plays a role during IAV infection.

### 5.2 Generation and analysis of radiation chimeras

The general strategy is shown in Figure 5.1A. Chimeras were generated at Liverpool University by James Stewart. Mice were subjected to whole body irradiation with 11 Gy in two doses 4 h apart using a <sup>137</sup>Cs source in a rotating closed chamber. Bone marrow was collected from male wild type C57BL/6-Ly5.1 (B6.SJL-*Ptprc*<sup>a</sup>*Pepc*<sup>b</sup>/BoyCrl; *Atg16L1*<sup>+/+</sup>) mice that are congenic for the CD45.1 allele or from  $\delta$ WD mice (that are congenic for CD45.2). The C57BL/6 CD45.1 marrows were used to enable confirmation of chimaerism by FACS analysis of bone-marrow-derived cells as littermate control and  $\delta$ WD mice are CD45.2 [Figure 5.1B]. The FACS analysis was done by James Stewart at Liverpool University.

### 5.3 $\delta$ WD mice reconstituted with wild type bone marrow remain highly sensitive to IAV

The radiation chimeras were used to see if a wild type *Atg16L1*<sup>+/+</sup> bone marrow could protect the susceptible  $\delta$ WD mice from lethal IAV infection. When challenged with IAV, wild type mice reconstituted with wild type *Atg16L1*<sup>+/+</sup> phagocytic cells [Figure 5.2A] started to recover and

**A****B**

**Figure 5.1** Confirmation of bone marrow transplant radiation chimaerism (operated by James Stewart at Liverpool University) **A.** Strategy for making bone-marrow chimaeras. **B.** Chimaerism was confirmed 12 weeks post-transplant in spleen cells by flow-cytometric analysis of congenic markers on leukocytes (CD45.1, CD45.2). Flow plot shows representative plot from one C57BL/6 WT (CD45.1) bone-marrow  $\rightarrow$   $\delta$ WD (CD45.2) recipient chimaera and one C57BL/6 WT (CD45.1) bone-marrow  $\rightarrow$  littermate control (CD45.2) recipient chimaera. All animals were  $> 95\%$  chimaeric.

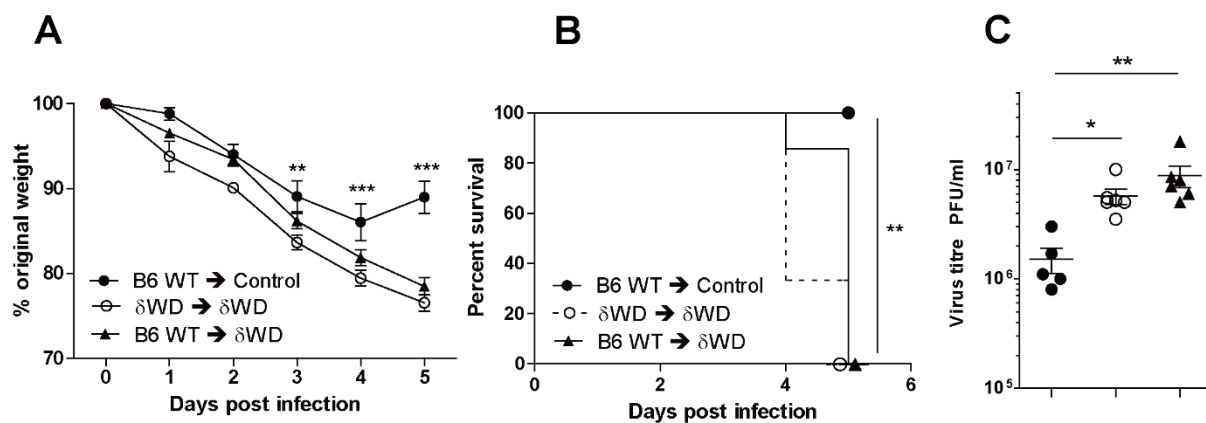


**Figure 5.2 Weight loss, mortality and viral titer following challenge of reconstituted mice with influenza virus.** Wild type *Atg16L1*<sup>+/+</sup> bone marrow was reconstituted in control (B6 WT → control [●] ) or  $\delta$ WD mice (B6 WT →  $\delta$ WD [○] ).  $\delta$ WD bone marrow was reconstituted in  $\delta$ WD mice ( $\delta$ WD →  $\delta$ WD [▲] ). Mice were given intranasal challenge of influenza virus strain X31 (1000pfu). Mice were monitored for weight loss (A) or mortality (B) at the indicated time points. Lung tissues (n=5 or 6) were taken at 5 d.p.i. and virus titer determined by plaque assay (done by Sharma Parul at University of Liverpool) (C), indicating the sensitivity to IAV is not caused by loss of non-canonical autophagy from by bone marrow-derived cells. Data represent the mean value  $\pm$  SEM. Analysis using the one way ANOVA with Tukey's post-hoc, showed a significant difference (\*p < 0.05).

regain weight at day 4. In contrast, when  $\delta$ WD mice were reconstituted with wild type bone marrow they remained highly sensitive to IAV [Figure 5.2A] with weight falling to 75% by day5 associated with highly mortality [Figure 5.2B] and increased viral titer in the lung [Figure 5.2C] (done by Sharma Parul at University of Liverpool), similar to those observed for  $\delta$ WD mice lacking non-canonical autophagy in all cells. This results suggest that a LAP<sup>+/+</sup> bone marrow cannot provide resistance to IAV when other tissues lack non-canonical autophagy.

Day5 p.i. Iba-1 (macrophages)

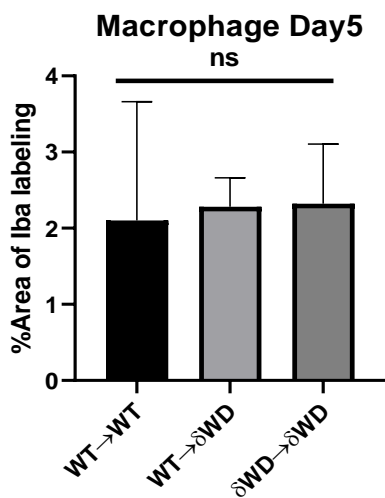
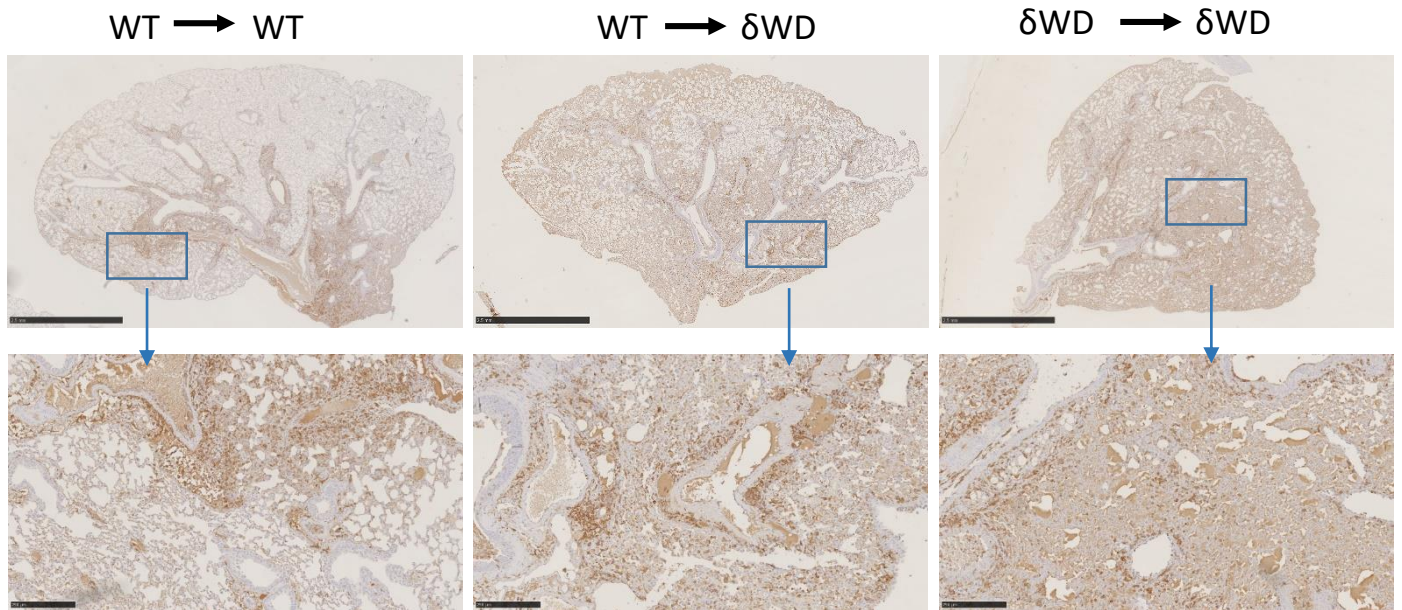
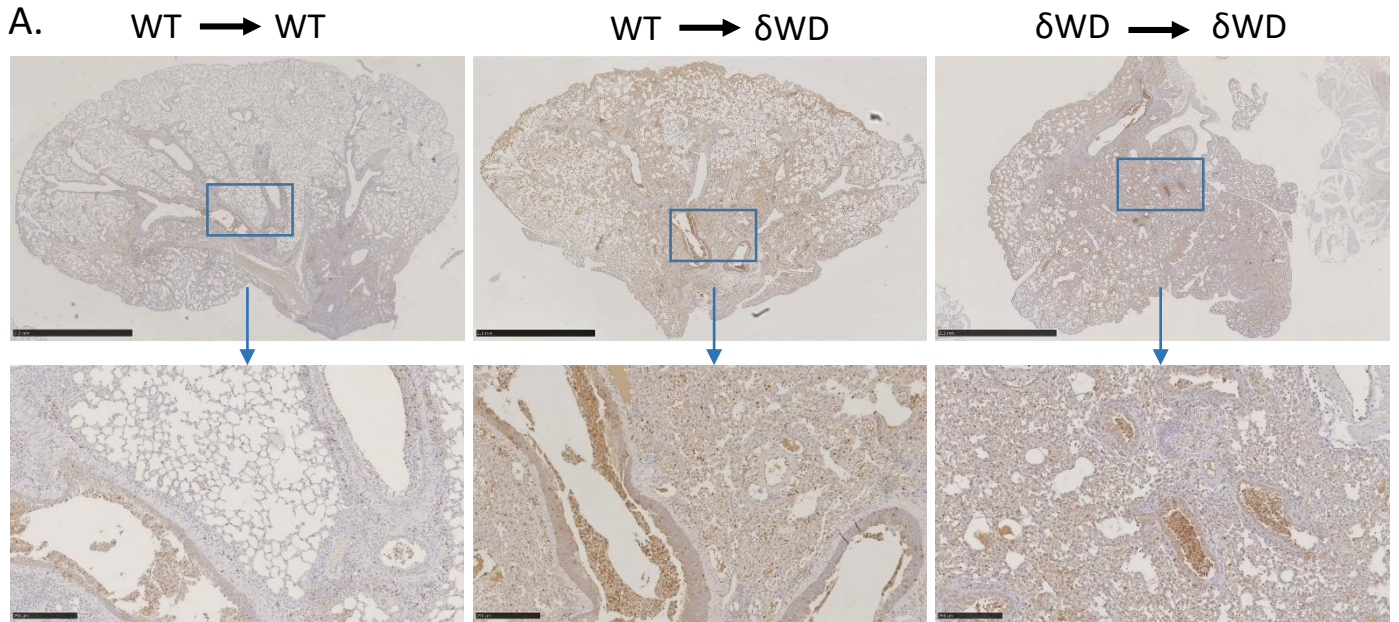


**Figure 5.3 Immunohistochemical analysis of lung following challenge with high dose influenza virus.** - Mice were irradiated and then reconstituted with wild type or  $\delta$ WD bone marrow as indicated. After being given intranasal challenge of influenza virus strain X31 (1000pfu), lungs from indicated mice were removed at day 5 d.p.i. Macrophages were detected by using anti-Iba-1, visualized with DAB and counter-stained with hematoxylin. Micrographs of representative areas from lungs of 2 mice are shown. Scale bars represent 2.5mm (upper panels) or 250 $\mu$ m (lower images). The percentage area of antibody labelling were quantified by ImageJ. Significance was determined by one way ANOVA (\* $p < 0.05$ ), data represent the mean value  $\pm$  SD.

## Day5 p.i. Ly6G (neutrophils)



## Day5 p.i. H3 (netosis)

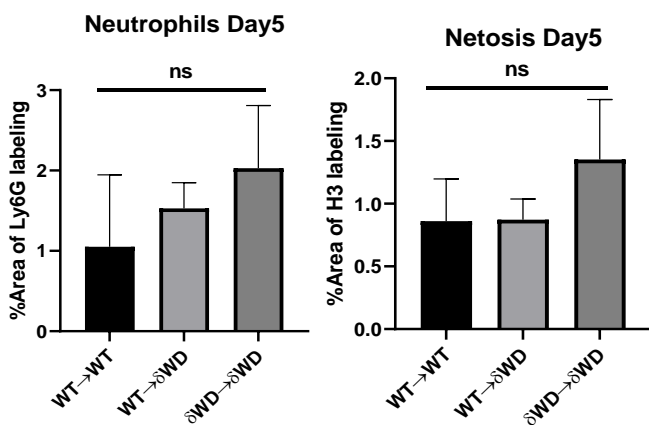
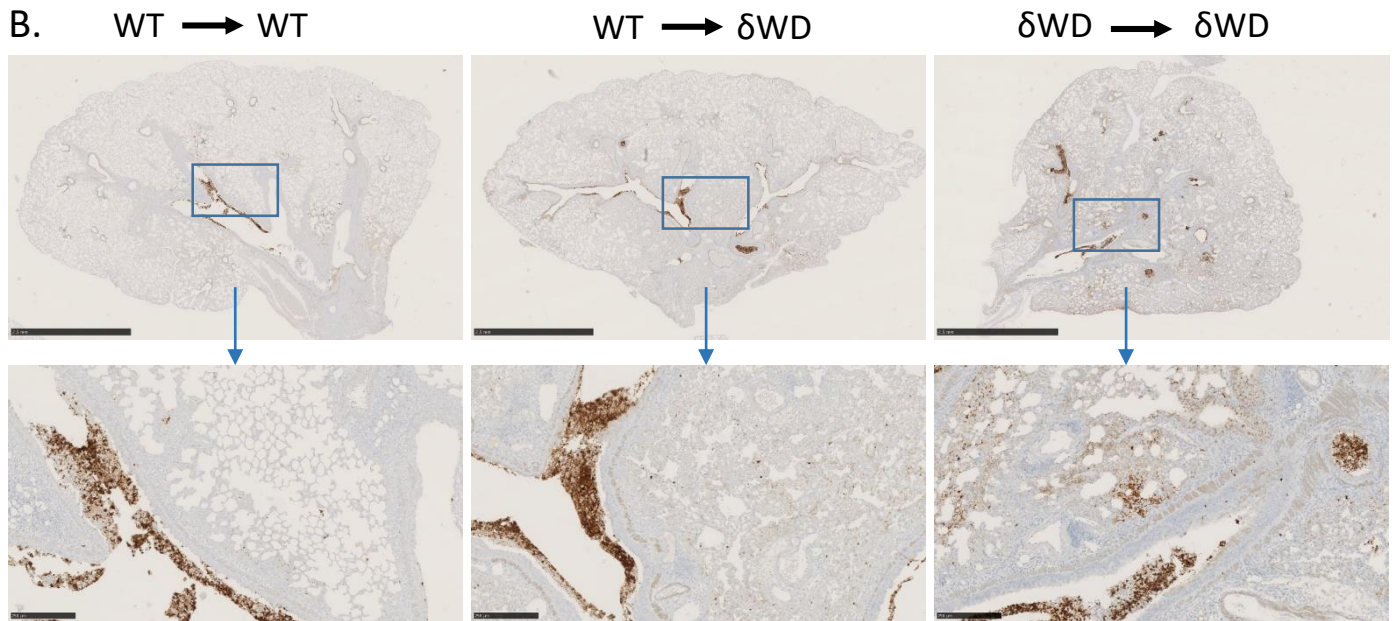


**Figure 5.4 Immunohistochemical analysis of lung following challenge with high dose influenza virus.** Mice were irradiated and then reconstituted with wild type or  $\delta$ WD bone marrow as indicated. After being given intranasal challenge of influenza virus strain X31 (1000pfu), lungs from indicated mice were removed at day 5 d.p.i. Neutrophils were detected by anti-Ly6G (**A**), and netosis with anti-H3 (**B**), visualized with DAB and counter-stained with hematoxylin. Micrographs of representative areas from lungs of 2 mice are shown. Scale bars represent 2.5mm (upper panels) or 250 $\mu$ m (lower images). The percentage area of antibody labeling were quantified by ImageJ. Significance was determined by one way ANOVA (\* $p < 0.05$ ), data represent the mean value  $\pm$  SD. 127

## 5.4 $\delta$ WD mice reconstituted with wild type bone marrow does not protect against immune infiltration into the lungs during IAV infection

According to weight loss and mortality measurement [Figure 5.2],  $\delta$ WD mice reconstituted with wild type bone marrow remained highly sensitive to IAV. The next experiments monitored inflammatory infiltration into the lungs. Mice were challenged with IAV X31 1000pfu and lungs taken at 5d p.i. were analysed by immunohistochemistry. Macrophages were detected by anti-Iba-1, neutrophils and netosis were detected by anti-Ly6G and anti-H3, visualized with DAB and counter-stained with hematoxylin. According to Figure 5.3 and 5.4A, the littermate controls reconstituted with wild type bone marrow cells failed to develop severe macrophage and neutrophil infiltration following IAV infection at day 5 pi. A preliminary survey of sections suggested that  $\delta$ WD mice reconstituted with wild type bone marrow displayed increased macrophage and neutrophil infiltration, similar to those observed for  $\delta$ WD mice lacking non-canonical autophagy in all cells. Quantification was attempted using ImageJ to assess DAB stain. Analysis of macrophage infiltration in Figure 5.3 suggested that macrophage staining was similar for all three mice. Similar analysis of neutrophils in Figure 5.4 showed that the percentage of area labelled by Ly6G when  $\delta$ WD mice were reconstituted with wild type bone marrow was higher than WT  $\rightarrow$  WT reconstitution, but lower than reconstitution of  $\delta$ WD with  $\delta$ WD bone marrow. There was a clear upward trend but this was not confirmed statistically. Netosis [Figure 5.4B] was observed in the bronchi and bronchioles in all the 3 mice models, while the WT to  $\delta$ WD and WT  $\rightarrow$  WT reconstitution displayed less in the lung parenchyma compares to reconstitution of  $\delta$ WD with  $\delta$ WD bone marrow. Although the statistical analysis failed to show significant differences between WT  $\rightarrow$   $\delta$ WD and WT  $\rightarrow$  WT reconstitutions, there was a trend for increased netosis in the  $\delta$ WD  $\rightarrow$   $\delta$ WD reconstitution.

## 5.5 Discussion and summary

The 'in vivo' data from the chimera reconstitution experiment [Result 5.2] suggested that  $\delta$ WD mice with a systemic defect in non-canonical autophagy in all tissues could not be rescued by reconstitution with wild type bone marrow cells. Reconstituted mice showed increased weight loss, higher mortality and higher virus titre in lung. Taken together with

chapter 4, these results suggest that protection of mice against excessive inflammation and severe IAV infection 'in vivo' is independent of immune cells, particularly LAP in phagocytes. A lack of involvement of LAP was surprising because the activation of LAP in phagocytic cells such as macrophages, dendritic cells and neutrophils by TLR signalling, NADP oxidase activation and ROS production would provide phagocytes with a powerful means of recognising and controlling microbial infection 'in vivo'. Activation of acid sphingomyelinase by *Listeria monocytogenes* (Gluschko et al 2018) and subsequent ROS production by NOX2, for example recruit LC3 to phagosomes. Similarly, activation of TLR2 and NOX2 by *Legionella dumoffi* signal ULK1-independent translocation of LC3 to single-membraned vacuoles containing Legionella (Hubber et al 2016). In both cases LC3 promotes fusion with lysosomes. The observation that virulence factors such as the GP63 metalloprotease of *Leishmania major* and melanin of *Aspergillus fumigates* prevent recruitment of NOX2 to phagosomes to prevent LAP (Matte et al 2016, Akoumianaki et al 2016, Kyrimizi 2018) further underlines the importance of LAP in phagocytes as defence against infection. While LAP provides a defence against several microbes 'in vitro', particularly for microbes with a tropism for macrophages, the data presented above suggest that LAP does not protect mice against IAV 'in vivo'. The intranasal infection model used in this study introduces IAV to airway epithelial cells and the results suggest that LC3-associated endocytosis in airway epithelium limits IAV infection before the virus reaches the lung associated immune system. This is supported by 'ex vivo' experiments carried out in the lab by PhD student Ben Bone showing that virus titres and interferon responses are 10-fold greater in lung explant cultures from  $\delta$ WD mice.

The results from immuno-histochemical analysis of lung were less clear cut. There was an upward trend for infiltration by neutrophils but differences in macrophages were difficult to observe. One explanation may lie in the limited sample size available and the d.p.i of sample collection. Sample collection was restricted by time available for analysis and the cost of 'in vivo' challenge experiments involving bone marrow reconstitution. A compromise was agreed where samples would be taken at day 5 d.p.i. Sample sizes were low because two mice were analysed for each reconstitution, and each mouse provided one section. The timing of sample collection may explain why differences in macrophages were not seen at day 5 because increases in macrophage infiltration were observed at day 7 in  $\delta$ WD mice [Figure 3.20]. It is possible that increased macrophage infiltration may be seen if samples were

analysed at day 7 d.p.i. Similarly, major neutrophil infiltration was observed in  $\delta$ WD mice at day 3, rather than day 5 [Figure 3.18 & 3.19].

It is interesting that reconstitution of  $\delta$ WD mice with WT bone marrow resulted in increased infiltration of neutrophils but the increase in netosis seen following reconstitution with  $\delta$ WD bone marrow was absent [Figure 5.4]. This may indicate increased netosis by neutrophils in  $\delta$ WD mice. This raises the possibility that the increased netosis in  $\delta$ WD mice is not only caused by high neutrophil infiltration but also due to the highly activated netosis process in  $\delta$ WD neutrophils. Whether the  $\delta$ WD neutrophils are more likely to activate netosis than WT neutrophils during IAV infection still needs to be demonstrated and is worthy of further study.

## **Chapter 6**

### **Result Part IV**

## Chapter 6: Role played by WD domain of ATG16L1 on acquired immune response following IAV infection

To investigate the role played by WD domain of ATG16L1 on activation of acquired immune responses during IAV infection, the population of immune cells in the lung from infected or uninfected mice was quantified by flow cytometry and antibody levels in the serum were quantified by enzyme-linked immunosorbent assay (ELISA).

### 6.1 Introduction and Aims:

Results from chapter 3 suggested that  $\delta$ WD deficiency in ATG16L1 could affect the innate immune response against IAV infection. It was therefore interesting to investigate the effect of  $\delta$ WD deficiency on adaptive immunity.

Compared to the innate immune system, the adaptive immune system is highly specific to a particular pathogen and it can provide a long-lasting protection. T and B lymphocytes are the key players in adaptive immunity against the IAV infection. T cells are predominantly produced in the thymus, mainly known as CD8<sup>+</sup> cytotoxic T cells and CD4<sup>+</sup> helper T cells. Helper T cells 'help' B cell maturation, and activation of cytotoxic T cells and macrophages. Whereas, cytotoxic T cells could restrict viral replication through lysis of virally infected cells (X. Chen et al., 2018), B cells are responsible for antibody production against invasive pathogens. The activation of T and B cells relies on the antigen presentation cells (APCs) such as macrophages and DCs. Upon IAV infection, internalized virus would be recognized and digested by the APCs in the lung leading to presentation of viral antigens on the MHC class I and II on the APCs plasma membrane. The APCs, mainly DCs, migrate from the lung to the draining lymph nodes and activate CD4<sup>+</sup> and CD8<sup>+</sup> T cells (Lambrecht & Hammad, 2012). T cells, which recognize the antigen presented by APCs, become activated and proliferate and migrate from the lymph nodes to the site of infection (Spitaels, Roose, & Saelens, 2016). Helper T cells are activated when they recognise antigen presented by MHC class II and provide help to B cell that encountered to the same antigen. This ultimately results in the production of protective antibodies against IAV. The aim of this chapter is to investigate whether the loss of the WD domain changes of immune cell populations and immunoglobulin production during IAV infection.

# 100 PFU X31

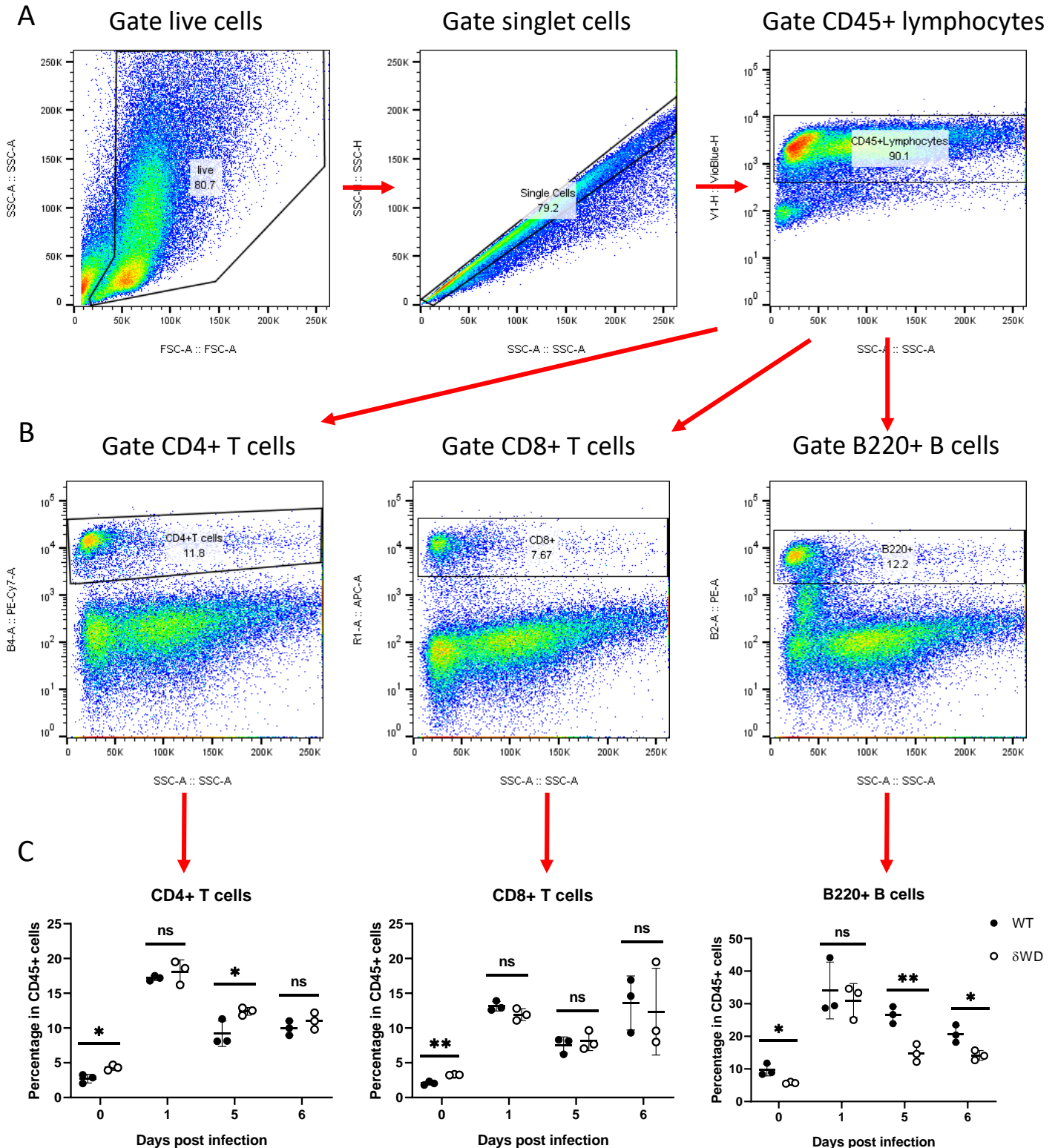


**Figure 6.1. Gating strategy used to identify T cells and B cells in mice lung.** (A) Cells suspensions were prepared from enzymatically digested mice lungs, after exclusion of doublets and debris, immune cells were identified by CD45 staining. (B) A sequential gating strategy was used to identify populations expressing specific markers: helper T cells (CD4+), cytotoxic T cells (CD8+) and B cells (B220+). (C) Percentages of each lymphocyte subsets in CD45+ cells were analysed at day 0, 1, 5 and 6 post infection. Lung samples were taken from mice that given intranasal challenge of influenza virus strain X31 (100pfu). FSC, forward scatter; SSC, side scatter. Values shown represent the mean  $\pm$  SD (n = 3). Significance was determined by multiple T test (\*p < 0.05).

# 100 PFU X31

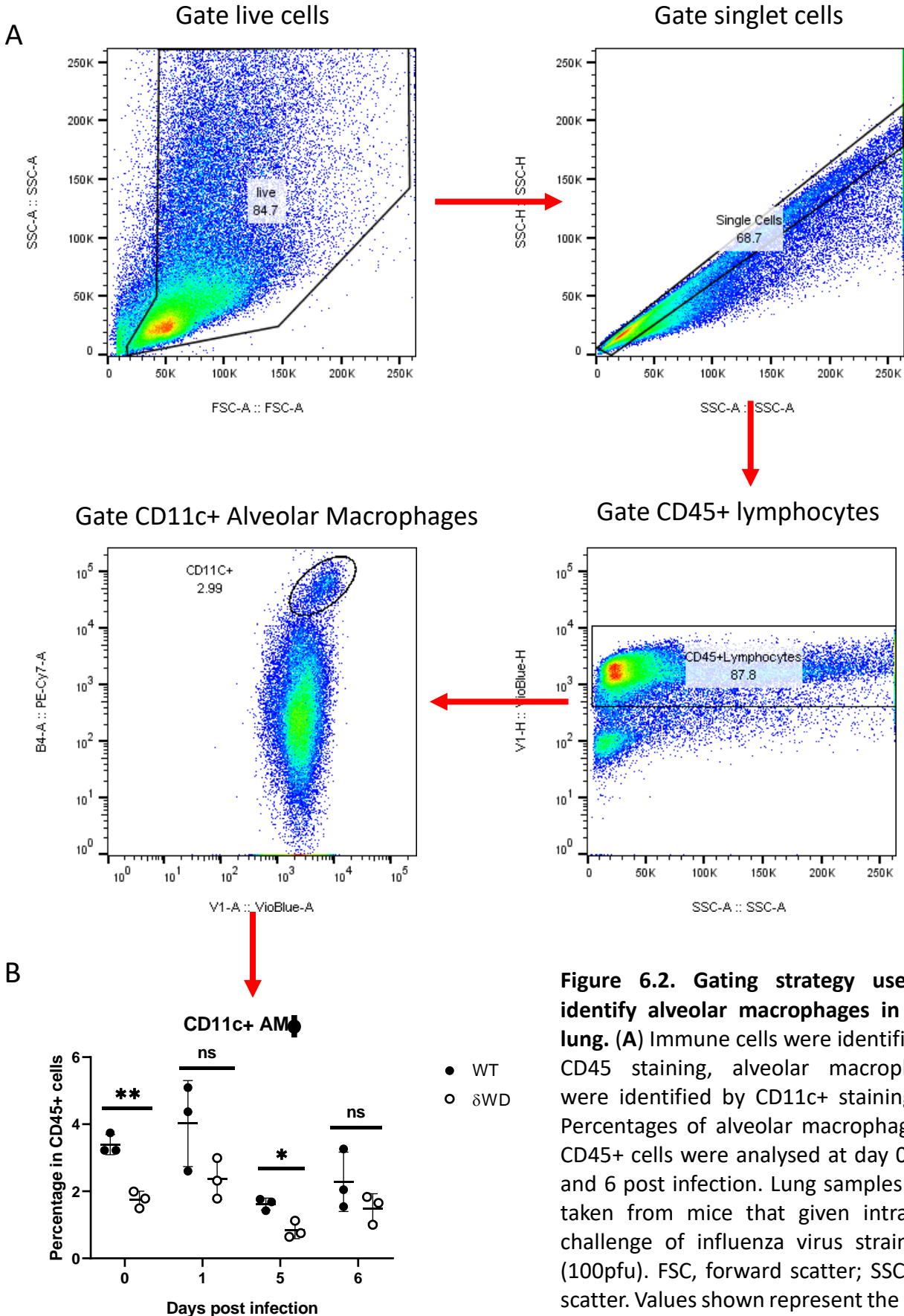


**Figure 6.2. Gating strategy used to identify alveolar macrophages in mice lung.** (A) Immune cells were identified by CD45 staining, alveolar macrophages were identified by CD11c+ staining. (B) Percentages of alveolar macrophages in CD45+ cells were analysed at day 0, 1, 5 and 6 post infection. Lung samples were taken from mice that given intranasal challenge of influenza virus strain X31 (100pfu). FSC, forward scatter; SSC, side scatter. Values shown represent the mean  $\pm$  SD (n=3). Significance was determined by multiple T test (\*p < 0.05). 134

# 1000 PFU X31

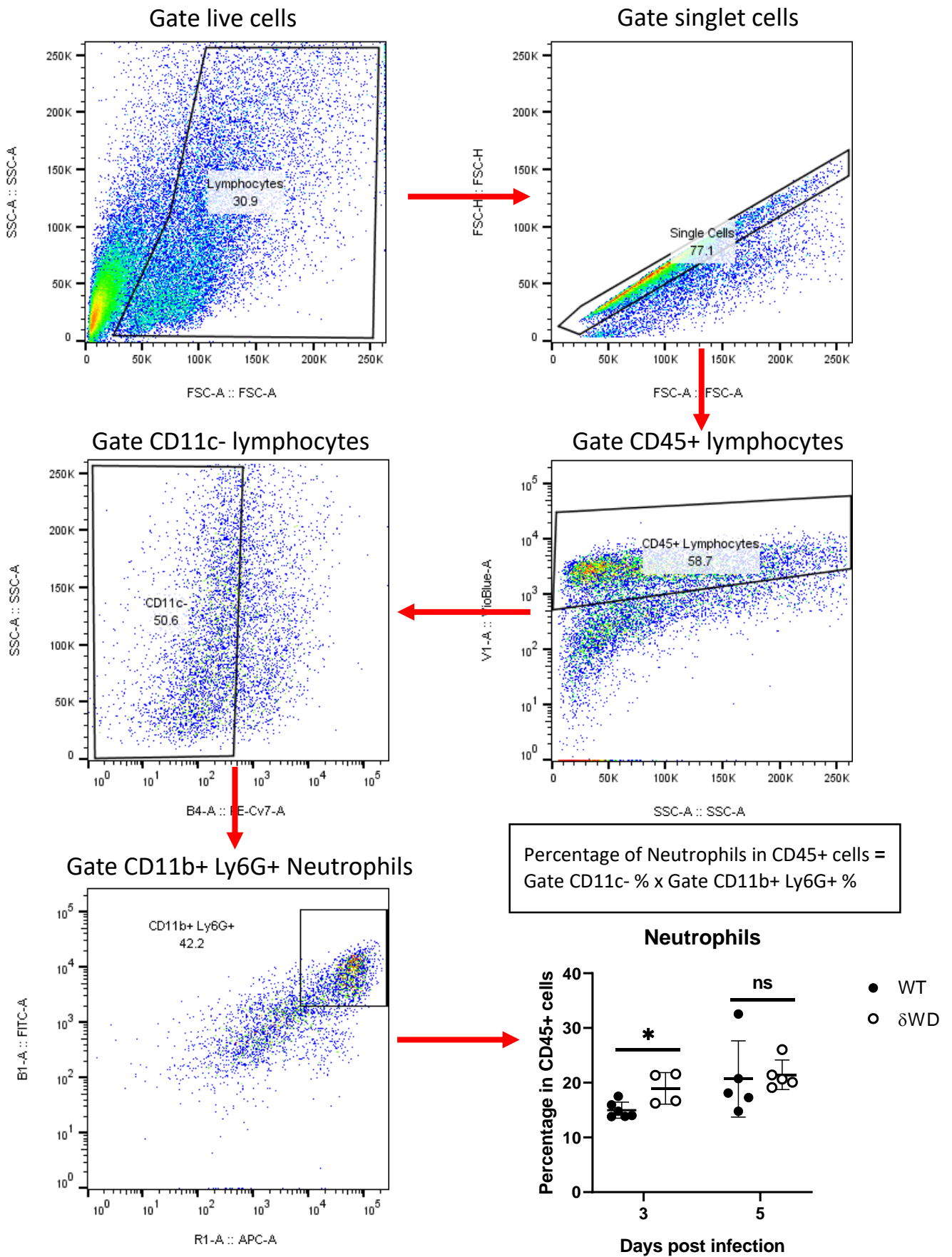


**Figure 6.3. Gating strategy used to identify neutrophils in mice lung.** (A) immune cells were identified by CD45 staining, neutrophils were identified by CD11c-, CD11b+ and Ly6G+ staining (B) Percentages of neutrophils in CD45+ cells were analysed at day 3 and 5 post infection. Lung samples were taken from mice that given intranasal challenge of influenza virus strain X31 (1000pfu). FSC, forward scatter; SSC, side scatter. Values shown represent the mean  $\pm$  SD (n=4-6). Significance was determined by multiple T test (\*p < 0.05). 135

# 1000PFU X31

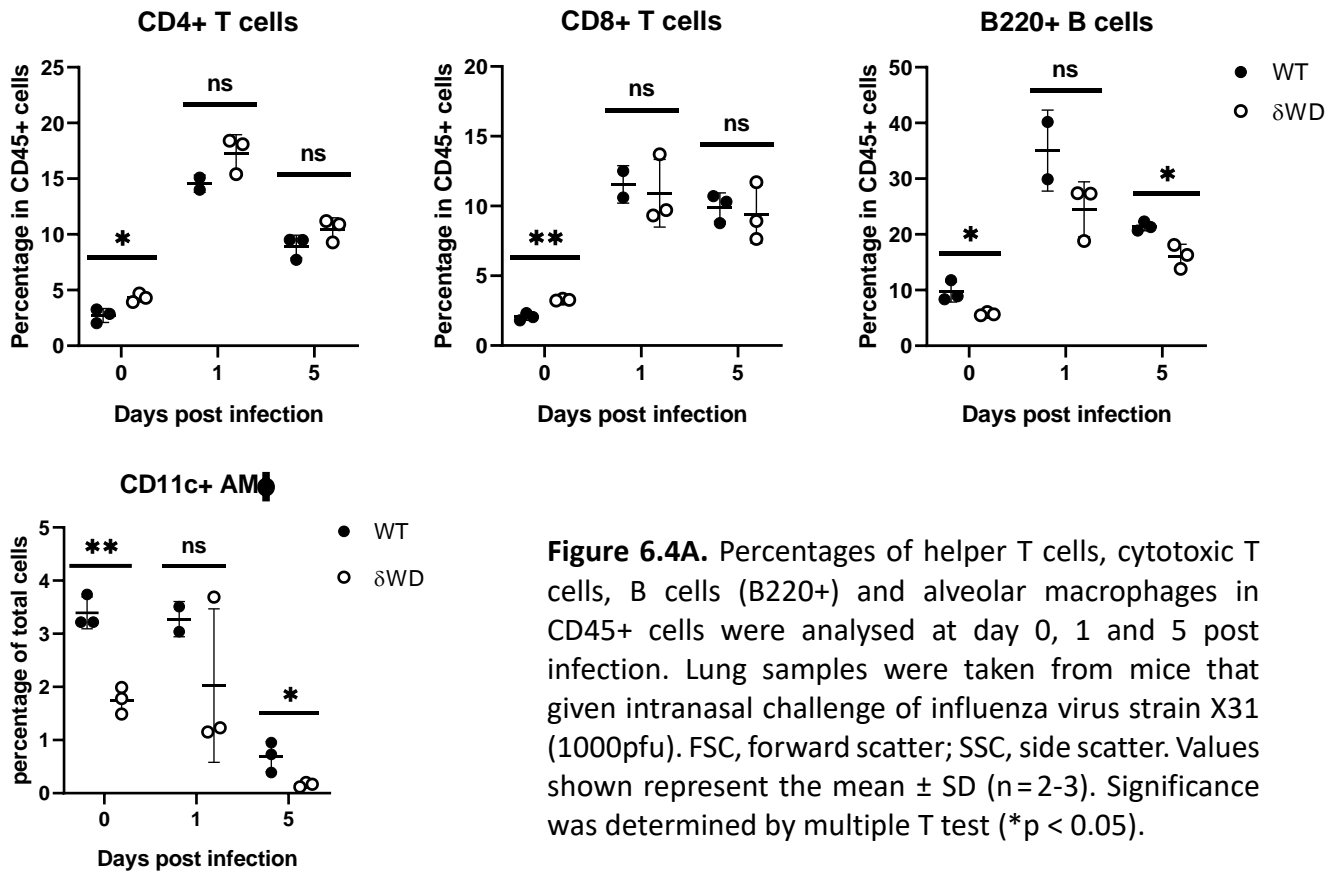


**Figure 6.4A.** Percentages of helper T cells, cytotoxic T cells, B cells (B220+) and alveolar macrophages in CD45+ cells were analysed at day 0, 1 and 5 post infection. Lung samples were taken from mice that given intranasal challenge of influenza virus strain X31 (1000pfu). FSC, forward scatter; SSC, side scatter. Values shown represent the mean  $\pm$  SD (n=2-3). Significance was determined by multiple T test (\*p < 0.05).

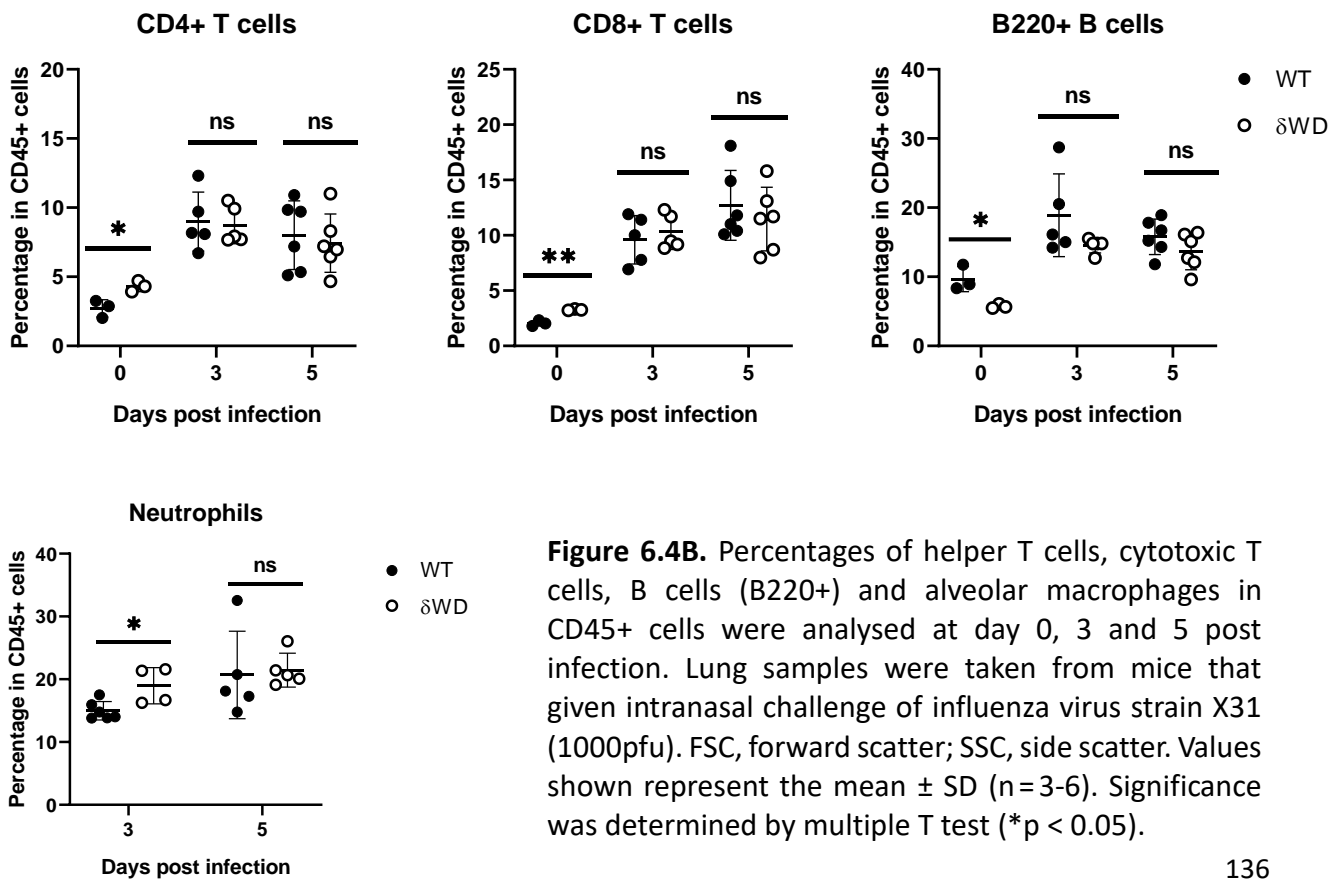


**Figure 6.4B.** Percentages of helper T cells, cytotoxic T cells, B cells (B220+) and alveolar macrophages in CD45+ cells were analysed at day 0, 3 and 5 post infection. Lung samples were taken from mice that given intranasal challenge of influenza virus strain X31 (1000pfu). FSC, forward scatter; SSC, side scatter. Values shown represent the mean  $\pm$  SD (n=3-6). Significance was determined by multiple T test (\*p < 0.05).

## 6.2 The effect of Atg16L1 WD domain in immune cells population on the lung during IAV infection

Mice were challenged with H3N2 X31 by inhalation, lungs were taken at the indicated days post infection (dpi). Lungs were processed to generate single cell suspensions for flow cytometry analysis. Two viral doses were applied to the mice model: 100pfu (low dose) and 1000pfu (high dose). The population of alveolar macrophages was assessed from the low dose (100pfu) infection at 1, 5 and 6 dpi, and the population of neutrophils and alveolar macrophages were assessed from the high dose (1000pfu) infection at 1, 3 and 5 dpi. The populations of T cells and B cells were assessed from both of the doses.

The gating strategy and percentages of each lymphocyte subset are indicated in Figure 6.1. Figure 6.1A shows how cells expressing leucocyte common antigen CD45<sup>+</sup> cells were identified within the lung cell suspension. In Figure 6.1B the CD45<sup>+</sup> population was analysed to identify helper T cells (CD4<sup>+</sup>), cytotoxic T cells (CD8<sup>+</sup>) and B cells (B220<sup>+</sup>). Figure 6.1C, shows the percentage cell distribution in the lungs of mice taken at the indicated times after challenge with IAV. The proportion of helper T cells (CD4<sup>+</sup>) and cytotoxic T cells (CD8<sup>+</sup>) within the CD45<sup>+</sup> lymphocytes in the lungs before infection were low at around 3%, with slightly higher, and statistically significant percentages seen in  $\delta$ WD mice compared to the littermate controls. Similarly, the percentage of B cells in lung was low before infection. This time there was a statistically significant decrease in B cells in  $\delta$ WD mice. The reason for these slight changes in lung lymphocyte populations before infection is unknown.

**Low dose influenza infection.** The percentages of all the three lymphocyte subsets within the CD45<sup>+</sup> cells increased after low dose IAV infection in both WT and  $\delta$ WD mice. This is seen on day 1pi around 4-fold increases in percentages of helper T cells, and 3-fold increases in percentages of cytotoxic T cells and B cells. There was no obvious difference in T cell populations between WT and  $\delta$ WD mice. A fall in helper T cells and B cells was observed at day 5 and 6 pi in both WT and  $\delta$ WD mice lung. During this period (day 5, 6 pi) B-cell populations fell faster in the  $\delta$ WD mice compared to the littermate controls.

The gating strategy for calculating the percentages of CD11c<sup>+</sup> alveolar macrophages in CD45<sup>+</sup> cells following low dose infection are indicated in Figure 6.2. According to Figure 6.2B, the

populations of alveolar macrophages were low (less than 5% of CD45+ cells) and remained low during infection.

**High dose influenza infection.** Two independent trials were carried out with high dose IAV challenge. The population of alveolar macrophages, T cells and B cells were assessed in the first trial, at day 1 and 5 pi, while, the populations of neutrophils, T cells and B cells were assessed in the second trial, at day 3 and 5 pi.

The gating strategy used to identify neutrophils in CD45+ cell populations is indicated in Figure 6.3. According to the first trial Figure 6.4A, the percentage of each cell type in the high dose infection were quite similar to the observation in the low dose infection. The percentage of T cell and B cells were increased in both WT and  $\delta$ WD mice after high dose IAV infection at day 1, followed by a decline at day 5. Again, there was a faster fall in B cells in  $\delta$ WD mice at day 5 pi. The experiment also studied CD11c+ alveolar macrophages, levels were low in lungs throughout infection and fell from 3-4% to less than 2% at day 5dpi.

The experiment above analysed 3 mice at each time point. The high dose challenge was repeated to generate a larger sample size of 3-5 mice at day 3 and 5 post infection. An analysis of neutrophils was included in this trial. Figure 6.4B shows analysis of 5 mice at day 1 and day 5 pi. Again, levels rose following infection but there was no obvious difference in the mean levels of T and B cells between day 3 and day 5 pi. Neutrophils represented 15-20% of CD45+ cells in the lung 3 days post infection with a small but significant increase in neutrophils in  $\delta$ WD mice.

The results are broadly in agreement with the histochemical results presented in Chapter 3 showing lymphocyte migration into the lungs after IAV infection. The results from the FACs analysis were not however as striking as the histochemical images. Large increases in macrophages were not evident at day 6, but increased neutrophils were seen at day 3. One reason for this may be down to sample preparation. Homogenisation of lung tissue might not be ideal as immune cells can be lysed during the long processes and that would affect cell recovery. This can be solved by collecting the lung lavage instead of the whole lung homogenates. The FACs experiment was repeated by James Stewart in University of Liverpool, with the lung lavage collected from the day 2 and 5 pi, with 1000pfu infection. Results (data not shown) suggest that rapid isolation of cells from lavage fluid preserves

lymphocyte populations leading to significantly higher neutrophil and macrophage percentage in  $\delta$ WD compared to litter mate control in day 2 and 5 pi, respectively. Interestingly, the percentage of alveolar macrophage, T cells and B cells in CD45+ lymphocytes all show decline after day 1 pi, [Figure 6.4A and B] this might be caused by displacement by the high neutrophil infiltration in the lung which also positive for CD45.

### 6.3 The effect of WD domain of Atg16L1 on immunoglobulin production during IAV infection

In order to investigate the effect of WD domain on immunoglobulin production during IAV infection, the immunoglobulin levels in the serum were quantified by Elisa using inactivated IAV as capture antigen. Serum was taken from mice challenged with H3N2 X31 1000 pfu, at day 1, 7 and 20 days pi. Serum from day 1 and 7 pi were used to test level of IgM, and day 20 pi was used to test IgG. IgM is first antibody to respond during infection, it usually associated with the early onset phase of an infection, while IgG is generally associated with long-term immunity or reactivity towards a pathogen.

According to Figure 6.5, the IgM level is increased in both of WT and  $\delta$ WD mice after infection, compared to the negative control. There was no difference between WT and  $\delta$ WD mice on day 1 pi, while the level of IgM is raised in  $\delta$ WD mice compared to WT on day 7 pi. Conversely, the level of IgG was higher in WT mice compared to  $\delta$ WD mice at 20 dpi. These results suggesting there are effects of Atg16L1 WD domain on immunoglobulin production during IAV infection. At the early stage of infection, the high level of IgM in  $\delta$ WD mice may be result from the high inflammation level present in the lung, whereas the low level of IgG at later stage might due to the low percentage of B cells in  $\delta$ WD mice.

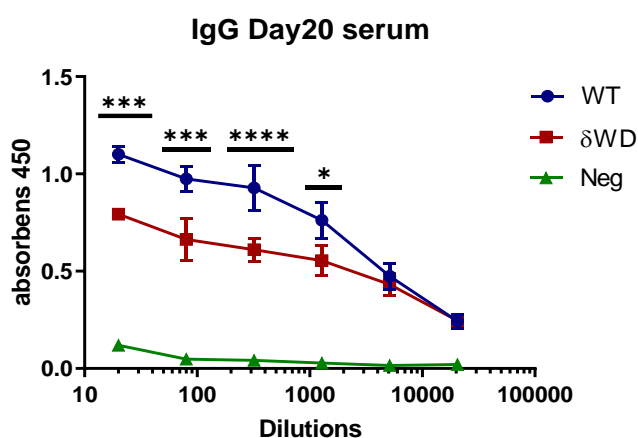
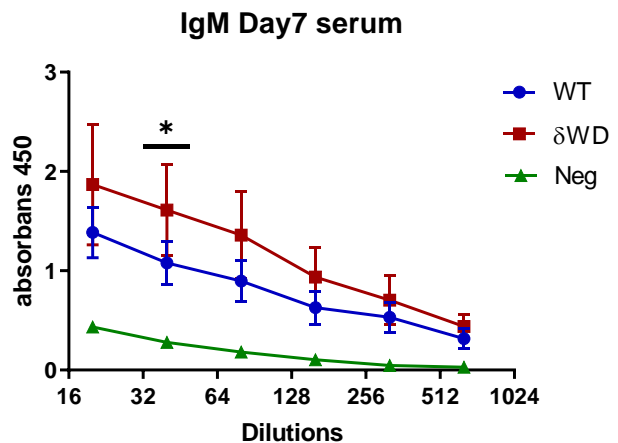
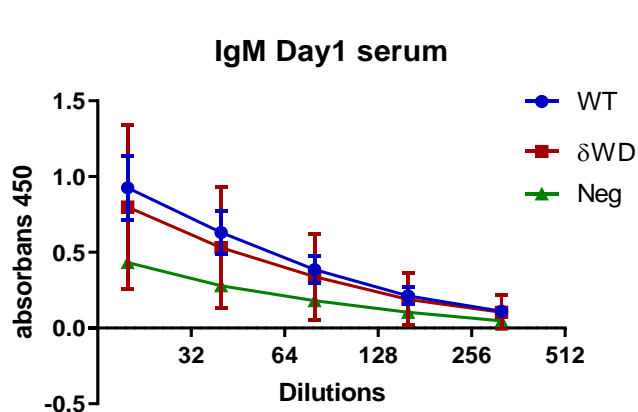


**Figure 6.5. Quantification of immunoglobulins level in the serum by Elisa following challenge of mice with high dose of influenza virus.** Mice were given intranasal challenge of influenza virus strain X31 (1000pfu). Serums were taken from mice (n=2-6) at the indicated times and analysed by Elisa. Values shown represent the mean  $\pm$  SD (n=2-6). Significance was determined by 2-way ANOVA with Sidak's multiple comparison test (\*p < 0.05).

## 6.4 Discussion

According to low dose day 5 pi, the CD45+ lymphocytes in  $\delta$ WD mice lung shows higher constitute of T cells, and low of alveolar macrophages and B cells compare to the littermate control, this is consistent with the uninfected lung samples. It suggests the WD deficiency in ATG16 barely affect the constitution of lymphocytes in the lung at early time point of low dose infection.

According to the high dose infection, the percentage of neutrophils in CD45+ lymphocytes is high in  $\delta$ WD mice lung compares to the litter mate control. This is consistent with the cytokines and pathology results in chapter 3, suggesting a high neutrophils infiltration in  $\delta$ WD mice lung at early time point high dose infection.

The percentage of alveolar macrophage, T cells and B cells in CD45+ lymphocytes all show decline after day 1 pi, it might cause by the high neutrophil infiltration in the lung which also positive in CD45.

The way of sample preparation from lung tissue homogenise might not be ideal as immune cells can be lysed during the long process, that would affect the results accuracy. This can be solved by collecting the lung lavage instead of the whole lung homogenise. The FACs experiment was repeated by James Stewart in University of Liverpool, with the lung lavage collected from the day 2 and 5 pi, with 1000pfu infection. Results (data not shown) suggest there is a significant high in neutrophils and macrophages percentage compares to litter mate control in day 2 and 5 pi, respectively. This suggests the WD deficiency would lead to high level of inflammatory cells infiltration in the lung after IAV infection. While, whether it affect the lymphocytes recruitment for acquired immunity still need to be demonstrate.

## **Chapter 7**

### **Discussion**

## Chapter 7 Discussion:

### 7.1 $\delta$ WD mice do not exhibit alterations in lymphocyte populations

During the progress of this PhD a LAP deficient mice model based on Rubicon KO has been established by Martinez et al (Martinez et al., 2015). However, Rubicon is also involved in a plethora of signalling pathways and by influencing NF- $\kappa$ B signalling, acts as a sentinel in inflammatory response. As a result, mice with LysMcre mediated loss of Rubicon from myeloid cells exhibit exaggerated inflammatory responses resulting in Lupus-like autoimmunity to apoptotic cells (Martinez et al., 2016). This phenotype makes the Rubicon KO mice less than ideal for studies of LAP and infection study LAP (Wong et al., 2018). The  $\delta$ WD mice (*Atg16L1* <sup>$\delta$ WD/ $\delta$ WD</sup>) lack the WD repeat domain of ATG16L1, but remain the ATG5-binding and CC-domain required for canonical autophagy are growing normally and maintain tissue homeostasis (Rai et al., 2019). In addition, alterations in lymphocyte populations seen in RUBICON<sup>LysMcre</sup> mice lacking non-canonical autophagy/LAP in myeloid cells (Martinez et al., 2016) were also absent from  $\delta$ WD mice. FACS results generated by Angela Man in the lab show, the distribution of T cell, B cell and macrophage populations in spleens were similar in  $\delta$ WD mice to littermate [Figure 7.1]. Therefore,  $\delta$ WD mice can be used as a suitable animal model to investigate the role of non-canonical autophagy or LAP during infection.

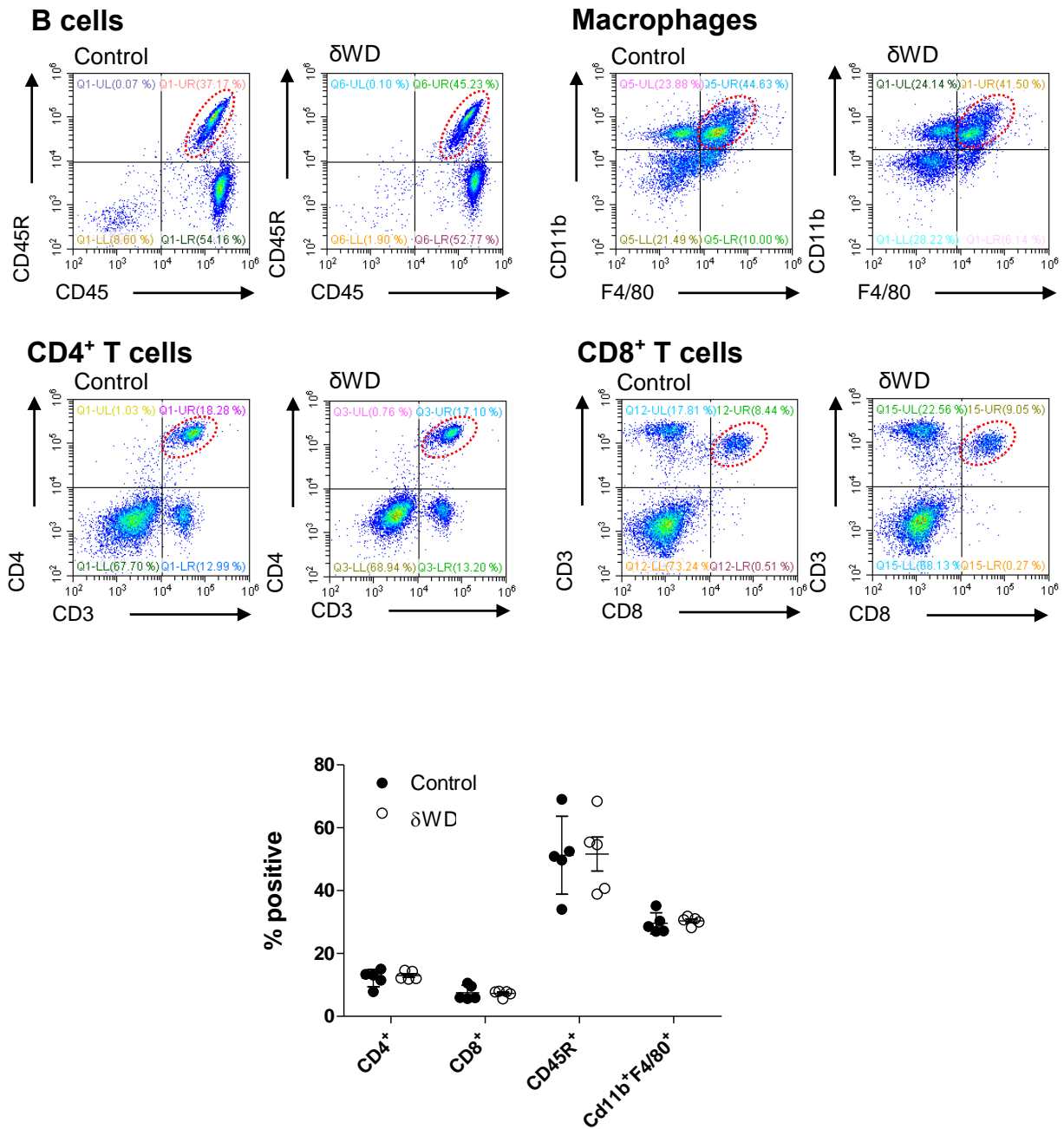


**Figure 7.1. Mice deficient in non-canonical autophagy have normal leukocyte populations.** The possibility that the loss of non-canonical autophagy resulted in changes in leukocyte populations was tested by analysing dissociated spleens by FACS using antibodies to T-cell subsets (CD3+, CD4+ and CD3+, CD8+), B-cells (CD45R/B220) and macrophages (CD11b, F40/80) Upper panel shows representative FACS profiles from n = 3 mice. Lower panel shows the percentage positive for each population. Significance was determined by T test (\*p < 0.05), data represent the mean value ± SEM.

## 7.2 correlative analysis across IAV mRNA level, cytokines expression level, viral titre and IAV histology quantification

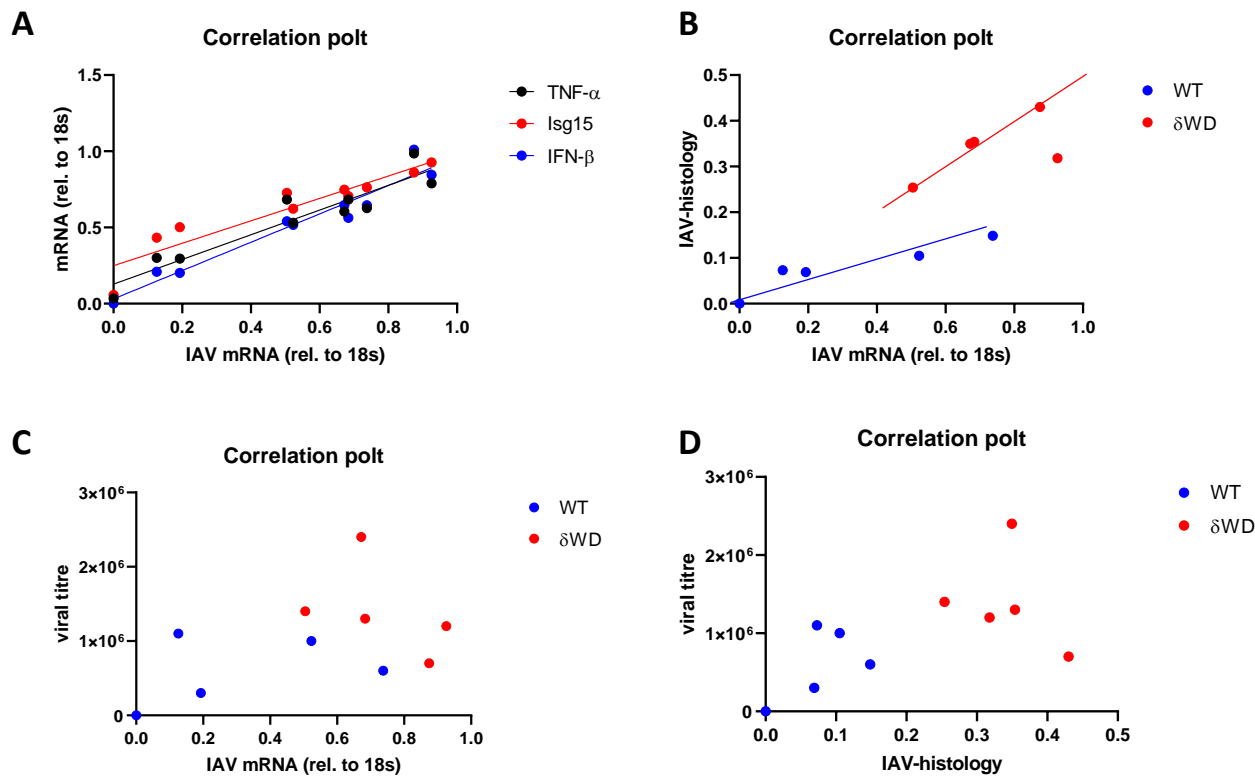


**Figure 7.2: The correlation plots between IAV mRNA level, cytokines expression level, viral titre and IAV histology quantification.** Mice were given intranasal challenge of influenza virus strain X31 (1000pfu). Lungs were removed from mice (n=5) at 3 day post infection and analysed for virus genome by q-PCR, plaque assay and histology quantification. **A.** Correlation between IAV mRNA level and cytokines expression level. **B.** Correlation between IAV mRNA level and IAV histology quantification level. **C.** Correlation between IAV mRNA level and viral titre by plaque assay. **D.** Correlation between IAV histology quantification level and viral titre by plaque assay.

Attempts were made to correlate data sets with individual mice. The aim was to determine for example if high virus titre correlated with increased cytokine expression. The results in Figure 7.2A show that there was a good positive correlation between the IAV mRNA level and cytokine expression level and a reasonable positive correlation between the IAV mRNA level and IAV antigen quantified from histology sections [Figure 7.2B]. It was not possible to see a clear correlation between the viral titre analysed by plaque assay and the IAV mRNA level [Figure 7.2C] or with the IAV quantified from histology sections [Figure 7.2D]. These results suggest that the increased cytokine expression might be triggered by high IAV replication and

viral m-RNA level in the lung which would stimulate innate immunity. The higher viral m-RNA would also explain the correlation with IAV protein in the lung sections. However, the high levels of IAV mRNA did not correlate with a high viral titre [Figure 7.2C], and high viral titre did not correlate with IAV protein in the lung sections. A possible reason could be that viral mRNA is incorporated into replication-defective particles. The possibility that the <sup>TM</sup>WD mutation could affect relative levels of defective virus articles is worthy of further study. In addition, the best correlations were obtained when the assays for different entities were the same. For example when qPCR is used to determine both viral RNA and cytokine mRNA there was a high correlation, but poor correlation when virus titre obtained from plaque assay is compared to histochemical analysis.

### 7.3 Could LAP in phagocytic cells play a role in controlling IAV infection?

The link between non-canonical autophagy TLR signalling, NADP oxidase activation and ROS production (Delgado, Elmaoued, Davis, Kyei, & Deretic, 2008; Sanjuan et al., 2007) provides phagocytes with a powerful means of restricting infection '*in vivo*'. Virulence factors such as the GP63 metalloprotease of *Leishmania major* and melanin of *Aspergillus fumigatus* prevent LC3 recruitment to phagosomes (Akoumianaki et al., 2016; Matte et al., 2016) and indicate the importance of non-canonical autophagy in phagocytes as a defence against prokaryotic pathogens. Radiation chimeras were used to test if phagocytic cells derived from wild type *Atg16L1*<sup>+/+</sup> bone marrow could protect the susceptible  $\delta$ WD mice from lethal IAV infection. When challenged with IAV, control mice reconstituted with wild type *Atg16L1*<sup>+/+</sup> phagocytic cells [Figure 5.2A] started to recover and regain weight at d 4 pi. In contrast,  $\delta$ WD mice reconstituted with wild type bone marrow remained highly sensitive to IAV [Figure 5.2A] with weight falling to 75% by day 5 associated with ca. log increases in viral titre in lung [Figure 5.2C], and inflammatory infiltration into the lung [Figure 5.4], similar to those observed for  $\delta$ WD mice lacking non-canonical autophagy in all cells. A reciprocal experiment used a knock in strategy [Figure 4.3] to generate mice where expression of the truncated *Atg16L1*  $\delta$ WD gene was restricted to myeloid cells ( $\delta$ WD<sup>phag</sup>). These mice, which lack non-canonical autophagy in myeloid cell lost weight at the same rate as controls following challenge [Figure 4.7 A] and failed to show the raised virus titre in lung [Figure 4.7 B] seen in  $\delta$ WD mice.

Similarly, the raised IL-1 $\beta$  pro-inflammatory cytokine profile and profuse macrophage and neutrophil infiltration into lung [Figure 4.10] seen in  $\delta$ WD mice were absent, and similar to littermate controls.

Critically, these results showed that sensitivity of  $\delta$ WD mice to IAV was not caused by a loss of non-canonical autophagy from myeloid cells. The ability of non-canonical autophagy in epithelial cells to protect against virus infection was therefore tested '*in vitro*'. This experiment was carried out by PhD students Benjamin Bone in our lab (data not shown). Virus titres in MEFs and lung explant cultures from  $\delta$ WD mice were 10-fold greater than controls. The MEFs from  $\delta$ WD mice also showed large increases in expression of interferon sensitive genes ISG15 and IFIT, as seen in lung '*in vivo*'. These increases in  $\delta$ WD mice occurred before differences in virus replication were detected suggesting that non-canonical autophagy slows release of viral RNA into the cytoplasm for interaction with RNA sensors. The results show that non-canonical autophagy in epithelial cells has an inherent ability to control influenza virus.

#### **7.4 How loss of non-canonical autophagy/LAP causes high viral titre and cytokine expression after infection**

To further understand the mechanisms, we attempt to investigate how LAP deficiency causes high viral titre and cytokines expression after infection. The most reasonable mechanism could be that a defect in the control of viral replication following loss of non-canonical autophagy in the lung epithelial cells, leads to a cytokine storm and tissue damage. Non-canonical autophagy in the lung epithelial cells may transfer IAV to lysosomes for degradation after entry. Thus, loss of non-canonical autophagy would result in the increased release of vRNA into nucleus for replication, and high viral titre in the lung. The high viral titre would trigger the expression of interferons and chemokines, especially the interferon sensitive genes ISG15, IFIT and neutrophils recruiting chemokine CXCL-1. Subsequently, neutrophils infiltrate to the lung, releasing large amount of pro-inflammatory cytokines such as IL-1 $\beta$ , TNF- $\alpha$  (Galani et al., 2017), which recruiting more immune cells to the site of infection and inducing cytokine storm and tissue damage. In addition, the excessive netosis induced by neutrophils in  $\delta$ WD mice could also lead to acute lung injury and venous thromboembolism (Storisteanu

et al., 2017). As a result, the  $\delta$ WD mice end up with high viral titre and cytokines expression, excessive neutrophils infiltration and netosis, acute lung injury and high mortality.

Apart from a high viral titre inducing excessive cytokine expression, non-canonical autophagy in lung epithelial cells might also play a role in controlling cytokines expression directly. According to Chapter 3 Figure 3.14, the q-PCR results on day2 suggest that CXCL-1 is more highly expressed in  $\delta$ WD mice than littermate controls, whereas IAV replication level shows no difference on day2, indicating the high expression level of CXCL-1 in  $\delta$ WD mice at early time point after infection might not due to the high viral replication levels. It gives a possibility that non-canonical autophagy might able to restrict cytokine over production induced by IAV infection independent of controlling viral replication. Mechanically, within infected epithelial cells, the single-stranded viral RNA in the cytosol is recognized by retinoic acid-inducible gene-1 (RIG-I), results in stimulating the expression of IFNs, and pro-inflammatory cytokines. Therefore, it is possible that, the non-canonical autophagy in lung epithelial cells, which could reduce the amount of viral RNA in the cytosol by promoting the fusion of virus-contain endosomes and lysosomes, is able to control the excessive expression of cytokines during IAV infection. To confirm this possibility, the activity of RIG-I during IAV infection is worth to investigate, if the activity of RIG-I is higher in  $\delta$ WD mice than littermate controls that would demonstrate the role played by non-canonical autophagy in controlling cytokines expression directly.

In addition, the LAP deficiency in DCs and macrophages might explain the excessive cytokine expression in  $\delta$ WD mice. In pDCs, TLR7 recognizes the ssRNA genomes contained within the influenza virion that are taken up into the endosome. TLR7 signalling via the adaptor MYD88 from distinct endosomes results in the activation of either nuclear factor- $\kappa$ B (NF- $\kappa$ B) or IFN-regulatory factor 7 (IRF7), which are transcription factors that are responsible for stimulating the expression of pro-inflammatory cytokines and type I IFNs, respectively (Iwasaki & Pillai, 2014). According to this, the high viral titre in  $\delta$ WD mice would lead to more cytokine production by pDCs, and result in cytokine storm. Besides, the cells dying following infection could be phagocytosed by macrophages, allowing double-stranded RNA (dsRNA) to be recognized by Toll-like receptor 3 (TLR3). This also leads to induction of nuclear factor- $\kappa$ B (NF- $\kappa$ B)-dependent pro-inflammatory cytokines and of type I interferon (IFN) and IFN-stimulated genes (ISGs) downstream of IFN-regulatory factor 3 (IRF3) (Iwasaki & Pillai, 2014). Therefore,

the high viral titre in  $\delta$ WD mice which causes more dying epithelial cells in the lung, would lead to stronger inflammatory response in macrophages, and the LAP deficiency in macrophages would aggravate the response by delaying the endosome fusion with lysosomes.

## 7.5 How does the WD domain of ATG16L1 promote lipidation of endolysosome compartments?

The mechanisms of how the WD domain of ATG16L1 drives LC3 lipidation during non-canonical autophagy and LAP in general, or during IAV infection are still unclear. Recent studies suggest however that the M2 protein of IAV and the v-ATPase complex might be involved. Non-canonical autophagy is induced in cells by drugs that raise the pH of endolysosome compartments (Florey et al., 2015). The M2 matrix protein of IAV acts as a proton-conducting channel that moves protons ( $H^+$ ) from the lumen of endosomes into the core of the virus. The acidification of the virus allows the release of vRNP into the cytoplasm (Dou et al., 2018). Studies suggest the proton channel activity of M2 is required for LC3 re-localisation onto the plasma membrane and peri-nuclear structures during IAV infection (Fletcher et al., 2018). Interestingly, this LC3 re-localisation induced by M2 requires WD40 domain of ATG16L1, while, the  $\Delta$ FBD of ATG16L1 lacking the WIPI2b and FIP200 binding sites) [Figure 7.3] which is required for canonical autophagy was not required (Fletcher et al., 2018). This study suggests that IAV-induced LC3 lipidation is driven predominantly by non-canonical autophagy rather than canonical autophagy.

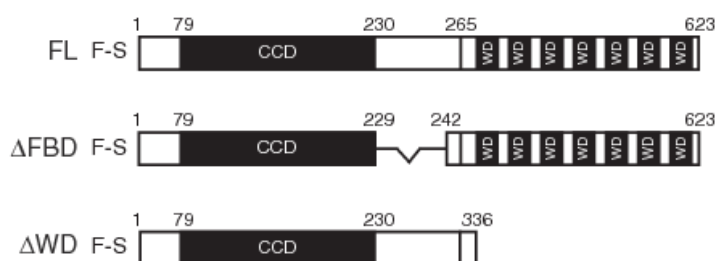


**Figure 7.3** Diagram of full-length (FL) 229–242 deletion ( $\Delta$ FBD) and 1–336 ( $\delta$ WD) ATG16L1 constructs used in this study. (Fletcher et al., 2018)

It is known that, ATG16L1 binding to WIPI2b and FIP200 through WIPI2b and FIP200 binding domain (FBD) is essential for driving LC3 conjugation to cellular membranes during canonical

autophagy. While, a recent study suggest that the membrane binding through WIPI2b can be compensated by C-terminal end of ATG16L1, indicating that WD domain is able to bind ATG16L1 onto membranes independent of WIPI and FIP200 (Lystad et al., 2019). Residues important for membrane binding have been identified at positions 266 and 319 in the linker region and phenylalanines 467 and 490 in the WD domain. Consistent with the fact that WD domain of ATG16L1 is required for LC3 lipidation, while ULK complex, Beclin-1 complex, WIPI2b and FBD of ATG16L1 are dispensable during non-canonical autophagy. However, the mechanisms of how WD domain of Atg16L1 detects endosomal membrane after changes in internal pH or osmotic balance are still unclear.

Interestingly, a very recent paper demonstrates that the WD domain of ATG16L1 could interact with v-ATPase in endolysosome membranes directly to bring LC3 onto the membrane for lipidation. SopF is secreted by the type 3 secretion system (T3SS1) of *Salmonella typhimurium*. SopF binds phosphoinositides in cell membranes to stabilise the vacuole containing *Salmonella*. SopF increases survival of *Salmonella* by disrupting association between v-ATPase and WD domain of ATG16L1 to block LC3 lipidation during xenophagy/LAP without affecting canonical autophagy. Similarly, during IAV entry, the v-ATPase in endosome membranes containing viral particles may facilitate ATG16L1 binding through the WD domain in response to changes in pH. Therefore, in  $\delta$ WD cells, the binding of ATG16L1 onto the endosomal membrane through WD40 and v-ATPase is abolished, as a result, LC3 lipidation onto viral-containing endosomes is impaired, leading to a delayed fusion and degradation by lysosomes.

## 7.6 Future work

The future work of this project would be based on 'in vitro' studies to work out the molecular mechanisms of how the WD domain of ATG16L1 and connection with LAP or LANDO effect IAV infection in detail. We assume that the lack of non-canonical autophagy pathway would lead to increased virus entry into the cell cytoplasm for transport to the nucleus and promote the viral replication. Therefore, viral entry needs to be quantified to demonstrate if non-canonical autophagy deficiency could result in increased viral entry at early stage of infection, for example from endosomes. Secondly, the role played by non-canonical autophagy in

controlling cytokines expression is worth investigating. The activity of RIG-I during IAV infection could be tested to see if non-canonical autophagy deficiency enhances the activity of RIG-I and results in an increased cytokine expression. Thirdly, the capability of netosis induced by  $\delta$ WD neutrophils need to be evaluated to determine if loss of WD-dependent non-canonical autophagy in neutrophils makes it more susceptible to netosis induction than WT neutrophils during IAV infection. The further mechanical study on ATG16L1 WD domain in IAV infection could be achieved by specifically inhibiting the function of ATG16L1 WD domain in LC3 recruitment. We could take advantage of SopF to block the binding between v-ATPase and WD domain of ATG16L1 in the WT cells to see if it could reduce the LC3 recruitment and increase the IAV infection level to  $\delta$ WD cells. Finally, our study suggesting that loss of WD domain in ATG16L1 results in susceptibility to IAV infection in mice model, this raises possibility that the T300A mutation in ATG16L1 which effect the function of WD domain, may have the same outcomes during IAV infection. The *ATG16L1* T300A mutation was known as a risk allele of Crohn's disease. People with Crohn's disease have abnormal Paneth cells due to decreased selective autophagy, reduced intracellular bacterial clearance, and increased cytokine release. It will be interesting to operate an IAV challenge with T300A mice model (available in our lab) to see if they also susceptible to IAV infection.

In conclusion, our study demonstrates the mice model with ATG16L1 WD domain deficiency are more susceptible to IAV infection. This is due to the loss of WD-dependent non-canonical autophagy pathway rather than canonical autophagy pathway. It highlights the important role of WD-dependent non-canonical autophagy in lung epithelial cells during IAV infection, and revealed a role for non-canonical autophagy in controlling inflammatory responses to restrict the cytokine storm and protect host from lethal infection. In addition, this study describes pathological progress of IAV infection at different time points and in different approaches, including viral titre, cytokines expression, pathology outcomes and acquired immunity response. These studies give us insight into what is happening in human cases of severe IAV infection. This provides a way of predicting illness progress and recovery, and can guide medical scientists towards a better understanding about individual variation in responses to IAV exposure based on the genetic background.

## References

- Aikawa, N. (1996). [Cytokine storm in the pathogenesis of multiple organ dysfunction syndrome associated with surgical insults]. *Nihon Geka Gakkai Zasshi*, *97*(9), 771-777.
- Akoumianaki, T., Kyrmizi, I., Valsecchi, I., Gresnigt, M. S., Samonis, G., Drakos, E., . . . Chamilos, G. (2016). Aspergillus Cell Wall Melanin Blocks LC3-Associated Phagocytosis to Promote Pathogenicity. *Cell Host Microbe*, *19*(1), 79-90. doi:10.1016/j.chom.2015.12.002
- Andreakos, E., Salagianni, M., Galani, I. E., & Koltsida, O. (2017). Interferon-lambdas: Front-Line Guardians of Immunity and Homeostasis in the Respiratory Tract. *Front Immunol*, *8*, 1232. doi:10.3389/fimmu.2017.01232
- Arasteh, J. M., (2012). Generation of mouse models to study the role of Atg16L1 in Inflammatory Bowel Disease (IBD). Faculty of Medicine and Health Sciences, University of East Anglia.
- Axe, E. L., Walker, S. A., Manifava, M., Chandra, P., Roderick, H. L., Habermann, A., . . . Ktistakis, N. T. (2008). Autophagosome formation from membrane compartments enriched in phosphatidylinositol 3-phosphate and dynamically connected to the endoplasmic reticulum. *J Cell Biol*, *182*(4), 685-701. doi:10.1083/jcb.200803137
- Baba, M., Takeshige, K., Baba, N., & Ohsumi, Y. (1994). Ultrastructural analysis of the autophagic process in yeast: detection of autophagosomes and their characterization. *J Cell Biol*, *124*(6), 903-913. doi:10.1083/jcb.124.6.903
- Beale, R., Wise, H., Stuart, A., Ravenhill, B. J., Digard, P., & Randow, F. (2014). A LC3-interacting motif in the influenza A virus M2 protein is required to subvert autophagy and maintain virion stability. *Cell Host Microbe*, *15*(2), 239-247. doi:10.1016/j.chom.2014.01.006
- Birgisdottir, A. B., Moulleron, S., Bhujabal, Z., Wirth, M., Sjøttem, E., Evjen, G., . . . Johansen, T. (2019). Members of the autophagy class III phosphatidylinositol 3-kinase complex I interact with GABARAP and GABARAP1 via LIR motifs. *Autophagy*, *15*(8), 1333-1355. doi:10.1080/15548627.2019.1581009
- Boada-Romero, E., Letek, M., Fleischer, A., Pallauf, K., Ramon-Barros, C., & Pimentel-Muinos, F. X. (2013). TMEM59 defines a novel ATG16L1-binding motif that promotes local activation of LC3. *Embo j*, *32*(4), 566-582. doi:10.1038/emboj.2013.8
- Boada-Romero, E., Serramito-Gomez, I., Sacristan, M. P., Boone, D. L., Xavier, R. J., & Pimentel-Muinos, F. X. (2016). The T300A Crohn's disease risk polymorphism impairs function of the WD40 domain of ATG16L1. *Nat Commun*, *7*, 11821. doi:10.1038/ncomms11821
- Bodemann, B. O., Orvedahl, A., Cheng, T., Ram, R. R., Ou, Y. H., Formstecher, E., . . . White, M. A. (2011). RalB and the exocyst mediate the cellular starvation response by direct activation of autophagosome assembly. *Cell*, *144*(2), 253-267. doi:10.1016/j.cell.2010.12.018
- Borthwick, L. A. (2016). The IL-1 cytokine family and its role in inflammation and fibrosis in the lung. *Semin Immunopathol*, *38*(4), 517-534. doi:10.1007/s00281-016-0559-z
- Bouvier, N. M., & Lowen, A. C. (2010). Animal Models for Influenza Virus Pathogenesis and Transmission. *Viruses*, *2*(8), 1530-1563. doi:10.3390/v20801530
- Camp, J. V., & Jonsson, C. B. (2017). A Role for Neutrophils in Viral Respiratory Disease. *Front Immunol*, *8*, 550. doi:10.3389/fimmu.2017.00550
- Carswell, E. A., Old, L. J., Kassel, R. L., Green, S., Fiore, N., & Williamson, B. (1975). An endotoxin-induced serum factor that causes necrosis of tumors. *Proc Natl Acad Sci U S A*, *72*(9), 3666-3670. doi:10.1073/pnas.72.9.3666
- Chen, L., Deng, H., Cui, H., Fang, J., Zuo, Z., Deng, J., . . . Zhao, L. (2018). Inflammatory responses and inflammation-associated diseases in organs. *Oncotarget*, *9*(6), 7204-7218. doi:10.18632/oncotarget.23208
- Chen, X., Khambu, B., Zhang, H., Gao, W., Li, M., Chen, X., . . . Yin, X. M. (2014). Autophagy induced by calcium phosphate precipitates targets damaged endosomes. *J Biol Chem*, *289*(16), 11162-11174. doi:10.1074/jbc.M113.531855

- Chen, X., Liu, S., Goraya, M. U., Maarouf, M., Huang, S., & Chen, J. L. (2018). Host Immune Response to Influenza A Virus Infection. *Front Immunol*, *9*, 320. doi:10.3389/fimmu.2018.00320
- Chiaretti, A., Pulitano, S., Conti, G., Barone, G., Buonsenso, D., Manni, L., . . . Riccardi, R. (2013). Interleukin and neurotrophin up-regulation correlates with severity of H1N1 infection in children: a case-control study. *Int J Infect Dis*, *17*(12), e1186-1193. doi:10.1016/j.ijid.2013.07.006
- Clausen, B. E., Burkhardt, C., Reith, W., Renkawitz, R., & Förster, I. (1999). Conditional gene targeting in macrophages and granulocytes using LysMcre mice. *Transgenic Research*, *8*(4), 265-277. doi:10.1023/a:1008942828960
- Coccia, E. M., Severa, M., Giacomini, E., Monneron, D., Remoli, M. E., Julkunen, I., . . . Uze, G. (2004). Viral infection and Toll-like receptor agonists induce a differential expression of type I and lambda interferons in human plasmacytoid and monocyte-derived dendritic cells. *Eur J Immunol*, *34*(3), 796-805. doi:10.1002/eji.200324610
- Cole, S. L., & Ho, L. P. (2017). Contribution of innate immune cells to pathogenesis of severe influenza virus infection. *Clin Sci (Lond)*, *131*(4), 269-283. doi:10.1042/cs20160484
- Cong, M., Iwaisako, K., Jiang, C., & Kisseleva, T. (2012). Cell signals influencing hepatic fibrosis. *Int J Hepatol*, *2012*, 158547. doi:10.1155/2012/158547
- Cottam, E. M., Maier, H. J., Manifava, M., Vaux, L. C., Chandra-Schoenfelder, P., Gerner, W., . . . Wileman, T. (2011). Coronavirus nsp6 proteins generate autophagosomes from the endoplasmic reticulum via an omegasome intermediate. *Autophagy*, *7*(11), 1335-1347. doi:10.4161/auto.7.11.16642
- Crisan, T. O., Plantinga, T. S., van de Veerdonk, F. L., Farcas, M. F., Stoffels, M., Kullberg, B. J., . . . Netea, M. G. (2011). Inflammasome-independent modulation of cytokine response by autophagy in human cells. *PLoS One*, *6*(4), e18666. doi:10.1371/journal.pone.0018666
- Cunha, L. D., Yang, M., Carter, R., Guy, C., Harris, L., Crawford, J. C., . . . Green, D. R. (2018). LC3-Associated Phagocytosis in Myeloid Cells Promotes Tumor Immune Tolerance. *Cell*, *175*(2), 429-441.e416. doi:10.1016/j.cell.2018.08.061
- De Filippo, K., Henderson, R. B., Laschinger, M., & Hogg, N. (2008). Neutrophil chemokines KC and macrophage-inflammatory protein-2 are newly synthesized by tissue macrophages using distinct TLR signaling pathways. *J Immunol*, *180*(6), 4308-4315. doi:10.4049/jimmunol.180.6.4308
- Delgado, M. A., Elmaoued, R. A., Davis, A. S., Kyei, G., & Deretic, V. (2008). Toll-like receptors control autophagy. *Embo j*, *27*(7), 1110-1121. doi:10.1038/emboj.2008.31
- Deretic, V. (2012). Autophagy as an innate immunity paradigm: expanding the scope and repertoire of pattern recognition receptors. *Curr Opin Immunol*, *24*(1), 21-31. doi:10.1016/j.coi.2011.10.006
- Deshmane, S. L., Kremlev, S., Amini, S., & Sawaya, B. E. (2009). Monocyte chemoattractant protein-1 (MCP-1): an overview. *J Interferon Cytokine Res*, *29*(6), 313-326. doi:10.1089/jir.2008.0027
- Dienz, O., Rud, J. G., Eaton, S. M., Lanthier, P. A., Burg, E., Drew, A., . . . Rincon, M. (2012). Essential role of IL-6 in protection against H1N1 influenza virus by promoting neutrophil survival in the lung. *Mucosal Immunol*, *5*(3), 258-266. doi:10.1038/mi.2012.2
- Dodington, D. W., Desai, H. R., & Woo, M. (2018). JAK/STAT - Emerging Players in Metabolism. *Trends Endocrinol Metab*, *29*(1), 55-65. doi:10.1016/j.tem.2017.11.001
- Dooley, H. C., Razi, M., Polson, H. E., Girardin, S. E., Wilson, M. I., & Tooze, S. A. (2014). WIPI2 links LC3 conjugation with PI3P, autophagosome formation, and pathogen clearance by recruiting Atg12-5-16L1. *Mol Cell*, *55*(2), 238-252. doi:10.1016/j.molcel.2014.05.021
- Dou, D., Revol, R., Ostbye, H., Wang, H., & Daniels, R. (2018). Influenza A Virus Cell Entry, Replication, Virion Assembly and Movement. *Front Immunol*, *9*, 1581. doi:10.3389/fimmu.2018.01581
- Edinger, T. O., Pohl, M. O., & Stertz, S. (2014). Entry of influenza A virus: host factors and antiviral targets. *J Gen Virol*, *95*(Pt 2), 263-277. doi:10.1099/vir.0.059477-0

- Elliott, M. R., Koster, K. M., & Murphy, P. S. (2017). Efferocytosis Signaling in the Regulation of Macrophage Inflammatory Responses. *J Immunol*, *198*(4), 1387-1394. doi:10.4049/jimmunol.1601520
- Enami, M. (1997). [Structure and function of influenza virus NS1 and NS2 proteins]. *Nihon Rinsho*, *55*(10), 2605-2609.
- Fadok, V. A., Bratton, D. L., Konowal, A., Freed, P. W., Westcott, J. Y., & Henson, P. M. (1998). Macrophages that have ingested apoptotic cells in vitro inhibit proinflammatory cytokine production through autocrine/paracrine mechanisms involving TGF-beta, PGE2, and PAF. *J Clin Invest*, *101*(4), 890-898. doi:10.1172/jci1112
- Fang, F. C. (2011). Antimicrobial actions of reactive oxygen species. *MBio*, *2*(5). doi:10.1128/mBio.00141-11
- Fislova, T., Gocnik, M., Sladkova, T., Durmanova, V., Rajcani, J., Vareckova, E., . . . Kostolansky, F. (2009). Multiorgan distribution of human influenza A virus strains observed in a mouse model. *Arch Virol*, *154*(3), 409-419. doi:10.1007/s00705-009-0318-8
- Fletcher, K., Ulferts, R., Jacquin, E., Veith, T., Gammoh, N., Arasteh, J. M., . . . Florey, O. (2018). The WD40 domain of ATG16L1 is required for its non-canonical role in lipidation of LC3 at single membranes. *Embo j*, *37*(4). doi:10.15252/embj.201797840
- Florey, O., Gammoh, N., Kim, S. E., Jiang, X., & Overholtzer, M. (2015). V-ATPase and osmotic imbalances activate endolysosomal LC3 lipidation. *Autophagy*, *11*(1), 88-99. doi:10.4161/15548627.2014.984277
- Florey, O., & Overholtzer, M. (2012). Autophagy proteins in macroendocytic engulfment. *Trends Cell Biol*, *22*(7), 374-380. doi:10.1016/j.tcb.2012.04.005
- Fodor, E. (2013). The RNA polymerase of influenza a virus: mechanisms of viral transcription and replication. *Acta Virol*, *57*(2), 113-122.
- Fujita, N., Morita, E., Itoh, T., Tanaka, A., Nakaoka, M., Osada, Y., . . . Yoshimori, T. (2013). Recruitment of the autophagic machinery to endosomes during infection is mediated by ubiquitin. *J Cell Biol*, *203*(1), 115-128. doi:10.1083/jcb.201304188
- Fukuyama, S., & Kawaoka, Y. (2011). The pathogenesis of influenza virus infections: the contributions of virus and host factors. *Curr Opin Immunol*, *23*(4), 481-486. doi:10.1016/j.coi.2011.07.016
- Galani, I. E., Triantafyllia, V., Eleminiadou, E. E., Koltsida, O., Stavropoulos, A., Manioudaki, M., . . . Andreakos, E. (2017). Interferon-lambda Mediates Non-redundant Front-Line Antiviral Protection against Influenza Virus Infection without Compromising Host Fitness. *Immunity*, *46*(5), 875-890.e876. doi:10.1016/j.immuni.2017.04.025
- Ganley, I. G. (2013). Autophagosome maturation and lysosomal fusion. *Essays Biochem*, *55*, 65-78. doi:10.1042/bse0550065
- Gannage, M., Dormann, D., Albrecht, R., Dengjel, J., Torossi, T., Ramer, P. C., . . . Munz, C. (2009). Matrix protein 2 of influenza A virus blocks autophagosome fusion with lysosomes. *Cell Host Microbe*, *6*(4), 367-380. doi:10.1016/j.chom.2009.09.005
- Garcia-Ramirez, R. A., Ramirez-Venegas, A., Quintana-Carrillo, R., Camarena, A. E., Falfan-Valencia, R., & Mejia-Arangure, J. M. (2015). TNF, IL6, and IL1B Polymorphisms Are Associated with Severe Influenza A (H1N1) Virus Infection in the Mexican Population. *PLoS One*, *10*(12), e0144832. doi:10.1371/journal.pone.0144832
- Ge, M. Q., Ho, A. W., Tang, Y., Wong, K. H., Chua, B. Y., Gasser, S., & Kemeny, D. M. (2012). NK cells regulate CD8+ T cell priming and dendritic cell migration during influenza A infection by IFN-gamma and perforin-dependent mechanisms. *J Immunol*, *189*(5), 2099-2109. doi:10.4049/jimmunol.1103474
- Glick, D., Barth, S., & Macleod, K. F. (2010). Autophagy: cellular and molecular mechanisms. *J Pathol*, *221*(1), 3-12. doi:10.1002/path.2697
- Gluschko, A., Herb, M., Wiegmann, K., Krut, O., Neiss, W. F., Utermohlen, O., . . . Schramm, M. (2018). The beta2 Integrin Mac-1 Induces Protective LC3-Associated Phagocytosis of *Listeria monocytogenes*. *Cell Host Microbe*, *23*(3), 324-337.e325. doi:10.1016/j.chom.2018.01.018

- Groves, H. T., McDonald, J. U., Langat, P., Kinnear, E., Kellam, P., McCauley, J., . . . Tregoning, J. S. (2018). Mouse Models of Influenza Infection with Circulating Strains to Test Seasonal Vaccine Efficacy. *Front Immunol*, *9*, 126. doi:10.3389/fimmu.2018.00126
- Guarner, J., & Falcon-Escobedo, R. (2009). Comparison of the pathology caused by H1N1, H5N1, and H3N2 influenza viruses. *Arch Med Res*, *40*(8), 655-661. doi:10.1016/j.arcmed.2009.10.001
- Guillot, L., Le Goffic, R., Bloch, S., Escriou, N., Akira, S., Chignard, M., & Si-Tahar, M. (2005). Involvement of toll-like receptor 3 in the immune response of lung epithelial cells to double-stranded RNA and influenza A virus. *J Biol Chem*, *280*(7), 5571-5580. doi:10.1074/jbc.M410592200
- Guo, H., Callaway, J. B., & Ting, J. P. (2015). Inflammasomes: mechanism of action, role in disease, and therapeutics. *Nat Med*, *21*(7), 677-687. doi:10.1038/nm.3893
- Guo, Z., Chen, L. M., Zeng, H., Gomez, J. A., Plowden, J., Fujita, T., . . . Sambhara, S. (2007). NS1 protein of influenza A virus inhibits the function of intracytoplasmic pathogen sensor, RIG-I. *Am J Respir Cell Mol Biol*, *36*(3), 263-269. doi:10.1165/rcmb.2006-0283RC
- Hanada, T., Noda, N. N., Satomi, Y., Ichimura, Y., Fujioka, Y., Takao, T., . . . Ohsumi, Y. (2007). The Atg12-Atg5 conjugate has a novel E3-like activity for protein lipidation in autophagy. *J Biol Chem*, *282*(52), 37298-37302. doi:10.1074/jbc.C700195200
- Harding, T. M., Morano, K. A., Scott, S. V., & Klionsky, D. J. (1995). Isolation and characterization of yeast mutants in the cytoplasm to vacuole protein targeting pathway. *J Cell Biol*, *131*(3), 591-602. doi:10.1083/jcb.131.3.591
- Harris, J., Hartman, M., Roche, C., Zeng, S. G., O'Shea, A., Sharp, F. A., . . . Lavelle, E. C. (2011). Autophagy controls IL-1beta secretion by targeting pro-IL-1beta for degradation. *J Biol Chem*, *286*(11), 9587-9597. doi:10.1074/jbc.M110.202911
- Heckmann, B. L., Boada-Romero, E., Cunha, L. D., Magne, J., & Green, D. R. (2017). LC3-Associated Phagocytosis and Inflammation. *J Mol Biol*, *429*(23), 3561-3576. doi:10.1016/j.jmb.2017.08.012
- Heckmann, B. L., & Green, D. R. (2019). LC3-associated phagocytosis at a glance. *J Cell Sci*, *132*(5). doi:10.1242/jcs.222984
- Heckmann, B. L., Teubner, B. J. W., Tummers, B., Boada-Romero, E., Harris, L., Yang, M., . . . Green, D. R. (2019). LC3-Associated Endocytosis Facilitates beta-Amyloid Clearance and Mitigates Neurodegeneration in Murine Alzheimer's Disease. *Cell*, *178*(3), 536-551.e514. doi:10.1016/j.cell.2019.05.056
- Henault, J., Martinez, J., Riggs, J. M., Tian, J., Mehta, P., Clarke, L., . . . Sanjuan, M. A. (2012). Noncanonical autophagy is required for type I interferon secretion in response to DNA-immune complexes. *Immunity*, *37*(6), 986-997. doi:10.1016/j.immuni.2012.09.014
- Hiscott, J., Nguyen, T. L., Arguello, M., Nakhaei, P., & Paz, S. (2006). Manipulation of the nuclear factor-kappaB pathway and the innate immune response by viruses. *Oncogene*, *25*(51), 6844-6867. doi:10.1038/sj.onc.1209941
- Huang, J., Canadien, V., Lam, G. Y., Steinberg, B. E., Dinauer, M. C., Magalhaes, M. A., . . . Brumell, J. H. (2009). Activation of antibacterial autophagy by NADPH oxidases. *Proc Natl Acad Sci U S A*, *106*(15), 6226-6231. doi:10.1073/pnas.0811045106
- Huang, J. H., Liu, C. Y., Wu, S. Y., Chen, W. Y., Chang, T. H., Kan, H. W., . . . Wu-Hsieh, B. A. (2018). NLRX1 Facilitates Histoplasma capsulatum-Induced LC3-Associated Phagocytosis for Cytokine Production in Macrophages. *Front Immunol*, *9*, 2761. doi:10.3389/fimmu.2018.02761
- Hubber, A., Kubori, T., Coban, C., Matsuzawa, T., Ogawa, M., Kawabata, T., . . . Nagai, H. (2017). Bacterial secretion system skews the fate of Legionella-containing vacuoles towards LC3-associated phagocytosis. *Sci Rep*, *7*, 44795. doi:10.1038/srep44795
- Hunter, C. A., & Jones, S. A. (2015). IL-6 as a keystone cytokine in health and disease. *Nat Immunol*, *16*(5), 448-457. doi:10.1038/ni.3153

- Hwang, I., Scott, J. M., Kakarla, T., Duriancik, D. M., Choi, S., Cho, C., . . . Kim, S. (2012). Activation mechanisms of natural killer cells during influenza virus infection. *PLoS One*, *7*(12), e51858. doi:10.1371/journal.pone.0051858
- Influenza Virus. (2009). *Transfus Med Hemother*, *36*(1), 32-39. doi:10.1159/000197314
- Ivashkiv, L. B., & Donlin, L. T. (2014). Regulation of type I interferon responses. *Nat Rev Immunol*, *14*(1), 36-49. doi:10.1038/nri3581
- Iwasaki, A., & Pillai, P. S. (2014). Innate immunity to influenza virus infection. *Nat Rev Immunol*, *14*(5), 315-328. doi:10.1038/nri3665
- Jaffer, U., Wade, R. G., & Gourlay, T. (2010). Cytokines in the systemic inflammatory response syndrome: a review. *HSR Proc Intensive Care Cardiovasc Anesth*, *2*(3), 161-175.
- Jin, M., Liu, X., & Klionsky, D. J. (2013). SnapShot: Selective autophagy. *Cell*, *152*(1-2), 368-368.e362. doi:10.1016/j.cell.2013.01.004
- Jo, E. K., Yuk, J. M., Shin, D. M., & Sasakawa, C. (2013). Roles of autophagy in elimination of intracellular bacterial pathogens. *Front Immunol*, *4*, 97. doi:10.3389/fimmu.2013.00097
- Johansen, T., & Lamark, T. (2011). Selective autophagy mediated by autophagic adapter proteins. *Autophagy*, *7*(3), 279-296. doi:10.4161/auto.7.3.14487
- Jung, C. H., Ro, S. H., Cao, J., Otto, N. M., & Kim, D. H. (2010). mTOR regulation of autophagy. *FEBS Lett*, *584*(7), 1287-1295. doi:10.1016/j.febslet.2010.01.017
- Kadowaki, N., Ho, S., Antonenko, S., Malefyt, R. W., Kastelein, R. A., Bazan, F., & Liu, Y. J. (2001). Subsets of human dendritic cell precursors express different toll-like receptors and respond to different microbial antigens. *J Exp Med*, *194*(6), 863-869. doi:10.1084/jem.194.6.863
- Kaplan, M. H. (2013). STAT signaling in inflammation. *Jakstat*, *2*(1), e24198. doi:10.4161/jkst.24198
- Killip, M. J., Fodor, E., & Randall, R. E. (2015). Influenza virus activation of the interferon system. *Virus Res*, *209*, 11-22. doi:10.1016/j.virusres.2015.02.003
- Kim, K. S., Jung, H., Shin, I. K., Choi, B. R., & Kim, D. H. (2015). Induction of interleukin-1 beta (IL-1beta) is a critical component of lung inflammation during influenza A (H1N1) virus infection. *J Med Virol*, *87*(7), 1104-1112. doi:10.1002/jmv.24138
- Kirkin, V., McEwan, D. G., Novak, I., & Dikic, I. (2009). A role for ubiquitin in selective autophagy. *Mol Cell*, *34*(3), 259-269. doi:10.1016/j.molcel.2009.04.026
- Klinkhammer, J., Schnepf, D., Ye, L., Schwaderlapp, M., Gad, H. H., Hartmann, R., . . . Staeheli, P. (2018). IFN-λ prevents influenza virus spread from the upper airways to the lungs and limits virus transmission. *Elife*, *7*. doi:10.7554/eLife.33354
- Klionsky, D. J. (2008). Autophagy revisited: a conversation with Christian de Duve. *Autophagy*, *4*(6), 740-743. doi:10.4161/auto.6398
- Klionsky, D. J., Cueva, R., & Yaver, D. S. (1992). Aminopeptidase I of *Saccharomyces cerevisiae* is localized to the vacuole independent of the secretory pathway. *J Cell Biol*, *119*(2), 287-299. doi:10.1083/jcb.119.2.287
- Kuballa, P., Nolte, W. M., Castoreno, A. B., & Xavier, R. J. (2012). Autophagy and the immune system. *Annu Rev Immunol*, *30*, 611-646. doi:10.1146/annurev-immunol-020711-074948
- Kundu, M., & Thompson, C. B. (2008). Autophagy: basic principles and relevance to disease. *Annu Rev Pathol*, *3*, 427-455. doi:10.1146/annurev.pathmechdis.2.010506.091842
- Lai, S. C., & Devenish, R. J. (2012). LC3-Associated Phagocytosis (LAP): Connections with Host Autophagy. *Cells*, *1*(3), 396-408. doi:10.3390/cells1030396
- Lam, G. Y., Cemma, M., Muise, A. M., Higgins, D. E., & Brumell, J. H. (2013). Host and bacterial factors that regulate LC3 recruitment to *Listeria monocytogenes* during the early stages of macrophage infection. *Autophagy*, *9*(7), 985-995. doi:10.4161/auto.24406
- Lambrecht, B. N., & Hammad, H. (2012). Lung dendritic cells in respiratory viral infection and asthma: from protection to immunopathology. *Annu Rev Immunol*, *30*, 243-270. doi:10.1146/annurev-immunol-020711-075021

- Le Goffic, R., Balloy, V., Lagranderie, M., Alexopoulou, L., Escriou, N., Flavell, R., . . . Si-Tahar, M. (2006). Detrimental contribution of the Toll-like receptor (TLR)3 to influenza A virus-induced acute pneumonia. *PLoS Pathog*, *2*(6), e53. doi:10.1371/journal.ppat.0020053
- Levine, B., & Kroemer, G. (2008). Autophagy in the pathogenesis of disease. *Cell*, *132*(1), 27-42. doi:10.1016/j.cell.2007.12.018
- Liu, Q., Zhou, Y. H., & Yang, Z. Q. (2016). The cytokine storm of severe influenza and development of immunomodulatory therapy. *Cell Mol Immunol*, *13*(1), 3-10. doi:10.1038/cmi.2015.74
- Liu, T., Zhang, L., Joo, D., & Sun, S. C. (2017). NF-kappaB signaling in inflammation. *Signal Transduct Target Ther*, *2*. doi:10.1038/sigtrans.2017.23
- Lu, Q., Yokoyama, C. C., Williams, J. W., Baldrige, M. T., Jin, X., DesRochers, B., . . . Virgin, H. W. (2016). Homeostatic Control of Innate Lung Inflammation by Vici Syndrome Gene Epg5 and Additional Autophagy Genes Promotes Influenza Pathogenesis. *Cell Host Microbe*, *19*(1), 102-113. doi:10.1016/j.chom.2015.12.011
- Lystad, A. H., Carlsson, S. R., de la Ballina, L. R., Kauffman, K. J., Nag, S., Yoshimori, T., . . . Simonsen, A. (2019). Distinct functions of ATG16L1 isoforms in membrane binding and LC3B lipidation in autophagy-related processes. *Nat Cell Biol*, *21*(3), 372-383. doi:10.1038/s41556-019-0274-9
- Martin, C. J., Peters, K. N., & Behar, S. M. (2014). Macrophages clean up: efferocytosis and microbial control. *Curr Opin Microbiol*, *17*, 17-23. doi:10.1016/j.mib.2013.10.007
- Martinez, J., Almendinger, J., Oberst, A., Ness, R., Dillon, C. P., Fitzgerald, P., . . . Green, D. R. (2011). Microtubule-associated protein 1 light chain 3 alpha (LC3)-associated phagocytosis is required for the efficient clearance of dead cells. *Proc Natl Acad Sci U S A*, *108*(42), 17396-17401. doi:10.1073/pnas.1113421108
- Martinez, J., Cunha, L. D., Park, S., Yang, M., Lu, Q., Orchard, R., . . . Green, D. R. (2016). Noncanonical autophagy inhibits the autoinflammatory, lupus-like response to dying cells. *Nature*, *533*(7601), 115-119. doi:10.1038/nature17950
- Martinez, J., Malireddi, R. K., Lu, Q., Cunha, L. D., Pelletier, S., Gingras, S., . . . Green, D. R. (2015). Molecular characterization of LC3-associated phagocytosis reveals distinct roles for Rubicon, NOX2 and autophagy proteins. *Nat Cell Biol*, *17*(7), 893-906. doi:10.1038/ncb3192
- Masud, S., Prajsnar, T. K., Torraca, V., Lamers, G. E. M., Benning, M., Van Der Vaart, M., & Meijer, A. H. (2019). Macrophages target Salmonella by Lc3-associated phagocytosis in a systemic infection model. *Autophagy*, *15*(5), 796-812. doi:10.1080/15548627.2019.1569297
- Matte, C., Casgrain, P. A., Seguin, O., Moradin, N., Hong, W. J., & Descoteaux, A. (2016). Leishmania major Promastigotes Evade LC3-Associated Phagocytosis through the Action of GP63. *PLoS Pathog*, *12*(6), e1005690. doi:10.1371/journal.ppat.1005690
- McNab, F., Mayer-Barber, K., Sher, A., Wack, A., & O'Garra, A. (2015). Type I interferons in infectious disease. *Nat Rev Immunol*, *15*(2), 87-103. doi:10.1038/nri3787
- Medzhitov, R. (2010). Inflammation 2010: new adventures of an old flame. *Cell*, *140*(6), 771-776. doi:10.1016/j.cell.2010.03.006
- Mizushima, N., Kuma, A., Kobayashi, Y., Yamamoto, A., Matsubae, M., Takao, T., . . . Yoshimori, T. (2003). Mouse Apg16L, a novel WD-repeat protein, targets to the autophagic isolation membrane with the Apg12-Apg5 conjugate. *J Cell Sci*, *116*(Pt 9), 1679-1688. doi:10.1242/jcs.00381
- Mokart, D., Capo, C., Blache, J. L., Delpero, J. R., Houvenaeghel, G., Martin, C., & Mege, J. L. (2002). Early postoperative compensatory anti-inflammatory response syndrome is associated with septic complications after major surgical trauma in patients with cancer. *Br J Surg*, *89*(11), 1450-1456. doi:10.1046/j.1365-2168.2002.02218.x
- Moynagh, P. N. (2005). The NF-kB pathway. *J Cell Sci*, *118*(20), 4589-4592. doi:10.1242/jcs.02579
- Murthy, A., Li, Y., Peng, I., Reichelt, M., Katakam, A. K., Noubade, R., . . . van Lookeren Campagne, M. (2014). A Crohn's disease variant in Atg16l1 enhances its degradation by caspase 3. *Nature*, *506*(7489), 456-462. doi:10.1038/nature13044

- Nayak, D. P., Hui, E. K., & Barman, S. (2004). Assembly and budding of influenza virus. *Virus Res*, *106*(2), 147-165. doi:10.1016/j.virusres.2004.08.012
- Neerincx, A., Castro, W., Guarda, G., & Kufer, T. A. (2013). NLRC5, at the Heart of Antigen Presentation. *Front Immunol*, *4*, 397. doi:10.3389/fimmu.2013.00397
- Neumann, G., Chen, H., Gao, G. F., Shu, Y., & Kawaoka, Y. (2010). H5N1 influenza viruses: outbreaks and biological properties. *Cell Res*, *20*(1), 51-61. doi:10.1038/cr.2009.124
- Nhu, Q. M., Shirey, K., Teijaro, J. R., Farber, D. L., Netzel-Arnett, S., Antalis, T. M., . . . Vogel, S. N. (2010). Novel signaling interactions between proteinase-activated receptor 2 and Toll-like receptors in vitro and in vivo. *Mucosal Immunol*, *3*(1), 29-39. doi:10.1038/mi.2009.120
- Oh, J. E., & Lee, H. K. (2013). Autophagy as an innate immune modulator. *Immune Netw*, *13*(1), 1-9. doi:10.4110/in.2013.13.1.1
- Parameswaran, N., & Patial, S. (2010). Tumor necrosis factor-alpha signaling in macrophages. *Crit Rev Eukaryot Gene Expr*, *20*(2), 87-103.
- Paun, A., & Pitha, P. M. (2007). The IRF family, revisited. *Biochimie*, *89*(6-7), 744-753. doi:10.1016/j.biochi.2007.01.014
- Petiot, A., Ogier-Denis, E., Blommaert, E. F., Meijer, A. J., & Codogno, P. (2000). Distinct classes of phosphatidylinositol 3'-kinases are involved in signaling pathways that control macroautophagy in HT-29 cells. *J Biol Chem*, *275*(2), 992-998. doi:10.1074/jbc.275.2.992
- Pimentel-Muinos, F. X., & Boada-Romero, E. (2014). Selective autophagy against membranous compartments: Canonical and unconventional purposes and mechanisms. *Autophagy*, *10*(3), 397-407. doi:10.4161/auto.27244
- Platanitis, E., & Decker, T. (2018). Regulatory Networks Involving STATs, IRFs, and NFκB in Inflammation. *Front Immunol*, *9*, 2542. doi:10.3389/fimmu.2018.02542
- Polson, H. E., de Lartigue, J., Rigden, D. J., Reedijk, M., Urbe, S., Clague, M. J., & Tooze, S. A. (2010). Mammalian Atg18 (WIPI2) localizes to omegasome-anchored phagophores and positively regulates LC3 lipidation. *Autophagy*, *6*(4), 506-522. doi:10.4161/auto.6.4.11863
- Prokunina-Olsson, L., Muchmore, B., Tang, W., Pfeiffer, R. M., Park, H., Dickensheets, H., . . . O'Brien, T. R. (2013). A variant upstream of IFNL3 (IL28B) creating a new interferon gene IFNL4 is associated with impaired clearance of hepatitis C virus. *Nat Genet*, *45*(2), 164-171. doi:10.1038/ng.2521
- Pulendran, B., & Maddur, M. S. (2015). Innate immune sensing and response to influenza. *Curr Top Microbiol Immunol*, *386*, 23-71. doi:10.1007/82\_2014\_405
- Qian, M., Fang, X., & Wang, X. (2017). Autophagy and inflammation. *Clin Transl Med*, *6*(1), 24. doi:10.1186/s40169-017-0154-5
- Rai, S., Arasteh, M., Jefferson, M., Pearson, T., Wang, Y., Zhang, W., . . . Wileman, T. (2019). The ATG5-binding and coiled coil domains of ATG16L1 maintain autophagy and tissue homeostasis in mice independently of the WD domain required for LC3-associated phagocytosis. *Autophagy*, *15*(4), 599-612. doi:10.1080/15548627.2018.1534507
- Ramos, I., & Fernandez-Sesma, A. (2015). Modulating the Innate Immune Response to Influenza A Virus: Potential Therapeutic Use of Anti-Inflammatory Drugs. *Front Immunol*, *6*, 361. doi:10.3389/fimmu.2015.00361
- Randall-Demllo, S., Chieppa, M., & Eri, R. (2013). Intestinal epithelium and autophagy: partners in gut homeostasis. *Front Immunol*, *4*, 301. doi:10.3389/fimmu.2013.00301
- Rengachari, S., Groiss, S., Devos, J. M., Caron, E., Grandvaux, N., & Panne, D. (2018). Structural basis of STAT2 recognition by IRF9 reveals molecular insights into ISGF3 function. *Proceedings of the National Academy of Sciences*, *115*(4), E601-E609. doi:10.1073/pnas.1718426115
- Romao, S., Gasser, N., Becker, A. C., Guhl, B., Bajagic, M., Vanoaica, D., . . . Munz, C. (2013). Autophagy proteins stabilize pathogen-containing phagosomes for prolonged MHC II antigen processing. *J Cell Biol*, *203*(5), 757-766. doi:10.1083/jcb.201308173

- Saitoh, T., Fujita, N., Jang, M. H., Uematsu, S., Yang, B. G., Satoh, T., . . . Akira, S. (2008). Loss of the autophagy protein Atg16L1 enhances endotoxin-induced IL-1beta production. *Nature*, *456*(7219), 264-268. doi:10.1038/nature07383
- Sakai, S., Kawamata, H., Mantani, N., Kogure, T., Shimada, Y., Terasawa, K., . . . Ochiai, H. (2000). Therapeutic Effect of Anti-Macrophage Inflammatory Protein 2 Antibody on Influenza Virus-Induced Pneumonia in Mice. *J Virol*, *74*(5), 2472-2476. doi:10.1128/jvi.74.5.2472-2476.2000
- Sandbulte, M. R., Spickler, A. R., Zaabel, P. K., & Roth, J. A. (2015). Optimal Use of Vaccines for Control of Influenza A Virus in Swine. *Vaccines (Basel)*, *3*(1), 22-73. doi:10.3390/vaccines3010022
- Sanjuan, M. A., Dillon, C. P., Tait, S. W., Moshiah, S., Dorsey, F., Connell, S., . . . Green, D. R. (2007). Toll-like receptor signalling in macrophages links the autophagy pathway to phagocytosis. *Nature*, *450*(7173), 1253-1257. doi:10.1038/nature06421
- Sawant, K. V., Poluri, K. M., Dutta, A. K., Sepuru, K. M., Troshkina, A., Garofalo, R. P., & Rajarathnam, K. (2016). Chemokine CXCL1 mediated neutrophil recruitment: Role of glycosaminoglycan interactions. *Sci Rep*, *6*, 33123. doi:10.1038/srep33123
- Scheller, J., Chalaris, A., Schmidt-Arras, D., & Rose-John, S. (2011). The pro- and anti-inflammatory properties of the cytokine interleukin-6. *Biochim Biophys Acta*, *1813*(5), 878-888. doi:10.1016/j.bbamcr.2011.01.034
- Schneider, W. M., Chevillotte, M. D., & Rice, C. M. (2014). Interferon-stimulated genes: a complex web of host defenses. *Annu Rev Immunol*, *32*, 513-545. doi:10.1146/annurev-immunol-032713-120231
- Schroder, K., Hertzog, P. J., Ravasi, T., & Hume, D. A. (2004). Interferon-gamma: an overview of signals, mechanisms and functions. *J Leukoc Biol*, *75*(2), 163-189. doi:10.1189/jlb.0603252
- Seo, S. U., Kwon, H. J., Song, J. H., Byun, Y. H., Seong, B. L., Kawai, T., . . . Kweon, M. N. (2010). MyD88 signaling is indispensable for primary influenza A virus infection but dispensable for secondary infection. *J Virol*, *84*(24), 12713-12722. doi:10.1128/jvi.01675-10
- Serramito-Gómez, I., Boada-Romero, E., & Pimentel-Muiños, F. X. (2016). Unconventional autophagy mediated by the WD40 domain of ATG16L1 is derailed by the T300A Crohn disease risk polymorphism. *Autophagy*, *12*(11), 2254-2255. doi:10.1080/15548627.2016.1216303
- Shaid, S., Brandts, C. H., Serve, H., & Dikic, I. (2013). Ubiquitination and selective autophagy. *Cell Death Differ*, *20*(1), 21-30. doi:10.1038/cdd.2012.72
- Shi, C. S., Shenderov, K., Huang, N. N., Kabat, J., Abu-Asab, M., Fitzgerald, K. A., . . . Kehrl, J. H. (2012). Activation of autophagy by inflammatory signals limits IL-1beta production by targeting ubiquitinated inflammasomes for destruction. *Nat Immunol*, *13*(3), 255-263. doi:10.1038/ni.2215
- Sivro, A., Stein, D. R., McKinnon, L. R. (2011). The Role of Cytokine Storm in Influenza Pathogenesis. Purple Paper, Issue No.23
- Sladkova, T., & Kostolansky, F. (2006). The role of cytokines in the immune response to influenza A virus infection. *Acta Virol*, *50*(3), 151-162.
- Slauch, J. M. (2011). How does the oxidative burst of macrophages kill bacteria? Still an open question. *Mol Microbiol*, *80*(3), 580-583. doi:10.1111/j.1365-2958.2011.07612.x
- Smith, C. A., Farrah, T., & Goodwin, R. G. (1994). The TNF receptor superfamily of cellular and viral proteins: activation, costimulation, and death. *Cell*, *76*(6), 959-962. doi:10.1016/0092-8674(94)90372-7
- Spitaels, J., Roose, K., & Saelens, X. (2016). Influenza and Memory T Cells: How to Awake the Force. *Vaccines (Basel)*, *4*(4). doi:10.3390/vaccines4040033
- Sprenkeler, E. G., Gresnigt, M. S., & van de Veerdonk, F. L. (2016). LC3-associated phagocytosis: a crucial mechanism for antifungal host defence against *Aspergillus fumigatus*. *Cell Microbiol*, *18*(9), 1208-1216. doi:10.1111/cmi.12616

- Storisteanu, D. M., Pocock, J. M., Cowburn, A. S., Juss, J. K., Nadesalingam, A., Nizet, V., & Chilvers, E. R. (2017). Evasion of Neutrophil Extracellular Traps by Respiratory Pathogens. *Am J Respir Cell Mol Biol*, *56*(4), 423-431. doi:10.1165/rcmb.2016-0193PS
- Superti, F., Agamennone, M., Pietrantonio, A., & Ammendolia, M. G. (2019). Bovine Lactoferrin Prevents Influenza A Virus Infection by Interfering with the Fusogenic Function of Viral Hemagglutinin. *Viruses*, *11*(1). doi:10.3390/v11010051
- Takehige, K., Baba, M., Tsuboi, S., Noda, T., & Ohsumi, Y. (1992). Autophagy in yeast demonstrated with proteinase-deficient mutants and conditions for its induction. *J Cell Biol*, *119*(2), 301-311. doi:10.1083/jcb.119.2.301
- Takeuchi, O., & Akira, S. (2010). Pattern recognition receptors and inflammation. *Cell*, *140*(6), 805-820. doi:10.1016/j.cell.2010.01.022
- Tam, A. B., Mercado, E. L., Hoffmann, A., & Niwa, M. (2012). ER stress activates NF-kappaB by integrating functions of basal IKK activity, IRE1 and PERK. *PLoS One*, *7*(10), e45078. doi:10.1371/journal.pone.0045078
- Tanaka, T., Narazaki, M., & Kishimoto, T. (2014). IL-6 in inflammation, immunity, and disease. *Cold Spring Harb Perspect Biol*, *6*(10), a016295. doi:10.1101/cshperspect.a016295
- Tate, M. D., Ioannidis, L. J., Croker, B., Brown, L. E., Brooks, A. G., & Reading, P. C. (2011). The role of neutrophils during mild and severe influenza virus infections of mice. *PLoS One*, *6*(3), e17618. doi:10.1371/journal.pone.0017618
- Tate, M. D., Pickett, D. L., van Rooijen, N., Brooks, A. G., & Reading, P. C. (2010). Critical Role of Airway Macrophages in Modulating Disease Severity during Influenza Virus Infection of Mice. *J Virol*, *84*(15), 7569-7580. doi:10.1128/jvi.00291-10
- Taubenberger, J. K., & Kash, J. C. (2010). Influenza virus evolution, host adaptation, and pandemic formation. *Cell Host Microbe*, *7*(6), 440-451. doi:10.1016/j.chom.2010.05.009
- Taubenberger, J. K., & Morens, D. M. (2006). 1918 Influenza: the mother of all pandemics. *Emerg Infect Dis*, *12*(1), 15-22. doi:10.3201/eid1201.050979
- Taubenberger, J. K., & Morens, D. M. (2008). The pathology of influenza virus infections. *Annu Rev Pathol*, *3*, 499-522. doi:10.1146/annurev.pathmechdis.3.121806.154316
- Taubenberger, J. K., & Morens, D. M. (2009). Pandemic influenza--including a risk assessment of H5N1. *Rev Sci Tech*, *28*(1), 187-202.
- Tavares, L. P., Teixeira, M. M., & Garcia, C. C. (2017). The inflammatory response triggered by Influenza virus: a two edged sword. *Inflamm Res*, *66*(4), 283-302. doi:10.1007/s00011-016-0996-0
- Tisoncik, J. R., Korth, M. J., Simmons, C. P., Farrar, J., Martin, T. R., & Katze, M. G. (2012). Into the eye of the cytokine storm. *Microbiol Mol Biol Rev*, *76*(1), 16-32. doi:10.1128/mmbr.05015-11
- Travassos, L. H., Carneiro, L. A., Ramjeet, M., Hussey, S., Kim, Y. G., Magalhaes, J. G., . . . Philpott, D. J. (2010). Nod1 and Nod2 direct autophagy by recruiting ATG16L1 to the plasma membrane at the site of bacterial entry. *Nat Immunol*, *11*(1), 55-62. doi:10.1038/ni.1823
- Tsai, S. Y., Segovia, J. A., Chang, T. H., Morris, I. R., Berton, M. T., Tessier, P. A., . . . Bose, S. (2014). DAMP molecule S100A9 acts as a molecular pattern to enhance inflammation during influenza A virus infection: role of DDX21-TRIF-TLR4-MyD88 pathway. *PLoS Pathog*, *10*(1), e1003848. doi:10.1371/journal.ppat.1003848
- Tschurtschenthaler, M., Adolph, T. E., Ashcroft, J. W., Niederreiter, L., Bharti, R., Saveljeva, S., . . . Kaser, A. (2017). Defective ATG16L1-mediated removal of IRE1 $\alpha$  drives Crohn's disease-like ileitis. *J Exp Med*, *214*(2), 401-422. doi:10.1084/jem.20160791
- Tsukada, M., & Ohsumi, Y. (1993). Isolation and characterization of autophagy-defective mutants of *Saccharomyces cerevisiae*. *FEBS Lett*, *333*(1-2), 169-174. doi:10.1016/0014-5793(93)80398-e
- Turner, M. D., Nedjai, B., Hurst, T., & Pennington, D. J. (2014). Cytokines and chemokines: At the crossroads of cell signalling and inflammatory disease. *Biochim Biophys Acta*, *1843*(11), 2563-2582. doi:10.1016/j.bbamcr.2014.05.014

- van den Brand, J. M., Haagmans, B. L., van Riel, D., Osterhaus, A. D., & Kuiken, T. (2014). The pathology and pathogenesis of experimental severe acute respiratory syndrome and influenza in animal models. *J Comp Pathol*, *151*(1), 83-112. doi:10.1016/j.jcpa.2014.01.004
- Ver Heul, A. M., Fowler, C. A., Ramaswamy, S., & Piper, R. C. (2013). Ubiquitin regulates caspase recruitment domain-mediated signaling by nucleotide-binding oligomerization domain-containing proteins NOD1 and NOD2. *J Biol Chem*, *288*(10), 6890-6902. doi:10.1074/jbc.M112.413781
- Vivier, E., Rautlet, D. H., Moretta, A., Caligiuri, M. A., Zitvogel, L., Lanier, L. L., . . . Ugolini, S. (2011). Innate or adaptive immunity? The example of natural killer cells. *Science*, *331*(6013), 44-49. doi:10.1126/science.1198687
- Wack, A., Terczyńska-Dyla, E., & Hartmann, R. (2015). Guarding the frontiers: the biology of type III interferons. *Nat Immunol*, *16*, 802. doi:10.1038/ni.3212
- Walzer, T., Dalod, M., Robbins, S. H., Zitvogel, L., & Vivier, E. (2005). Natural-killer cells and dendritic cells: "l'union fait la force". *Blood*, *106*(7), 2252-2258. doi:10.1182/blood-2005-03-1154
- Wang, W., Xu, L., Su, J., Peppelenbosch, M. P., & Pan, Q. (2017). Transcriptional Regulation of Antiviral Interferon-Stimulated Genes. *Trends Microbiol*, *25*(7), 573-584. doi:10.1016/j.tim.2017.01.001
- Weber, A., Wasiliew, P., & Kracht, M. (2010). Interleukin-1 (IL-1) pathway. *Sci Signal*, *3*(105), cm1. doi:10.1126/scisignal.3105cm1
- Wileman, T. (2013). Autophagy as a defence against intracellular pathogens. *Essays Biochem*, *55*, 153-163. doi:10.1042/bse0550153
- Wilson, M. I., Dooley, H. C., & Tooze, S. A. (2014). WIPI2b and Atg16L1: setting the stage for autophagosome formation. *Biochem Soc Trans*, *42*(5), 1327-1334. doi:10.1042/bst20140177
- Wong, S. W., Sil, P., & Martinez, J. (2018). Rubicon: LC3-associated phagocytosis and beyond. *Febs j*, *285*(8), 1379-1388. doi:10.1111/febs.14354
- Xiong, Q., Li, W., Li, P., Yang, M., Wu, C., & Eichinger, L. (2018). The Role of ATG16 in Autophagy and The Ubiquitin Proteasome System. *Cells*, *8*(1). doi:10.3390/cells8010002
- Yamamoto, H., Kakuta, S., Watanabe, T. M., Kitamura, A., Sekito, T., Kondo-Kakuta, C., . . . Ohsumi, Y. (2012). Atg9 vesicles are an important membrane source during early steps of autophagosome formation. *J Cell Biol*, *198*(2), 219-233. doi:10.1083/jcb.201202061
- Yang, Z., & Klionsky, D. J. (2009). An overview of the molecular mechanism of autophagy. *Curr Top Microbiol Immunol*, *335*, 1-32. doi:10.1007/978-3-642-00302-8\_1
- Yang, Z., & Klionsky, D. J. (2010). Mammalian autophagy: core molecular machinery and signaling regulation. *Curr Opin Cell Biol*, *22*(2), 124-131. doi:10.1016/j.ceb.2009.11.014
- Yorihuzi, T., & Ohsumi, Y. (1994). *Saccharomyces cerevisiae* MATa mutant cells defective in pointed projection formation in response to alpha-factor at high concentrations. *Yeast*, *10*(5), 579-594. doi:10.1002/yea.320100503
- Yoshii, S. R., Kuma, A., Akashi, T., Hara, T., Yamamoto, A., Kurikawa, Y., . . . Mizushima, N. (2016). Systemic Analysis of Atg5-Null Mice Rescued from Neonatal Lethality by Transgenic ATG5 Expression in Neurons. *Dev Cell*, *39*(1), 116-130. doi:10.1016/j.devcel.2016.09.001
- Yu, L., Chen, Y., & Tooze, S. A. (2018). Autophagy pathway: Cellular and molecular mechanisms. *Autophagy*, *14*(2), 207-215. doi:10.1080/15548627.2017.1378838
- Zaffagnini, G., & Martens, S. (2016). Mechanisms of Selective Autophagy. *J Mol Biol*, *428*(9 Pt A), 1714-1724. doi:10.1016/j.jmb.2016.02.004
- Zhang, J. M., & An, J. (2007). Cytokines, inflammation, and pain. *Int Anesthesiol Clin*, *45*(2), 27-37. doi:10.1097/AIA.0b013e318034194e
- Zhang, L., & Wang, A. (2012). Virus-induced ER stress and the unfolded protein response. *Front Plant Sci*, *3*, 293. doi:10.3389/fpls.2012.00293
- Zuniga, J., Torres, M., Romo, J., Torres, D., Jimenez, L., Ramirez, G., . . . Selmán, M. (2011). Inflammatory profiles in severe pneumonia associated with the pandemic influenza A/H1N1

virus isolated in Mexico City. *Autoimmunity*, 44(7), 562-570.  
doi:10.3109/08916934.2011.592885

## **Acknowledgement:**

First, I would like to express my sincere appreciation to my primary supervisor Prof. Tom Wileman, for providing me the Ph.D position in University of East Anglia, arousing my interest and giving me the opportunity to develop as a biological scientist. I would also like to thank my supervisory team Tom Wileman, Ulrike Mayer and Simon Carding for all of the help and support they have provided during my entire Ph.D career.

Second, I would like to thank Prof. James Steward (University of Liverpool), for all of his help of arranging and operating animal infection experiment in University of Liverpool, Sharma Parul (University of Liverpool) for her help of the FACs and Chimera experiment, and Anja Kipar at (University of Zurich) for her help of the histology work.

Third, I am grateful my lab members: Matthew Jefferson, Shashank Rai, Benjamin Bone, Weijiao Zhang, Timothy Pearson, Aleksandra Zhekova and Angela Man for all of the technical and spiritual support they provided. I would like to thank Penny Powell for the brilliant advices she suggested for my work. I would also like to thank Dr. Julia Maryam for establishing the mouse models used in my study.

Last but not least, I would like to thank my family to provide the finical and psychological supports to encourage me for chasing my dreams. I appreciate my husband Chao Guo, who travel from China to England for keeping company and taking care of me for 2 years allow me to concentrate on my works.